

JOURNAL OF

CHROMATOGRAPHY A

INCLUDING ELECTROPHORESIS AND OTHER SEPARATION METHODS

EDITORS

U.A.Th. Brinkman (Amsterdam)
 R.W. Giese (Boston, MA)
 J.K. Haken (Kensington, N.S.W.)
 C.F. Poole (London)
 L.R. Snyder (Orinda, CA)
 S. Terabe (Hyogo)

EDITORS, SYMPOSIUM VOLUMES,
 E. Heftmann (Orinda, CA), Z. Deyl (Prague)

EDITORIAL BOARD

D.W. Armstrong (Rolla, MO)
 W.A. Aue (Halifax)
 P. Boček (Brno)
 P.W. Carr (Minneapolis, MN)
 J. Crommen (Liège)
 V.A. Davankov (Moscow)
 G.J. de Jong (Groningen)
 Z. Deyl (Prague)
 S. Dilli (Kensington, N.S.W.)
 Z. El Rassi (Stillwater, OK)
 H. Engelhardt (Saarbrücken)
 M.B. Evans (Hatfield)
 S. Fanali (Rome)
 G.A. Guiochon (Knoxville, TN)
 P.R. Haddad (Hobart, Tasmania)
 I.M. Hais (Hradec Králové)
 W.S. Hancock (Palo Alto, CA)
 S. Hjertén (Uppsala)
 S. Honda (Higashi-Osaka)
 Cs. Horváth (New Haven, CT)
 J.F.K. Huber (Vienna)
 J. Janák (Brno)
 P. Jandera (Pardubice)
 B.L. Karger (Boston, MA)
 J.J. Kirkland (Newport, DE)
 E. sz. Kováts (Lausanne)
 C.S. Lee (Ames, IA)
 K. Macek (Prague)
 A.J.P. Martin (Cambridge)
 E.D. Morgan (Keele)
 H. Poppe (Amsterdam)
 P.G. Righetti (Milan)
 P. Schoenmakers (Amsterdam)
 R. Schwarzenbach (Dübendorf)
 R.E. Shoup (West Lafayette, IN)
 R.P. Singhal (Wichita, KS)
 A.M. Sioum (Marseille)
 D.J. Strydom (Boston, MA)
 T. Takagi (Osaka)
 N. Tanaka (Kyoto)
 K.K. Unger (Mainz)
 P. van Zoonen (Bilthoven)
 R. Verpoorte (Leiden)
 Gy. Vigh (College Station, TX)
 J.T. Watson (East Lansing, MI)
 B.D. Westerlund (Uppsala)

EDITORS, BIBLIOGRAPHY SECTION

Z. Deyl (Prague), J. Janák (Brno), V. Schwarz (Prague)

ELSEVIER

JOURNAL OF CHROMATOGRAPHY A

INCLUDING ELECTROPHORESIS AND OTHER SEPARATION METHODS

Scope. The *Journal of Chromatography* publishes papers on all aspects of **chromatography, electrophoresis** and other separation methods. Contributions consist mainly of research papers dealing with chromatographic theory, instrumental developments and their applications. Section A covers all areas except biomedical applications of separation science which are published in section B: *Biomedical Applications*.

Submission of Papers. The preferred medium of submission is on disk with accompanying manuscript. Manuscripts (in English; four copies are required) should be submitted to: Editorial Office of *Journal of Chromatography A*, P.O. Box 681, 1000 AR Amsterdam, Netherlands, Telefax (+31-20) 485 2304. Review articles are invited or proposed in writing to the Editors who welcome suggestions for subjects. An outline of the proposed review should first be forwarded to the Editors for preliminary discussion prior to preparation. Submission of an article is understood to imply that the article is original and unpublished and is not being considered for publication elsewhere. For copyright regulations, see below.

Subscription information. For 1996 Vols. 715–748 of *Journal of Chromatography A* (ISSN 0021-9673) are scheduled for publication. Subscription prices for *Journal of Chromatography A + B* (combined), or for section A or B are available upon request from the publisher. Subscriptions are accepted on a prepaid basis only and are entered on a calendar year basis. Issues are sent by surface mail except to the following countries where air delivery via SAL is ensured: Argentina, Australia, Brazil, Canada, China, Hong Kong, India, Israel, Japan, Malaysia, Mexico, New Zealand, Pakistan, Singapore, South Africa, South Korea, Taiwan, Thailand, USA. For all other countries airmail rates are available upon request. Claims for missing issues must be made within six months of our publication (mailing) date. Please address all your requests regarding orders and subscription queries to: Elsevier Science B.V., Journal Department, P.O. Box 211, 1000 AE Amsterdam, Netherlands. Tel.: (+31-20) 485 3642; Fax: (+31-20) 485 3598. Customers in the USA and Canada wishing information on this and other Elsevier journals, please contact Journal Information Center, Elsevier Science Inc., 655 Avenue of the Americas, New York, NY 10010, USA, Tel. (+1-212) 633 3750, Telefax (+1-212) 633 3764.

Abstracts/Contents Lists published in Analytical Abstracts, Biochemical Abstracts, Biological Abstracts, Chemical Abstracts, Chemical Titles, Chromatography Abstracts, Current Awareness in Biological Sciences (CABS), Current Contents/Life Sciences, Current Contents/Physical, Chemical & Earth Sciences, Deep-Sea Research/Part B: Oceanographic Literature Review, Excerpta Medica, Index Medicus, Mass Spectrometry Bulletin, PASCAL-CNRS, Referativnyi Zhurnal, Research Alert and Science Citation Index.

US Mailing Notice. *Journal of Chromatography A* (ISSN 0021-9673) is published weekly (total 52 issues) by Elsevier Science B.V., (Sara Burgerhartstraat 25, P.O. Box 211, 1000 AE Amsterdam, Netherlands). Annual subscription price in the USA US\$ 6863.00 (US\$ price valid in North, Central and South America only) including air speed delivery. Second class postage paid at Jamaica, NY 11431. **USA POSTMASTERS:** Send address changes to *Journal of Chromatography A*, Publications Expediting, Inc., 200 Meacham Avenue, Elmont, NY 11003. Airfreight and mailing in the USA by Publications Expediting.

Advertisements. The Editors of the journal accept no responsibility for the contents of the advertisements. Advertisement rates are available on request. Advertising orders and enquiries may be sent to *International:* Elsevier Science, Advertising Department, The Boulevard, Langford Lane, Kidlington, Oxford, OX5 1GB, UK; Tel: (+44) (0) 1865 843565; Fax: (+44) (0) 1865 843952. *USA and Canada:* Weston Media Associates, Dan Lipner, P.O. Box 1110, Greens Farms, CT 06436-1110, USA; Tel: (203) 261 2500; Fax: (203) 261 0101. *Japan:* Elsevier Science Japan, Ms Noriko Kodama, 20-12 Yushima, 3 chome, Bunkyo-Ku, Tokyo 113, Japan; Tel: (+81) 3 3836 0810; Fax: (+81) 3 3839 4344.

See inside back cover for Publication Schedule and Information for Authors.

© 1995 ELSEVIER SCIENCE B.V. All rights reserved.

0021-9673/95/\$09.50

No part of this publication may be reproduced, stored in a retrieval system or transmitted in any form or by any means, electronic, mechanical, photocopying, recording or otherwise, without the prior written permission of the publisher, Elsevier Science B.V., Copyright and Permissions Department, P.O. Box 521, 1000 AM Amsterdam, Netherlands.

Upon acceptance of an article by the journal, the author(s) will be asked to transfer copyright of the article to the publisher. The transfer will ensure the widest possible dissemination of information.

Special regulations for readers in the USA – This journal has been registered with the Copyright Clearance Center, Inc. Consent is given for copying of articles for personal or internal use, or for the personal use of specific clients. This consent is given on the condition that the copier pays through the Center the per-copy fee stated in the code on the first page of each article for copying beyond that permitted by Sections 107 or 108 of the US Copyright Law. The appropriate fee should be forwarded with a copy of the first page of the article to the Copyright Clearance Center, Inc., 222 Rosewood Drive, Danvers, MA 01923, USA. If no code appears in an article, the author has not given broad consent to copy and permission to copy must be obtained directly from the author. The fee indicated on the first page of an article in this issue will apply retroactively to all articles published in the journal, regardless of the year of publication. This consent does not extend to other kinds of copying, such as for general distribution, resale, advertising and promotion purposes, or for creating new collective works. Special written permission must be obtained from the publisher for such copying.

No responsibility is assumed by the Publisher for any injury and/or damage to persons or property as a matter of products liability, negligence or otherwise, or from any use or operation of any methods, products, instructions or ideas contained in the materials herein. Because of rapid advances in the medical sciences, the Publisher recommends that independent verification of diagnoses and drug dosages should be made.

Although all advertising material is expected to conform to ethical (medical) standards, inclusion in this publication does not constitute a guarantee or endorsement of the quality or value of such product or of the claims made of it by its manufacturer.

Ⓢ The paper used in this publication meets the requirements of ANSI/NISO Z39.48-1992 (Permanence of Paper).

Printed in the Netherlands

CONTENTS

(Abstracts/Contents Lists published in *Analytical Abstracts*, *Biochemical Abstracts*, *Biological Abstracts*, *Chemical Abstracts*, *Chemical Titles*, *Chromatography Abstracts*, *Current Awareness in Biological Sciences (CABS)*, *Current Contents/Life Sciences*, *Current Contents/Physical, Chemical & Earth Sciences*, *Deep-Sea Research/Part B: Oceanographic Literature Review*, *Excerpta Medica*, *Index Medicus*, *Mass Spectrometry Bulletin*, *PASCAL-CNRS*, *Referativnyi Zhurnal*, *Research Alert* and *Science Citation Index*)

Editorial

by R.W. Giese v

REVIEW

Optimisation of selectivity in capillary electrophoresis with emphasis on micellar electrokinetic capillary chromatography
by H. Corstjens, H.A.H. Billiet, J. Frank and K.Ch.A.M. Luyben (Delft, Netherlands) 1

REGULAR PAPERS

Column Liquid Chromatography

Method of increasing the sensitivity of liquid chromatography-atmospheric pressure chemical ionization mass spectrometry
using a semi-micro column
by T. Adachi, M. Nemoto and Y. Ito (Saitama, Japan) (Received 16 May 1995) 13

High-performance liquid chromatography of C₆₀, C₇₀, and higher fullerenes on tetraphenylporphyrin-silica stationary phases
using strong mobile phase solvents
by J. Xiao and M.E. Meyerhoff (Ann Arbor, MI, USA) (Received 9 May 1995) 19

Retention mechanisms of polycyclic aromatic nitrogen heterocyclics on bonded amino phases in normal-phase liquid
chromatography
by H. Carlsson and C. Östman (Solna, Sweden) (Received 2 March 1995) 31

Determination of hydroxy-substituted polycyclic aromatic hydrocarbons by high-performance liquid chromatography with
electrochemical detection
by M.T. Galceran and E. Moyano (Barcelona, Spain) (Received 8 May 1995) 41

Surface modification of microporous polyamide membranes with hydroxyethyl cellulose and their application as affinity
membranes
by T.C. Beeskow, W. Kusharyoto, F.B. Anspach, K.H. Kroner and W.-D. Deckwer (Braunschweig, Germany)
(Received 2 May 1995) 49

Simultaneous determination of amino acids and biogenic amines by reversed-phase high-performance liquid chromatography
of the dabsyl derivatives
by I. Krause, A. Bockhardt, H. Neckermann, T. Henle and H. Klostermeyer (Freising, Germany) (Received 4 May
1995) 67

Microcalorimetric characterization of the anion-exchange adsorption of recombinant cytochrome b₅ and its surface-charge
mutants
by D.S. Gill, D.J. Roush, K.A. Shick and R.C. Willson (Houston, TX, USA) (Received 22 March 1995) 81

Chromatographic and chemometric investigation of the chemical defence mechanism of poplar tree genotypes against a bark
fungine parasite
by C. Baiocchi, E. Marengo, M.A. Roggero and D. Giacosa (Turin, Italy) and A. Giorcelli and S. Toccari (Casale
Monferrato, Italy) (Received 9 May 1995) 95

Ion-exchange mechanisms of some transition metals on a mixed-bed resin with a complexing eluent
by P. Janvion, S. Motellier and H. Pitsch (Fontenay-aux-Roses, France) (Received 2 May 1995) 105

Field-Flow Fractionation

Influence of bulk and surface composition on the retention of colloidal particles in thermal field-flow fractionation
by P.M. Shiundu and J.C. Giddings (Salt Lake City, UT, USA) (Received 9 May 1995) 117

(Continued overleaf)

ห้องสมุดมหาวิทยาลัยเทคโนโลยีพระจอมเกล้าธนบุรี
21 ตุลาคม 2538

Contents (continued)

Gas Chromatography

- Solution properties of amorphous co- and terpolymers of styrene as examined by inverse gas chromatography
by V.I. Bogillo (Kiev, Ukraine) and A. Voelkel (Poznań, Poland) (Received 8 May 1995) 127

Electrophoresis

- Double-chain surfactants with two sulfonate groups as micelle-forming reagents in micellar electrokinetic chromatography of naphthalene derivatives
by H. Harino, M. Tanaka, T. Araki, Y. Yasaka, A. Masuyama, Y. Nakatsuji, I. Ikeda and K. Funazo (Osaka, Japan) and S. Terabe (Hyogo, Japan) (Received 8 May 1995) 135
- Determination of the enantiomeric purity of 5,6-dihydroxy-2-aminotetralin by high-performance capillary electrophoresis with crown ether as chiral selector
by P. Castelnovo and C. Albanesi (Milan, Italy) (Received 8 May 1995) 143
- Determination of chiral reagent purity by capillary electrophoresis
by A. Engström, H. Wan, P.E. Andersson and B. Josefsson (Stockholm, Sweden) (Received 17 May 1995) 151
- Separation of formoterol enantiomers and detection of zeptomolar amounts by capillary electrophoresis using laser-induced fluorescence
by S. Cherkaoui, M. Faupel and E. Francotte (Basel, Switzerland) (Received 17 May 1995) 159
- Pre-column derivatization of proteins to enhance detection sensitivity for sodium dodecyl sulfate non-gel sieving capillary electrophoresis
by E.L. Gump and C.A. Monnig (Riverside, CA, USA) (Received 17 May 1995) 167
- Improvement in the determination of food additive dyestuffs by capillary electrophoresis using β -cyclodextrin
by S. Razee, A. Tamura and T. Masujima (Hiroshima, Japan) (Received 16 May 1995) 179

SHORT COMMUNICATIONS

Column Liquid Chromatography

- High-performance liquid chromatographic determination of denatonium benzoate in ethanol with 5% polyvinylpyrrolidone
by A. Faulkner and P. DeMontigny (West Point, PA, USA) (Received 2 May 1995) 189
- Determination of amphoteric surfactants in cosmetic cleansing products by high-performance liquid chromatography on a cation-exchange column
by A. Tegeler, W. Ruess and E. Gmahl (Darmstadt, Germany) (Received 16 May 1995) 195

LETTER TO THE EDITOR

- Experiences with HPLC-grade solvents
by J.J. Kirkland (Newport, DE, USA) 199

JOURNAL OF CHROMATOGRAPHY A

VOL. 715 (1995)

JOURNAL OF CHROMATOGRAPHY A

INCLUDING ELECTROPHORESIS AND OTHER SEPARATION METHODS

EDITORS

U.A.Th. BRINKMAN (Amsterdam), R.W. GIESE (Boston, MA), J.K. HAKEN (Kensington, N.S.W.),
C.F. POOLE (London), L.R. SNYDER (Orinda, CA), S. TERABE (Hyogo)

EDITORS, SYMPOSIUM VOLUMES

E. HEFTMANN (Orinda, CA), Z. DEYL (Prague)

EDITORIAL BOARD

D.W. Armstrong (Rolla, MO), W.A. Aue (Halifax), P. Boček (Brno), P.W. Carr (Minneapolis, MN), J. Crommen (Liège), V.A. Davankov (Moscow), G.J. de Jong (Groningen), Z. Deyl (Prague), S. Dilli (Kensington, N.S.W.), Z. El Rassi (Stillwater, OK), H. Engelhardt (Saarbrücken), M.B. Evans (Hatfield), S. Fanali (Rome), G.A. Guiochon (Knoxville, TN), P.R. Haddad (Hobart, Tasmania), I.M. Hais (Hradec Králové), W.S. Hancock (Palo Alto, CA), S. Hjertén (Uppsala), S. Honda (Higashi-Osaka), Cs. Horváth (New Haven, CT), J.F.K. Huber (Vienna), J. Janák (Brno), P. Jandera (Pardubice), B.L. Karger (Boston, MA), J.J. Kirkland (Newport, DE), E. sz. Kováts (Lausanne), C.S. Lee (Ames, IA), K. Macek (Prague), A.J.P. Martin (Cambridge), E.D. Morgan (Keele), H. Poppe (Amsterdam), P.G. Righetti (Milan), P. Schoenmakers (Amsterdam), R. Schwarzenbach (Dübendorf), R.E. Shoup (West Lafayette, IN), R.P. Singhal (Wichita, KS), A.M. Siouffi (Marseille), D.J. Strydom (Boston, MA), T. Takagi (Osaka), N. Tanaka (Kyoto), K.K. Unger (Mainz), P. van Zoonen (Bilthoven), R. Verpoorte (Leiden), Gy. Vigh (College Station, TX), J.T. Watson (East Lansing, MI), B.D. Westerlund (Uppsala)

EDITORS, BIBLIOGRAPHY SECTION

Z. Deyl (Prague), J. Janák (Brno), V. Schwarz (Prague)



ELSEVIER

Amsterdam – Lausanne – New York – Oxford – Shannon – Tokyo

J. Chromatogr. A, Vol. 715 (1995)

© 1995 ELSEVIER SCIENCE B.V. All rights reserved.

0021-9673/95/\$09.50

No part of this publication may be reproduced, stored in a retrieval system or transmitted in any form or by any means, electronic, mechanical, photocopying, recording or otherwise, without the prior written permission of the publisher, Elsevier Science B.V., Copyright and Permissions Department, P.O. Box 521, 1000 AM Amsterdam, Netherlands.

Upon acceptance of an article by the journal, the author(s) will be asked to transfer copyright of the article to the publisher. The transfer will ensure the widest possible dissemination of information.

Special regulations for readers in the USA – This journal has been registered with the Copyright Clearance Center, Inc. Consent is given for copying of articles for personal or internal use, or for the personal use of specific clients. This consent is given on the condition that the copier pays through the Center the per-copy fee stated in the code on the first page of each article for copying beyond that permitted by Sections 107 or 108 of the US Copyright Law. The appropriate fee should be forwarded with a copy of the first page of the article to the Copyright Clearance Center, Inc., 222 Rosewood Drive, Danvers, MA 01923, USA. If no code appears in an article, the author has not given broad consent to copy and permission to copy must be obtained directly from the author. The fee indicated on the first page of an article in this issue will apply retroactively to all articles published in the journal, regardless of the year of publication. This consent does not extend to other kinds of copying, such as for general distribution, resale, advertising and promotion purposes, or for creating new collective works. Special written permission must be obtained from the publisher for such copying.

No responsibility is assumed by the Publisher for any injury and/or damage to persons or property as a matter of products liability, negligence or otherwise, or from any use or operation of any methods, products, instructions or ideas contained in the materials herein. Because of rapid advances in the medical sciences, the Publisher recommends that independent verification of diagnoses and drug dosages should be made.

Although all advertising material is expected to conform to ethical (medical) standards, inclusion in this publication does not constitute a guarantee or endorsement of the quality or value of such product or of the claims made of it by its manufacturer.

Ⓜ The paper used in this publication meets the requirements of ANSI/NISO Z39.48-1992 (Permanence of Paper).

Printed in the Netherlands



ELSEVIER

Journal of Chromatography A, 715 (1995) v

JOURNAL OF
CHROMATOGRAPHY A

Editorial: Letters to the Editor

“Letters” in scientific journals bring up, formally or informally, ideas, comments, opinions, stories, experiences, advice, disagreements, insights, assessment, elaborations, and so forth. Certainly these aspects exist in separation science. With this issue of our Journal, we encourage our readers to communicate more with each other in this format. Contributions should be sent to the Editorial Office in Amsterdam (see cover for full address). Submissions will be subject to the usual refereeing procedure. Normally a Letter should be no longer than two printed pages.

This issue contains a Letter contribution from Jack Kirkland relating a recent experience in troubleshooting. Some HPLC columns underwent a peculiar demise in his laboratory. Jack is not the easiest person to fool in the area of HPLC, but a solvent manufacturer managed to do it (of course, only for a short time).

We hope to hear from you, and thereby have the Journal cover more of the broad spectrum of separation science.

Roger W. Giese

Review

Optimisation of selectivity in capillary electrophoresis with emphasis on micellar electrokinetic capillary chromatography

H. Corstjens*, H.A.H. Billiet, J. Frank, K.Ch.A.M. Luyben

Department of Biochemical Engineering, Delft University of Technology, Julianalaan 67, 2628 BC Delft, Netherlands

Abstract

Separations in capillary electrophoresis and especially in micellar electrokinetic capillary chromatography are characterised by a large number of parameters and therefore difficult to optimise. This paper reviews recent approaches suitable for optimisation of selectivity in capillary electrophoresis.

Typical features of optimisation strategies applicable to capillary electrophoresis and micellar electrokinetic capillary chromatography in particular are discussed. A distinction is made between statistical approaches, using fitting procedures of polynomial equations, and practical optimisation schemes, based on physicochemical models describing the migration behaviour.

Besides speeding up the search in finding satisfactory separation conditions, additional knowledge may be obtained about the migration and separation mechanism(s) when a systematic approach is applied. However, due to the complexity and the number of available optimisation schemes, these approaches should not be used as black-box systems. The analyst has a crucial role in optimising a separation.

Contents

1. Introduction	1
2. Statistical approaches in the optimisation of CE	3
3. Optimisation procedures based on physicochemical models	4
3.1. Global approaches in the optimisation of CE	5
3.2. Practical approaches in the optimisation of CE	7
4. Conclusions	9
References	10

1. Introduction

Capillary electrophoresis (CE) is a rapidly expanding analytical technique that can be used to separate many different compounds. The separation of biological molecules such as pep-

tides, proteins [1–6] and nucleic acids [7,8] as well as inorganic ions [9,10] and pollutants [11,12] has been reported in the literature. In spite of the fact that CE is characterised by a high efficiency, the desired separation is often only obtained after considerable experimentation. Although the adjustment of system parameters, like sample characteristics to introduce

* Corresponding author.

stacking [13,14], the use of electrokinetic injection with its discriminating capabilities [15,16] or the selection of an appropriate detection wavelength for detection or spectral recognition [17,18], should not be overlooked, system optimisation will not be dealt with. The purpose of the present review is to give an overview of the guidelines and strategies that are currently available to achieve an adequate selectivity with the minimum number of experiments.

Selectivity in capillary zone electrophoresis (CZE) is strongly influenced by the pH of the buffer. In addition, the type and concentration of buffer and the presence of an organic modifier can affect both selectivity and efficiency. In micellar electrokinetic capillary chromatography (MECC), a special mode of CE [19], two additional parameters have a remarkable influence on the separation, i.e. the type and concentration of surfactant. As a result numerous factors will affect MECC experiments.

The temperature affects different physico-chemical parameters like viscosity, pK_a and pH values, absolute mobilities and the critical micellar concentration (cmc) of various surfactants and thus the separation. As a result, an efficient temperature control is inevitable in method development and although temperature changes can be used to improve the selectivity [20,21], we will focus on methods in which the temperature is assumed to be constant.

Clearly, an appropriate optimisation strategy should be used to find good separation conditions in the shortest time and/or after only a few experiments. Basically, all optimisation strategies consist of three distinct steps: the choice of the appropriate parameter(s) and the parameter space, a model or algorithm to describe the migration behaviour and a criterion to evaluate the resulting electropherogram. For an overview the reader is referred to Ref. [22].

The choice of the parameter(s) to be optimised is mainly influenced by the analytical technique itself and therefore, this choice often seems quite obvious. In contrast, the choice of the limits of each parameter, which usually defines the parameter space, is more difficult to rationalise. Although generally the absolute minimum and

maximum value of a parameter is physically defined, these limits seldom will be the actual limits used in the optimisation procedure. For example, optimisation of the pH as the parameter having much influence on selectivity in CZE is a rather obvious choice. However, the actual pH range under investigation is difficult to define without relevant knowledge about the sample to separate. In this respect dissociation constants as well as pH stability data are essential in CZE. Unfortunately, in many cases relevant data concerning the sample under investigation are not available so that the experience of the analyst becomes important.

After the choice of the appropriate parameters and their limiting values, experiments must be performed to explore the migration of the solutes as a function of the parameter(s). A description of the behaviour of the analytical system in the entire parameter space is then generally obtained by interpolation using an algorithm that relates the migration of the solutes to the parameter(s). Differences can be found among the various models used and the theoretical basis underlying the model can be quite different. Approaches based on physicochemical properties like dissociation constants, mobility data and diffusion coefficients of the solutes and buffer properties like ionic strength and pH as well as models based on strictly mathematical equations, treated in a statistical way, are reported. It is clear that there is a correlation between the accuracy of the model and the time and effort it takes to satisfactorily predict the migration behaviour of different solutes and hence to find good separation conditions.

The final step in the optimisation strategy is the evaluation of the migration behaviour of the solutes predicted in the parameter space in terms of the quality of the separation. The goal of an optimisation may vary considerably from one case to another, e.g. the separation of two enantiomers requires a different criterion than a peptide map in which many different unknown solutes must be detected. Therefore, this goal must be translated into appropriate objective mathematical functions, defining the criterion. The criterion relates the quality of an observed

electropherogram to a desired one and this choice is critical and affects both the optimisation procedure to follow and the results obtained. Furthermore, it is not necessary to search for the global optimum in the parameter space but it satisfies to find experimental conditions resulting in sufficient separation. Many different criteria are proposed in the literature and some of them, which are used in the optimisation of chromatographic experiments but are also useful in CE, can be found in Ref. [22]. Recently, Hayashi et al. [23] studied the precision and throughput in MECC and concluded that these statistical parameters are suitable as criteria in MECC. The criterion should always be carefully evaluated in relation to the ultimate goal of the analyst.

Although for high-performance liquid chromatography (HPLC) several optimisation schemes have been published [22], these approaches often require substantial modification before they can be used to optimise a CE separation. Recently, some books on capillary electrophoresis have paid some attention to method development and optimisation strategies in CE [24-26]. In the first part of this review the possibility to apply statistical approaches is discussed, while in the second part some feasible optimisation schemes are commented.

2. Statistical approaches in the optimisation of CE

The optimisation of CE and especially MECC experiments is complex due to the number of parameters affecting the separation. Further complications can arise from the mutual interaction of the parameters. Examples illustrating this phenomenon have been reported both for micellar liquid chromatography [27] and MECC [24]. This explains why the development of physicochemical models describing the separation mechanisms is not an easy task. Often the behaviour of the system is approximated by simple mathematical equations for which only a minimum amount of knowledge is required.

An example of such an approach is the use of

a simplex algorithm. The principle of a simplex method is covered extensively by the literature [22,28]. In general, the simultaneous optimisation of n parameters results from a fitting procedure of the response (or criterion) y with a first-order model to the parameters x as shown in Eq. 1.

$$y = b_0 + b_1x_1 + b_2x_2 + \dots + b_nx_n \quad (1)$$

The optimum is approached in a sequential way constructing geometrical figures (called simplex) in the parameter space using previous experimental results. These sequences are repeated until the separation is satisfactory or until no further improvement is observed.

The advantage of this approach is that it is applicable to any type and number of parameters and that knowledge about the separation mechanism is not required to calculate the response or define the parameter settings for the next measurement. However, an important drawback of the simplex method is the large number of experiments that is generally needed to reach the optimum. This is clearly illustrated by Castagnola et al. [29], who optimised pH, concentration of organic modifier and concentration of surfactant in the separation of derivatised amino acids. Although the variable-sized weighted simplex optimisation design was used to speed up the procedure, still 10 to 15 steps were required to reach separation conditions that are satisfactory in terms of the mean resolution of all the relevant peak pairs. In addition, the choice of the starting conditions is very critical since different starting conditions can lead to different solutions. Finally, it should be noted that by applying simplex methods much information is lost since only the information of the last $n + 1$ experiments is retained. An adequate description of the response surface is not obtained in this way and this is a serious disadvantage when the response surface is complex.

Another multi-parameter optimisation procedure, called the overlapping resolution mapping scheme (ORM), was introduced for CE by Li and co-workers [30-35]. After defining the parameters and the accompanying parameter

space, the initial experiments are performed, and the response (resolution R_s) of each peak pair is used to determine the coefficients of a polynomial equation that not only accounts for the effect of each parameter but also includes mathematical interaction effects between the parameters, expressed as $x_i x_j$ -terms in Eq. 2:

$$R_s = a_1 x_1 + a_2 x_2 + a_3 x_3 + a_{12} x_1 x_2 + a_{13} x_1 x_3 + a_{23} x_2 x_3 + a_{123} x_1 x_2 x_3 \quad (2)$$

Once the coefficients of the polynomial equations are known, the resolution for each peak pair over the whole parameter space can be predicted and visualised as a resolution map. The optimum separation conditions can then be deduced from an overlay of all the resolution maps. Applications of this method include the separation of solutes such as sulphonamides [30,31], flavonoids [31,32], derivatised amino acids [33,34], drug substances [34] and porphyrins [35].

It should be realised that in this strategy peaks are not identified, hence the actual migration behaviour of the solutes is not followed. Significant errors may result from changes in the relative peak positions. This problem was discerned by Glajch et al. [36], who initially developed the ORM approach for HPLC. Due to such effects the response surface may be complex and discontinuous, and overlapping of the resolution maps can then be expected to yield unreliable results. For this reason peak tracking should be considered as a valuable asset, and this task is much facilitated by using advanced detection techniques such as diode-array spectrophotometry or mass spectrometry.

A third type of experimental design that has been shown to be useful for optimisation purposes is the Plackett–Burman statistical design, which is a fractional factorial design that can be used if the number of parameters is one less than a multiple of four. Dummies should be added to meet the required number of parameters. A dummy can be used to estimate the variability of the system and the significance of the effects found for the true physical parameters. Statistical treatment of the data can often be used for

the screening of many parameters and the models used to describe the results of the experiments are typically first-order in each parameter. The most important parameters found with this screening procedure can then be studied in a full multi-level factorial design.

Vindevoegel and Sandra [37] used this approach to obtain a satisfactory separation of a mixture of testosterone esters. Seven parameters are evaluated by means of eight initial experiments in which the effect of pH and the concentrations of buffer, acetonitrile, sodium dodecyl sulphate (SDS) and sodium heptyl sulphate on the analysis time, the noise, the efficiency and the resolution are studied. Interpretation of the results should, however, be done very carefully since the observed changes in migration behaviour may be due to multiple interactions.

An important advantage of these factorial-design type of procedures is that they are applicable under many different experimental circumstances and that there is no restriction concerning the type of solutes and parameters in the optimisation. However, since in this way no general rules are obtained concerning migration mechanisms, the results are restricted to the separation under investigation. A change in the separation conditions requires that the whole procedure has to be followed over again.

3. Optimisation procedures based on physicochemical models

When relevant knowledge of the mechanism of a given type of separation is available, optimisation protocols can be developed that make use of these separation principles, expressed by an appropriate algorithm.

In Section 3.1, approaches in which fundamental equations describing the migration behaviour and the resolution will be treated. These general equations are based on a theoretical description of the separation process. The parameters describing the migration are then evaluated and adjusted to reach a maximum value of the resolution. In such a way, global guidelines,

pointing to the desired migration behaviour, can be formulated. However, the translation of these guidelines into practical separation conditions is often not obvious, and therefore the practical applicability is limited.

In Section 3.2, specific physicochemical models are shown describing the migration behaviour of particular solutes as a function of one or more parameters. The experimental separation conditions can then be adjusted in such a way that the criterion reaches satisfying values. Clearly, these procedures are suitable to solve practical optimisation problems.

3.1. Global approaches in the optimisation of CE

In MECC uncharged solutes are separated according to differences in micellar solubility. In analogy with HPLC, the equations describing the capacity factor k' and the resolution R_s in MECC are based on a classical chromatographic description as shown in Eqs. 3 and 4 [38].

$$k' = \frac{t_r - t_{eo}}{t_{eo}(1 - t_r/t_{mc})} \quad (3)$$

$$R_s = \frac{\sqrt{N}}{4} \cdot \frac{\alpha - 1}{\alpha} \cdot \frac{k'_j}{1 + k'_j} \cdot \frac{1 - t_{eo}/t_{mc}}{1 + (t_{eo}/t_{mc})k'_i} \quad (4)$$

Here, t_r is the migration time of the solute, t_{mc} is the migration time of a solute totally solubilised in the micelles (e.g. Sudan III), t_{eo} is the migration time of an uncharged solute that has no interaction at all with the micelles (e.g. methanol), α is the selectivity and defined as the ratio of two capacity factors, N is the number of theoretical plates and subscripts i and j denote two (closely migrating) compounds. The definition of the capacity factor k' is clearly analogous to the conventional chromatographic definition of the capacity factor as expressed in Eq. 5:

$$k'_{chrom.} = \frac{t_r - t_0}{t_0} \quad (5)$$

where t_0 is the retention time of a non-retained solute and the additional term in the de-

nominator in Eq. 3 accounts for the size of the migration window in MECC.

It is obvious that this limited migration range, expressed as the ratio t_{mc} over t_{eo} , is important with respect to the peak capacity and separation capabilities of a micellar system. This is illustrated in Fig. 1, showing three simulated electropherograms of two solutes having identical α -values but different values of k' . The separation is superior at intermediate values of k' (electropherogram B in Fig. 1). Low capacity factors result in relatively small micellar interactions and a lack of selectivity and high capacity factor

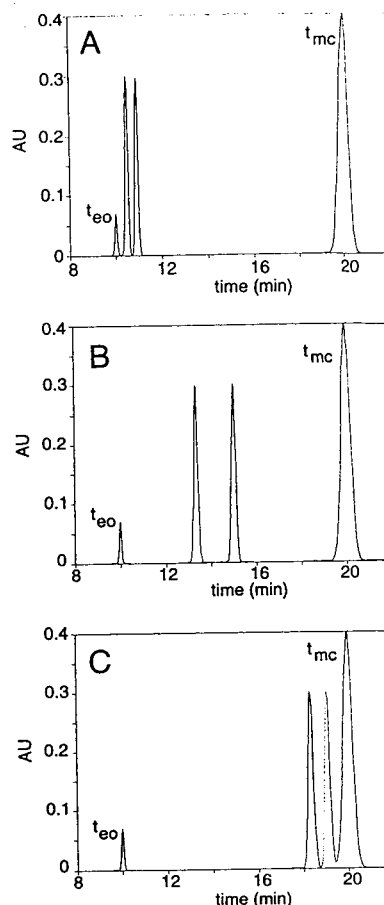


Fig. 1. Simulated electropherograms illustrating the drawbacks of a limited elution range, typical for MECC. Both the migration window ($t_{mc}/t_{eo} = 2$) and the selectivity ($\alpha = 2$) are held constant. (A) $k'_i = 0.1$; $k'_j = 0.2$. (B) $k'_i = 1$; $k'_j = 2$. (C) $k'_i = 10$; $k'_j = 20$.

values result in longer migration times as well as in bad separations because all the solutes are migrating close to t_{mc} .

Extension of the migration window can be achieved by altering the electroosmotic and/or the micellar electrophoretic mobility [39,40]. Recently, Ahuja et al. [41] demonstrated the use of a mixed pseudo-stationary micellar phase of SDS and Brij 35. The electroosmotic and micellar electrophoretic mobilities are matched by adjusting the ratio of the concentration of Brij 35 and SDS so that the micellar mobility equals the electroosmotic mobility but has the opposite sign. This results in a real stationary micellar phase and an infinite migration range is obtained, even at relatively high pH values (ca. 7) where electroosmotic velocities are significant.

The prediction of conditions for optimal separation of neutrals in MECC, formulated by Foley [42] is based on the assumption that selectivity is mainly determined by the partitioning of the neutral solutes between the water and the micellar phase. Accordingly, the concentration of surfactant is the most important parameter to be optimised in that case.

The surfactant concentration $[M]$ is related to the capacity factor k' as shown in Eq. 6:

$$[M] = \frac{k' + \nu \cdot cmc \cdot (k' + P_{wm})}{\nu \cdot (k' + P_{wm})} \quad (6)$$

$$\approx \frac{k'}{P_{wm} \cdot \nu} + cmc, \quad P_{wm} > k'$$

where P_{wm} is the partition coefficient of a given solute for the water and the micellar phase, ν is the partial molar volume of the surfactant and cmc is the critical micelle concentration. Assuming that both N and α are independent of k' , the optimum capacity factor $k'_{opt(R_s)}$ is derived from the classical resolution equation (Eq. 4):

$$k'_{opt(R_s)} = \sqrt{\frac{t_{mc}}{t_{eo}}} \quad (7)$$

Substitution of $k'_{opt(R_s)}$ in Eqs. 6 and 4 allows the calculation of the optimal surfactant concentration (equation not shown) and the corresponding best resolution, respectively:

$$R_s = \frac{\sqrt{N}}{4} \cdot \frac{\alpha - 1}{\alpha} \cdot \frac{\sqrt{t_{mc}/t_{eo}} - \sqrt{t_{eo}/t_{mc}}}{2 + \sqrt{t_{mc}/t_{eo}} + \sqrt{t_{eo}/t_{mc}}} \quad (8)$$

By adjusting the concentration of surfactant it is possible to optimise a separation, independent of the hydrophobicity of the solutes. The same can be done to optimise the resolution per unit time (equations not shown). It is obvious that both approaches do not predict the same optimal parameter settings.

The authors conclude that there is an optimal region for the capacity factor. In general, intermediate values of k' are preferable. Low values of k' will lead to a short analysis time but will suffer from bad resolution, except for samples that are very easy to separate. High capacity factors result in excessive retention and a loss in resolution since all the solutes migrate close to t_{mc} . This phenomenon is not known in conventional column chromatography.

Ghowsi et al. [43] have rewritten the equations based on chromatographic principles using an electrophoretic approach in MECC for neutral solutes. The resolution is not only expressed as a function of the capacity factor but also as a function of μ_{ep}^* , which is the average effective electrophoretic mobility of a neutral solute. N is dependent on the capacity factor and thus on the effective migration time of each solute separately, and in addition, the efficiency is characterised by a Van Deemter-like behaviour of plate number versus voltage.

Using these equations Ghowsi et al. [43] performed a theoretical optimisation for three modes of MECC differing in the net migration velocity of the micelles. Although the approach and the accompanying equations are quite different compared to the optimisation procedure of Foley [42], the results are very similar: when the micelles move to the positive electrode, resolution is maximal if the neutral solute is carried by the micelles to the same extent as the solute is carried by the electroosmotic flow in the opposite direction. Obviously, the analysis time will then be infinite. When the micelles are stationary or moving to the negative electrode, the optimum capacity factor can be calculated by deriving the appropriate equations, and it can be

shown that maximum resolution will be reached for k' values close to 5. In a more qualitative way Terabe et al. [38] came to a similar conclusion starting with equations derived for conventional chromatography.

Based on these global guidelines, together with many experimental observations, Terabe [44] has formulated an introductory guide for optimisation in MECC, which is summarised by the flow chart in Fig. 2. Here, theoretical knowledge is translated in experimental CE-conditions. The first experiment is performed with standard MECC-conditions, and based on this result, the analyst is advised to change the experimental settings concerning the type and concentration of surfactant or other buffer additives so that optimal capacity factor values are approached. The applicability is demonstrated by Bevan et al. [45], who optimised the resolution for mixtures of synthetic oligonucleo-

tides. Although small deviations from theory were observed, high concentrations of urea at various SDS-concentrations, organic modifiers and the use of bile salts and cationic micelles could be used to control the capacity factors and increase the chances to find good separation conditions.

3.2. Practical approaches in the optimisation of CE

It is obvious that for charged solutes the pH will be the first parameter of choice. Kennedler and Friedl [46] have derived a relation between the resolution of monovalent ions in CZE and the pH of the buffer. Both selectivity and efficiency depend on the charge number, and thus for weak electrolytes on the pH as expressed by Eq. 9 for two solutes i and j :

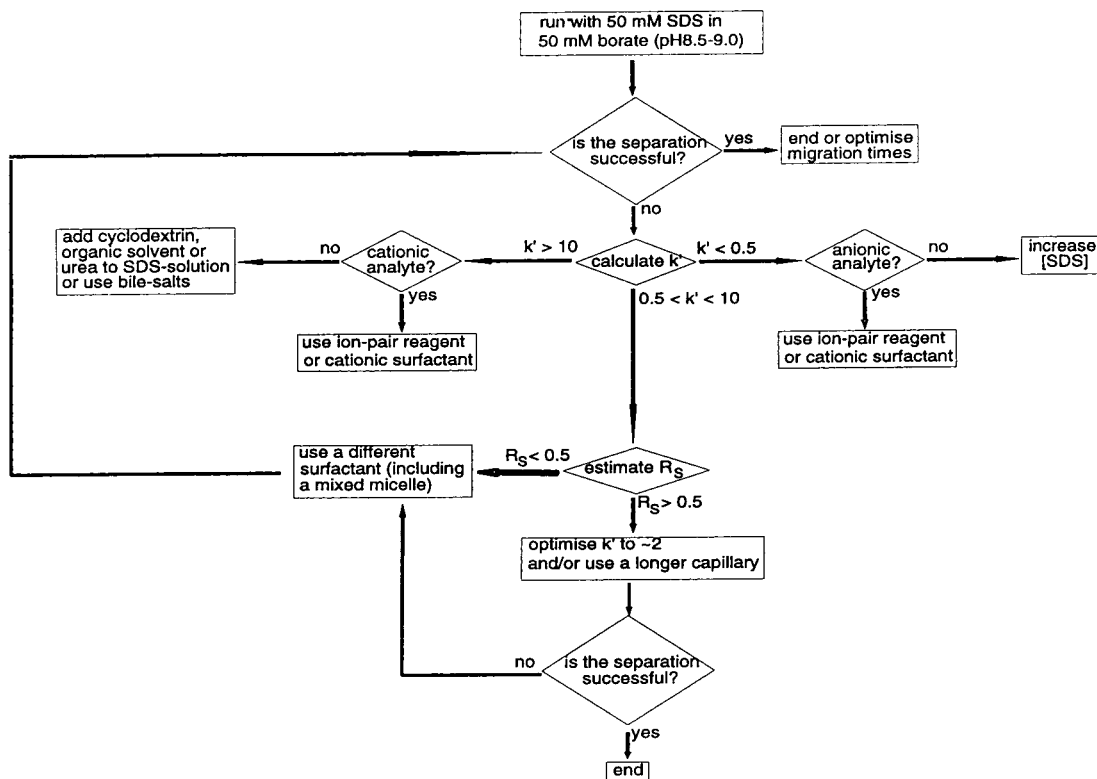


Fig. 2. Introductory guide to the method development of a MECC experiment formulated by Terabe [44].

$$R_{ji} = \frac{\left(\frac{\mu_{\text{act},i}}{\mu_{\text{act},j}} - 1\right) + \left(\frac{\mu_{\text{act},i}}{\mu_{\text{act},j}} \Delta_j - \Delta_i\right)}{(1 - \Delta_i)^{3/2} + \frac{\mu_{\text{act},i}}{\mu_{\text{act},j}} (1 - \Delta_j)^{3/2}} \sqrt{\frac{e_0 U}{32kT}} \quad (9)$$

where μ_{act} is the actual mobility, $\Delta_i = 10^{\text{p}K_{a,i} - \text{pH}}$, $\Delta_j = 10^{\text{p}K_{a,j} - \text{pH}}$, e_0 is the electric charge, k is the Boltzmann constant, T is the absolute temperature and U is the applied voltage. This equation was also extended to multivalent ions [47]. The resolution as a function of pH of the buffer and applied voltage was calculated for different solutes and optimal settings can easily be deduced. As expected, the predicted resolution is a complex function of the pH in the case of multivalent ions.

Use of these relations requires accurate knowledge about the acid–base properties of the solutes and in the study cited above, the relevant $\text{p}K_a$ values were taken from the literature. In addition, the mobilities of the solutes have to be known very precisely, and since not much literature data is available, these values should be determined experimentally by measuring the migration time of a solute as a function of the pH. Obviously, this requires a large number of experiments.

It is recognised by the authors that the model proposed is limited by the lack of consistent data on the analyte properties [48]. Nevertheless, both for mono- and multivalent ions an optimal pH was predicted, resulting in a baseline separation of the entire series of substituted benzoic acids and phenols investigated. It was found that a change of the pH as small as 0.04 may have a dramatic influence on the resolution, and in spite of uncertainties in both the mobilities and the dissociation constants, this effect is predicted by this approach.

Jacquier et al. [49] also optimise the pH for the separation of monovalent ions. With only one experiment when the $\text{p}K_a$ value is known and two experiments when the dissociation constant is unknown, the migration time of a solute over the pH range can be predicted. In addition, an estimate of the molecular diffusion coefficient and hence the peak width is obtained. The electroosmotic flow is modelled in a very simple

way using the dissociation constant of the silanol groups.

Although in this approach the number of experiments is very limited and also some uncertainty remains concerning the electroosmotic mobility and the dissociation constants, the predicted behaviour of the solutes is in reasonable agreement with the experimental results. Using this strategy, the separation of three different solute mixtures: three chlorophenol geometric isomers, three nitrophenol geometric isomers and three chloroaniline geometric isomers was rapidly achieved.

The mobility of several monovalent substituted phenols is predicted by Smith and Khaledi [50] modelling the electrophoretic mobility μ_{ep} as a function of the pH of the buffer and the acid dissociation constant K_a :

$$\mu_{\text{ep}} = \mu_{\text{A}^-} \cdot \frac{K_a / [\text{H}^+]}{1 + K_a / [\text{H}^+]} \quad (10)$$

where μ_{A^-} is the electrophoretic mobility of the anionic form of the acid. The parameters μ_{A^-} and K_a can be determined by fitting Eq. 10 to the measured μ_{ep} as a function of pH.

Although this approach is analogous to that of Friedl and Kenndler [47], there are also some important differences. The $\text{p}K_a$ values obtained by fitting Eq. 10 to the experimental data are apparent dissociation constants depending on the actual CE conditions, and they are not necessarily close to literature data. (Titration data illustrate that for amino acids and small peptides apparent dissociation constants may differ significantly [51], illustrating the effect of the surfactant on the dissociation behaviour of these solutes.) As few as four measurements may be sufficient to obtain a reliable fit. Here, the choice of the pH range to be scanned is important and is more easy when physicochemical data of the solutes are available. Limitations on the actual prediction of migration times is discerned so that the migration order prediction for closely migrating peaks may fail, especially for solutes having almost identical $\text{p}K_a$ or mobility values.

The well-known observed linear relation between the capacity factor and the concentration of surfactant in MECC was used by Pyell and

Bütehörn [52] to increase resolution. Two experiments at different SDS concentrations enable the calculation of k' and thus migration times of all the solutes at different concentrations of SDS. This one-parameter optimisation procedure resulted in baseline separation of a mixture of seven methylnitroanilines. Furthermore, the optimisation of the concentration of modifiers like urea and glucose was performed in a similar way, using appropriate logarithmic relations between the migration and the concentration of the modifier.

The description of the behaviour of ionisable solutes in a micellar system is complicated due to the combination of the electrophoretic and chromatographic migration mechanisms. Khaledi and co-workers extended the procedure described earlier to the separation of both negatively [53–55] and positively [55,56] charged solutes in a micellar system. Here, the two important parameters are pH and the micellar concentration. Assuming that the net migration of an ionisable solute is the weighted average of the migration parameter of the solute in the associated (a) or non-associated (b) forms both in the aqueous and micellar phase, the net mobility of an ionisable solute can be expressed as:

$$\mu_{ep} = F_{aq,a} \cdot \mu_{aq,a} + F_{aq,b} \cdot \mu_{aq,b} + (F_{mc,a} + F_{mc,b}) \cdot \mu_{mc} \quad (11)$$

where μ_{aq} is the mobility of the solute in the aqueous phase in the associated and non-associated forms, respectively (subscripts a and b), μ_{mc} is the mobility of the micelle and the F -values are the mole fractions of the solute in the micellar and aqueous phase (subscripts mc and aq) in the associated and non-associated forms. Ion-pair formation between the charged solute and the oppositely charged surfactant constitutes an additional mechanism affecting migration, which is also considered. Note that this ion-pair complex and the uncharged solute molecules in the aqueous phase are assumed to migrate with the electroosmotic velocity and that μ_{eo} is not included in Eq. 11 since it is not important in the estimation of the electrophoretic mobility. Rewriting Eq. 11 results in a general expression which relates the mobility of a solute to all

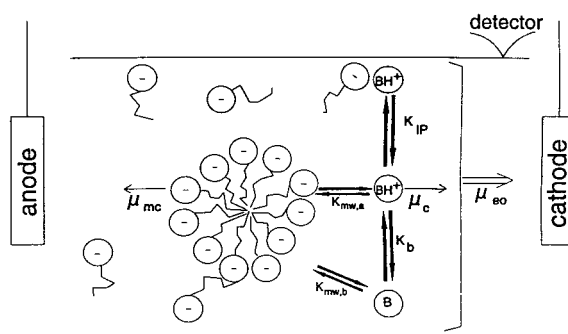


Fig. 3. Relevant equilibria of a cationic solute (BH^+ and B) in a micellar system containing negatively charged micelles. From Ref. [55].

possible equilibrium constants, acid–base dissociation constants, pH and mobilities of the micellar phase and the solute under investigation (equation not shown). Four situations can be distinguished: an acid or basic solute that migrates in a micellar system containing positively or negatively charged micelles. For each case, the general mobility expression is then rewritten and simplified, e.g. ion-pair formation is only considered for oppositely charged solute and surfactant molecules.

As an example, the relevant interactions between a weak base and a negatively charged surfactant are schematically illustrated in Fig. 3. Consequently, the relevant apparent parameters are estimated using five experiments at different pH and SDS concentration settings. Subsequently, the mobility of each solute can be predicted over the entire pH and SDS range. The equations were experimentally verified and the results are briefly summarised in Table 1. Note that fine-tuning of the separation of the aromatic amines was achieved by adding SDS and acetonitrile and this is done independent of the proposed optimisation strategy, and this means that insight in the separation mechanisms is required.

4. Conclusions

The use of a systematic optimisation strategy in the development of CE applications is highly recommended and should be preferred to trial and error. In this way satisfactory separation

Table 1

Predicting capabilities of migration times of charged solutes in MECC using the phenomenological approach developed by the group of Khaledi

Solute–buffer system	Predicting capabilities	Remark
Acidic solutes–anionic micelle	++	–
Basic solutes–anionic micelle	+	Ion-pair formation is assumed to be very important and free BH^+ is not present The separation is further improved increasing the SDS concentration (improved peak shape) and adding 10% acetonitrile (extends the migration window)

conditions are established in the shortest time and/or with only a few experiments. Furthermore, detailed information on the separation mechanisms may be obtained. This will be of great use in the development of different applications by the analyst and will facilitate the improvement of existing optimisation schemes and the introduction of new and better strategies in method development.

At present there is a wide choice of optimisation procedures. For some of these strategies only a minimal knowledge of separation principles is needed, while other approaches, based on the assumption of a particular separation mechanism, require more specific information about the solutes to separate. The choice of a particular strategy depends on the goal of the analyst and the feasibility of such an approach.

An important aspect of optimisation is the proper choice of the parameter(s) and the parameter space. In some cases the significance of this aspect seems to be underestimated, but, unfortunately, general rules do not exist. The choice of the type of parameter may seem obvious in most cases but the choice of the parameter space is more complicated, more difficult to justify and often influenced by the analyst's experience. It should be realised that badly chosen "start conditions" may drastically reduce the chances to find useful separation conditions. Due to the high complexity and the linking of the parameters, a multi-parameter approach in which several parameters are optimised simultaneously in combination with a peak identification procedure should be favoured.

More knowledge of CE separations makes predictions of the migration behaviour more accurate, but a good balance should be found between the required knowledge of the analytical system and the effort required to obtain it. In some cases this knowledge is already included in the optimisation approach by the designer, so it does not need to be provided by the analyst. However, the lack of physicochemical data often hampers such optimisation protocols.

None of the strategies discussed here can be used as a black-box or a stand-alone system. The analyst himself is an important factor, and by choosing the appropriate optimisation strategy he has a major influence on the outcome of the optimisation procedure. Adequate interpretation of the measurements can be of decisive importance. Therefore it remains crucial that the strategy or the algorithm as well as the separation technique is known in detail by the analyst.

References

- [1] P.D. Grossman, J.C. Colburn, H.H. Lauer, R.G. Nielsen, R.M. Riggin, G.S. Sittampalam and E.C. Rickard, *Anal. Chem.*, 61 (1989) 1186.
- [2] M.A. Stregé and A.L. Lagu, *Anal. Biochem.*, 210 (1993) 402.
- [3] M. Gilges, H. Husmann, M. Kleemiß, S.R. Motsch and G. Schomburg, *J. High Resolut. Chromatogr.*, 15 (1992) 452.
- [4] M.H.J.M. Langenhuizen and P.S.L. Janssen, *J. Chromatogr.*, 638 (1993) 311.
- [5] T. Yashima, A. Tsuchiya, O. Morita and S. Terabe, *Anal. Chem.*, 64 (1992) 2981.

- [6] K.A. Cobb and M.V. Novotny, *Anal. Chem.*, 64 (1992) 879.
- [7] V. Dolnik, J. Liu, J.F. Banks, Jr., M.V. Novotny and P. Boček, *J. Chromatogr.*, 480 (1989) 321.
- [8] A. Guttman and N. Cooke, *Anal. Chem.*, 63 (1991) 2038.
- [9] A. Weston, P.R. Brown, A.L. Heckenberg, P. Jandik and W.R. Jones, *J. Chromatogr.*, 602 (1992) 249.
- [10] T. Kaneta, S. Tanaka, M. Taga and H. Yoshida, *Anal. Chem.*, 64 (1992) 798.
- [11] C.P. Ong, C.L. Ng, N.C. Chong, H.K. Lee and S.F.Y. Li, *J. Chromatogr.*, 516 (1990) 263.
- [12] C.P. Ong, H.K. Lee and S.F.Y. Li, *J. Chromatogr.*, 542 (1991) 473.
- [13] D.S. Burgi and R.L. Chien, *Anal. Chem.*, 63 (1991) 2042.
- [14] J.L. Beckers and M.T. Ackermans, *J. Chromatogr.*, 629 (1993) 371.
- [15] X. Huang, M.J. Gordon and R.N. Zare, *Anal. Chem.*, 60 (1988) 375.
- [16] C.S. Effenhauser, *Anal. Methods Instrum.*, 1 (1993) 172.
- [17] D.F. Swaile and M.J. Sepaniak, *J. Microcol. Sep.*, 1 (1989) 155.
- [18] D.N. Heiger, P. Kaltenbach and H.-J.P. Sievert, *Electrophoresis*, 15 (1994) 1234.
- [19] S. Terabe, K. Otsuka, K. Ichikawa, A. Tsuchiya and T. Ando, *Anal. Chem.*, 56 (1984) 111.
- [20] C.W. Whang and E.S. Yeung, *Anal. Chem.*, 64 (1992) 502.
- [21] Y. Baba, M. Tshukako, T. Sawa and M. Akashi, *J. Chromatogr.*, 632 (1993) 137.
- [22] P.J. Schoenmakers, *Optimization of Chromatographic Selectivity*, Elsevier, Amsterdam, 1986.
- [23] Y. Hayashi, R. Matsuda and S. Terabe, *Chromatographia*, 37 (1993) 149.
- [24] N.A. Guzman, *Capillary Electrophoresis Technology*, Dekker, New York, 1993.
- [25] P. Camilleri, *Capillary Electrophoresis: Theory and Practice*, CRC Press, Boca Raton, FL, 1993.
- [26] H.J. Issaq, G.M. Janini, K.C. Chan and Z. El-Rassi, *Adv. Chromatogr.*, 35 (1995) 101.
- [27] J.K. Strasters, S. Kim and M.G. Khaledi, *J. Chromatogr.*, 586 (1991) 221.
- [28] D.L. Massart, B.G.M. Vandeginste, S.N. Deming, Y. Michotte and L. Kaufman, *Chemometrics: A Textbook*, Elsevier, Amsterdam, 1988.
- [29] M. Castagnola, D.V. Rossetti, L. Cassiano, R. Rabino, G. Nocca and B. Giardina, *J. Chromatogr.*, 638 (1993) 327.
- [30] C.L. Ng, H.K. Lee and S.F.Y. Li, *J. Chromatogr.*, 598 (1992) 133.
- [31] C.L. Ng, C.P. Ong, H.K. Lee and S.F.Y. Li, *J. Microcol. Sep.*, 5 (1993) 191.
- [32] C.L. Ng, C.P. Ong, H.K. Lee and S.F.Y. Li, *Chromatographia*, 34 (1992) 166.
- [33] Y.F. Yik and S.F.Y. Li, *Chromatographia*, 35 (1993) 560.
- [34] C.L. Ng, Y.L. Toh, S.F.Y. Li and H.K. Lee, *J. Liq. Chromatogr.*, 16 (1993) 3653.
- [35] Y.J. Yao, H.K. Lee and S.F.Y. Li, *J. Chromatogr.*, 637 (1993) 195.
- [36] J.L. Glajch, J.J. Kirkland, K.M. Squire and J.M. Minor, *J. Chromatogr.*, 199 (1980) 57.
- [37] J. Vindevogel and P. Sandra, *Anal. Chem.*, 63 (1991) 1530.
- [38] S. Terabe, K. Otsuka and T. Ando, *Anal. Chem.*, 57 (1985) 834.
- [39] A.T. Balchunas and M.J. Sepaniak, *Anal. Chem.*, 59 (1987) 1466.
- [40] K. Otsuka and S. Terabe, *J. Microcol. Sep.*, 1 (1989) 150.
- [41] E.S. Ahuja, E.L. Little, K.R. Nielsen and J.P. Foley, *Anal. Chem.*, 67 (1995) 26.
- [42] J.P. Foley, *Anal. Chem.*, 62 (1990) 1302.
- [43] K. Ghowsi, J.P. Foley and R.J. Gale, *Anal. Chem.*, 62 (1990) 2714.
- [44] S. Terabe, *J. Pharm. Biomed. Anal.*, 10 (1992) 705.
- [45] C.D. Bevan, I.M. Mutton and A.J. Pipe, *J. Chromatogr.*, 636 (1993) 113.
- [46] E. Kenndler and W. Friedl, *J. Chromatogr.*, 608 (1992) 161.
- [47] W. Friedl and E. Kenndler, *Anal. Chem.*, 65 (1993) 2003.
- [48] W. Friedl and E. Kenndler, *Fresenius J. Anal. Chem.*, 348 (1994) 576.
- [49] J.C. Jacquier, C. Rony and P.L. Desbene, *J. Chromatogr. A*, 652 (1993) 337.
- [50] S.C. Smith and M.G. Khaledi, *Anal. Chem.*, 65 (1993) 193.
- [51] M.G. Khaledi and A.H. Rodgers, *Anal. Chim. Acta*, 239 (1990) 121.
- [52] U. Pyell and U. Bütehörn, *Chromatographia*, 40 (1995) 175.
- [53] M.G. Khaledi, S.C. Smith and J.K. Strasters, *Anal. Chem.*, 63 (1991) 1820.
- [54] S.C. Smith and M.G. Khaledi, *J. Chromatogr.*, 632 (1993) 177.
- [55] C. Quang, J.K. Strasters and M.G. Khaledi, *Anal. Chem.*, 66 (1994) 1646.
- [56] J.K. Strasters and M.G. Khaledi, *Anal. Chem.*, 63 (1991) 2503.



ELSEVIER

Journal of Chromatography A, 715 (1995) 13–18

JOURNAL OF
CHROMATOGRAPHY A

Method of increasing the sensitivity of liquid chromatography–atmospheric pressure chemical ionization mass spectrometry using a semi-micro column

Takeshi Adachi^{a,*}, Masami Nemoto^a, Yuji Ito^b

^aPharmaceutics Laboratory, Pharmaceutical Research Laboratories, Taisho Pharmaceutical Co. Ltd., 1-403 Yoshinocho, Ohmiya, Saitama 330, Japan

^bAnalytical Laboratory, OTC Research Laboratories, Taisho Pharmaceutical Co. Ltd., 1-403 Yoshinocho, Ohmiya, Saitama 330, Japan

First received 29 November 1994; revised manuscript received 16 May 1995; accepted 17 May 1995

Abstract

A method for increasing the signal intensity of liquid chromatography–atmospheric chemical ionization mass spectrometry (LC–APCI–MS) using a semi-micro column was studied. Prostaglandin E₁ was used as a model compound. However, this method was not effective for detection with APCI–MS without an improved APCI interface, in which the diameter of the micro-pipe on the APCI interface was decreased from 0.1 to 0.05 mm. The signal intensity of APCI–MS detection using a semi-micro column with an improved APCI interface was five times that obtained with use of a conventional column.

1. Introduction

Liquid chromatographic techniques are in common use in analytical, biological and other types of studies, and LC–MS in particular is widely used as a powerful analytical tool. However, LC–MS suffers from certain problems, including the inability to use non-volatile buffer solutions as the mobile phase and low sensitivity compared with GC–MS. Non-volatile buffer solutions for use as mobile phases have been reported with column-switching techniques [1,2] or with the use of suppressor in ion chromatography [3]. Derivatization methods have been

reported for increasing the sensitivity of detection [4,5]. The use of a semi-micro or micro column technique for LC–MS to increase sensitivity has already been reported for fast atom bombardment ionization [6], electrospray ionization [7,8] and ionspray ionization [9] interfaces, but there has been no report of such use for an atmospheric pressure chemical ionization (APCI) interface. A semi-micro column leads to less band spreading of solutes and higher numbers of theoretical plates than does a conventional column, and therefore has been used to increase the signal intensity with ultraviolet, fluorescence and other types of detection for HPLC. In this study, we attempted to increase the signal intensity for prostaglandin E₁ as a

* Corresponding author.

model compound using a semi-micro column for LC-APCI-MS.

2. Experimental

2.1. Materials and reagents

Prostaglandin E₁ (PGE₁) was purchased from Funakoshi (Tokyo, Japan). A 100 μg/ml solution of PGE₁ was prepared in 10% (w/w) ethanol. The deionized water used in all experiments was obtained from a Milli-Q system (Waters, Milford, MA, USA). All other solvents and reagents were of analytical-reagent or HPLC grade.

2.2. LC-APCI-MS systems and conditions

A Model M-1000 LC-APCI-MS system connected with a Model L-6200 liquid chromatograph (Hitachi, Tokyo, Japan) was used. A 10-μl volume of sample solution was injected with a microsyringe through a Model 7125 loop injector with a 20-μl loop (Rheodyne, Cotati, CA, USA). Separation was performed on a Develosil ODS-5 column (particle size 5 μm; Nomura Chemical, Seto, Japan). The semi-micro column (150 × 2.0 mm I.D.) and the conventional column (150 × 4.6 mm I.D.) were stainless-steel tubes and the flow-rates were 0.2 and 1.0 ml/min, respectively. The tubes connected with the injector, the column and the mass spectrometer were polyether-ether-ketone (PEEK) tubes of 0.13 and 0.25 mm I.D. for the semi-micro column and the conventional column, respectively. The other operating conditions were as reported previously [10].

3. Results and discussion

In this study, PGE₁, the characteristics of which had already been studied with LC-APCI-MS using a conventional column [10], was used as a model compound, and had a base ion peak at m/z 337 ($[M + H - H_2O]^+$) in the APCI mass

spectrum. When a semi-micro column was used as the separation column, the PGE₁ peak was very broad on LC-APCI-MS, and the signal intensity was about twice that with a conventional column (Fig. 1). These findings suggested the presence of diffusion of PGE₁ in the APCI interface. A block diagram of the APCI interface is shown in Fig. 2. The flow route was closed between the injector and the micro-pipe of the APCI interface, but was open between the micro-pipe and the first aperture. Therefore, it was thought that diffusion of mobile phase occurred between the micro-pipe and the first aperture, and PGE₁ was assigned the broad peak on LC-APCI-MS. In fact, the PGE₁ peak was sharp and exhibited a high intensity with UV detection. The pressure in the micro-pipe fell to about 4–5 kg/cm² when the semi-micro column was used from 20–30 kg/cm² when the conventional column was used, because the flow-rate changed to 0.2 ml/min from 1 ml/min, respectively.

This low pressure was also thought to be responsible for the broad peak on LC/APCI-MS. For that reason, suppression of diffusion of mobile phase and solute and increase in the pressure in the micro-pipe are required to obtain a sharp PGE₁ peak.

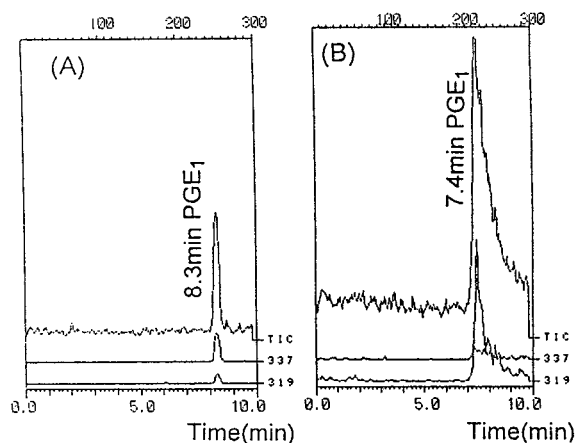


Fig. 1. Total ion current chromatograms ($m/z = 200-500$ with 2 s per scan) of 100 ng of PGE₁ on (A) conventional column and (B) semi-micro column.

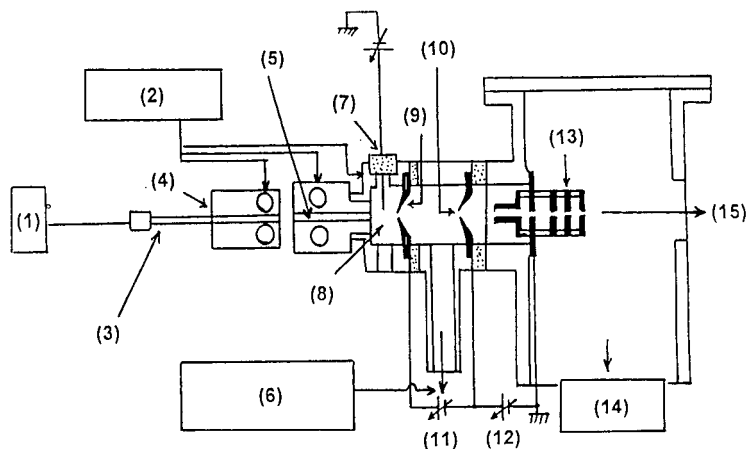


Fig. 2. Block diagram of the APCI interface: 1 = HPLC unit; 2 = electric source for heating; 3 = micro-pipe; 4 = vaporizer; 5 = desolvation; 6 = vacuum pump; 7 = needle electrode for corona discharge; 8 = APCI ion source housing; 9 = first aperture; 10 = second aperture; 11 = electric source for drift voltage; 12 = electric source for ion acceleration; 13 = quadruple lens; 14 = vacuum pump; 15 = mass MS spectrometer.

3.1. Adjustment of micro-pipe position

Initially, the micro-pipe position was adjusted to increase signal intensity and sharpen the PGE₁ peak. Normally, the micro-pipe was set on the vaporizer heating block in an appropriate position and the micro-pipe [Fig. 2 (3)] was moved toward the first aperture [Fig. 2 (9)], since it was thought that the PGE₁ peak shape was broad owing to the poor arrival of the mobile phase vapour and the solute at the needle electrode for corona discharge and the first aperture due to low pressure in the micro-pipe, but this method was not effective in increasing signal intensity or improving the peak shape even when the micro-pipe was moved 3 cm towards the first aperture. These findings suggested that increasing the pressure in the micro-pipe was necessary.

3.2. Postcolumn addition of solvent

Next, postcolumn addition of solvent was attempted. This method was aimed at increasing the pressure in the micro-pipe and suppressing diffusion of solutes in the column. The addition pump used was a Model 6010 (Hitachi), which

was connected to a T-connector at the post-column. With addition of 0.8 ml/min of mobile phase, the peak intensity and the PGE₁ peak shape were the same as those obtained using the conventional column. These findings indicated there was diffusion of the solute after column separation. In order to suppress diffusion, hexane, which is not miscible with water, was used as an additional solvent. This method increased the sensitivity of APCI-MS to about 2–3 times that of the conventional column, but the peak shape was not markedly improved.

3.3. Improvement of micro-pipe

The inside diameter of the micro-pipe is 0.1 mm, and this diameter is justified with use of a conventional column. When a semi-micro column is used, this diameter decreases the pressure in the micro-pipe, and the correct diameter for use is about 0.05 mm. Therefore, improvement of the micro-pipe by using a 0.05 mm I.D. was attempted. The micro-pipe consisted of a heating stem block and stainless-steel tube (1/16 in., 0.1 mm I.D.), and the stainless-steel tube was removed from the heating stem block of the micro-pipe. Next, a stainless-steel tube of 0.5 mm I.D.

was inserted into the heating stem block as a guide-pipe. In addition, a tube of 0.05 mm I.D. prepared from Polisil Tubing (GL Sciences, Tokyo, Japan), which features a polymer coated on fused-silica tubing was inserted into the guide-pipe, and was fixed with a union and connectors.

This improved micro-pipe was set on the vaporizer block and chromatographic analyses were performed. A fivefold increase in peak intensity compared with that with a conventional column was obtained, along with improvement of the peak shape compared with that with a 0.1 mm I.D. micro-pipe (see Fig. 4).

Certain factors were considered as reasons for these findings. One was proper suppression of band spreading of solutes on the column. The vaporization area of the mobile phase was also thought to be such a factor, but the vaporization areas on the conventional and semi-microcolumns did not differ greatly (1.7 and 1.3 cm², respectively). These areas were measured from areas of change in colour of thermal paper that had been positioned at the first aperture position. The state of the mist of the vapour was thought to be another such factor, since the states of nebulized mist from 0.1 to 0.05 mm I.D. micro-pipes differed appropriately, whereas mist particles from the 0.05 mm I.D. micro-pipe were smaller than those from the 0.1 mm I.D. micro-pipe. Vapour mist composed of smaller particles yields a good efficiency of vaporization and collisions with the solvent, which is ionized by a corona discharge, and solute are increased, yielding a high signal intensity. However, a fivefold increase in intensity was obtained with the semi-micro column and this increase corresponded to the decrease in column cross-sectional area. Therefore, the factor responsible for sensitivity was suppression of band spreading of solutes in the semi-micro column, and improvement of the micro-pipe with a small diameter resulted in optimum mobile phase vapour conditions for analysis using a semi-micro column.

3.4. Mass spectra of PGE₁

PGE₁ mass spectra measured under several sets of conditions are shown in Fig. 3. The mass

spectrum obtained using a conventional column had a base peak at m/z 337 $[(M + H - H_2O)^+]$, Fig. 3A), but that obtained using a semi-micro column and a 0.1 mm I.D. micro-pipe had a base peak at m/z 319 $[(M + H - 2H_2O)^+]$, Fig. 3B). A fragment ion peak at m/z 333 also appeared in the latter spectrum but not in the spectrum obtained using the conventional column. This peak at m/z 333 was thought to represent $(M + H - 3H_2O + MeOH)^+$. This difference in the mass spectra was due to the difference in the moving times of mobile phase in the vaporizer region; for the conventional and semi-micro columns with flow-rates of 1 and 0.2 ml/min, the moving times were about 20 and 100 ms, respectively. Thus, using the semi-micro column, PGE₁ was heated for a longer time than in the conventional column. When the micro-pipe position was slid 3 cm for the first aperture, the mass spectrum obtained was the same as that for the semi-micro column (Fig. 3C). When hexane was added to mobile phase postcolumn, the ratio of peaks with m/z 319 and 337 differed from that for the conventional column. The moving time of the mobile phase with the post-addition method was the same as that with the conventional column, but the heats of vaporization of the mobile phase and the mixture of mobile phase and hexane differed [11]. This difference in heats of vaporization influenced the mass spectra. When a micro-pipe of 0.05 mm I.D. was used and the flow-rate was set at 0.2 ml/min, the moving time in the vaporizer region was 25 ms, and this time and the heat of vaporization of mobile phase were the same as those for the conventional column. The mass spectrum obtained was the same as that for the conventional column (Fig. 3E). Thus, comparison of mass spectra indicated that the method using a micro-pipe of 0.05 mm I.D. was also effective.

3.5. Application

The semi-micro column method was used for the identification of a degradation product of PGE₁. The degraded sample used was a PGE₁ solution (100 μg/ml, pH 7.0 phosphate buffer) stored for 1 h at 60°C. The residual PGE₁ level in this sample was about 80% (peak area per-

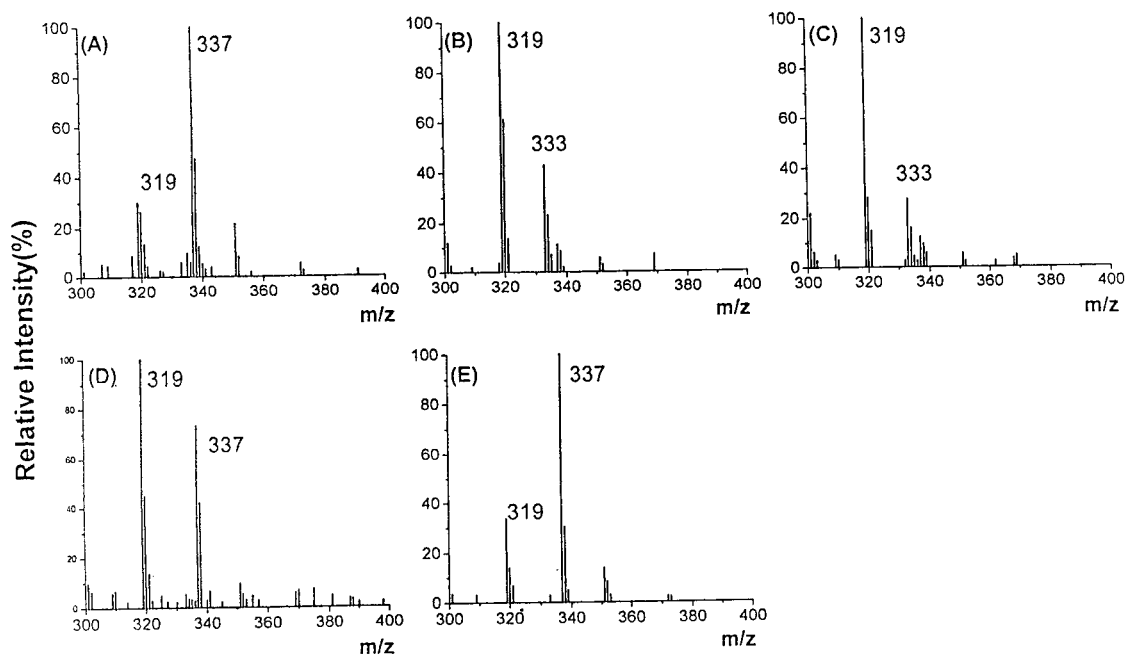


Fig. 3. PGE₁ mass spectra: (A) conventional column; (B) semi-micro column with normal micro-pipe; (C) semi-micro column with micro-pipe positioned forward (5 mm); (D) semi-micro column with postcolumn addition of hexane; (E) semi-micro column with improvement of micro-pipe.

centage with UV detection: 210 nm). Portions of 10 μ l of this solution were subjected to LC-APCI-MS using a conventional column and a semi-micro column, and the results are shown in Fig. 4. The PGE₁ peak appeared at a retention time of 6.8 min of on the conventional column

and at 7.5 min on the semi-micro column, although both columns had a linear flow-rate of 6 cm/min. This difference in retention time is thought to be due to differences in the conditions of column packing and the lot numbers of the packing materials.

With use of the semi-micro column a degradation product was detected behind the PGE₁ peak (retention time 12.0 min), but with use of the conventional column the degradation product was not clearly detected in the same intensity range. The spectrum of this peak was the same as that previously reported for PGA₁ [10], and this degradation peak was in fact identified as that of PGA₁. In addition, a very small unknown peak was present on the LC-APCI-MS trace just before the PGE₁ peak (retention time 6.4 min). This peak could not be identified, but its spectrum was the same as that of PGE₁; it may therefore have been the 8-epimer of PGE₁.

These findings indicated when a small amount of a compound is to be identified by LC-APCI-MS, the use of a semi-micro column as the analytical column is more advantageous than the use of a

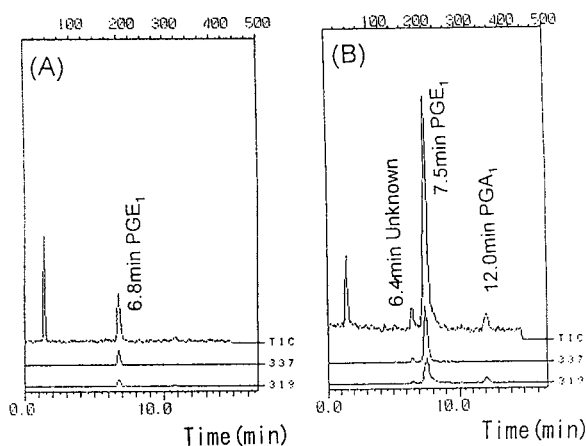


Fig. 4. Total ion current chromatograms ($m/z = 200-500$ with 2 s per scan) of 10 μ l of degraded PGE₁ sample on (A) conventional column and (B) semi-micro column.

conventional column if the same volume of sample for analysis is to be injected. We believe that our semi-micro column method will be effective for any analyte.

References

- [1] N. Asakawa, H. Ohe, M. Tsuno, Y. Nezu, Y. Yoshida and T. Sato, *J. Chromatogr.*, 541, (1991) 231.
- [2] P.S. Kokkonen, W.M.A. Niessen, U.R. Tjaden and J. van der Greef, *J. Chromatogr.*, 565, (1991) 265.
- [3] R.A.M. van der Hoeven, W.M.A. Niessen, H.A. Schols, C. Bruggink, A.G.J. Voragen and J. van der Greef, *J. Chromatogr.*, 627, (1992) 63.
- [4] J. Paulson and C. Lindberg, *J. Chromatogr.*, 554, (1991) 149.
- [5] R.J. Vreeken, M. Honing, B.L.M. van Baar, T.T. Ghijsen, G.J. de Jong and U.A.Th. Brinkman, *Biol. Mass Spectrom.*, 22 (1993) 621.
- [6] J.E. Evans, A. Ghosh, B.A. Evans and M.R. Natowicz, *Biol. Mass Spectrom.*, 22, (1993) 331.
- [7] R.A. Newman, A. Furntes, T.Y. Minor, K.T. McManus and D.A. Garteiz, *J. Liq. Chromatogr.*, 17, (1994) 403.
- [8] R.P. Schneider, J.F. Ericson, M.J. Lynch and H.G. Fouda, *Biol. Mass Spectrom.*, 22, (1993) 595.
- [9] T. Wachs, J.C. Conboy, F. Garcia and J.D. Henion, *J. Chromatogr. Sci.*, 29 (1991) 357.
- [10] T. Adachi, N. Yunoki, Y. Ito and H. Hayashi, *Bunseki Kagaku*, 43 (1994) 189.
- [11] T. Adachi, M. Nisio, N. Yunoki, Y. Ito and H. Hayashi, *Anal. Sci.*, 10 (1994) 457.



ELSEVIER

Journal of Chromatography A, 715 (1995) 19–29

JOURNAL OF
CHROMATOGRAPHY A

High-performance liquid chromatography of C₆₀, C₇₀, and higher fullerenes on tetraphenylporphyrin–silica stationary phases using strong mobile phase solvents

Jie Xiao, Mark E. Meyerhoff*

Department of Chemistry, The University of Michigan, Ann Arbor, MI 48109, USA

First received 27 February 1995; revised manuscript received 9 May 1995; accepted 11 May 1995

Abstract

The HPLC separation of C₆₀, C₇₀, and higher fullerenes on a tetraphenylporphyrin–silica stationary phase is investigated using pure carbon disulfide, chlorobenzene, *p*-xylene, and toluene as mobile phases. Selectivity factors (α) for C₇₀/C₆₀ separations using these solvents are determined to be 1.8, 3.2, 3.8, and 4.3, respectively. Thermodynamic studies reveal that an exothermic interaction takes place between the fullerene and porphyrin stationary phase in the presence of such solvents. Higher fullerenes (up to C₉₄) can be separated quickly at 90°C using CS₂–toluene (45:55, v/v) as the mobile phase. The high solubility of fullerenes in these solvents dramatically increases the overall potential with regard to preparative fullerene purification. The inability of an alternative protoporphyrin–silica phase to separate C₆₀/C₇₀ using the same mobile phases supports a retention mechanism based on simultaneous face-to-face and face-to-edge π – π interactions between the immobilized tetraphenylporphyrin and the fullerenes.

1. Introduction

The discovery of Buckminster fullerene [1], C₆₀, and related higher fullerene structures has evoked a flurry of research in the fields of chemistry, physics, and materials science [2]. This increase in research activities has necessitated the development of improved purification methods for this new class of molecules [3–5]. Currently, HPLC techniques play an integral role in the separation and purification of fullerenes and several stationary phases have been

developed specifically for fullerene (including higher fullerenes) separations [4,6–21].

The difficulty in chromatographic purification of fullerenes lies in their relative insolubility. As pointed out previously by Sun and co-workers [23] as well as Pirkle and Welch [24], this low solubility [22] in organic solvents commonly used as eluents (e.g., hexane, *n*-pentane, dichloromethane, and acetonitrile) makes preparative fullerene separations on conventional supports tedious. Only the use of strong solvents [i.e., toluene or carbon disulfide (CS₂)] as mobile phases would enable large-scale purification of the higher fullerenes [14,15,24–27]. Thus, a faster and more efficient chromatographic process, not curbed by solubility limitations, is urgently

* Corresponding author.

needed to increase the amount of isolated fullerenes obtained from a single crude soot extract.

Recently it has been reported [28,29] that stationary phases based upon tetraphenylporphyrin immobilized on silica gel supports can be useful in anion-exchange separations of aromatic carboxylates/sulfonates, and in reversed-phase separations of polycyclic aromatic hydrocarbons (PAHs) by HPLC. In addition, preliminary data demonstrated that the tetraphenylporphyrin–silica stationary phase can achieve the highest reported selectivity factor for the separation of C_{60}/C_{70} in 100% toluene [30]. Further, we have also shown that single-step HPLC separation of metallofullerenes (e.g., $La@C_{82}$ and $Y@C_{82}$) can be achieved using a 10-cm column packed with zinc(II) tetraphenylporphyrin–silica [31].

In continuing the investigation of this new stationary phase, we report herein: (i) the separation of C_{60} and C_{70} with four strong fullerene solvents, i.e., toluene, *p*-xylene, chlorobenzene, and carbon disulfide, as mobile phases; (ii) thermodynamic studies for these separations; and (iii) the separation of higher fullerenes (up to C_{94}) in a single injection of crude extract with a very strong mobile phase of CS_2 –toluene (45:55, v/v), within 8 min at 90°C. We further illustrate that the phenyl group of the immobilized porphyrin is critical for separation of fullerenes by reporting results for similar separations using a protoporphyrin–silica phase.

2. Experimental

2.1. Apparatus

The HPLC system consisted of a Spectra Physics (San Jose, CA, USA) SP 8700 solvent delivery system, a Spectra-Physics SP 4290 computing integrator, a Kratos (Ramsey, NJ, USA) Spectroflow 773 variable-wavelength UV–Vis detector, and a Rhyodyne (Cotati, CA, USA) Model 7010 sample valve. Columns were thermostated using a Fisher Scientific water jacket connected to a Fisher Scientific (Pittsburgh, PA,

USA) Model 80 Isotemp constant-temperature circulator. Dead volume of the column was determined by the injection of a CS_2 solution in toluene while using toluene as the mobile phase.

2.2. Chemicals

Fullerenes were produced via a d.c. carbon arc method similar to that described by Parker et al. [32]. The reactor featured water-cooled collection surfaces, variable arc gap, and forced helium flow across the gap to decrease slag formation. The fullerene-containing soot was Soxhlet extracted for 16 h with toluene, followed by a second extraction with pyridine. The resulting deep-red solutions were filtered through a 0.45- μ m cellulose nitrate filter (Millipore, Bedford, MA, USA) prior to drying at 130°C under vacuum. The total yield of crude fullerene extract was approximately 8.0 wt.%, with the pyridine extract containing a greater percentage of higher fullerenes. HPLC-grade toluene, *p*-xylene, and carbon disulfide as well as analytical-reagent grade chlorobenzene were obtained from Aldrich (Milwaukee, WI, USA).

2.3. Preparation of the stationary phase

The zinc(II) tetraphenylporphyrin–silica [$Zn(pCPTPP)$ –silica] stationary phase was prepared in a manner similar to that described elsewhere [28]. In brief, the unsymmetrical phenyl-substituted tetraphenylporphyrin, [5-(*p*-carboxyphenyl)-10,15,20-triphenyl]porphyrin [H_2 -($pCPTPP$)], was covalently attached to aminopropyl silica gel (10 μ m) via an amide bond. The residual amine sites on the stationary phase were acetylated by refluxing the support in acetic anhydride. Finally, to prepare the metallated support, 2 g of $H_2(pCPTPP)$ –silica was refluxed in 50 ml dimethylformamide containing 0.8 g $ZnCl_2$. Typical porphyrin surface coverages were in the range 0.2–0.4 μ mol/m², based on data from elemental analysis of the final stationary-phase material [28]. The porphyrin–silicas were packed into 250 × 4.6 mm I.D. stainless-steel

tubes by the downfall slurry method at a pressure of 41.4 MPa.

2.4. Matrix-assisted laser desorption time-of-flight mass spectrometry (MALDI-TOF-MS)

MALDI-TOF-MS was performed on a VESTEC-2000 instrument (Houston, TX, USA). The wavelength of the laser was 337 nm. A saturated 2,5-dihydrobenzoic acid solution (about 50 mM) with 50% aqueous acetonitrile containing 0.1% TFA was used as the matrix. An amount of 1 μ l of fullerene solution in carbon disulfide was analyzed on the flat surface of the probe tip (2 mm diameter) with the matrix. The insulin A chain (FW = 2531.6) was used as the internal standard to calibrate the m/z output of the system.

3. Results and discussion

In order to fully explore the versatility of columns packed with tetraphenylporphyrin–silica and to acquire more information regarding the nature of the interactions between the immobilized tetraphenylporphyrin and fullerenes, four different strong solvents, i.e. toluene, *p*-xylene, chlorobenzene, and carbon disulfide, were examined as mobile phases to separate C_{60} and C_{70} . Typical chromatograms for C_{60} and C_{70} separations using these solvents are shown in Fig. 1. Table 1 summarizes the solubility of C_{60} , capacity factors (k'), and selectivity factors ($\alpha_{C_{70}/C_{60}}$) in these solvents. To keep the chromatographic conditions consistent, a detector wavelength of 430 nm was selected, which is above the UV cutoff of carbon disulfide (390 nm), although fullerenes do not absorb strongly in this region. To perform the separation, a 20- μ l solution of C_{60} and C_{70} in toluene (1 mg/ml each) was injected into a 250 \times 4.6 mm I.D. column packed with zinc(II) tetraphenylporphyrin–silica (10 μ m). As shown in Table 1, retention times of C_{60} and C_{70} follow a trend that correlates with the inverse of their solubilities in the given mobile-phase solvent; that is, fullerene retention time in CS_2 < in

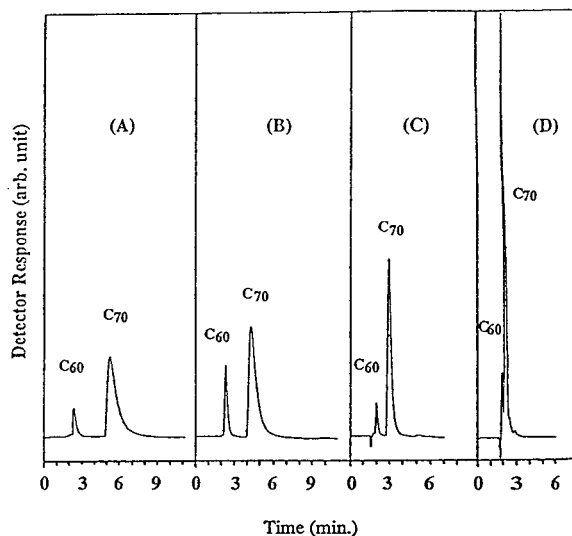


Fig. 1. Separation of C_{60} and C_{70} on the Zn(pCPTPP)–silica stationary phase. Column: 250 \times 4.6 mm I.D. stainless-steel column. Flow-rate: 2 ml/min. Detection: UV, 430 nm (0.100 AUFS). Injection: 20 μ l of fullerene solution in toluene. Temperature: 30°C. Mobile phase: (A) toluene, (B) *p*-xylene, (C) chlorobenzene, and (D) carbon disulfide.

chlorobenzene < in *p*-xylene < in toluene. These results are consistent with other reports on less selective columns [14,26], where increasing the percentage of a stronger fullerene solvent, usually toluene, in the mobile phase decreases the retention of the fullerenes. Interestingly, it has been reported that the separation on poly(styrene-divinylbenzene) gel switches from an adsorption (i.e., C_{70} elutes after C_{60}) to a size-exclusion (i.e., C_{70} elutes before C_{60}) type of mechanism when the carbon disulfide content in a CS_2 – CH_2Cl_2 mobile phase is increased beyond 60% [27]. The porphyrin-based stationary phase, however, still behaves as a normal adsorption-type column, even when using 100% CS_2 as the mobile phase, suggesting that the fullerene interaction with the immobilized porphyrin is quite strong. Although only complete solubility data for C_{60} has appeared in the literature, retention of C_{70} on the porphyrin-based column indicates that its solubility follows the same pattern as that of C_{60} . In comparing the selectivity achieved for C_{70} and C_{60} separation on the tetraphenylporphyrin–silica stationary phase to that obtained

Table 1

Solubility of C_{60} , capacity factors (k') of C_{60} and C_{70} , and selectivity factors (α) for C_{70} and C_{60} using different mobile-phase solvents^a

Mobile phase	Solubility of C_{60} (mg/ml) ^b	Capacity factor of C_{60}	Capacity factor of C_{70}	Selectivity factor for C_{70}/C_{60}
Toluene	2.8	0.56	2.43	4.3
<i>p</i> -Xylene	5.2	0.51	1.92	3.8
Chlorobenzene	7.0	0.27	0.87	3.2
Carbon disulfide	7.9	0.17	0.31	1.8

^a HPLC conditions as in Fig. 1.

^b From Ref. [22].

on two commercial columns (“Buckyprep” and “Buckyclutcher”), which have been touted as the best for fullerene separations, the tetraphenylporphyrin column has an $\alpha_{C_{70}/C_{60}}$ of 4.3 using 100% toluene, compared to $\alpha_{C_{70}/C_{60}} = 1.8$ for the “Buckyprep” column [15] (packed with 2-pyrenal-1-ethyl-silica) and $\alpha_{C_{70}/C_{60}} = 1.45$ for the “Buckyclutcher” column [33] (packed with 3,3,3-tri-dinitrobenzoxyl-propyl-silica) under the same conditions. Therefore, the tetraphenylporphyrin stationary phase is capable of operating with fullerene solvents even stronger than toluene as the mobile phase while still yielding excellent separation of C_{70} and C_{60} .

Some peak asymmetry (tailing) is observed for the C_{60} and C_{70} bands in the chromatograms shown in Fig. 1. This was typical for all columns studied. Peak tailing decreased as the solvent strength of the mobile phase increased, i.e., tailing in $CS_2 <$ in chlorobenzene $<$ in *p*-xylene $<$ in toluene (see Fig. 1). Injection of mixtures made from pure C_{60} and C_{70} eliminated the possibility that the presence of higher fullerenes, which elute after C_{70} , contributed to C_{70} tailing. One possible factor that can influence peak profiles is the kinetics of fullerene interaction with the immobilized porphyrin on the silica support. Indeed, slow “off” and/or “on” adsorption rate constants may contribute to the asymmetric peak profiles observed. In this situation, a stronger solvent used as the mobile phase can increase the rate of a slow kinetic step, and thereby improve the symmetry of peak profiles. In addition, since kinetics are temperature dependent, increasing the column temperature is

an effective means of improving peak symmetry (see below). Another possible explanation for the tailing observed is the self-complexing of fullerenes in solution, which has been recently reported by researchers [34]. A small amount of this complex may be retained longer on porphyrin column, resulting in a tailing after the “parent” peak. Higher solubility and an increase in operating temperature are also unfavorable for the formation of such self-complexes [34].

Although carbon disulfide is a very strong solvent for fullerenes, the Zn(pCPTPP)-silica column exhibits an $\alpha_{C_{70}/C_{60}} = 1.8$ using this solvent as a mobile phase (see Table 1). To our knowledge, no existing HPLC column is capable of separating C_{60} and C_{70} in 100% CS_2 . Unfortunately, due to the low efficiency of the porphyrin-silica column used here, C_{60} and C_{70} are not baseline resolved. However, it is likely that better resolution could be achieved with a more efficiently packed column (the current column typically has $N = 700$). It should also be noted that the capacity factors of C_{60} and C_{70} (0.16 and 0.31) in this separation are much lower than the optimum value (5–10). If the surface coverage (ϕ) of porphyrin stationary phase could be increased from the present $0.2 \mu\text{mol}/\text{m}^2$ to $2 \mu\text{mol}/\text{m}^2$ (e.g., increasing the ϕ value ten-fold) via an improved porphyrin immobilization method, the capacity factors ($k' = K \cdot \phi$) for C_{60} and C_{70} would be 1.6 and 3.1, respectively. This would improve the resolution (R_s) by a factor of three in accordance with the classical equation defining the resolution of solutes on chromatographic columns.

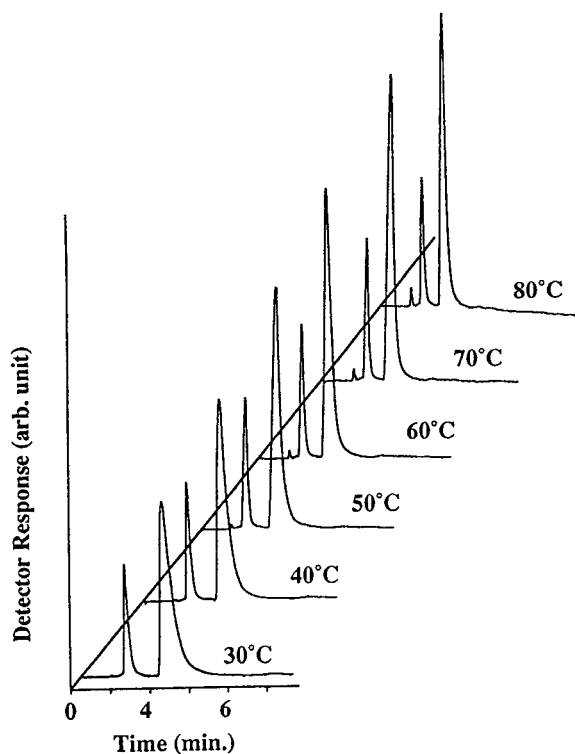


Fig. 2. Temperature effect on separation of C_{60} and C_{70} . Column: 250×4.6 mm I.D. Zn(pCPTPP)-silica. Mobile phase: *p*-xylene. Flow-rate: 2 ml/min. Detection: UV-Vis, 430 nm (0.100 AUFS). Injection: $20 \mu\text{l}$ of fullerene solution in toluene. Temperatures: 30, 40, 50, 60, 70, and 80°C .

To evaluate the thermodynamic parameters governing fullerene adsorption onto the tetraphenylporphyrin stationary phase, chromatograms were obtained at various temperatures. Fig. 2 shows chromatograms of C_{60} and C_{70} with *p*-xylene as the mobile phase at different temperatures. The profile of the C_{70} peak improves as the temperature is elevated. This may be a further indication (see above) that the tailing of the C_{70} peak is due to slow kinetics for fullerene interaction with the immobilized porphyrin as well as self-complexation of fullerenes.

Fig. 2 clearly demonstrates that increasing the column temperature results in a decrease in retention and asymmetry of both the C_{60} and C_{70} peaks when employing *p*-xylene as the mobile phase. Moreover, the van 't Hoff plots of C_{60} and C_{70} , Figs. 3A and 3B, show the same trend for the other three solvents examined. Due to the low boiling point of CS_2 , it was studied only over the temperature range 30 – 70°C , while the range 30 – 80°C was examined for the other solvents. In the temperature range studied, the van 't Hoff plots are all quite linear. The enthalpies of transfer (see Table 2) are calculated from the slopes of the van 't Hoff plots according to the equation

$$\ln(k') = -\frac{\Delta G}{RT} + \ln \phi = -\frac{\Delta H}{RT} + \frac{\Delta S}{R} + \ln \phi \quad (1)$$

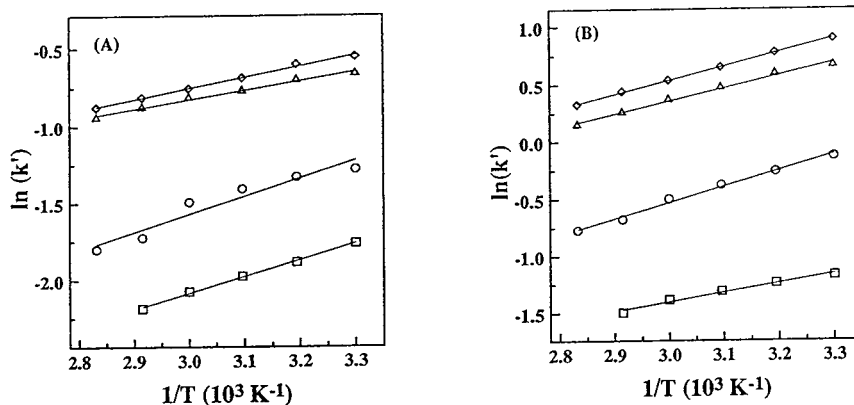


Fig. 3. Plot of $\ln(k')$ vs. $1/T$ for C_{60} (A) and C_{70} (B) on the Zn(pCPTPP)-silica stationary phase. Mobile phase: toluene (\diamond), *p*-xylene (\triangle), chlorobenzene (\circ), and carbon disulfide (\square). Flow-rate: 2 ml/min. Detection: UV-Vis, 430 nm (0.100 AUFS). Injection: $20 \mu\text{l}$ of fullerene solution in toluene.

Table 2

Enthalpy of transfer (ΔH) for the separation of fullerenes on tetraphenylporphyrin–silica stationary phase using different mobile-phase solvents (kJ/mol)

Enthalpy	Mobile phase			
	Carbon disulfide	Chlorobenzene	<i>p</i> -Xylene	Toluene
ΔH of C_{60}	-9.4	-10.1	-5.7	-6.1
ΔH of C_{70}	-7.2	-11.9	-9.8	-10.2

A similar normal temperature dependence of fullerene separation has been reported previously for a dimethoxyphenylpropyl-bonded silica phase [18]. However, an unusual temperature effect on the retention of C_{60} and C_{70} has been reported for a CSP 1 support [24], the “Buckyclutter 1” stationary phase [33], the dinitrobenzoylphenylglycine (DNBPG), as well as the (*R*)-(-)-2-(2,4,5,7-tetranitro-9-fluorenylideneaminoxy propionic acid (TAPA) stationary phase [14]. Retention times for C_{60} and C_{70} on these stationary phases increase, rather than decrease, as the column temperature is raised. The authors did not propose a clear explanation for this unusual behavior. From Table 2, the negative sign of the ΔH s means that the adsorption of C_{60} and C_{70} on the immobilized porphyrin column is exothermic. In addition, the separation of PAHs, the planar analogs of fullerenes, on the tetraphenylporphyrin–silica stationary phase [29] has the same temperature dependence as that of fullerenes. This consistency in the temperature dependence of fullerenes and PAHs supports a proposed π - π interaction retention mechanism (see below).

An unusual temperature effect with CS_2 is shown in Fig. 4, in which selectivity factors for C_{70}/C_{60} are plotted versus temperature. With toluene, *p*-xylene, or chlorobenzene as the mobile phase, elevating the temperature decreases the selectivity factor. However, the selectivity factor for C_{70} over C_{60} increases rather than decreases, as column temperature is raised when using CS_2 as the eluent. The relationship between the change in selectivity factor $\alpha_{i,j}$ ($=k'_i/k'_j$) and temperature can be expressed as

$$\frac{\alpha_{T_1}}{\alpha_{T_0}} = \exp \left[\frac{(T_1 - T_0) \Delta(\Delta H)}{T_1 T_0 R} \right] \quad (2)$$

where $\Delta(\Delta H)$ is $\Delta H_i - \Delta H_j$ (solute *i* is more retained than solute *j*). Usually in chromatography as observed with toluene, *p*-xylene, and chlorobenzene as mobile phases, the ΔH s for C_{60} (-6.1, -5.7, and -10.1 kJ/mol, respectively) are smaller than those of C_{70} (-10.2, -9.8, and -11.9 kJ/mol, respectively); thus, according to Eq. 2, the higher the column temperature, the smaller the α value. However, the ΔH of C_{60} in carbon disulfide (-9.4 kJ/mol) is larger than that of C_{70} (-7.2 kJ/mol), so that increasing the

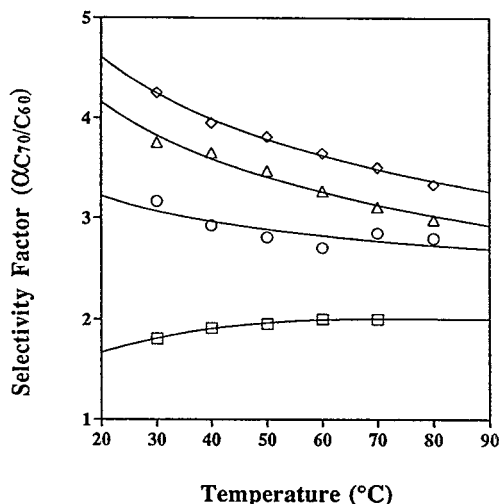


Fig. 4. Plot of $\alpha_{C_{70}/C_{60}}$ versus temperature on the Zn(pCPTPP)–silica stationary phase. Mobile phase: toluene (◇), *p*-xylene (△), chlorobenzene (○), and carbon disulfide (□). Flow-rate: 2 ml/min. Detection: UV-Vis, 430 nm (0.100 AUFS). Injection: 20 μ l of fullerene solution in toluene.

temperature results in an increase, rather than a decrease, in the selectivity factor (α). This unusual behavior reveals that the entropy effect predominates retention in carbon disulfide, whereas the enthalpy effect predominates retention in the other three solvents. It is speculated that the high electronic density of the π -orbitals of the sulfur atoms in carbon disulfide somehow interacts differently with the π -electrons of fullerenes when compared with π -electrons of toluene, xylene, and chlorobenzene. It is also possible, however, that CS_2 more effectively solvates the porphyrin stationary phase, and this may further contribute to the unusual temperature dependence observed. A clearer understanding of this abnormal behavior will require a more detailed investigation.

Using a stronger solvent as the mobile phase in fullerene separations on the porphyrin–silica columns dramatically increases the solubility of the higher fullerenes, enabling both the detection and purification of higher fullerenes to be achieved much more rapidly than with conventional columns. Fig. 5 shows a typical rapid separation obtained for a single injection of a pyridine extract of crude soot, which contains higher fullerenes. Matrix-assisted laser desorption time-of-flight mass spectra (MALDI-TOF-MS) of each of the six fractions collected are shown in Fig. 6. Due to the very low laser power used, fragmentation of fullerene ions is minimized. Thus, the bands in the chromatogram shown in Fig. 5 can easily be assigned. In some spectra, a small portion of previous peak components are seen because of peak tailing. Further, due to the great similarity between higher fullerenes (i.e., only two carbon atoms difference (2.5%) between C_{76} and C_{78}), C_{76} and C_{78} are not baseline resolved and C_{82} and C_{84} co-elute. It should be noted, however, that a mixture of very strong fullerene solvents (45% CS_2 –55% toluene) was used as the mobile phase, and better resolution of these components is possible by using a weaker mobile phase (e.g., toluene or toluene–hexane).

In our previous work [29], the tetraphenylporphyrin-based stationary phase was demonstrated to have a shape (planar versus nonpla-

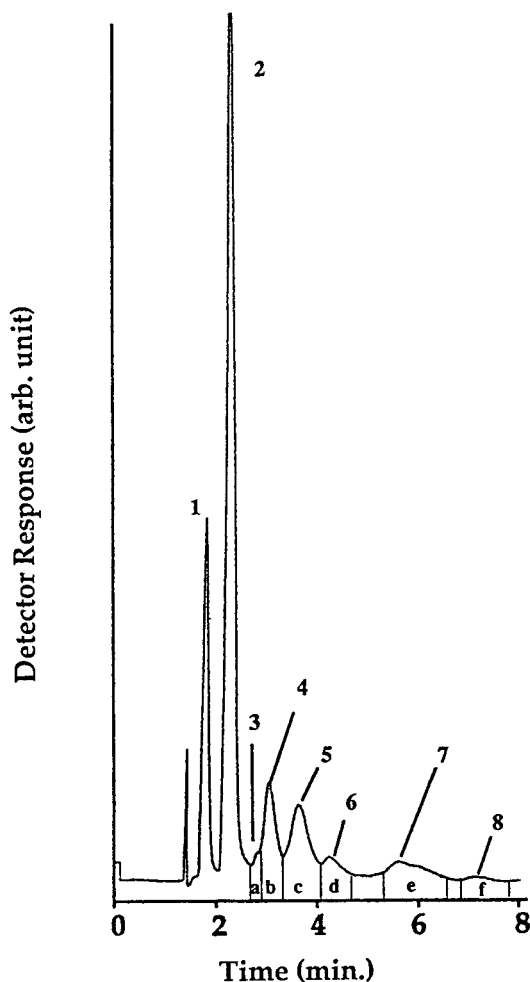


Fig. 5. HPLC chromatogram of higher fullerenes on the Zn(pCPTPP)–silica stationary phase. Mobile phase: carbon disulfide–toluene (45:55, v/v). Injection: 50 μl toluene solution of a pyridine extract of graphite soot. Flow-rate: 2 ml/min. Detection: UV, 430 nm (0.150 AUFS). Temperature: 90°C. Peak identity: (1) C_{60} , (2) C_{70} , (3) C_{76} , (4) C_{78} , (5) C_{82} , and C_{84} , (6) C_{86} , (7) C_{88} , C_{90} , and C_{92} , (8) C_{94} ; (a)–(f) are fractions for mass spectrometry in Fig. 6 (* indicates the major components).

nar) selectivity for PAHs, based on face-to-face π – π interactions between π -electron systems on the porphyrin ring and the PAH. It is thought that the *meso* phenyl groups do not play a significant role in PAH retention. However, the unique convex surface of fullerenes may render

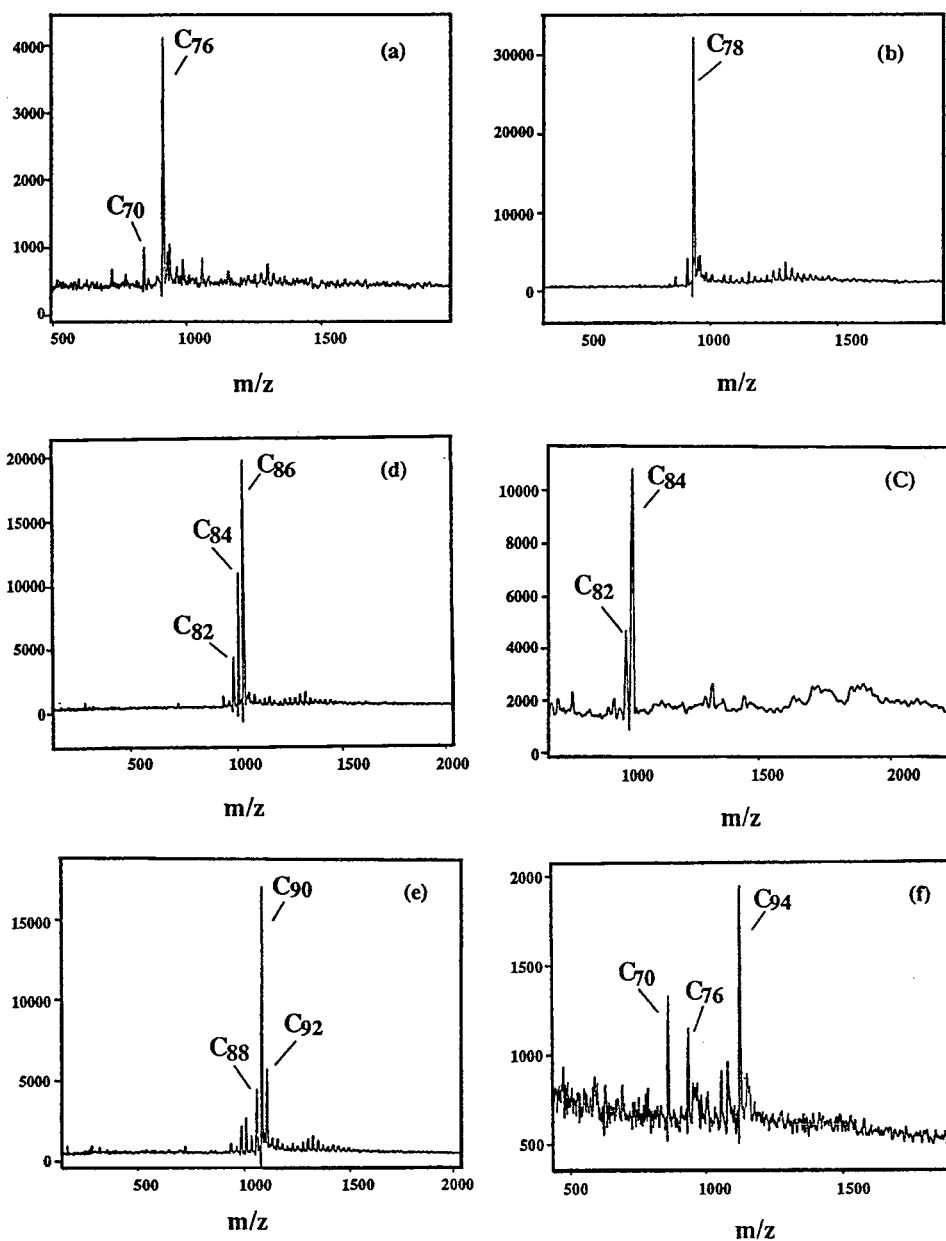


Fig. 6. MALDI-TOF-MS of six fractions (a)–(f) in Fig. 5. Mass spectrometry conditions are described in the Experimental section.

these analytes better able to undergo three-dimensional (3D) interaction with immobilized tetraphenylporphyrin stationary phase than planar PAH molecules. Single-crystal X-ray studies [35] reveal that the four *meso* phenyl rings in

tetraphenylporphyrin are perpendicular to the porphyrin ring, rather than co-planar. Therefore, another interaction is possible, between the fullerene “face” and the “edge” of the *meso* phenyl groups. This type of face-to-edge π - π

interaction in chromatographic recognition has been reported previously by Pirkle et al. [36], and such arrangements are found in the crystal structures of proteins [37], peptides [38], and small molecules [39], and also have been the subject of theoretical calculations [40]. Since tetraphenylporphyrin may be capable of simultaneous face-to-face and face-to-edge π - π interactions with the fullerenes, this extra dimension with respect to the interaction between the immobilized tetraphenylporphyrin and fullerene may account for the very high selectivity achieved. In Fig. 7, the 3D structures of C_{60} and zinc(II) tetraphenylporphyrin (ZnTPP) are shown at the same scale to reveal their relative sizes. Buckminsterfullerene (C_{60}) with a diameter of 7.1 Å looks like a soccer ball [41], while C_{70} with a central diameter of 6.9 Å and a longitudinal axis of 7.8 Å looks like a football [42]. Theoretical simulations predict that even C_{100} has a longitudinal length of only 15 Å. ZnTPP with its 6.8×6.8 Å porphyrin ring and four *meso* phenyl groups, that are diagonally approximately 11 Å apart, appears to form a π -electron cavity and behaves as a half of "basket" to host fullerenes. As shown in Fig. 7a, the larger the fullerene cage (C_{70} versus C_{60}), the more contact area the solute has to interact with the ZnTPP cavity, resulting in a stronger π - π interaction and, therefore, a longer retention

time. Indeed, the molecular-shape selectivity observed on the tetraphenylporphyrin-silica phase is so sensitive that even the small difference in shape between C_{70} and C_{60} yields a very large difference in retention.

To further support this retention mechanism, we have prepared a protoporphyrin-silica stationary phase [43]. Compared with the tetraphenylporphyrin structure, protoporphyrin does not possess four phenyl rings at the *meso* positions. As shown in Fig. 8, under similar conditions, C_{60} and C_{70} can still be separated but with much poorer selectivity. Because the higher surface coverage of protoporphyrin [$2.8 \mu\text{mol}/\text{m}^2$ for Zn(pCPTPP)] rules out the possibility that these results are due to less coverage of stationary phase ($k' = K \cdot \phi$), the shorter retention time and poorer C_{70}/C_{60} selectivity appears due to a much smaller partition coefficient (K) for each solute. As illustrated in Fig. 7b, the absence of the π -electron cavity in the protoporphyrin stationary phase results in less π - π interaction sites, further suggesting the critical contribution of the *meso* phenyl groups (see Fig. 7a) to the fullerene separations on tetraphenylporphyrin-silica columns.

4. Conclusion

In summary, immobilized tetraphenylporphyrins offer unprecedented selectivity for the separation of fullerenes over previously reported columns. With this newly developed stationary phase, the strong fullerene solvents carbon disulfide, chlorobenzene, and *p*-xylene, in addition to toluene, can be used for the first time as mobile phases to efficiently separate C_{60} and C_{70} and higher fullerenes. Higher fullerenes (up to C_{94}) can be quickly separated within 8 min using a 45% CS_2 -55% toluene mixture as the mobile phase while operating the column at 90°C. This work demonstrates the great potential of tetraphenylporphyrin-silica stationary phase for the large-scale purification of higher fullerenes. In contrast to other fullerene selectors, the separation of fullerenes on tetraphenylporphyrin-silica behaves normally as the temperature in-

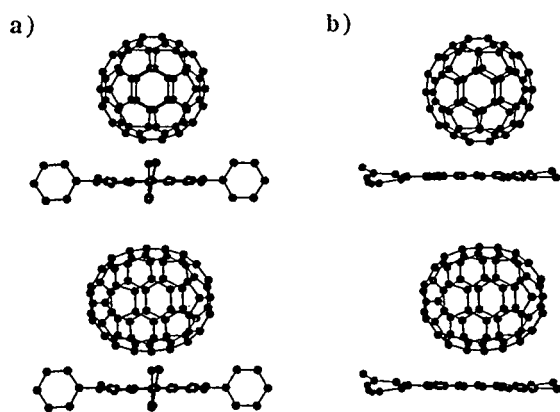


Fig. 7. Three-dimensional molecular modeling for the interaction of zinc tetraphenylporphyrin (ZnTPP) (a) and protoporphyrin IX (b) with Buckminsterfullerene (C_{60}) (top) and C_{70} (bottom).

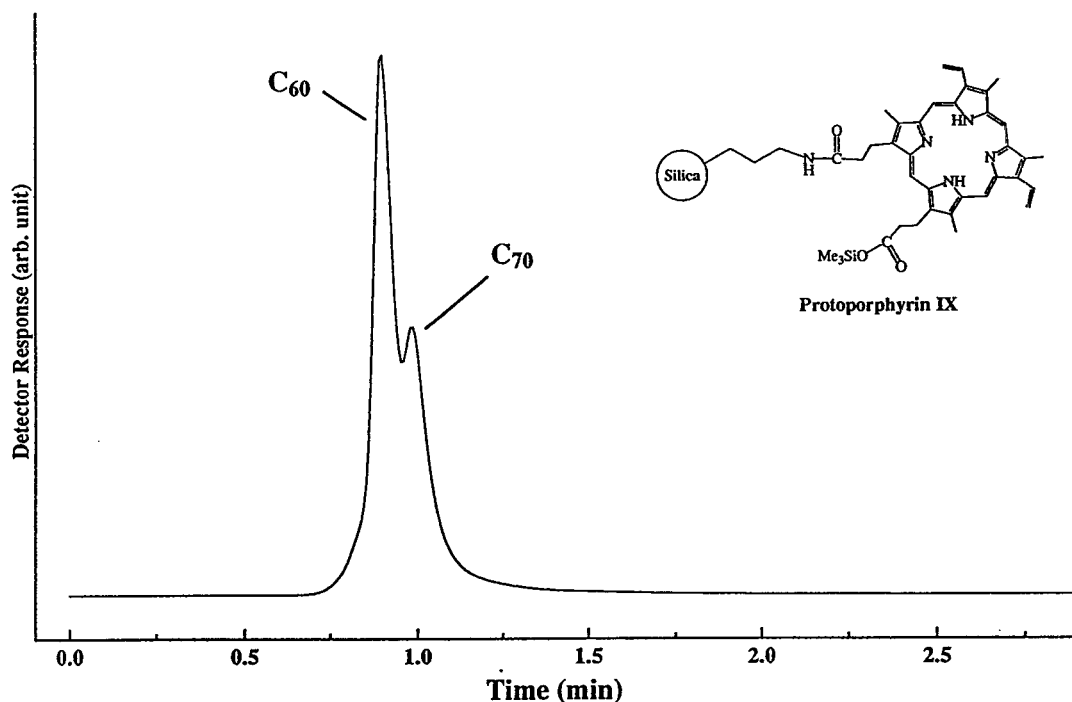


Fig. 8. Separation of C_{60} and C_{70} on the column packed with immobilized protoporphyrin-silica. Mobile phase: toluene. Flow-rate: 1 ml/min. Detection: UV-Vis, 430 nm (0.100 AUFS). Injection: 20 μ l of fullerene solution in toluene. Temperature: ambient.

creases, indicating that the adsorption interaction is exothermic. An unusual temperature effect on the selectivity factor of C_{60} and C_{70} in carbon disulfide is observed. At present, the reason for this atypical behavior is not clear. A possible retention mechanism that relies upon simultaneous face-to-face and face-to-edge π - π interactions between fullerenes and tetraphenylporphyrin is further supported by new results obtained with columns packed with a protoporphyrin-silica phase.

Acknowledgements

We gratefully acknowledge The Anspec Co. (Ann Arbor, MI, USA) for use of their column packing equipment and Prof. Francis and his group at The University of Michigan for providing the fullerenes. J.X. wishes to thank Dr. Chris Kibbey for his help and encouragement.

This work was supported by a grant from the National Science Foundation (CHE-9401376).

References

- [1] W.L.D. Lamb, K. Fostiropoulos and D.R. Huffman, *Nature*, 347 (1990) 354.
- [2] H.W. Kroto, A.W. Allaf and S.P. Balm, *Chem. Rev.*, 91 (1991) 1213.
- [3] D.M. Cox, S. Behal, M. Disko, S.M. Gorum, M. Greany, C.S. Hsu, E.B. Kollin, J. Millar, J. Ribbins, W. Robbins, R.D. Sherwood and P. Tindall, *J. Am. Chem. Soc.*, 113 (1991) 2940–2944.
- [4] F. Diederich, R.L. Whetten, C. Thilgen, R. Ettl, L. Chao and M.M. Alvarez, *Science*, 254 (1991) 1768–1770.
- [5] F. Diederich and R.L. Whetten, *Acc. Chem. Res.*, 25 (1992) 119–126.
- [6] J.M. Hawkins, T.A. Lewis, S.D. Loren, A. Meyer, J.R. Heath, Y. Shibato and R.J. Saykally, *J. Org. Chem.*, 55 (1990) 6250.
- [7] C.J. Welch and W.H. Pirkle, *J. Chromatogr.*, 609 (1990) 89.

- [8] H. Ajie, H.M. Alvarez, S.J. Anz, R.D. Beck, F. Diederich, K. Fostiropoulos, D.R. Huffman, W. Kratschner, Y. Rubin, K.E. Schriver, D. Sensharma and R.L. Whetten, *J. Phys. Chem.*, 94 (1990) 8630.
- [9] F. Diederich, R. Ettl, Y. Rubin, R.L. Whetten, R. Beck, M. Alvarez, S. Anz, D. Sensharma, F. Wudl, K.C. Khemani and A. Koch, *Science*, 252 (1991) 548.
- [10] M. Diack, R.L. Hettich, R.N. Compton and G. Guiochon, *Anal. Chem.*, 64 (1992) 2143.
- [11] Y. Cui, S.T. Lee, S.V. Olesik, W. Flory and M. Mearini, *J. Chromatogr.*, 625 (1992) 131.
- [12] K. Cabrera, G. Wieland and M. Schafer, *J. Chromatogr.*, 644 (1993) 396–399.
- [13] A. Gügel and K. Müllen, *J. Chromatogr.*, 628 (1993) 23–29.
- [14] M. Diack, R.N. Compton and G. Guiochon, *J. Chromatogr.*, 639 (1993) 129–140.
- [15] K. Kimata, K. Hosoya, T. Araki and N. Tanaka, *J. Org. Chem.*, 58 (1993) 282–283.
- [16] A.D. Darwish, H.W. Kroto, R. Taylor and D.R.M. Walton, *J. Chem. Soc. Chem. Commun.*, 115 (1994) 5–16.
- [17] M. Diack, R.I. Hettich, R.N. Compton and G. Guiochon, *Anal. Chem.*, 64 (1992) 2143–2148.
- [18] K. Jinno, H. Ohta, Y. Saito, T. Uemura, H. Nagashima, Y.L. Chen, G. Luehr, J. Archer, J.C. Fetzer and W.R. Biggs, *J. Chromatogr.*, 648 (1993) 71–77.
- [19] K. Jinno, T. Uemura, H. Olhta, H. Nagashima and K. Itoh, *Anal. Chem.*, 65 (1993) 2650–2654.
- [20] J. Anacleto and M. Quilliam, *Anal. Chem.*, 65 (1993) 2236–2242.
- [21] K. Kihuchi, N. Nakahara and T. Wakabayashi, *Chem. Phys. Lett.*, 188 (1992) 177–180.
- [22] R.S. Ruoff, D.S. Tse, R. Malhotra and D.C. Lorents, *J. Phys. Chem.*, 97 (1993) 3379.
- [23] Y. Wu, Y.Z. Sun Gu, Q. Wang, X. Zhou, Y. Xiong and Z. Jin, *J. Chromatogr.*, 648 (1993) 491–496.
- [24] W.H. Pirkle and C.J. Welch, *J. Org. Chem.*, 56 (1991) 6973.
- [25] A. Gügel, M. Becker, D. Hammel, L. Mindach, J. Räder, T. Simon, M. Wagner and K. Müller, *Angew. Chem. Int. Ed. Eng.*, 31 (1992) 644.
- [26] C.J. Welch, S.R. Perrin and W.H. Pirkle, PittCon '93, Atlanta, GA, USA, 1993, Abstract 212P.
- [27] D.L. Stalling, K.C. Kuo, C.Y. Guo and S. Saim, *J. Liq. Chromatogr.*, 16 (1993) 699–722.
- [28] C.E. Kibbey and M.E. Meyerhoff, *Anal. Chem.*, 65 (1993) 2189–2196.
- [29] C.E. Kibbey and M.E. Meyerhoff, *J. Chromatogr.*, 641 (1993) 49–55.
- [30] C.E. Kibbey, M.R. Savina, B. Parseghian, M.E. Meyerhoff and A.H. Francis, *Anal. Chem.*, 65 (1993) 3717–3719.
- [31] J. Xiao, M. Savina, G.B. Martin, A.H. Francis and M.E. Meyerhoff, *J. Am. Chem. Soc.*, 116 (1994) 9341–9242.
- [32] D.H. Parker, P. Wurtz, K. Chatterjee, K.R. Lykke, J.E. Hunt, M.J. Pellin, J.C. Hemminger, D.M. Gruen and L.M. Stock, *J. Am. Chem. Soc.*, 113 (1991) 7499–7503.
- [33] W.H. Pirkle and C.J. Welch, Materials Research Society Conference, 1993.
- [34] Y.-P. Sun and C.E. Bunker, *Nature (London)*, 365 (1993) 398.
- [35] D.M. Collins, W.R. Scheidt and J.L. Hoard, *J. Am. Chem. Soc.*, 94 (1972) 6689–6696.
- [36] W.H. Pirkle, C.J. Welch and M.H. Hyun, *J. Chromatogr.*, 607 (1992) 26–130.
- [37] S.K. Burley and G.A. Petsko, *Science*, 229 (1985) 23.
- [38] I.Z. Siemion, *Z. Naturforsch. Teil B*, 45 (1990) 1324.
- [39] A.V. Muechldorf, D. Van Engen, J.C. Warner and A.D. Hamilton, *J. Am. Chem. Soc.*, 110 (1988) 6561.
- [40] P. Linse, *J. Am. Chem. Soc.*, 114 (1992) 4367.
- [41] W.I.F. David, R.M. Ibberson, J.C. Matthewman, K. Prassides, T.J.S. Dennis, J.P. Hare, H.W. Kroto, R. Taylor and D.R.M. Walton, *Nature*, 353 (1991) 147–149.
- [42] D.R. McKenzie, C.A. Davis, D.J.H. Cockayne, D.A. Muller and A.M. Vassallo, *Nature*, 355 (1992) 622–624.
- [43] J. Xiao and M.E. Meyerhoff, in preparation.

Retention mechanisms of polycyclic aromatic nitrogen heterocyclics on bonded amino phases in normal-phase liquid chromatography

Håkan Carlsson, Conny Östman*

Division of Analytical Chemistry, National Institute of Occupational Health, S-171 84 Solna, Sweden

First received 22 August 1994; revised manuscript received 2 March 1995; accepted 5 April 1995

Abstract

Two aminoalkyl bonded phases, aminopropylsilica and dimethylaminopropylsilica, operated in the normal-phase mode were investigated regarding the retention mechanisms of polycyclic aromatic nitrogen heterocyclics (PANHs). By blocking active interaction sites with methyl substituents, the retention mechanisms could be ascertained. The bonded functional groups of the aminoalkyl stationary phases were found to be the primary adsorption sites. Hydrogen bonding was found to be the dominant retention mechanism for carbazole-type PANHs on both stationary phases and for acridine-type PANHs on the aminopropyl phase. For acridine-type PANHs on dimethylaminopropylsilica, retention was found to be mainly due to electron donor–acceptor interaction. Residual silanols on the stationary phase support material on these non-end-capped bonded phases were found to contribute only slightly to the retention of both acridine- and carbazole-type PANHs. A strong dependence of retention on steric hindrance of the *n*-electrons on the nitrogen of acridine-type solutes was shown. Further, the necessity to consider not only the polarity and solvent strength but also the selectivity of the mobile phase is demonstrated.

1. Introduction

Polycyclic aromatic nitrogen heterocyclics (PANHs) with a single endocyclic nitrogen heteroatom, can be divided into two classes: acridines, which contain a pyridine ring with a lone pair electrons on the nitrogen, and carbazoles, containing a pyrrole ring with a hydrogen bonded to the nitrogen atom. Acridine-type PANHs are slightly basic owing to the unshared electron pair of the nitrogen atom not participating in the aromatic delocalization. In carbazole-

type PANHs the unshared electron pair is incorporated into the aromatic π orbitals and the imino hydrogen of these compounds gives these PANHs weak acidic properties.

The Snyder–Scowinski adsorption–displacement model [1,2] has been successfully used in order to explain the retention of polar molecules, including PANHs, on the amino-propylsilica stationary phase [3–5]. In this model, the solute and solvent molecules are expected to compete for positions in a monomolecular layer formed on the surface of the adsorbent. Primarily a monolayer of the solvent is formed on the adsorbent surface. As the solute

* Corresponding author.

migrates through the column, it competes for the active adsorption sites and retention occurs via solvent displacement–solute adsorption.

However, the specific mechanism of interaction is not considered in the displacement model. Normal bonded phases based on silica are heterogenic materials that contain three forms of surface adsorption sites [6]. They are supposed to consist of the functional groups of the bonded phase, residual silica support silanols and mixed sites as a result of interaction between the functional groups and the residual silanols.

In the aminopropylsilica stationary phase, the adsorbent surface silanol groups are substituted with aminopropyl groups. The surface coverage is about $2 \mu\text{mol}/\text{m}^2$, compared with $8 \mu\text{mol}/\text{m}^2$ for the silanol groups of unmodified silica [3]. On the Nucleosil-NH₂ bonded stationary phase, the mean distance between the aminopropyl anchoring sites has been found to be 9.5 \AA [7]. The amino group is a strong Lewis base, i.e., an electron donor, and thus shows specific interactions with electron acceptor solutes.

The retention behaviour of PANHs in normal-phase HPLC using bonded stationary phases is dependent on a number of solute–stationary phase interactions. Possible mechanisms are interactions between the stationary phase and (1) the solute aromatic π -electron system [8,9], (2) the lone pair of electrons of the acridine nitrogen heteroatom [8] and (3) the hydrogen atom attached to the carbazole nitrogen heteroatom [10]. In normal-phase chromatography the acid–base properties of the PANHs [8] and steric effects, i.e., the accessibility of the nitrogen atom [8,11], have an impact on retention. Further, if the bonded phase is not end-capped, the unreacted acidic silanol groups on the silica support material may also play a part in the solute–stationary phase interaction [12].

Some different views have been put forward regarding the retention mechanism of PANHs on the aminopropylsilica phase. Some workers have stated that this phase behaves like a deactivated silica [4] and that the residual silanols are of major importance for the retention of PANH [7]. Others have proposed that the primary inter-

action site of the aminopropylsilica stationary phase is the amino group [3,13]. Solutes containing fused aromatic ring systems, such as polycyclic aromatic hydrocarbons (PAHs) and PANHs, are assumed to interact by a charge-transfer mechanism involving the lone pair of electrons of the aminopropylsilica and the π -electron cloud of the solutes [9]. This is an electron donor–acceptor (EDA) interaction where the amino group of the stationary phase acts as an electron donor and the fused aromatic ring system of the adsorbed solute acts as an electron acceptor [7]. The solute–stationary phase EDA interaction is assumed to be planar. This has been demonstrated by slightly twisted polyphenyls having a weaker retention than flat fused arenes [9].

Few descriptions of the dimethylaminopropylsilica stationary phase have been published. This phase can be regarded as a methyl-substituted aminopropylsilica where the two amino hydrogens of the bonded functional group have been replaced by methyl substituents. Owing to the free electron pair of the amino nitrogen, this stationary phase may also act like an electron donor. It can thus be assumed that the dimethylaminopropylsilica will interact with fused aromatic ring systems with an EDA mechanism similar to that of the aminopropylsilica phase. However, the replacement of the hydrogens of the amino group by methyl groups will exclude some of the possible mechanisms involved in the retention of PANH.

2. Experimental

2.1. Chemicals

Reference substances of acridine-type PANHs (Fig. 1) were purchased from Promochem (Wesel, Germany). The carbazole-type reference substances were kindly provided by Professor M. Zander. Each component was dissolved in pentane–hexane (10:90) (Rathburn, Walkerburn, UK) at a concentration of approximately $10 \text{ ng}/\mu\text{l}$.

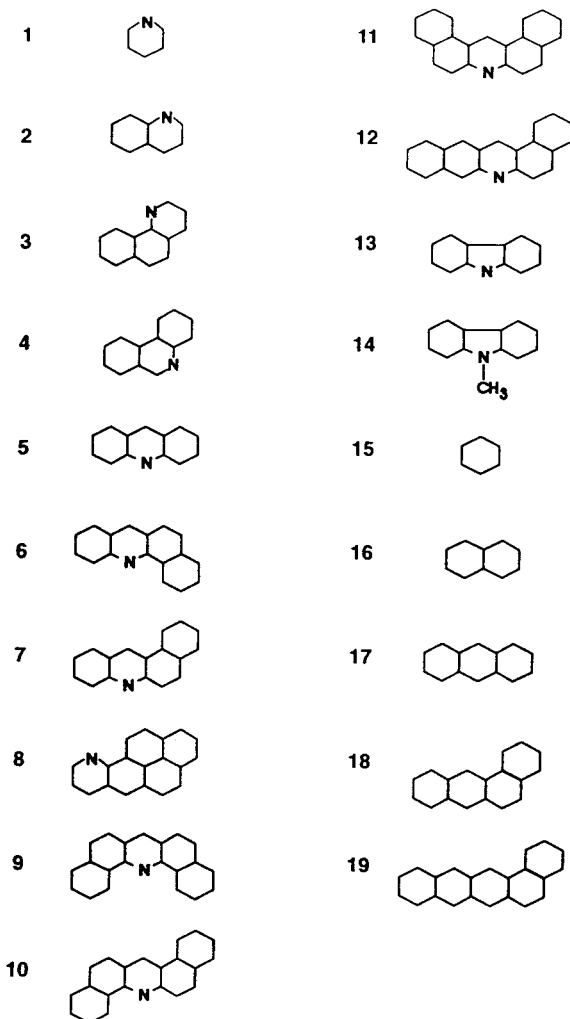


Fig. 1. Structures of the solutes: 1 = pyridine; 2 = quinoline; 3 = benzo[*h*]quinoline; 4 = phenanthridine; 5 = acridine; 6 = benz[*c*]acridine; 7 = benz[*a*]acridine; 8 = 10-azabenz[*a*]pyrene; 9 = dibenz[*c,h*]acridine; 10 = dibenz[*a,h*]acridine; 11 = dibenz[*a,j*]acridine; 12 = dibenz[*a,i*]acridine; 13 = carbazole; 14 = 9-methylcarbazole; 15 = benzene; 16 = naphthalene; 17 = anthracene; 18 = benz[*a*]anthracene; 19 = dibenz[*a,i*]anthracene.

2.2. HPLC columns

Two amino bonded phase columns from Macherey–Nagel (Düren, Germany) were used:

aminopropylsilica (Nucleosil-NH₂, 200 × 4 mm I.D.) and dimethylaminopropylsilica [Nucleosil-N(CH₃)₂, 200 × 4 mm I.D.]. Data on the surface coverage of these two phases were not supplied by the manufacturer. Berendsen et al. [14] calculated the surface coverage for synthesized amino and dimethylamino phases as 2.35 and 3.11 μmol/m², respectively. Both of the modified stationary phases were manufactured using Nucleosil 100-5 as the silica base material. This consists of spherical particles with a pore size of 100 Å and a diameter of 5 μm. The pore volume is 1.0 ml/g and the surface area 350 m²/g. A Nucleosil 100-5 column (200 × 4 mm I.D.) containing the silica base material was also used during the investigation.

2.3. Mobile phases

Hexane, methyl *tert*.-butyl ether (MTBE) and dichloromethane (DCM) were used as mobile phase components. All solvents were of HPLC grade (Rathburn) and were used as received. Regarding the aminopropylsilica and the dimethylaminopropylsilica stationary phases, hexane at a flow-rate of 2.0 ml/min was used during the retention measurements to investigate interaction mechanisms. The retention of carbazole and acridine on the unmodified Nucleosil silica base material was measured using a mobile phase composition of DCM–hexane (40:60). When investigating the influence of steric hindrance of adjacent benzene rings, a mobile phase consisting of MTBE–hexane (10:90) was used in order to obtain reasonable retention times for the unshielded acridine-type PANHs (*k'* > 100 when using pure hexane). When investigating solvent effects, mobile phase compositions consisting of 0, 10, 20, 33 and 50% of polar modifier, either MTBE or DCM, in hexane were used.

2.4. HPLC instrumentation

The HPLC system consisted of an injector (Model 7125; Rheodyne, Cotati, CA, USA)

equipped with a 20- μ l injection loop, an HPLC pump (Model 590 programmable solvent delivery module; Waters, Milford, MA, USA) and a UV detector (Model 655A; Hitachi, Tokyo, Japan) monitoring the effluent at 254 nm. Retention time measurements were performed at $20 \pm 2^\circ\text{C}$. A PC-based laboratory data system (ELDS Pro; Chromatography Data Systems, Svartsjö, Sweden) was used for registering, storing and processing the detector signals. Prior to investigation, each column was allowed to equilibrate overnight using a flow of 0.2 ml/min of the mobile phase. The system dead time (t_0) was determined as the first baseline disturbance due to the elution of pentane. Retention time (t_r) was measured as the peak maximum calculated by applying a polynomial function to the obtained data points collected at a sampling rate of 5 Hz. The reported capacity factors (k'), calculated as $k' = (t_r - t_0)/t_0$, where t_0 is the dead time, are the means of five replicate determinations. For all k' values the relative standard deviation was $<4\%$ and mostly $<3\%$, except for acridine on the aminopropylsilica using hexane as mobile phase.

3. Results and discussion

The two aminoalkyl stationary phases were manufactured using the same silica base material and had similar surface coverages of the bonded phase. By studying the retention properties on these two related phases it was possible to determine some of the retention mechanisms of PANHs in more detail. It should be noted that the investigation was made using Nucleosil silica-based packings and the results may differ when using other packings based on other silicas.

3.1. Interaction mechanisms

PAHs are assumed to interact with the amino stationary phase by an EDA type of interaction mechanism [7]. Owing to the delocalized aromatic π -electrons, the PAH solute acts as an electron acceptor and the amino group as a strong n-electron donor [9]. When plotting $\log k'$ (Table 1) versus the number of π -electrons for the five PAHs on the amino and the dimethylamino columns, two straight ($r > 0.999$), parallel (slope 0.193 ± 0.005 and 0.204 ± 0.015 ,

Table 1

Capacity factors (k') and relative retentions versus anthracene (α) for some selected polycyclic aromatic hydrocarbons and polycyclic aromatic nitrogen heterocyclics on the aminopropylsilica and the dimethylaminopropylsilica stationary phases with hexane as mobile phase at a flow-rate of 2.0 ml/min

Compound	Stationary phase			
	Aminopropylsilica		Dimethylaminopropylsilica	
	k'	α	k'	α
Benzene	0.39	0.22	0.14	0.18
Naphthalene	0.83	0.46	0.35	0.44
Anthracene	1.80	1	0.80	1
Benz[<i>a</i>]anthracene	3.84	2.13	1.63	2.04
Dibenz[<i>a,i</i>]anthracene	8.69	4.83	3.82	4.77
Pyridine	58.6	32.5	6.20	7.75
Quinoline	77.5	43.1	6.96	8.70
Acridine	161	89.7	7.55	9.44
Benz[<i>a</i>]acridine	>200	>111	11.4	14.2
Dibenz[<i>a,i</i>]acridine	>200	>111	21.4	26.8
Carbazole	116	64.6	162	203
9-Methylcarbazole	5.63	3.13	1.97	2.46

respectively, at a confidence level of 95%) lines over a range of $\log k'$ of approximately 0.9 were obtained. Thus, both columns demonstrated similar selectivity towards PAHs, but the dimethylamino phase exhibited weaker retention. It is therefore plausible to assume that the same major retention mechanism, a charge-transfer interaction [7,9], is acting in both cases.

The introduction of the two methyl substituents on the amino group introduces two competing mechanisms, a steric and an inductive effect, that will change the retention when comparing the two stationary phases. Steric effects by the more bulky methyl groups yield a larger distance for the charge-transfer interaction and thus a decrease in retention. On the other hand, an increase in retention would be the result of the inductive effect on addition of methyl groups due to stronger electron donor properties of the nitrogen lone pair of electrons. The observed decrease in retention on the dimethylamino phase, a factor of ca. 2.5, demonstrate that the steric effect of the methyl groups is of greater importance than the increased electron density on the amino nitrogen for this EDA interaction.

Carbazole has three linear fused rings, two six-membered and one five-membered ring, and fourteen electrons participating in the electron delocalization, including the unshared electron pair of the nitrogen heterocyclic atom. The compound possess weak acidic properties due to the hydrogen atom on the pyrrolic ring. Thus, in the case of carbazole-type compounds, three retention mechanisms are possible: (1) charge-transfer interaction as described above; (2) hydrogen bonding interaction between the acidic imino hydrogen attached to the nitrogen heteroatom of the solute and the nitrogen lone pair of electrons of the stationary phase amino group [4]; and (3) hydrogen bonding between the solute imino hydrogen and residual silanols on the adsorbent surface. These interactions are possible on both the aminopropyl- and the dimethylaminopropylsilica stationary phases.

That hydrogen bonding is the major retention mechanism for carbazole-type compounds is obvious from the strong decrease in retention on

replacing the imino hydrogen of carbazole with a methyl group (9-methylcarbazole). No hydrogen bonding is then possible and the retention on the aminopropyl phase decreases from $k' = 116$ to 5.63, a factor of >20 (Table 1). A stronger effect was found for the dimethylaminopropylsilica phase, where this factor was >80 . That this is due to hydrogen bonding to the bonded amino group of the stationary phase and not residual silanols is obvious from the following: in the next paragraph it is clearly demonstrated that the basic solute acridine has only a minor interaction with the residual silanols of the acidic silica surface. The retention of carbazole on the unsubstituted silica base material using DCM–hexane (40:60) was found to be >100 times weaker than for acridine. It is therefore obvious that carbazole has to exhibit an even weaker interaction with residual silanols on these two bonded amino stationary phases. Further, the introduction of methyl substituents on the amino group of the stationary phase increased the retention of carbazole from $k' = 116$ to 162, a factor of 1.4. This is attributed to the inductive effect of the methyl groups on the stationary phase that increase the electron density of the amino nitrogen, resulting in a stronger hydrogen bonding interaction. 9-Methylcarbazole exhibits a stronger retention than anthracene (5.63 and 1.80, respectively) on the aminopropyl column. As the polar interaction site of carbazole is blocked by the methyl substituent, the increased retention is attributed to the inductive effect of the heterocyclic nitrogen of the solute increasing the electron acceptor ability of the π -electron system, thus yielding stronger EDA complex formation than for anthracene.

Acridine has a similar structure to anthracene. Both compounds consist of three linear fused-six membered rings, with fourteen π -electrons involved in the electron delocalization. On the aminopropylsilica the k' value for acridine was found to be 161 compared with 1.80 for anthracene (Table 1). This increased retention can be attributed to (1) an increased charge-transfer interaction with stronger EDA complex formation involving the delocalized π -electrons [7], (2)

a hydrogen bonding interaction between the weakly basic solute nitrogen lone pair of electrons and the amino hydrogens of the stationary phase [4] and/or (3) hydrogen bonding to residual silanols of the adsorbent surface. On the dimethylaminopropylsilica phase the possibility of hydrogen bonding with the amino group was eliminated by replacing the amino hydrogens with methyl groups. From the strong decrease in the retention of acridine, from $k' = 161$ to 7.55, it is clear that the major retention mechanism does not involve hydrogen bonding to the residual silanols as stated by Hammers et al. [7].

That the EDA interaction is a minor retention mechanism for PANHs is evident from the retentions of anthracene, carbazole and 9-methylcarbazole, $k' = 1.80$, 116 and 5.63, respectively, on the aminopropylsilica phase. In the last two compounds the n -electrons of the heterocyclic nitrogen participate in the electron delocalization. Further, the hydrogen bonding site, the carbazole imino hydrogen, is blocked by a methyl substituent in 9-methylcarbazole. No hydrogen bonding is therefore possible between the solute nitrogen lone pair of electrons and the amino hydrogens of the aminopropylsilica stationary phase. Hence, the only remaining retention mechanism is EDA complex formation. 9-Methylcarbazole has a retention approximately three times stronger than that of anthracene owing to the inductive effect of the nitrogen atom on the electron-accepting properties of the delocalized electrons. The retention of carbazole is, however, >20 times stronger than that of 9-methylcarbazole, clearly demonstrating a stronger interaction due to hydrogen bonding.

The steric effect on the retention of anthracene and 9-methylcarbazole by the methyl groups of the dimethylaminosilica is a decrease by a factor of about 2–3 while the decrease in the retention of acridine is a factor of about 21. The obvious reason for this 7–10 times stronger decrease is the blocking of the hydrogen bonding to the bonded functional amino group of the adsorbent. The stronger retention of acridine compared with anthracene on the dimethylaminopropylsilica is attributed, in analogy with 9-methylcarbazole, to increased EDA com-

plex formation due to the inductive effect of the heterocyclic nitrogen atom.

With an increasing number of aromatic rings attached to the pyridine or pyrrole rings, the relative contribution of hydrogen bonding will decrease. This is demonstrated in Fig. 2 by the non-linear plot of $\log k'$ obtained from the dimethylaminopropylsilica phase vs. number of π -electrons for five aromatic compounds with 1–5 aromatic rings containing one pyridine ring in the structure, i.e., pyridine, quinoline, acridine, benz[*a*]acridine and dibenz[*a,i*]acridine. The five corresponding unsubstituted PAHs demonstrate a linear dependence ($r > 0.999$) on the number of π -electrons. Regarding the pyridine-type compounds, the slope of the line approaches closer to the slope for the PAHs as the number of aromatic rings increases. This behaviour demonstrates that the retention mechanism of pyridine-type compounds consists of more than one interaction. One is the EDA complexation, which is a linear function of the number of aromatic rings, as for the PAHs, and another interaction has a decreasing influence on retention as the number of rings increases. The

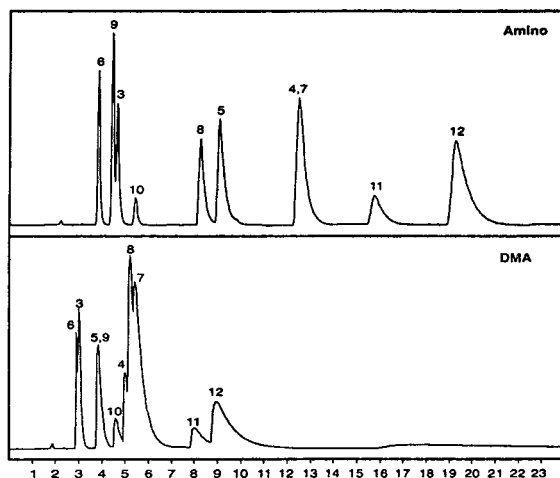


Fig. 2. Chromatograms of a mixture of the acridine-type PANHs listed in Table 2. The peak numbering correspond to the numbers in Fig. 1. Amino = aminopropylsilica stationary phase; DMA = dimethylaminopropylsilica stationary phase. Mobile phase: methyl *tert.*-butyl ether–hexane (10:90) at a flow-rate of 2.0 ml/min. UV detection at 254 nm.

remaining, possible interaction on this phase is hydrogen bonding to residual silanols of the adsorbent surface. It can therefore be concluded that this interaction gives a small contribution to the retention of acridine-type compounds on the dimethylaminopropylsilica and thus also on the aminopropylsilica phase. Hence the residual silanols on the stationary phase support material on these non-end-capped bonded phases can play only a minor role in the retention mechanism for both acridine- and carbazole-type compounds.

3.2. Steric hindrance

There is a shielding effect of the nitrogen atom lone pair of electrons by benzo and methyl groups adjacent to the nitrogen heteroatom of acridine-type PANHs that decreases the strength of the hydrogen bonding interaction with the stationary phase due to steric interaction [8]. This effect was investigated using a mobile phase composition of MTBE–hexane (10:90) in order to obtain reasonable retention times for unshielded acridine compounds with four and five aromatic rings (Table 2). Acridine had $k' = 6.0$ on the aminopropylsilica phase. For the un-

shielded five-ring compound dibenz[*a,i*]acridine, $k' = 13.7$. By shielding the nitrogen lone pair of electrons with one and two adjacent benzo substituents, as in dibenz[*a,h*]acridine and dibenz[*c,h*]acridine, k' was reduced to 3.2 and 2.4, respectively. For the aminopropylsilica phase, all five investigated PANHs with three to five aromatic rings (benzo[*h*]quinoline, benz[*c*]acridine, 10-azabenz[*a*]pyrene, dibenz[*a,h*]acridine and dibenz[*c,h*]acridine) having the nitrogen lone pair of electrons shielded by one or two adjacent benzo substituent groups eluted prior to acridine. Their relative retentions with respect to acridine were in the range 0.3–0.5. This effect is much more pronounced on the aminopropylsilica than the dimethylaminopropylsilica phase. The latter has a corresponding selectivity factor range of 0.7–1.6 for the shielded compounds. This is due to the strong contribution of hydrogen bonding to the retention of acridine type compounds on the former stationary phase. As a decrease in capacity factor due to shielding is observed also for the dimethylaminopropylsilica phase, this implies that the nitrogen lone pair of electrons contribute to the charge-transfer interaction with the stationary phase. Chromatograms obtained on the two stationary phases of a

Table 2

Capacity factors (k') and relative retentions versus acridine (α) for some selected acridine-type PANHs on aminopropylsilica and diamethylaminopropylsilica stationary phases

Compound	Stationary phase			
	Aminopropylsilica		Dimethylaminopropylsilica	
	k'	α	k'	α
Benz[<i>c</i>]acridine ^a	1.89	0.31	1.67	0.67
Dibenz[<i>c,h</i>]acridine ^b	2.37	0.39	2.51	1.00
Benzo[<i>h</i>]quinoline ^a	2.61	0.43	1.67	0.67
Dibenz[<i>a,h</i>]acridine ^a	3.19	0.53	3.30	1.31
10-Azabenz[<i>a</i>]pyrene ^a	5.45	0.53	4.03	1.61
Acridine	6.04	1	2.51	1
Benz[<i>a</i>]acridine	8.69	1.44	4.55	1.81
Phenanthridine	8.93	1.48	3.64	1.45
Dibenz[<i>a,j</i>]acridine	11.2	1.86	6.85	2.72
Dibenz[<i>a,i</i>]acridine	13.7	2.27	7.87	3.14

Mobile phase: methyl *tert.*-butyl ether–hexane (10:90) at a flow-rate of 2.0 ml/min.

^a Nitrogen atom shielded by one adjacent benzene ring.

^b Nitrogen atom shielded by two adjacent benzene rings.

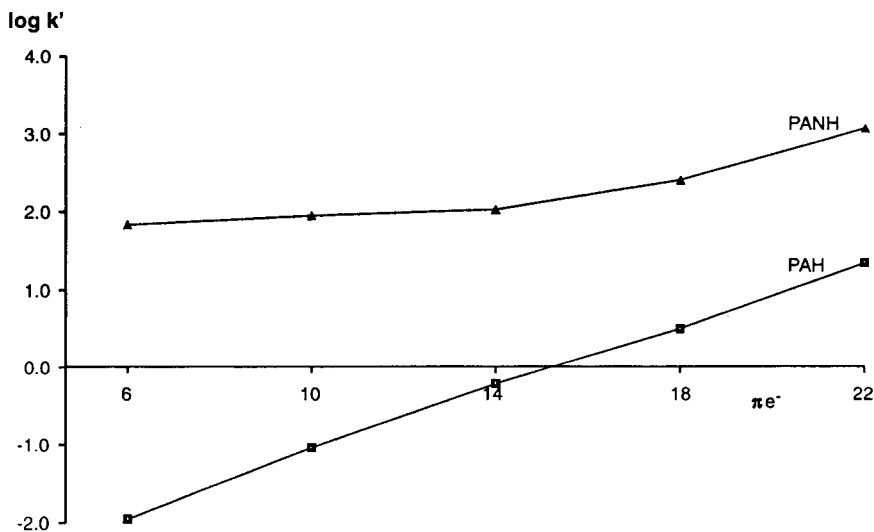


Fig. 3. $\log k'$ as a function of the number of π -electrons for PAHs and acridine-type PANHs with 1–5 aromatic rings. Dimethylaminopropylsilica stationary phase with hexane as mobile phase at a flow-rate of 2.0 ml/min. Mean of five replicate measurements.

mixture of the ten acridine-type PANHs listed in Table 2 are shown in Fig. 3.

3.3. Solvent effects

MTBE and DCM mixed with hexane were used as mobile phases. The concentrations of the polar modifiers in hexane were 0, 10, 20, 33 and 50%. In Fig. 4, $\log k'$ for acridine is plotted vs. mobile phase composition for the amino- and dimethylaminopropylsilica phases. On the amino phase the retention of acridine is stronger when using DCM as a polar modifier than when using MTBE, in spite of the higher solvent strength of DCM compared with MTBE, $\epsilon^0 = 0.42$ and 0.38, respectively. On the dimethylamino phase, on the other hand, the retention of acridine is stronger when using MTBE, which is in accordance with the solvent strength of these two polar modifiers. The addition of a polar mobile phase modifier will increase the solubility of acridine in the mobile phase. If this was the only mechanism, acridine would have a stronger retention on both stationary phases when using MTBE as modifier. However, MTBE is an aprotic, dipolar

solvent and a proton acceptor with a slightly basic character. Hydrogen bonding can therefore occur between the MTBE ether oxygen and the amino hydrogens of the aminopropylsilica phase. This is not possible on the dimethylaminopropylsilica phase owing to the methyl groups attached to the amino nitrogen. Hence there is a possibility of adsorption site competition with the solvent when using MTBE as mobile phase modifier on the aminopropylsilica [7]. The conclusion is that the hydrogen bonding interaction of acridine with the amino hydrogens of the aminopropylsilica phase is reduced in strength by adsorption site competition with MTBE. As DCM is unable to interact with the amino hydrogens by hydrogen bonding, retention is influenced only by an increased solubility of acridine in the mobile phase.

Regarding carbazole, the addition of a polar modifier decreases the retention on both columns, which is in accordance to the solvent strength of the two polar solvents, i.e., the addition of DCM gives the shortest retention. As carbazole interacts by hydrogen bonding to the lone pair of electrons on the amino nitrogen, no

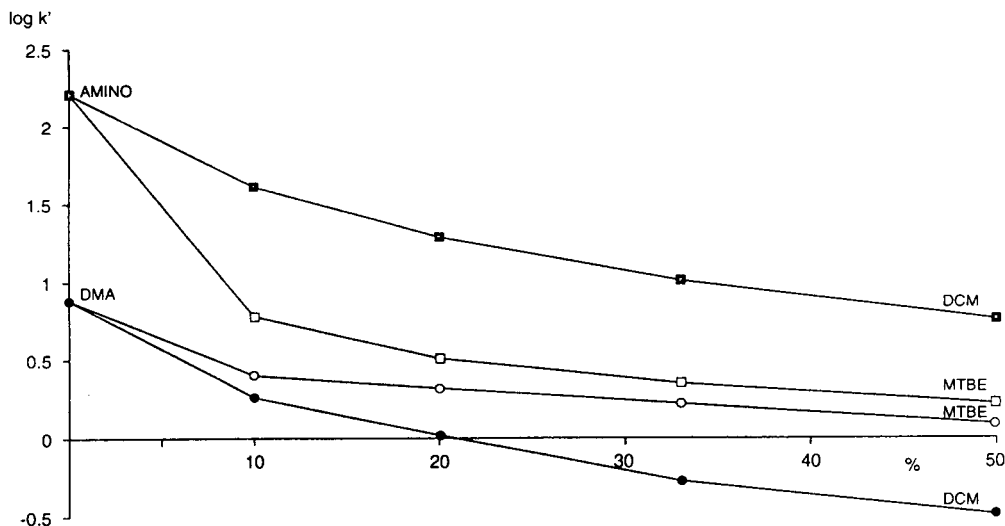


Fig. 4. Log k' for acridine as a function of the percentage of the polar modifiers dichloromethane (DCM) and methyl *tert.*-butyl ether (MTBE) in the hexane mobile phase. Squares = aminopropylsilica stationary phase; circles = dimethylaminopropylsilica stationary phase; closed symbols = DCM; open symbols = MTBE. Mean of five replicate measurements.

adsorption site competition involving the mobile phase can occur regarding the retention of carbazole on either of the two stationary phases.

These results emphasize the importance of hydrogen bonding of the mobile phase to the stationary phase as a contributor to the retention mechanism. It is therefore necessary to consider not only the polarity and solvent strength, but also the selectivity of the mobile phase.

References

- [1] L.R. Snyder, *Principles of Adsorption Chromatography*, Marcel Dekker, New York, 1968.
- [2] E. Soczewinski, *Anal. Chem.*, 41 (1969) 179–182.
- [3] L.R. Snyder and T.C. Schunk, *Anal. Chem.*, 54 (1982) 1764–1772.
- [4] P.L. Scolla and R.J. Hurtubise, *J. Chromatogr.*, 357 (1986) 127–138.
- [5] P.L. Smith and W.T. Cooper, *J. Chromatogr.*, 410 (1987) 249–265.
- [6] P.L. Smith and W.T. Cooper, *Chromatographia*, 25 (1988) 55–60.
- [7] W.E. Hammers, M.C. Spanjer and C.L. De Ligny, *J. Chromatogr.*, 174 (1979) 291–305.
- [8] H. Colin, J.-M. Schmitter, G. Guiochon, *Anal. Chem.*, 53 (1981) 625–631.
- [9] D. Karlesky, D.C. Shelly and I.M. Warner, *J. Liq. Chromatogr.*, 174 (1979) 291–305.
- [10] T. Nakazawa, M. Kuroki and Y. Tsunamhima, *J. Chromatogr.*, 211 (1981) 388–391.
- [11] K. Kamata and N. Motohashi, *J. Chromatogr.*, 319 (1985) 331–340.
- [12] Y. Tang, Dissertation, City University of New York, New York, 1989.
- [13] M.C. Hennion, C. Picard, C. Combellas, M. Caudet and R. Rosset, *J. Chromatogr.*, 210 (1981) 211–228.
- [14] G.E. Berendsen, K.A. Pikaart, L. de Galan and C. Olieman, *Anal. Chem.*, 52 (1980) 199.



ELSEVIER

Journal of Chromatography A, 715 (1995) 41–48

JOURNAL OF
CHROMATOGRAPHY A

Determination of hydroxy-substituted polycyclic aromatic hydrocarbons by high-performance liquid chromatography with electrochemical detection

M.T. Galceran*, E. Moyano

Departament de Química Analítica, Universitat de Barcelona, Diagonal 647, 08028 Barcelona, Spain

First received 28 November 1994; revised manuscript received 8 May 1995; accepted 16 May 1995

Abstract

Conditions were established for the determination of hydroxy-substituted polynuclear aromatic hydrocarbons (hydroxy-PAHs) using high-performance liquid chromatography with electrochemical detection. Reversed-phase chromatography with methanol–aqueous phosphate buffer (pH 3.0) (50:50) was adopted for the separation of the hydroxy-PAHs. The figures of merit were calculated; the detection limits (signal-to-noise ratio = 2:1) ranged from 20 to 200 pg. The method was applied to the determination of these compounds in an aerosol sample and 5-hydroxyindane, 2-hydroxy-9-fluorenone and 2-nitro-1-naphthol were tentatively identified at the pg/m³ level. The presence of 2-nitro-1-naphthol (0.2 ng/m³) was confirmed by gas chromatography–mass spectrometry.

1. Introduction

Polycyclic aromatic hydrocarbons (PAHs) constitute a class of organic compounds which are generated in a variety of combustion processes and released to atmosphere preferentially associated with submicron-size particles [1,2]. It has been known for more than three decades that organic extracts of the fine particulate organic matter (POM) collected in ambient urban air are carcinogenic [3,4].

When released into a polluted atmosphere, particle-adsorbed PAHs are exposed to a variety of gaseous co-pollutants. These include stable molecules and highly reactive intermediates, both free radicals and electronically excited molecular species resulting from absorption of

radiation. Polar functional groups are introduced by chemical reactions with these species, giving several PAH derivatives including compounds with hydroxy, ketone, quinone and nitro substituents on the parent PAH. The transformation reactions may show seasonal variations [5]; a major pathway for PAH degradation in winter is probably the reaction with nitrogen oxides and with the resulting acids. Photochemical reactions with oxygen and reactions with secondary air pollutants such as ozone, peroxyacetyl nitrate and hydroxyl and hydroperoxyl radicals are expected to be high in summer.

It has been shown by the Ames test that the moderately polar derivatives have significant mutagenicity compared with PAHs [6–8]. Nevertheless, the polar fractions of the aerosol extracts have been characterized to a limited extent. Moderately polar compounds such as nitro- and

* Corresponding author.

oxy-PAHs have been found in aerosol samples [9–12] and the mutagenicity of the extracts has been attributed to the presence of these compounds. In addition, compounds of higher polarity, such as hydroxy-PAHs [13], nitrated lactone derivatives [14] and aliphatic and aromatic carboxylic acids and their hydroxy derivatives [15,16], have also been identified.

Although gas chromatography with selective detectors has been used in the determination of the hydroxy-PAHs [16], HPLC with electrochemical detection is an option to be considered for these relatively highly polar compounds, since high selectivity and sensitivity are achieved. To our knowledge, this technique has not been used for the determination of hydroxy-PAHs.

Electrochemical detection is only possible for compounds that have oxidizable or reducible functional groups within the potential window of the measuring electrode. For instance, reduction of oxy- and nitro-PAHs has been used for the determination of these compounds [9–12]. Furthermore, hydroxy-PAHs can be detected by oxidation with conventional solid electrodes at positive potentials. The reactions on the electrode surface (Fig. 1) are very similar to those of phenols [17].

This paper describes the application of HPLC with electrochemical detection (ED) for the determination of some hydroxy-PAHs in urban aerosols. The optimum separation conditions and working potential were established and the quality parameters were calculated. Atmospheric aerosol samples were analysed and some of the

hydroxy-PAH derivatives were found at pg/m^3 levels.

2. Experimental

2.1. Chemicals

Analytical-reagent grade dichloromethane (Panreac, Barcelona, Spain), acetone (Carlo Erba, Milan, Italy) and methanol (Merck, Darmstadt, Germany) were used for the extraction of organic compounds from atmospheric aerosols. For the mobile phase, HPLC-grade methanol (Merck) and water purified with a Culligan (Barcelona, Spain) system were used. The buffer solutions were prepared with analytical-reagent grade phosphoric acid (Merck) and potassium dihydrogenphosphate (Merck). The compounds listed in Table 1 were provided by Carlo Erba, EGA Chemie (Steinheim, Germany), Fluka (Buchs, Switzerland), Janssen-Chimica (Geel, Belgium) and Merck. Bond-Elut C_{18} (500 mg) cartridges and coupling pieces were obtained from Analytichem International (ICT, Basle, Switzerland).

A stock standard solution was prepared containing 0.2 mg/ml of each in methanol, and 2,4-dibromophenol from EGA Chemie (Steinheim, Germany) was used as an internal standard.

2.2. Chromatographic conditions

HPLC was carried out with a Knauer (Bad Homburg, Germany) Model 64 pump and an ESA (Bedford, MA, USA) Coulochem 5100A detector with a dual-electrode analytical cell (ESA Model 5011) equipped with two working electrodes, a large-surface-area coulometric electrode and a high-efficiency amperometric electrode, a counter electrode and a Pd reference electrode. A $0.2\text{-}\mu\text{m}$ ESA graphite filter was placed before the analytical cell. A Merck-Hitachi D-2500 Chromato-Integrator integrator (Merck), was used. The sample was introduced by a Rheodyne (Cotati, CA, USA) Model 7125 injector with a loop of $20\ \mu\text{l}$. An RP-Select-B

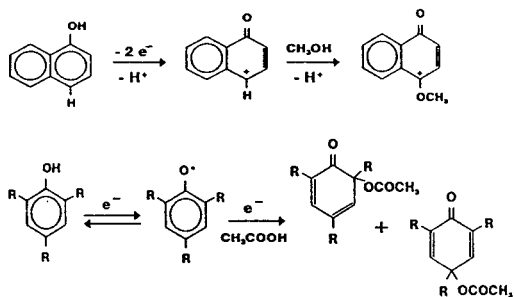
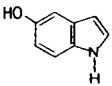
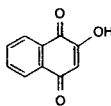
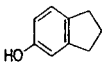
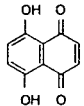
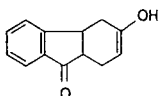
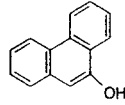
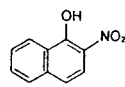


Fig. 1. Hydroxy-PAH electrochemical reactions.

Table 1
Hydroxy-PAHs studied

No.	Compound	Abbreviation	Structure
1	5-Hydroxyindole	5-HI	
2	2-Hydroxy-1,4-naphthoquinone	2-H-1,4-NQ	
3	5-Hydroxyindane	5-IOH	
4	5,8-Dihydroxy-1,4-naphthoquinone	5,8-DH-1,4-NQ	
5	2-Hydroxy-9-fluorenone	2-H-9-FLO	
6	9-Hydroxyphenanthrene	9-HF	
7	2-Nitro-1-naphthol	2-N-1-N	

(5 μm , 150 \times 4 mm I.D.) reversed phase column with a Nucleosil C₁₈ precolumn (5 μm , 30 \times 4 mm I.D.) was used.

GC-MS was carried out with a Varian SATURN III GC/MS ion-trap detector) equipped with both a waveform generator and a Varian Model 8200 autosampler. SATURN Revision C software was used for data acquisition in the full-scan electron impact (EI) ionization mode. For the gas chromatographic separation, a DB-17 fused-silica capillary column (30 m \times 0.25 mm I.D.) (J&W Scientific, Folsom, CA, USA) with a 0.25- μm film thickness was used with helium as carrier gas at a linear velocity of 30 cm/s. The temperature was held at 60°C for 1

min, programmed to 180°C at 30°C/min and then to 270°C at 10°C/min, and maintained at 270°C for 10 min. The injector, the interface and the ion-trap temperatures were 260, 250 and 270°C, respectively. An ionization energy of 70 eV and a mass range of 50–250 u at 1 scan/s were used.

A Supelco (Gland, Switzerland) Visiprep SPE vacuum manifold was used for the clean-up procedure.

2.3. Sample collection

Atmospheric aerosols were collected in one of the main avenues of Barcelona, 10 m above

street level. This area has a high volume of traffic. The samples were collected on thermally treated filters (300°C for 2 h) using a Sierra Misco Model 650 high-volume sampler and a Whatman EPM-2000 20.3 × 25.4 cm glass-fibre filter-paper (Whatman International, Maidstone, UK). After collection, the filters were stored in at -30°C in the dark until analysis.

2.4. Preparation of samples

The filters were cut into four pieces and each piece was subjected to ultrasonic extraction, first with dichloromethane and then with methanol. The extracts were mixed and after filtration they were concentrated to dryness by rotary evaporation. The residue was redissolved in dichloromethane (50 ml) and subjected to liquid-liquid partitioning with 0.1 M NaOH (3 × 10 ml). Dichloromethane in the aqueous phase was removed using rotary evaporation. Finally, the aqueous extract was acidified to pH 4 and used for the solid-phase extraction as follows.

First, the C₁₈ cartridge was cleaned with 10 ml of acetonitrile, 10 ml of acetone, 10 ml of methanol and 10 ml of water (pH 4) consecutively. The aqueous extract was introduced at a flow-rate of 4–5 ml/min and the column was washed with 10 ml of water (pH 4). After drying, the hydroxy-PAHs were eluted with 2 ml of methanol. The solvent was evaporated under nitrogen and the residue was dissolved in 500 µl of dichloromethane for GC-MS analysis or 1 ml of mobile phase and 10 µl of 2,4-dibromophenol (40 µg/ml) as internal standard for HPLC analysis.

3. Results and discussion

A standard solution (1 mg/ml) of seven hydroxy-PAHs (5-HI, 2-H-1,4-NQ, 5-IOH, 5,8-DH-1,4-NQ, 2-H-9-FLO, 9-HF and 2-N-1-N) was used and 2,4-dibromophenol was added as an internal standard. These compounds may be formed in the atmosphere due to reactions

between PAHs and OH radicals and some have been detected in atmospheric aerosols [18].

Different binary phases of methanol and 40 mM phosphoric acid-potassium dihydrogenphosphate buffer (pH 3) from 70:30 to 45:55 were tested. The buffer solution provides the pH, the conductivity and the ionic strength needed for the electrochemical reactions. 5,8-DH-1,4-NQ gave tailing peaks, probably owing to the interactions with the silica support. The tailing effect was reduced by the addition of 3.5% acetic acid to the mobile phase. In addition, a decrease in methanol content produced an increase in the analysis time, and resolutions were improved except for 9-HF and 2-N-1-N. Further, the elution order of 2-H-9-FLO and 5,8-DH-1,4-NQ changed when the percentage of methanol in the mobile phase decreased. The optimum separation for all substances was obtained with the mobile phase methanol-phosphoric acid-sodium dihydrogenphosphate buffer (40 mM, pH 3) (50:50) plus 7% acetic acid (Fig. 2).

The optimum working potential was obtained from the hydrodynamic voltammograms of the compounds under the separation conditions previously established. Fig. 3 shows the hydrodynamic voltammograms. The working potential chosen was the potential that gave the best response for all the compounds. Good values were obtained at +550 mV for 5-HI, 5-IOH, 5,8-DH-1,4-NQ, 2-H-9-FLO and 9-HF, but at this potential 2-H-1,4-NQ, 2-N-1-N and the internal standard (2,4-dibromophenol) gave no response. High responses were obtained at potentials near +800 mV for all the compounds. At more positive potentials, increases in both the background noise and the residual current occurred owing to the oxidation of the mobile phase. Therefore, +800 mV was chosen as the optimum potential, although a slight decrease in the responses of 5,8-DH-1,4-NQ, 9-HF and 2-H-9-FLO was observed. Adsorption of the sub-products from the electrochemical reactions or polymerization on the electrode surface may be the cause of the decrease in the relative intensities.

Calibration for hydroxy-PAHs using peak areas in the range 0.2–20 µg/ml was carried out

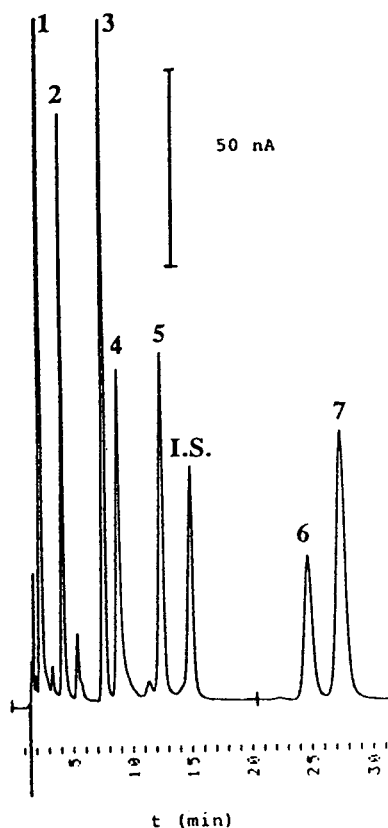


Fig. 2. Chromatogram of hydroxy-PAHs (20 μ l, 0.4 μ g/ml). Mobile phase: methanol–phosphoric acid–sodium dihydrogenphosphate buffer (40 mM, pH 3) (50:50) plus 3.5% acetic acid in buffer solution. Peaks: 1 = 5-HI; 2 = 2-H-1,4-NQ; 3 = 5-IOH; 4 = 5,8-DH-1,4-NQ; 5 = 2-H-9-FLO; 6 = 9-HF; 7 = 2-N-1-N.

under the optimum separation conditions for each compound. The correlation coefficients of the calibration functions for eight concentration levels from 0.01 to 1 μ g/ml (two replicates) were better than 0.9994 for all the hydroxy-PAHs. Five replicate determinations of 8 ng (0.4 μ g/ml solution) of each hydroxy-PAH in the mobile phase were carried out under the optimum conditions to determine the precision of the analysis. The relative standard deviations (R.S.D.) were in the range 0.9–4.5%.

The detection limits of the HPLC–ED system were determined as three times the signal-to-

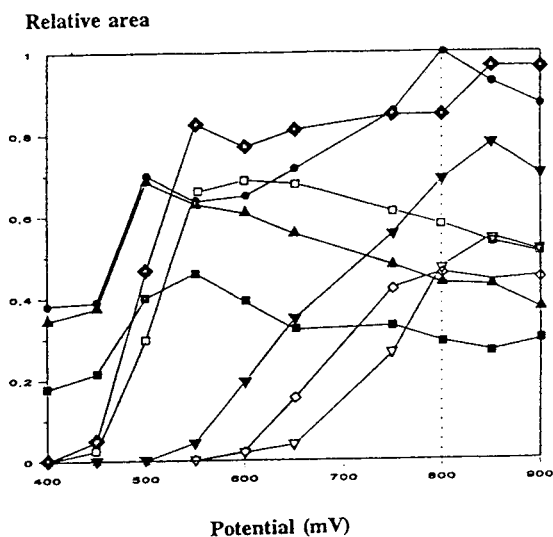


Fig. 3. Hydrodynamic voltammograms: ▲ = 5-HI; ● = 2-H-1,4-NQ; ▽ = 5-IOH; ◇ = 5,8-DH-1,4-NQ; ▼ = 2-H-9-FLO; ◆ = internal standard; □ = 9-HF; ■ = 2-N-1-N.

noise ratio for peak areas using standard solutions. For the early peaks, 5-HI, 5-IOH and 2-H-1,4-NQ, the detection limits were low, 30, 105 and 90 pg, respectively. The higher value obtained for 5,8-DH-1,4-NQ, 220 pg, may be related to its low response at the working potential (+800 mV) (Fig. 3). The compounds that eluted with relatively long retention times gave high detection limits of 200 pg for 2-H-9-FLO, 240 pg for 2-N-1-N and 300 pg for 9-HF.

The method presented was mainly developed to determine PAH derivatives in samples of environmental concern, and hydroxy-PAHs were determined in various atmospheric aerosols. Fig. 4A shows a typical chromatogram of a winter atmospheric aerosol and Fig. 4B shows the chromatogram obtained when the sample was spiked with 6 μ g of hydroxy-PAHs per gram of particulate matter. These chromatograms indicate that 2-nitro-1-naphthol can be present in the extract. Minor peaks at the retention times of 2-hydroxy-9-fluorenone and 5-hydroxyindane appeared, suggesting that these compounds could be present in the extract. The concentration of 2-N-1-N in the sample was calculated by HPLC–

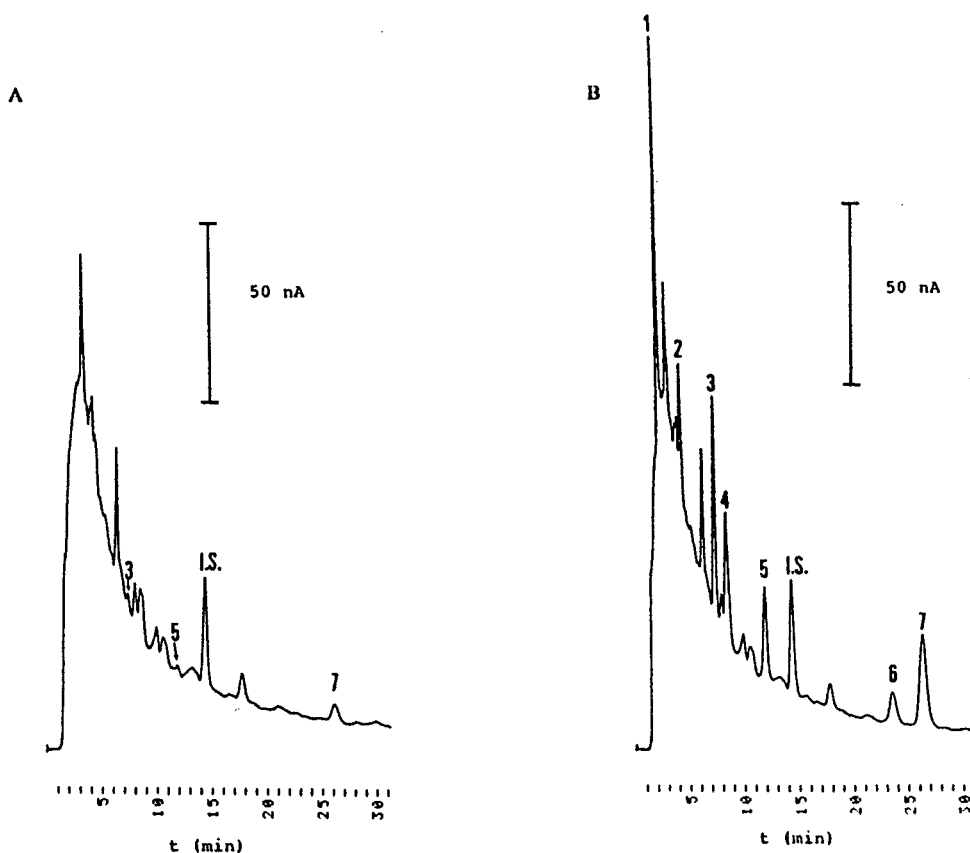


Fig. 4. HPLC of (A) atmospheric aerosol sample and (B) spiked atmospheric aerosol sample. Chromatographic conditions as in Fig. 2. Peaks: 1 = 5-HI; 2 = 2-H-1,4-NQ; 3 = 5-IOH; 4 = 5,8-DH-1,4-NQ; 5 = 2-H-9-FLO; 6 = 9-HF; 7 = 2-N-1-N.

ED using 2,4-dibromophenol as internal standard, and was found to be 0.21 ng/m^3 in air and $19 \text{ } \mu\text{g/g}$ in particulate matter. The concentrations of the 5-IOH and 2-H-9-FLO, tentatively identified by HPLC-ED, would be of the order of the detection limits for real samples, which are always higher than those obtained for standard solutions. For hydroxy-PAHs in aerosol samples, the detection limits calculated from the spiked sample were 0.8–2.5 ng injected into the chromatograph, 5–30 times higher than those obtained from standard solutions. The highest differences were observed for the early-eluted peaks owing to the baseline tail. Taking into account the recovery of the preconcentration

step, these values mean that the detection limits of these compounds in real samples would be of the order of $0.03\text{--}0.2 \text{ ng/m}^3$, depending on the compound.

In order to confirm the presence of hydroxy-PAHs in the aerosol samples, the extracts dissolved in dichloromethane were injected into a GC-MS system. Only 2-N-1-N was identified in the winter sample; its spectrum and the total ion chromatogram are given in Fig. 5. The concentrations of 2-H-9-FLO and 5-IOH, of the order of 0.05 ng/m^3 according to their detection limits by HPLC-ED, were not high enough for their identification by GC-MS.

Although there are few data in the literature

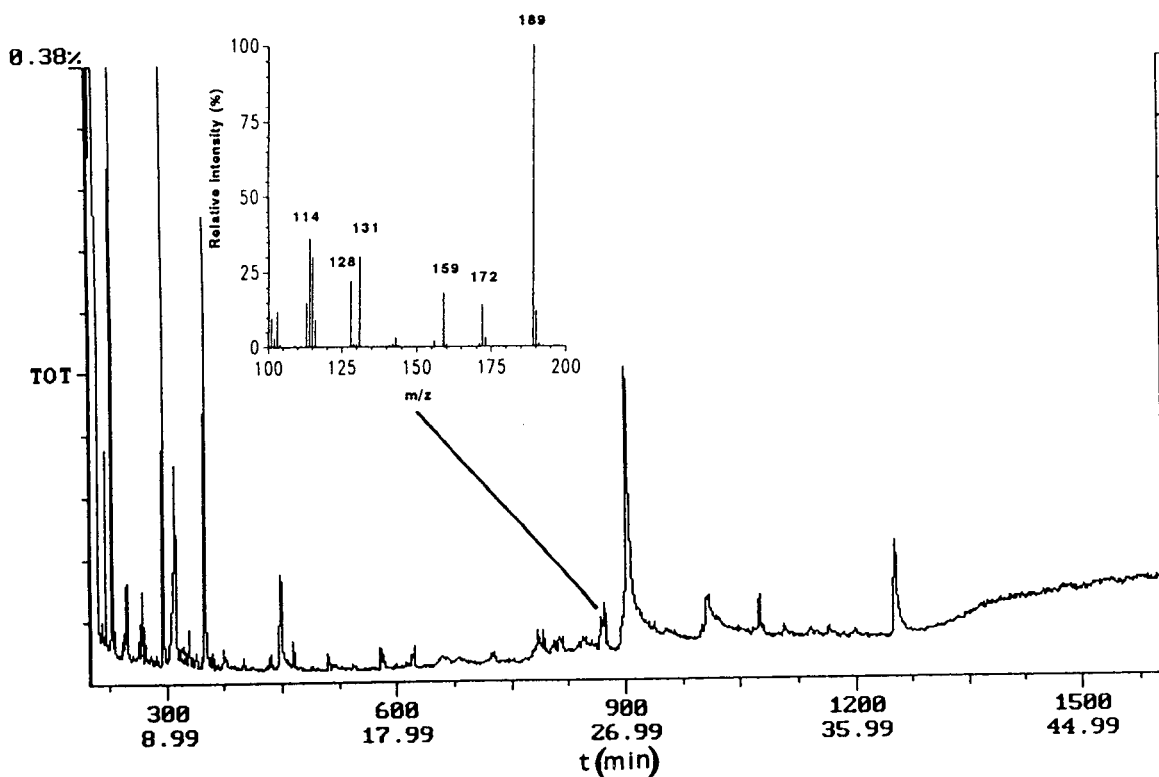


Fig. 5. Total ion gas chromatogram of an atmospheric aerosol sample and mass spectrum of the compound identified (2-N-1-N).

about hydroxy-PAHs in atmospheric aerosols, our results agree with the values found by Nishioka et al. [13], who reported concentrations for hydroxylated nitro polycyclic aromatic compounds in urban air particulate extracts between 0.01 and 0.6 ng/m³.

4. Conclusions

The use of liquid chromatography with electrochemical detection for the determination of hydroxy-PAHs has been assessed. Separation and determination conditions to provide detection at the subnanogram level were established. The selectivity, linearity and sensitivity of the method were studied. The method was applied

to the determination of hydroxy-PAHs in atmospheric aerosol samples.

Acknowledgement

Varian Iberica is acknowledged for the loan of the GC-MS instrument.

References

- [1] L. Van Vaeck and K. Van Cauwenberghe, *Atmos. Environ.*, 12 (1978) 2229.
- [2] L. Van Vaeck, G. Broddin and K. Van Cauwenberghe, *Environ. Sci. Technol.*, 13 (1979) 1494.
- [3] J. Leiter, M.B. Shimkin and M.J. Shear, *J. Natl. Cancer Inst.*, 3 (1942) 155.

- [4] J. Leiter and M.J. Shear, *J. Natl. Cancer Inst.*, 3 (1943) 455.
- [5] M. Moller and I. Alfheim, *Atmos. Environ.*, 14 (1980) 83.
- [6] W.C. Hueper, P. Kotin, E.C. Tabor, W.W. Payne, H.K. Falk and E. Sawiki, *Arch. Pathol.*, 74 (1962) 89.
- [7] T.C. Pederson and J.S. Slak, *Appl. Toxicol.*, 1 (1981) 54.
- [8] H. Stray, S. Mano, A. Mikalsen and M. Oehme, *J. High Resolut. Chromatogr. Chromatogr. Commun.*, 7 (1984) 74.
- [9] S.M. Rappaport, Z.L. Jin and X.B. Xu, *J. Chromatogr.*, 240 (1982) 145.
- [10] Z.L. Jin and S.M. Rappaport, *Anal. Chem.*, 55 (1983) 1778.
- [11] K.P. Ang, B.T. Tay and H. Gunasingham, *Int. J. Environ. Stud.*, 29 (1987) 163.
- [12] M.T. Galceran and E. Moyano, *Talanta*, 40 (1993) 615.
- [13] M.L. Nishioka, C.C. Howard, D.A. Contos, L.M. Ball and J. Lewtas, *Environ. Sci. Technol.* 22 (1988) 908.
- [14] J. Arey, W.P. Harger, D. Helming and R. Atkinson, *Mutat. Res.*, 281 (1992) 67.
- [15] Y. Yokouchi and Y. Ambe, *Atmos. Environ.*, 9 (1986) 1727.
- [16] E. Wauters, F. Vangaever, P. Sandra and M. Verzele, *J. Chromatogr.*, 170 (1979) 133.
- [17] V.D. Parker, in M.M. Baizer (Editor), *Organic Electrochemistry*, Marcel Dekker, New York, 1969.
- [18] J.M. Bayona, K.E. Markides and M.L. Lee, *Environ. Sci. Technol.*, 22 (1988) 1440.



ELSEVIER

Journal of Chromatography A, 715 (1995) 49–65

JOURNAL OF
CHROMATOGRAPHY A

Surface modification of microporous polyamide membranes with hydroxyethyl cellulose and their application as affinity membranes

T.C. Beeskow, W. Kusharyoto, F.B. Anspach*, K.H. Kroner, W.-D. Deckwer

Biochemical Engineering Division, GBF, Gesellschaft für Biotechnologische Forschung mbH, Mascheroder Weg 1, D-38124 Braunschweig, Germany

First received 14 March 1995; revised manuscript received 2 May 1995; accepted 4 May 1995

Abstract

Activated membranes for covalent immobilization of hydroxyethyl cellulose (HEC) were obtained by reaction of microfiltration nylon membranes (N66) with bisoxirane or formaldehyde. Covalent linkage of HEC was essential for the reduction of non-specific interactions with proteins and yielded a HEC coating as a layer of extended coils at the porous network of the membrane after both activation methods, thus reducing the water permeability of the modified membranes. Immobilization of iminodiacetic acid (IDA) onto HEC-coated membranes via standard oxirane chemistry provided IDA affinity membranes with almost identical properties to IDA chromatographic sorbents. The extended coil structure of the coating accounts for protein capacities higher than a theoretical monolayer coverage would yield. The thermodynamics of the interaction of metal chelate affinity (MCA) membranes with the proteins lysozyme, ovalbumin (OVA) and concanavalin A (Con A) demonstrated that dissociation constants $K_D > 10^{-5} M$ are unsuitable for the retention of target proteins on a single membrane disc. This was demonstrated by the separation of a protein mixture of lysozyme ($K_D \approx 10^{-5} M$) and Con A ($K_D \approx 10^{-7} M$) on an MCA membrane.

1. Introduction

Over the last few years affinity membranes have been introduced in downstream processing of proteins as protein adsorbers [1–4]. In order to overcome the main drawbacks of classical soft gels, such as compressibility and slow process rates, microporous membranes with various covalently bound affinity ligands were employed [5]. In such membranes the transport of the biomolecules to the affinity ligands occurs mainly

by convection. The low diffusional resistance leads to faster adsorption kinetics [6,7]. These benefits were investigated in membrane chromatographic systems employing stacked membranes [8,9] or hollow fibres [10]. The high volumetric throughput combined with a membrane-based immunoaffinity purification process allowed the purification of recombinant proteins from dilute solutions [10]. In principle, these membranes are capable to handle crude cell or microbial suspensions. An integration of separation by microfiltration and adsorption of target products or contaminants by affinity membranes

* Corresponding author.

has been demonstrated by means of cross-flow filtration [11]. Typical ligands used are ion-exchange groups [2,3,9], pseudobiospecific ligands such as reactive dyes [1,8,12] or metal chelators [13,14] and biospecific ligands such as protein A, protein G or receptor molecules [10,15,16].

Most of the polymers used in manufacturing of microfiltration membranes, such as nylon, polysulfone or polyethylene, display undesirable surface characteristics leading to difficulties in processing protein solutions. Proteins tend to adsorb strongly on these membrane surfaces. Different approaches were undertaken to remedy this problem, such as preparation of copolymers for membrane formation, use of hydrophillic alloying polymers, preparation of adsorptive coatings, introduction of hydrophillic groups into polymer backbones and covalent surface coatings by hydrophillic coating polymers, as reviewed by Klein et al. [17]. This review and a patent of Azad and Goffe [18] demonstrated that end groups of polysulfone membranes can be activated by oxirane chemistry to bind hydroxyethyl cellulose (HEC) covalently. A reduction of non-specific protein adsorption was observed and a higher density of reactive sites for immobilization of protein A was produced. End group modification of nylon-6 membranes ensuing polysaccharide immobilization was reported by Klein and Feldhoff [19]. The resulting composite membrane was applicable for covalent attachment of BSA or Cibacron Blue. Also polymer-grafted membranes with ion exchange, metal chelate, reactive dye and histidine ligands were used as affinity membranes [20–22].

The objective of this study was the development of a hydrophillic membrane combining the functional properties of microporous polyamide membranes, such as high consistency of the pore size distribution and mechanical rigidity, and the combination of chemical reactivity and low protein adsorption of HEC. Nylon membranes have only a low concentration of terminal amino groups [19,23], the direct activation of the nylon matrix leading to low ligand densities using metal chelators or triazine dyes [24–26]. Another problem of nylon membranes is the non-specific adsorption of proteins [27–29]. Immobilization

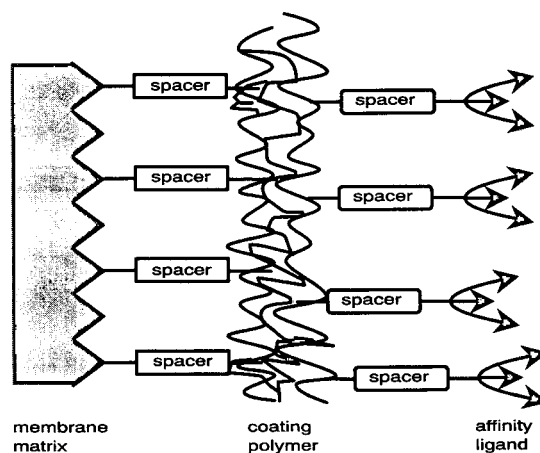


Fig. 1. Scheme of an affinity membrane as obtained by covalent immobilization of a polymer on a membrane matrix and additional linkage of affinity ligands.

of HEC onto nylon membranes was expected to exhibit low non-specific binding of proteins and proper binding capacities for affinity ligands. The initial activation of the nylon matrix by bisoxirane or formaldehyde was directed at the covalent immobilization of HEC to the membrane surface via amino end-groups or amide groups in the nylon chain. The HEC coatings were compared for their non-specific protein adsorption. After the subsequent activation of the HEC hydroxyl groups by epibromohydrin or bisoxirane, iminodiacetic acid (IDA), a metal chelator, was immobilized on the HEC-coated membrane surface. In Fig. 1 a schematic illustration of such an affinity membrane is shown. The adsorption of different model proteins on the metal chelate affinity (MCA) membrane was investigated.

2. Experimental

2.1. Materials

Microfiltration membranes (Ultipor N 66, NXG 29325, 0.45 μm) were a gift from Pall (Dreieich, Germany). Epibromohydrin, 1,4-butanediol diglycidyl ether (bisoxirane), sodium dodecyl sulphate (SDS), CaCl_2 , Cibacron Blue

F3G-A, and hydroxyethyl cellulose (Cellosize WP 40) (HEC) were obtained from Fluka (Neu-Ulm, Germany). Acetic acid, disodium EDTA, iminodiacetic acid (IDA), MnCl_2 , Na_2CO_3 , ethanol and Triton X-100 were purchased from E. Merck (Darmstadt, Germany). HCl, NaOH, NaCl, CuCl_2 and formaldehyde were obtained from Riedel-de Haen (Seelze, Germany). Ovalbumin (Grade V) (OVA), concanavalin A (Con A), sodium borohydride and imidazole were obtained from Sigma (Munich, Germany). Bovine hemoglobin ($2 \times$ cryst., lyophil., research grade) and hen egg white lysozyme were purchased from Serva (Heidelberg, Germany). Porofil was purchased from Coulter Electronics (Krefeld, Germany).

2.2. Methods

Activation of nylon membranes with bisoxirane

Five membrane discs (47 mm diameter) were shaken for 15 h at 353 K in a solution of 9 ml

bisoxirane–1 ml ethanol–1 ml 25 mM Na_2CO_3 , pH 11. After activation the membranes were washed three times with water at room temperature (Fig. 2a).

Activation of nylon membranes with formaldehyde

Nylon membranes were activated with formaldehyde according to a procedure described by Cairns et al. [30] using nylon fibres, which was modified to account for membrane discs. Ten membrane discs (47 mm diameter) were incubated for 7 h at 333 K in a solution of 20 ml formaldehyde (>36.5% w/w) and 0.2 ml phosphoric acid (85% w/w). The membranes were washed several times with water at 313 K (Fig. 2b).

Coupling of HEC

Each membrane disc was shaken in 5 ml of a 2% HEC solution (w/w) for 30 min at room temperature. Then the disc was placed onto a

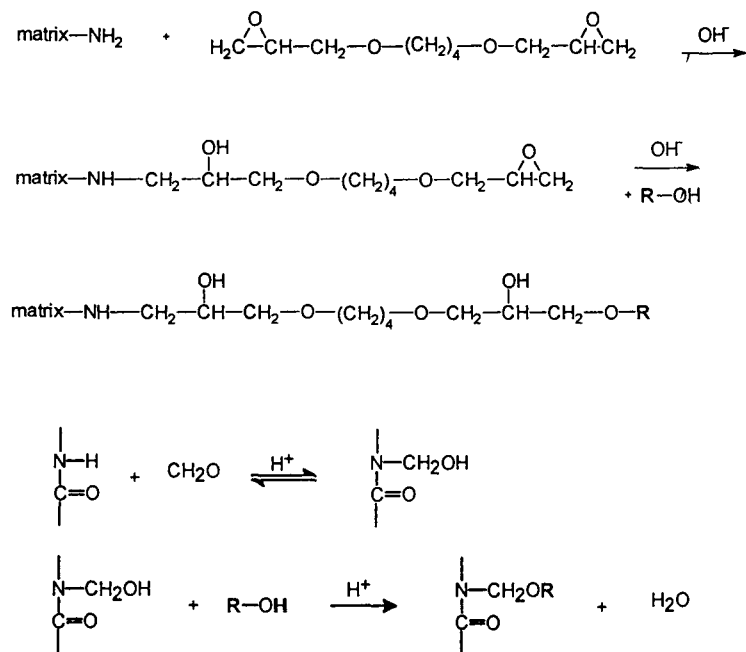


Fig. 2. Reaction scheme for covalent immobilization on nylon membranes. (a) Modification of nylon amino end groups by bisoxirane ensuing immobilization of polysaccharides (ROH), such as hydroxyethyl cellulose (HEC). (b) Activation of nylon amide groups, followed by immobilization of HEC.

sintered glass filter holder and the remaining HEC solution was sucked slowly through the membrane disc by reduced pressure until no further drop was formed at the filtrate side. Subsequently the wetted membrane disc was dried in an oven. Formaldehyde-activated membranes were coated at pH 2 and dried for 45 min at 363 K. Bisoxirane-activated membranes were dried at 393 K for 14 h after coating at pH 11. To compare the HEC coating of activated and non-activated membranes, membranes without prior activation were treated with HEC under the same conditions. The amount of bound HEC was determined after washing.

Washing procedures

In order to check the stability of the coating the membranes were treated with different washing solutions. A membrane disc was shaken three times for 1 h at room temperature in 0.1 M NaOH, 1% Triton X-100 or 0.1% SDS. Afterwards the membrane was shaken for 2 days with several water changes to displace the liquid applied for washing.

Determination of HEC density

Using a bicinchoninic acid (BCA) assay (Pierce, Rockford, IL, USA) the amount of bound HEC was determined. The HEC-coated membrane was incubated in 10 ml of 2 M HCl at 363 K for 4 h in order to decompose HEC in glucose monomers by acid hydrolysis. An amount of 2.1 ml of 1 M NaOH was added to 1 ml of the supernatant. Then 2 ml of BCA reagent was mixed with 0.5 ml of the glucose containing solution and incubated for 30 min at 333 K. The absorbance was monitored at 562 nm. The amount of bound HEC was calculated using a calibration plot of distinct glucose concentrations, yielded from known HEC concentrations after acid hydrolysis, versus absorbance as described above.

Activation of HEC-coated membranes

An amount of 80 mg of sodium borohydride was dissolved in 12 ml 2 M NaOH. Then 20 ml of water and 4 ml of epibromohydrin or 4 ml of bisoxirane were added. Three membranes were

shaken in the reaction medium for 3 h either at 323 K for reaction with epibromohydrin or at room temperature for bisoxirane. Finally, the membranes were washed at least three times with water.

Immobilization of IDA and Cu(II)

A 1-g portion of IDA was dissolved in 10 ml 25 mM Na₂CO₃. The reaction medium was adjusted to pH 12 with 6 M NaOH. The immobilization occurred overnight at 323 K while the activated membrane was shaken in the solution described above. The membrane was washed several times with water and then charged with Cu(II) by shaking it for 1 h in 20 ml of 10 mM CuCl₂ dissolved in 50 mM acetate pH 5. Afterwards it was washed three times with water and then equilibrated with buffer as required.

Determination of non-specific binding-sites by hemoglobin adsorption

A membrane disc of 47 mm diameter was equilibrated by shaking it three times in 25 mM phosphate buffer–0.5 M NaCl, pH 7. Then the membrane was shaken for exactly 1 h at room temperature in 5 ml of 100 mg/l hemoglobin dissolved in the equilibration buffer. Control experiments without membranes were run under identical conditions. The absorbance of the supernatant was measured at 405 nm using an Ultrospec Plus 4054 UV–Vis spectrophotometer (Pharmacia, Freiburg, Germany). The protein concentration was calculated from a calibration plot. Finally, the amount of adsorbed hemoglobin was calculated from the concentration difference of the supernatants with and without membrane.

Determination of hydraulic permeability and K_L -value

K_L is defined as the pressure required to displace the wetting water from the largest pore of the membrane [31]. It was determined at the transition from diffusive air flow to capillary air flow, as the water is expelled from the largest pores of the membrane. Hydraulic permeability and K_L -value were determined to check whether

the pores of the membrane were blocked by the coating method. Therefore, pressure was applied on a water container via a Palltronic FFE 02 (Pall, Dreieich, Germany), utilizing it as a pressure controlling unit. The membrane was placed in an SM 16254 filter holder (Sartorius, Göttingen, Germany) connected to the water container. After 50 ml of pre-filtered deionized water (0.2- μm microfiltration membrane) were flushed through the membrane at 500 mbar, the time to process 100 ml water was measured and converted into the hydraulic permeability. For determination of K_L the water container was removed to reduce the dead volume.

Pore size distribution of membranes

The pore size distribution of active pores in the membranes was evaluated by means of a Coulter Porometer II (Coulter Electronics, Krefeld, Germany). The Porometer records the gas flow as a function of the applied pressure during displacement of a wetting fluid from an initially saturated membrane. This extension of the bubble-point method (ASTM F316) to the wet-dry method (ASTM 2499) is described by Klein [32]. A fluorohydrocarbon with low surface tension (Porofil) was used as wetting fluid. The dry membrane (25 mm diameter) was dipped in Porofil for 5 min at room temperature. After wetting, the pore size distribution was evaluated automatically by taking the ratios of wet to dry gas flow for a given pressure range.

Specific surface area of membranes

Specific surface areas of membranes were determined by N_2 -sorption using the ASAP 2000 system (Micromeritics, Neuss, Germany) and employing the BET II Model [33]. Since N_2 is a small molecule, the specific surface area of both the large flow-through pores and the smaller pores inside the porous network of the nylon membranes are accessible by this method.

Determination of Cu(II) capacity

Cu(II)-loaded membranes were suspended for 30 min in 20 ml 20 mM disodium EDTA. The supernatant was fed to the furnace of an atomic absorption spectrophotometer (Perkin-Elmer,

Type 2100) and the absorbance monitored at 324.7 nm. The Cu(II) concentration was calculated using a calibration plot.

Determination of protein adsorption isotherms

Single membrane discs were placed in an ultrafiltration cell (Amicon 8050, membrane area 13.4 cm^2). Constant flow-rates of 2 ml/min were maintained by means of a peristaltic pump (Pharmacia LKB P1) connected to the filtrate line. Mixing of the protein solution in the ultrafiltration cell was secured with a magnetic stirrer at approximately 300 rpm. The absorbance of the protein solution at 280 nm was monitored using a Pharmacia Uvicord S II UV-monitor with flow-through cell connected to a Pharmacia REC 101 recorder (Pharmacia, Freiburg, Germany). The solution was recirculated from the ultrafiltration cell through the UV-monitor back to the cell. A sample of protein solution of known volume (0.2–1 ml) and concentration (1–2 mg/l) was injected into 4 ml binding buffer in the ultrafiltration cell. After apparent equilibrium was achieved, i.e. no change of protein concentration in solution during circulation, another injection followed. A calibration plot was obtained in the same way without a membrane in the ultrafiltration cell. The protein concentration at each apparent equilibrium was calculated from the calibration plot. The stationary-phase protein concentration was calculated by difference and plotted against the protein concentration. Binding buffer for adsorption of lysozyme and OVA was 25 mM phosphate–0.5 M NaCl, pH 7. Con A adsorption was carried out in 25 mM phosphate–0.5 M NaCl–traces of CaCl_2 , MnCl_2 , pH 6, in order to bind the dimer. All experiments were carried out at room temperature.

Fractionation of a two-component model protein solution

The metal chelate membranes were charged with Cu(II) as described above. After equilibration with 25 mM phosphate buffer–0.5 M NaCl–traces of CaCl_2 , MnCl_2 , pH 6, a volume of 4 ml equilibration buffer was mixed in the ultrafiltration cell with 0.5 ml of 1 g/l lysozyme and 0.5 ml

of 1 g/l Con A dissolved in equilibration buffer. This solution was filtered through the membrane at a flow-rate of 2 ml/min. After washing the proteins were eluted either with 200 mM imidazole dissolved in buffer or 20 mM disodium EDTA.

Sandwich affinity membranes

The metal chelate membrane was loaded with Cu(II) as described above. Con A was adsorbed onto the membrane at a ligand density of 400 $\mu\text{g cm}^{-2}$ as described above. This sandwich affinity membrane, which utilizes the lectin as affinity ligand, was employed for OVA adsorption. The isotherm was determined as described for the MCA membranes.

SDS-PAGE

Protein fractions were analyzed with a Pharmacia Phast System according to the manufacturer's instructions on SDS 8–25% PAGE under reducing conditions similar to the procedure of Laemmli [34] and made visible by silver staining [35].

3. Results and discussion

According to the technical information of the manufacturer the isotropic membranes are made of nylon 66 with accessible amino and carboxy-

late groups in a 1:1 molar ratio. Polyester fibres are utilized as support layers. Characteristic data of Ultipor N66 (NXG 29325) are nominal pore size 0.45 μm , mass/plane surface $6.7 \cdot 10^{-3} \text{ g cm}^{-2}$, specific surface area (BET II) 7.1 m^2/g and 150 μm thickness.

3.1. Immobilization of HEC

Activation of the nylon 66 polymer with bisoxirane or formaldehyde resulted in densities of active sites of at least 80 nmol cm^{-2} of epoxide groups or 2 $\mu\text{mol cm}^{-2}$ of N-methylol groups (Fig. 2), respectively [36]. The higher density of N-methylol groups is attributed to the modification of the amide groups of the nylon polymer by formaldehyde. The following immobilization of HEC provided a HEC coating which was covalently linked by reactions yielding either alkoxy- or N-alkoxymethyl derivatives (Fig. 2). As control, non-activated membranes were reacted with HEC under otherwise identical reaction conditions. The stability of these coatings was checked by different washing procedures. Afterwards the amount of immobilized HEC was determined for activated and compared with non-activated membranes. Both activation procedures resulted in a HEC density of at least 0.5 mg cm^{-2} (Figs. 3a and b); thus no remarkable difference of the coating efficiency was found with both activation procedures.

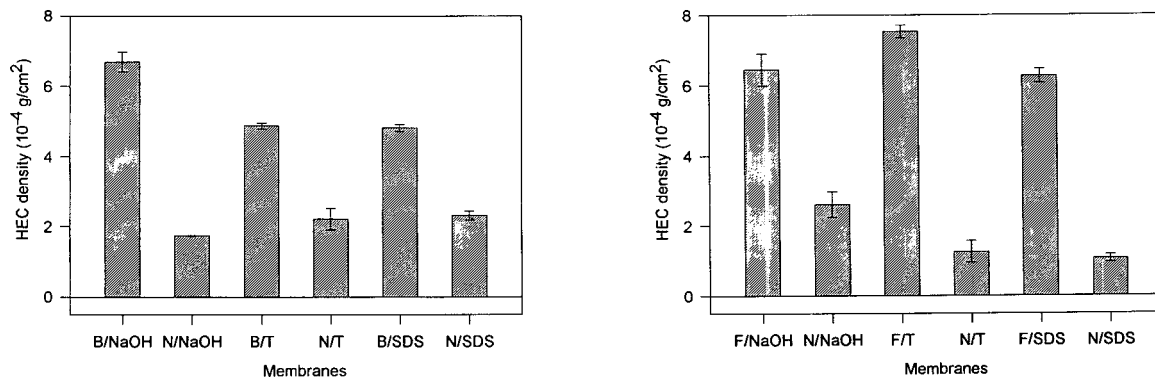


Fig. 3. Amount of immobilized HEC and influence of different washing procedures after HEC immobilization [0.1 M NaOH (NaOH), 1% Triton X-100 (T), 0.1% SDS (SDS)]. (a) After bisoxirane activation of the nylon matrix (B) or without nylon activation (N). (b) Amount of bound HEC after formaldehyde activation of the nylon matrix (F) or without nylon activation (N). Data were obtained as duplicates using two membranes.

It is important to note that HEC is also adsorbed to non-activated membranes. Although a reduction of HEC density was measured, especially after treatment with 0.1% SDS or Triton X-100, the adhesive forces were sufficient to hold fractions of HEC polymers in place during the different washing procedures, as displayed with non-activated membranes (Figs. 3a and b). This implies that HEC was attached in partially covalent and adsorptive manner at the inner porous surface of the membrane. However, HEC density was significantly higher for activated than for non-activated membranes.

It is well known that macromolecule chains do not adsorb on polymer surfaces in a film- or rod-like form. Instead, they build up coils on the membrane surface [37]. The coil dimension depends on the strength of interaction between matrix and the adsorbed polymer, the distance of covalent linkages and the diameter of the macromolecule in a given liquid. Therefore, it is plausible that the coated membrane surfaces consist of loops and tails of HEC chains freely moving inside the pores.

3.2. Non-specific interactions

The influence of HEC coating on the reduction of non-specific interactions was investigated as outlined in the Experimental section. Hemoglobin was chosen as surface active protein [38] which has been found to adsorb onto nylon membranes (Fig. 4). Significant reduction of hemoglobin adsorption on all covalently linked HEC-coated membranes was observed as compared to non-treated nylon membranes (Figs. 4a and b). Hemoglobin adsorption was also reduced on non-activated membranes which were treated with HEC under identical conditions employed for activation, however, without the activating reagent as control. The ionic detergent SDS (0.1%) and the non-ionic detergent Triton X-100 (0.1%) [39] were more efficient in the removal of physically adsorbed HEC than washing with 0.1 M NaOH. These results demonstrate that interactions between HEC polymers and nylon are quite strong, demanding for strong de-

tergents if physically adsorbed HEC ought to be washed out thoroughly.

Washing exposes non-specific binding sites from both activated and non-activated membranes. Usually, HEC density and hemoglobin adsorption were inversely related with both physically adsorbed and covalently bound HEC. Hence, the presence of HEC in the pore structure of the membranes is responsible for a reduction of non-specific hemoglobin adsorption. Nylon activation prior to HEC coating was essential to yield lowest hemoglobin adsorption. If formaldehyde was chosen for activation, less non-specific interactions remained compared to bisoxirane even after washing with detergents. This could be due to a more homogeneous distribution of HEC at the membrane surface, caused by multiple covalent binding of the HEC polymer as a result of the higher density of N-methylol groups at the nylon chains.

Considerable differences in hemoglobin adsorption were also noticed after HEC coating of non-activated membranes (control experiments) employing either reaction conditions for bisoxirane or formaldehyde activation. At 393 K partial dehydration may have taken place during the 14-h reaction time, leading to some covalent linkages between nylon and HEC of undetermined origin. At the lower temperature and shorter reaction time employed with formaldehyde-activated membranes, HEC was only physically adsorbed and apparently completely displaced by the detergents. A plausible explanation of the higher hemoglobin adsorption on those membranes which demonstrated higher HEC coating after adsorption (Fig. 3a, N/NaOH, etc.) and washing with detergent compared to washing with NaOH cannot be given. One might assume that 0.1 M NaOH was not able to displace those polymer chains which were held closest to nylon, but the detergent did at least partially. If that is true, a more homogeneous coating would be left after washing with NaOH, despite a lower HEC density, providing less non-specific interaction with hemoglobin.

Since a slight increase of hemoglobin adsorption was noticed after washing original nylon membranes with SDS, maybe originating from

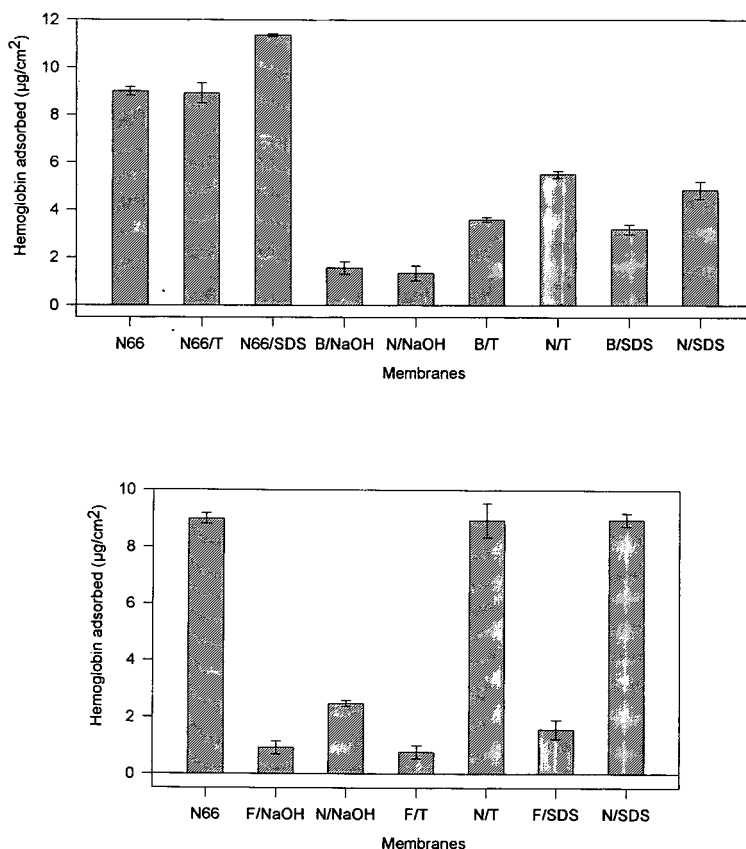


Fig. 4. Non-specific adsorption of hemoglobin on HEC-coated membranes. Influence of washing procedures. Original membrane (N66); (a) reaction conditions for HEC coating: 2% HEC at pH 11; (N) HEC coating without prior activation; (B) HEC coating on bisoxirane-activated membranes. (b) Reaction conditions for HEC coating: 2% HEC at pH 2; (N) HEC coating without prior activation; (F) HEC coating on formaldehyde-activated membranes. Washing conditions: 0.1 M NaOH (NaOH); 1% Triton X-100 (T), 0.1% SDS (SDS). Data were obtained as duplicates using two membranes.

adsorbed SDS, only Triton X-100 was employed in the following as washing reagent after HEC coating. No evidence was found that Triton X-100 would stick on HEC-coated nylon membranes, thus it was completely removed by washing with water.

Remaining non-specific interactions with HEC-coated nylon membranes were compared with those of non-modified nylon membranes in the filtration mode by using lysozyme as model protein (Fig. 5). Equilibrium isotherms obtained with coated membranes displayed a shallow shape, indicating very weak non-specific interactions. By contrast, approximately a three-fold amount of lysozyme was adsorbed on the origi-

nal nylon membranes. No discrimination between the two activation methods was apparent which is in contrast to the hemoglobin adsorption (Fig. 4). Possibly a different mechanism accounts for the interactions of hemoglobin and lysozyme with nylon, leading to a better recognition of insufficiently coated membrane surfaces by hemoglobin.

3.3. Hydrodynamic properties

The pore sizes of the HEC-coated membranes are 40 nm smaller on average than those of the original membranes (Table 1), which represents a reduction of approximately 10%. The K_L -value

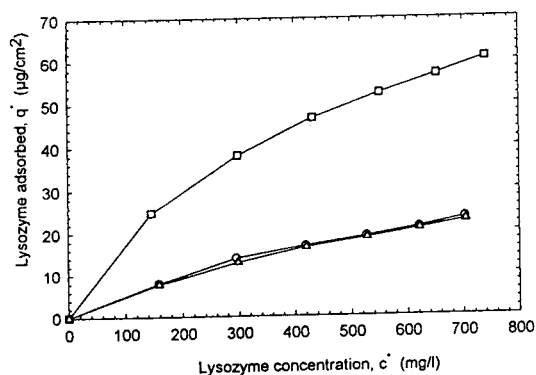


Fig. 5. Lysozyme adsorption isotherms for nylon membranes with and without HEC coating in 25 mM phosphate, pH 7, 0.5 M NaCl. (\square) N66; (\circ) B/HEC; (\triangle) F/HEC. Reduction of non-specific binding is observed with HEC-coated membranes independent of the activation method.

did not change significantly after modification; thus the maximum pore size of the membrane is almost not affected. By contrast, the hydraulic permeability is reduced to approximately 57% after HEC coating (Table 1). Both activation methods demonstrated comparable data as judged from these analysis.

The specific surface area of the original nylon membranes ($7.1 \text{ m}^2/\text{g}$), as determined by N_2 sorption, is reduced after the modification process, yielding $5.9 \text{ m}^2/\text{g}$ and $6.0 \text{ m}^2/\text{g}$ for B/HEC and F/HEC, respectively. Taking into consideration the 8% increase in weight of the membranes after coating, the porous network of the nylon

membrane, as accessible by N_2 , is not affected significantly by the HEC coating. The remaining surface area still indicates the existence of a porous network after the coating process. Total blockage of the pores, as would result from a compact HEC precipitate, should have been indicated by a much lower specific surface area, accounting for the geometrical surface of the membranes only.

The decrease in hydraulic permeability indicates that the HEC polymers stay inside the pores, thus reducing the pore size. Assuming a reduction of the mean flow pore size from 0.66 to $0.63 \mu\text{m}$, as evaluated from the porometer data, the hydraulic permeability of a capillary pore would be reduced to 91% only, employing the Hagen–Poiseuille law. One reason for the difference between the theoretical permeability and the observed value could be blockage of parts of the flow-through pores of the membrane. This would have only minor effects on the evaluation of data determined by the wet and dry method or the K_L -value, since both methods include flow-through pores only. On the other hand, the same degree of reduction of the gas flow should have been observed as for the water flow. However, this was not the case; approximately a 20% reduction of the gas flow was measured compared to approximately 40% for the water flow. Consequently, pore blockage cannot fully explain these results.

Another interpretation of the observed reduc-

Table 1
Characteristic data of nylon membranes with and without HEC coating

Membrane	Wet and dry porosity			K_L -value (mbar)	Hydraulic permeability ($\text{ml min}^{-1} \text{cm}^{-2} \text{bar}^{-1}$)
	Minimum flow pore diameter (μm)	Mean flow pore diameter (μm)	Maximum flow pore diameter (μm)		
N 66	0.46	0.66	0.80	2550	22.4
				2550	23.0
B/HEC	0.42	0.63	0.76	2700	13.1
				2700	13.0
F/HEC	0.40	0.63	0.75	2400	12.8
				2400	12.9

Data were achieved as duplicates using two membranes, except for N66.

tion in permeability meets better with the specific properties of polymers. HEC polymers are open coils on the membrane surface in an aqueous environment. The existence of hydrogels is discussed by Klein et al. [17], although no estimation was provided regarding the space a HEC coating might require. The major problem is that the crosslinking of HEC during the coating reaction is unknown. However, a rough estimate of its structure should be possible. HEC is a flexible polymer with high extension in water as derived from polymer–solvent interactions [40]. Since data accounting for the thickness of adsorbed HEC layers in water are not available, experimental data from the adsorption of polysaccharides on silica particles may be used instead, such as described by Baudin et al. [41]. For example, pullulan, which is a neutral linear polysaccharide of β -1,6-linked maltotriose units, adsorbs in a poor affinity-type. The hydrodynamic layer thickness is 19 and 24 nm using pullulan of molecular masses 200 000 and 400 000, respectively. The radius of gyration (R_G) of these polymers in water is 19 and 28 nm; hence, it is very close to the hydrodynamic layer thickness. The environment for adsorbed polymer chains on a surface corresponds most to that of semi-dilute solutions where polymer coils overlap strongly but the volume fraction remains small [37]. If one end of the polymer chain is attached covalently to a surface, the density of chemical linkages defines the polymer's shape. Consequently, the chains are disposed like adjacent mushrooms if the distance (D) between two linkages is larger than the coil size ($D > 2R_G$). If the density of linkages is higher ($D < 2R_G$), a brush results from enlarged chains.

For HEC of molecular mass 350 000 (manufacturer information), as employed in this study, a radius of gyration of 20 nm is a conservative estimation. On the other hand, a HEC mass of $5.5 \cdot 10^{-4} \text{ g cm}^{-2}$, as determined by the BCA assay, corresponds to a HEC density of 1.6 nmol cm^{-2} . Taking into account a closed packed monolayer of HEC coils, the specific surface area of $7.1 \text{ m}^2/\text{g}$ and the mass per plane surface of $6.7 \cdot 10^{-3} \text{ g cm}^{-2}$, a diameter of 7.6 nm for one HEC sphere is calculated. An R_G of 20 nm, as is estimated in water, would demand for

strong overlapping of polymer chains at the membrane surface, which is entropically unfavourable. Therefore, HEC polymer chains should stay in an enhanced cylindrical shape inside the pores of the membrane, thereby reducing overlapping. Taking the radius of gyration as the radius of a hemisphere of adsorbed HEC at the nylon surface, a layer thickness of 20 nm would result, which is in accordance with experimental data determined for pullulan [41]. Assuming a constant volume of the HEC sphere and a radius of 10 nm at the nylon surface, which again is a conservative estimation, the sphere will deform to a cylinder with a height of 50 nm, corresponding to the layer thickness. Hence the mean flow pore size would be reduced at least from 0.66 to $0.56 \mu\text{m}$, ensuing a reduction of the hydraulic permeability to 72%. This corresponds much better to the experimental value (57%).

Taking into consideration an enhanced cylindrical shape of the HEC coating, K_L -values and pore sizes determined by the wet and dry method should not change dramatically. Flexible polymer chains have only a minor influence on the pressure required to empty the wetted pore system, since mainly capillary forces and the surface tension need to be overcome. The gel-like structure of the polymer chains will increase mainly the viscosity of the solvent close to the membrane surface but not its general physical properties. Consequently, the pore size of the nylon network is still determining for the evaluation of these data.

3.4. Chemical properties

After having demonstrated that only minor non-specific interactions of HEC-coated membranes and proteins remain, these membranes need to be activated before immobilization of affinity ligands. In order to employ the same immobilization procedures as with hydrophilic chromatographic matrices, e.g. agarose, HEC-coated membranes were activated with epibromohydrin and bisoxirane. After that, IDA was immobilized onto the activated membranes and charged with Cu(II) ions to obtain MCA membranes. By measuring the amount of charged Cu(II) a precise method is available for

determination of the IDA density on these membranes.

In order to get high Cu(II) capacities, covalent binding of HEC is essential, such as found after bisoxirane ($\approx 100 \text{ nmol cm}^{-2}$ for B/HEC/B and F/HEC/B) and epibromohydrin activation (150 nmol cm^{-2} for B/HEC/E, F/HEC/E), respectively (Fig. 6). By contrast, Cu(II) capacities on non-covalently coated HEC membranes (N/HEC/E and N/HEC/B) are similar to those on membranes without HEC coating (N66/E and N66/B), which all were significantly lower than those on covalently coated membranes. Thus, the activation of hydroxyl groups of HEC is mainly responsible for these high Cu(II) capacities and not the remaining functional groups at the nylon matrix, as could be speculated.

Only minor differences among covalently coated membranes were found. Epibromohydrin activation leads to approximately 60% higher Cu(II) capacities than bisoxirane activation. On chromatographic matrices the same order is found, which is commonly attributed to a higher crosslinking of bisoxirane with the matrix due to its spacer length. Probably the same is true for HEC-coated membranes.

3.5. Adsorption isotherms of MCA membranes

Equilibrium isotherms obtained from the adsorption of lysozyme onto the different MCA

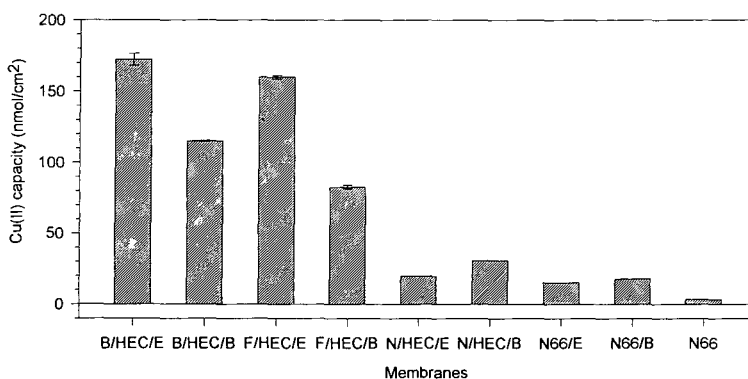


Fig. 6. Cu(II) capacity of MCA membranes obtained by IDA immobilization after different activation procedures. Covalent immobilization of HEC yields significantly higher capacities. Data were obtained as duplicates using two membranes.

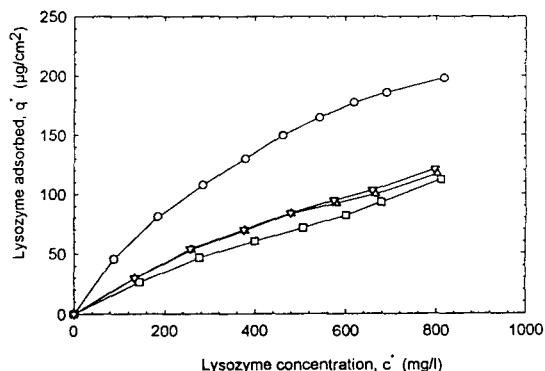


Fig. 7. Lysozyme adsorption isotherms for MCA membranes in 25 mM phosphate, pH 7, 0.5 M NaCl. (○) B/HEC/B/IDA:Cu(II); (▽) B/HEC/E/IDA:Cu(II); (△) F/HEC/B/IDA:Cu(II); (□) F/HEC/E/IDA:Cu(II).

membranes are displayed in Fig. 7. The data points reflect experimental results which were fitted employing the Langmuirean model for adsorption, $q^* = c^* q_m / (K_D + c^*)$. From the fitting, the apparent dissociation constant, K_D , and the maximum capacity, q_m , were evaluated. The maximum capacity for all membranes was found to be in the same range of $300 \pm 30 \mu\text{g cm}^{-2}$, but the shape of the isotherms differed. K_D of B/HEC/B/IDA:Cu(II) ($4 \cdot 10^{-5} \text{ M}$) was less than half the K_D of the other membranes [$(9 \pm 1) \cdot 10^{-5} \text{ M}$], indicating a stronger interaction between lysozyme and bisoxirane-linked IDA for B/HEC membranes despite a 60% lower Cu(II) capacity compared to epibromohydrin-linked IDA. Apparent K_D 's of about 10^{-4} M corre-

spond to unusually weak interaction of IDA:Cu(II) with lysozyme, commonly being found one order of magnitude lower. Probably the accessibility of the IDA:Cu(II) chelate immobilized in the HEC coils on the membrane surface is restricted. It is known that lysozyme possesses one surface-exposed histidine responsible for binding onto metal chelate sorbents [42]. However, this histidine residue needs to come close to the coordination sphere of the membrane-bound metal chelate to be adsorbed. The longer spacer obtained after bisoxirane activation may improve this. In MCA chromatography the apparent dissociation constant is inversely related to the ligand density over a certain range [43]. Thus, for lysozyme the metal chelate density seems to be higher after bisoxirane activation than after epibromohydrin activation. Since the opposite is true, a considerable fraction of metal chelate ligands is not accessible to the protein.

The shape of the isotherms and the maximum capacity on F/HEC membranes displayed only minor differences between both activation procedures. As indicated after immobilization of IDA, less Cu(II) was bound on these membranes than on bisoxirane-activated membranes despite a slightly higher HEC density. This might reflect the more compact structure of HEC on formaldehyde-activated membranes. Consequently, spacers and chelate ligands will be less accessible on these membranes as well. Since lysozyme contains only one histidine for interaction with the metal chelate, it is more sensitive to changes in the accessibility of chelate ligands. This is found in the differences of the adsorption isotherms of lysozyme on F/HEC and B/HEC membranes, which are less marked on F/HEC membranes.

Another model protein for characterization of MCA matrices is Con A. Con A exposes several histidines at its surface; thus the discrimination of more or less accessible metal chelate ligands is not as distinct as with lysozyme. The lectin dimer binds strongly onto IDA:Cu(II) chelates at pH 6 by the interaction of several surface-located histidine residues [44,45]. The equilibrium adsorption isotherms in Fig. 8 confirm these strong

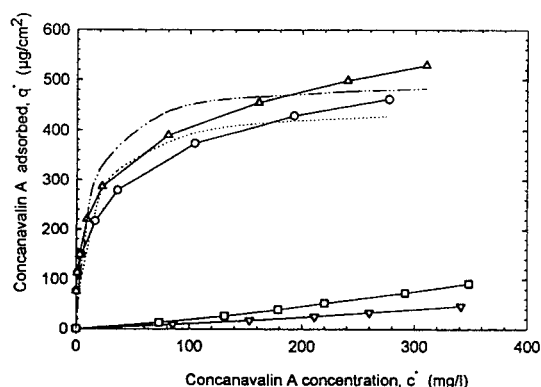


Fig. 8. Concanavalin A adsorption isotherms for different membranes, 25 mM phosphate, pH 6, 0.5 M NaCl, including trace amounts of Ca(II) and Mn(II). (Δ) B/HEC/E/IDA:Cu(II); (\circ) B/HEC/B/IDA:Cu(II); (\square) N66; (∇) B/HEC. Dotted lines are obtained by iteration assuming Langmuir isotherms.

interactions also for MCA membranes. They are very steep at low protein concentrations. Fitting of the data by the Langmuirean model is not successful, as indicated by non-linearity of the double reciprocal plot (data not shown). Nevertheless, the apparent dissociation constants were estimated by iteration based on a non-linear least-squares curve-fitting algorithm from Marquardt [46], showing some deviation from the real K_D . Dissociation constants of $2 \cdot 10^{-7}$ and $3 \cdot 10^{-7}$ M, as obtained by iteration, confirm the strong interactions of Con A onto the metal chelates. In comparison, Con A adsorption onto the B/HEC membrane without metal chelate ligands was very low (Fig. 8). Proteins are well-known to interact weakly with many surfaces in a non-specific manner [47]. In the case of Con A this might be the reason for the non-Langmuirean adsorption of Con A on the metal chelate membranes. Another important fact to consider is the behaviour of Con A to build multimers of different extent depending on the pH and the concentration of Con A [48]. This could result in multimer or multilayer adsorption, particularly at higher equilibrium concentrations. A further explanation could be polarization on the membrane which builds up during the filtration process, leading to additional Con A adsorption at higher protein concentration.

In the case of Con A no influence of the spacer on the shape of the isotherms was observed; thus the type of interaction did not change and the metal chelates are accessible regardless whether short or long spacers were used. Therefore, the slightly higher Con A capacity obtained after epibromohydrin activation can be explained by the higher Cu(II) capacity of the membrane. This was also found by El-Rassi et al. [44].

The metal chelate membranes with formaldehyde-bound HEC coating exhibit similar Con A adsorption isotherms, with slightly lower capacities of approximately $380 \mu\text{g cm}^{-2}$. Con A capacities were reproducible with all types of membranes after elution of Cu(II) and Con A by EDTA. Elution of the lectin was not observed at 200 mM imidazole, which again points to a very tight binding.

3.6. Separation of model proteins on MCA membranes

The distinct affinities of lysozyme and Con A for the IDA:Cu(II) chelate, as indicated by the adsorption isotherms, were utilized to fractionate a mixture of both proteins. The protein mixture was flushed once through B/HEC membranes with the chelate immobilized either by a bisoxirane or a epibromohydrin spacer. Both membranes adsorbed Con A completely; hence it was not found in a corresponding SDS-PAGE gel (Fig. 9). However, lysozyme was found in the filtrates. Rinsing with buffer caused complete elution of lysozyme from the membranes. Obviously, the relatively weak interactions between the immobilized metal chelates and lysozyme cannot retain the protein during extensive washing. Elution of large amounts of lysozyme from IDA:Cu(II) membranes was also found by Serafica et al. [13] with buffer containing 0.1 M NaCl. By contrast, with chromatographic sorbents elution of lysozyme is not described during washing; however, this is due to a better efficiency (larger number of theoretical plates) of the column setup.

With a 200 mM imidazole step gradient only small fractions of Con A elute from the

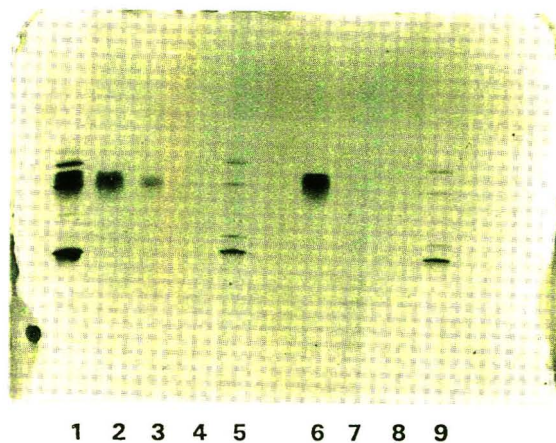


Fig. 9. SDS-PAGE gels of the fractionation of a Con A-lysozyme mixture; lane 2–5, fractionation by B/HEC/B/IDA:Cu(II); lane 6–9, fractionation by B/HEC/E/IDA:Cu(II). Lane 1: protein mixture; lane 2, 6: break-through fraction; lane 3, 7: washing filtrate; lane 4, 8: 200 mM imidazole elution; lane 5, 9: 20 mM EDTA elution; lane 2 and 6: lysozyme only; lane 5 and 9: Con A only.

IDA:Cu(II) membrane activated with bisoxirane. No Con A was found in the filtrate using membranes activated with epibromohydrin. Con A elution was achieved from both membranes by elution of Cu(II) by 20 mM EDTA. This is another proof that interactions between Con A and the metal chelate membrane are indeed metal chelate interactions; the proteins were not retained by non-specific interactions.

3.7. Accessibility of large ligands

In order to investigate the accessibility of large ligands, a sandwich affinity membrane of metal chelate-immobilized Con A was chosen. Con A was immobilized onto a B/HEC/E/IDA:Cu(II) MCA membrane. Such sandwich affinity chromatographic sorbents are described by Horváth and co-workers [44,49]. The carbohydrate binding site of Con A retains completely its affinity towards carbohydrates and glycoproteins since the immobilization by metal chelate adsorption leads to orientation of the affinity ligand [45]. Affinity interactions of OVA with either the IDA:Cu(II) chelate or Con A takes place at different sites on the surface of the protein. One

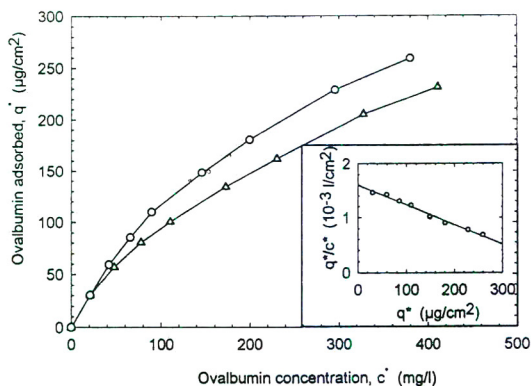


Fig. 10. Adsorption isotherms of OVA on a MCA membrane and a sandwich affinity membrane, 25 mM phosphate, pH 7, 0.5 M NaCl. (○) B/HEC/E/IDA:Cu(II):Con A; (Δ) B/HEC/E/IDA:Cu(II). The linearity of the Scatchard plot indicates specific interactions of the sandwich affinity membrane (inset).

histidine residue is available for interaction with the metal chelate [50], whereas the carbohydrate site is responsible for interaction with Con A. The adsorption isotherms of OVA on the metal chelate and the sandwich affinity membrane are displayed in Fig. 10. The maximum capacity of the sandwich system ($453 \mu\text{g cm}^{-2}$) is slightly higher than that of the metal chelate membrane ($419 \mu\text{g cm}^{-2}$) assuming Langmuirean adsorption. There is strong evidence that OVA binds specifically to Con A, as indicated by the linearity of the Scatchard plot. Con A capacity of the sandwich membrane was approximately $400 \mu\text{g cm}^{-2}$, as estimated from the Con A isotherm on the metal chelate membrane (Fig. 8) obtained

experimentally. This corresponds to 7.5 nmol cm^{-2} of the Con A dimer. The maximum capacity of OVA on the sandwich membrane corresponds to $10.1 \text{ nmol cm}^{-2}$. This indicates clearly the good accessibility of the large ligand Con A. The slightly higher OVA capacity of the sandwich membrane compared to the metal chelate membrane and the binding ratio OVA/Con A of 1.3 indicates that one Con A dimer can adsorb more than one OVA molecule. Possibly, both binding sites of the Con A dimer are partly accessible for OVA.

3.8. Theoretical considerations of protein adsorption on MCA membranes

Table 2 displays the thermodynamic data obtained for the adsorption of different proteins on metal chelate membranes by fitting to the Langmuirean model. The apparent dissociation constants are in a similar range as described for particulate sorbents, as used in immobilized metal chelate interaction chromatography [51,52]. This confirms the mainly specific interactions of the affinity membranes with the model proteins. The influence of the membrane matrix is only minor, almost similar to hydrophillic chromatographic matrices.

The dimensions of lysozyme, Con A dimer and OVA are $4.5 \times 3 \times 3 \text{ nm}$ [53], $8.4 \times 4 \times 3.9 \text{ nm}$ [54] and $7 \times 4.5 \times 5 \text{ nm}$ [55], respectively. Because the orientations of the adsorbed proteins are not known, the surface area covered by one protein molecule is calculated utilizing smallest and largest values of protein dimensions building a rectangle at the membrane surface.

Table 2

Thermodynamic constants of MCA membranes and proteins, as determined from Langmuir adsorption isotherms

MCA membrane	Protein	Maximum capacity, q_m ($\mu\text{g cm}^{-2}$)	Apparent dissociation constant, K_D (M)
B/HEC/B/IDA:Cu(II)	Lysozyme	321	$4 \cdot 10^{-5}$
B/HEC/E/IDA:Cu(II)	OVA	419	$6 \cdot 10^{-6}$
B/HEC/B/IDA:Cu(II)	Con A	451	$3 \cdot 10^{-7}$

Consequently, a range of monolayer adsorption of the proteins is calculated. Theoretically, a membrane of 1 cm^2 comprising 435 cm^2 internal surface area would adsorb 77–116 μg lysozyme (M_r 14 400), 114–245 μg Con A (M_r 53 000 for the dimer) or 93–144 μg OVA (M_r 45 000) in a monolayer. However, maximum capacities are two- to five-fold higher than theoretical monolayer capacities (Table 2). This can be attributed to the HEC coils on the membrane surface. Since nitrogen sorption is performed on a dehydrated membrane surface, the extended HEC polymer chains on the nylon membrane are collapsed and compact like a film. Thus, the specific surface area from N_2 sorption must be different from the surface “perceived” by proteins in an aqueous environment. Considering the size of the proteins employed (3 to 10 nm), adsorption is not only possible on the out-ranging positions of the HEC layer, it will take place on inner locations of the expanded HEC coils as well ($\approx 50 \text{ nm}$ thickness). Therefore, more proteins can be adsorbed than calculated for a monolayer. By contrast, monolayer adsorption was experienced by lysozyme adsorption onto nylon membranes (Fig. 5) [24,26]. Protein adsorption in expanded HEC coils does imply that at least partial transport by diffusion is taking place. Thus, in polymer-coated membranes protein transport does not occur by convection only.

4. Conclusions

Covalent coating of nylon microfiltration membranes by HEC is a basic requirement to minimize non-specific adsorption of proteins and to allow an effective immobilization of affinity ligands. Both activation of amino end groups by bisoxirane and amide groups by formaldehyde results in stable HEC coatings which display very little remaining non-specific interactions with proteins.

The hydroxyl groups of HEC are a suitable matrix for activation procedures known from hydrophilic chromatographic supports, such as agarose. Thus, very similar chemical reactions could be utilized to immobilize affinity ligands. Small ligands, such as metal chelates, as well as

large ligands, like Con A, are accessible after immobilization onto these HEC-coated membranes.

The structure of the HEC polymer represents expanded coils on the membrane surface. These coils are responsible for the reduction of the hydraulic permeability of up to 43% but also for two- to five-fold higher protein capacities of the affinity membranes than monolayer adsorption would yield.

Formaldehyde-activated membranes produce a more compact structure of the HEC coating at close proximity to the nylon matrix compared to bisoxirane-activated membranes. This results in slightly lower protein capacities and reduced accessibilities of the immobilized ligands. However, these minor differences would not justify the preference of one of these methods.

Thermodynamic data of protein adsorption demonstrates that affinity interactions can be utilized without alteration of their specificity, which might have occurred through the modification and immobilization processes. From the current results it can be derived that dissociation constants $K_D > 10^{-5} \text{ M}$ are unsuitable for the retention of target proteins on a single membrane disc. With affinity systems demonstrating stronger interactions, the potential of these affinity membranes as a tool for protein purification is indicated.

Acknowledgements

Financial support was provided by the German Federal Ministry of Research and Technology and the German Federal Ministry of Education and Research (“Hochschulnachwuchsförderungsprogramm”, HSP II). We thank Pall, Dreieich, Germany for the support of T.C. Beeskow and the gift of the membranes.

List of abbreviations

Chemicals

Bisoxirane	1,4-butanediol ether,	diglycidyl
------------	-----------------------	------------

Con A	concanavalin A,
Disodium EDTA	disodium salt of ethylenediaminetetraacetic acid,
HEC	hydroxyethyl cellulose,
Hemoglobin	bovine hemoglobin,
IDA	iminodiacetic acid,
Lysozyme	hen egg white lysozyme,
OVA	ovalbumin,
SDS	sodium dodecyl sulphate.

B/HEC/E	epibromohydrin-activated B/HEC,
IDA:Cu(II)	chelate formed after charging IDA with Cu(II),
IDA:Cu(II):Con A	sandwich affinity sorbent formed by adsorption of Con A on IDA:Cu(II).

Washing procedures

Indicated is: membrane/washing solution.	
B/NaOH	washing of HEC-coated membranes after bisoxirane activation of the nylon matrix with 0.1 M NaOH,
N/T	washing of HEC-coated membranes without prior activation of the nylon matrix with 1% Triton X-100,
F/SDS	washing of HEC-coated membranes after formaldehyde activation of the nylon matrix with 0.1% SDS.

Membranes

N66	original, non-treated nylon membrane,
MCA membrane	metal chelate affinity membrane,
B/HEC	HEC-coated membrane after bisoxirane activation of the nylon matrix,
F/HEC	HEC-coated membrane after formaldehyde activation of the nylon matrix,
N/HEC	HEC coating without prior activation of the nylon matrix,
F/HEC/B	bisoxirane-activated F/HEC,
B/HEC/B	bisoxirane-activated B/HEC,
F/HEC/E	epibromohydrin-activated F/HEC,

References

- [1] B. Champluvier and M.-R. Kula, *Biotechnol. Bioeng.*, 40 (1992) 33.
- [2] D. Lütkemeyer, M. Bretschneider, H. Büntemeyer and J. Lehmann, *J. Chromatogr.*, 639 (1993) 57.
- [3] O.-W. Reif and R. Freitag, *J. Chromatogr. A*, 654 (1993) 29.
- [4] P. Langlotz, S. Krause and K.H. Kroner, *F&S Filtrieren und Separieren*, 5 (1991) 62.
- [5] S. Brandt, R.A. Goffe, S.B. Kessler, J.L. O'Connor and S.E. Zale, *Bio/Technology*, 6 (1988) 779.
- [6] J.L. Coffman, D.K. Roper and E.N. Lightfoot, *Bio-separation*, 4 (1994) 183.
- [7] M. Unarska, P.A. Davies, M.P. Esnouf and B.J. Bellhouse, *J. Chromatogr.*, 519 (1990) 53.
- [8] K.-G. Briefs and M.-R. Kula, *Chem. Eng. Sci.*, 47 (1992) 141.
- [9] J.A. Gerstner, R. Hamilton and S.M. Cramer, *J. Chromatogr.*, 596 (1992) 173.
- [10] M. Nachman, A.R.M. Azad and P. Bailon, *Biotechnol. Bioeng.*, 40 (1992) 564.
- [11] K.H. Kroner, in J.G. Crespo and K.W. Böddeker (Editors), *Membrane Processes in Separation and Purification*, NATO ASI Series, Series E: Applied Science 272, Kluwer Academic Publishers, Dordrecht, 1994, p. 109.
- [12] S. Krause, K.H. Kroner and W.-D. Deckwer, *Biotechnol. Tech.*, 5 (1991) 199.
- [13] G.C. Serafica, J. Pimbley and G. Belfort, *Biotechnol. Bioeng.*, 43 (1994) 21.
- [14] O.-W. Reif, V. Nier, U. Bahr and R. Freitag, *J. Chromatogr. A*, 664 (1994) 13.
- [15] P. Langlotz and K.H. Kroner, *J. Chromatogr.*, 591 (1992) 107.
- [16] R. Mandaro, S. Roy and K.C. Hou, *Bio/Technology*, 5 (1987) 928.
- [17] E. Klein, E. Eichholz and D.H. Yeager, *J. Membrane Sci.*, 90 (1994) 69.
- [18] A.R.M. Azad and R.A. Goffe, *Patent Cooperation Treaty Publication No. WO 90/04609*, 1990.
- [19] E. Klein and P.A. Feldhoff, *EP 0 441 660 A1*, 1991.
- [20] H. Iwata, K. Saito, S. Furusaki, T. Sugo and J. Okamoto, *Biotechnol. Progr.*, 7 (1991) 412.
- [21] W. Demmer, H.-H. Hörl, A.-R. Weiss, E. Wünn and D. Nußbaumer, *Proc. 5th Eur. Congr. Biotechnol.*, Vol. 2, Munksgaard, Copenhagen, 1990, p. 766.

- [22] S. Mandjiny and M.A. Vijayalakshmi, in C. Rivat and J.-F. Stoltz (Editors), *Biotechnology of Blood Proteins*, Vol. 227, John Libbey Eurotext, 1993, p. 189.
- [23] K. Kugel, A. Moseley, G.B. Harding and E. Klein, *J. Membrane Sci.*, 74 (1992) 115.
- [24] B. Champluvier and M.-R. Kula, *J. Chromatogr.*, 539 (1991) 315.
- [25] B. Champluvier and M.-R. Kula, in D.L. Pyle (Editor), *Separations for Biotechnology*, Vol. 2, Elsevier, London, 1990, p. 295.
- [26] F.B. Anspach and T.C. Beeskow, *Proc. IMSTEC*, Sydney, Australia, 1992, p. 278.
- [27] C. Sarry and H. Sucker, *Pharm. Technol.*, 10 (1992) 72.
- [28] C. Sarry and H. Sucker, *Pharm. Technol.*, 1 (1993) 60.
- [29] A.M. Pitt, J. Parenter. *Sci. Technol.*, 41 (1987) 110.
- [30] T.L. Cairns, H.D. Foster, A.W. Larchar, A.K. Schneider and R.S. Schreiber, *J. Am. Chem. Soc.*, 71 (1949) 651.
- [31] D.B. Pall, E.A. Kirnbauer and B.T. Allen, *Colloids Surf.*, 1 (1980) 235.
- [32] E. Klein, *Affinity Membranes: Their Chemistry and Performance in Adsorptive Separation Processes*, John Wiley, New York, 1991, p. 101.
- [33] S.J. Gregg and K.S.W. Sing, *Adsorption, Surface Area and Porosity*, Academic Press, New York, 1982, p. 42.
- [34] U.K. Laemmler, *Nature*, 227 (1970) 680.
- [35] L.A. Butcher and J.K. Tomkins, *Anal. Biochem.*, 148 (1986) 384.
- [36] T.C. Beeskow and F.B. Anspach, in preparation
- [37] P.G. de Gennes, *Adv. Colloid Interface Sci.*, 27 (1987) 189.
- [38] J.A. Braatz, A.H. Heifetz and C.L. Kehr, *J. Biomater. Sci. Polymer Ed.*, 3 (1992) 451.
- [39] B. Ersson, L. Rydén and J.-C. Janson, in J.-C. Janson and L. Rydén (Editors), *Protein Purification, Principles, High Resolution Methods and Applications*, VCH Publishers, New York, 1989, p. 3.
- [40] W. Brown and D. Henley, *Makromol. Chem.*, 75 (1964) 179.
- [41] I. Baudin, A. Ricard and R. Auderbert, *J. Colloid Interface Sci.*, 138 (1990) 324.
- [42] Y.-J. Zhao, E. Sulkowski and J. Porath, *Eur. J. Biochem.*, 202 (1991) 1115.
- [43] H.-J. Wirth, K.K. Unger and M.T.W. Hearn, *Anal. Biochem.*, 208 (1993) 16.
- [44] Z. El Rassi, Y. Truei, Y.-F. Maa and C. Horváth, *Anal. Biochem.*, 169 (1988) 172.
- [45] F.B. Anspach and G. Altmann-Haase, *Biotechnol. Appl. Biochem.*, 20 (1994) 323.
- [46] D.W. Marquardt, *J. Soc. Ind. Appl. Math.* 11 (1963) 431.
- [47] J.D. Andrade and V. Hlady, *Adv. Polym. Sci.*, 79 (1986) 1.
- [48] G.M. Edelman, B.A. Cunningham, G.N. Reeke, J.W. Becker, M.J. Waxdal and J.L. Wang, *Proc. Natl. Acad. Sci. USA*, 69 (1972) 2580.
- [49] D. Corradini, Z. El Rassi, C. Horváth, G. Guerra and W. Horne, *J. Chromatogr.*, 458 (1988) 1.
- [50] Z. El Rassi and C. Horváth, *J. Chromatogr.*, 359 (1986) 241.
- [51] M. Belew, T.-T. Yip, L. Andersson and J. Porath, *J. Chromatogr.*, 403 (1987) 197.
- [52] F.B. Anspach, *J. Chromatogr. A*, 676 (1994) 249.
- [53] T. Imoto, L.N. Johnson, A.C.T. North, D.C. Phillips and J.A. Rupley, in P.D. Boyer (Editor), *The Enzymes*, Vol. 7, Academic Press, London, 1972, p. 692.
- [54] G.N. Reeke, Jr., J.W. Becker and G.M. Edelman, *J. Biol. Chem.*, 250 (1975) 1525.
- [55] P.E. Stein, A.G.W. Leslie, J.T. Finch and R.W. Carrell, *J. Mol. Biol.*, 221 (1991) 941.



ELSEVIER

Journal of Chromatography A, 715 (1995) 67-79

JOURNAL OF
CHROMATOGRAPHY A

Simultaneous determination of amino acids and biogenic amines by reversed-phase high-performance liquid chromatography of the dabsyl derivatives

Ingolf Krause*, Annette Bockhardt, Herbert Neckermann, Thomas Henle, Henning Klostermeyer

Forschungszentrum für Milch und Lebensmittel, Institut für Chemie und Physik, Technische Universität München-Weihenstephan, Voettinger Str. 45, D-85350 Freising, Germany

First received 13 February 1995; revised manuscript received 4 May 1995; accepted 15 May 1995

Abstract

An efficient, sensitive and reliable method for the simultaneous determination of dabsyl derivatives of numerous proteinogenic and physiological amino acids and biogenic amines in complex matrices by reversed-phase high-performance liquid chromatography (RP-HPLC) is described. A linear relation between peak area and concentration was observed from 1.25 to 1250 pmol and the detection limit was between 0.12 and 0.52 pmol. The average repeatability ranged between 1.3 and 3.1%, and the recovery values between 98 and 104%. An automated derivatization/injection unit clearly improved the performance of the method. Triethylamine was found to be a very effective additive to optimize separation efficiency. The method was successfully applied to the analysis of amino acids from protein hydrolyzates and of amino acid and biogenic amines of biological samples and food. More than 40 compounds could be separated simultaneously.

1. Introduction

After the introduction of dabsyl chloride as a pre-column derivatization reagent for amino acids [1] as well as primary and secondary amines [2], numerous applications have been published, most of them related to the analysis of amino acids in biological fluids or protein hydrolyzates by high-performance liquid chromatography (HPLC) [3-12,17]. Several advan-

tages of the dabsyl method over pre- or post-column derivatization with OPA, FMOC, PITC or fluorescamine were reported [6,13,14], e.g. dabsyl derivatives of primary and secondary amino acids are stable at room temperature and detection can be carried out in the visible region ($\lambda = 436-460$ nm) with high specificity and sensitivity at the picomole level [3-4,6].

Several modifications of the basic method of Chang et al. [3] were directed to optimize dabsylation and chromatographic separation [4-8,10,12]. The stability of the dabsyl derivatives, which is commonly described as being "perfect" up to 4 weeks at room temperature

* Corresponding author.

[5,8,14,16] or over one year at -20°C [16–18], has been questioned by Vendrell and Avilés [12]. Observations of these authors clearly indicated that peak-area values of certain amino acids (bis-dabsylated lysine, tyrosine and histidine) are not reproducible from one experiment to another if the standard conditions of Chang et al. [3] for derivatization are applied. Furthermore, a non-quantitative derivatization yield of several proteinogenic amino acids (aspartic acid, glutamic acid, serine, threonine, arginine) was found [5]. Vendrell and Avilés [12] proposed to increase the final concentration of dabsyl chloride and to adjust properly the concentration of organic solvent in the reaction mixture to overcome these problems.

Chromatographic separations of the dabsyl derivatives of selected physiological amino acids, decarboxylated amino acids (taurine, β -alanine, γ -amino butyric acid) and selected polyamines (putrescine, spermine, spermidine) as well as of phosphorylated amino acids were published by several authors [2,4,10,11,15].

In addition, the influence of chromatographic parameters such as pH, buffer composition, ionic strength, organic modifier, temperature, column length and type on the separation efficiency of certain amino acids has been described [5–7,9,12,17], but most of these parameters were only tested on the separation of the 18 hydrolyzate amino acids or selected additional compounds. Although several methods for the determination of biogenic amines in food or biological material have been reported—for a review see Refs. [19–21]—a simultaneous determination of biogenic amines and amino acids, including the precursors of biogenic amines, has not yet been published.

Our attempt was to develop a method for the simultaneous determination of proteinogenic and physiological amino acids as well as biogenic amines with special focus on derivatization yield and derivative stability, even in complex matrices as food or biological material, thus providing a flexible method for several fields of applications.

2. Experimental

2.1. Materials

Doubly recrystallized dabsyl chloride, triethylamine (sequencing grade) and 6 M HCl were from Pierce (Rockford, IL, USA), dimethylformamide and ANOTOP filter were obtained from Merck (Darmstadt, Germany). Ultrafiltration inserts (UFC, M_r cut-off: 5000) were from Millipore (Eschborn, Germany). Acetone and bis-2-carboxyethyl-sulfide (3,3'-thiodipropionic acid, TDPA) were from Fluka (Neu-Ulm, Germany) and acetonitrile was from Riedel-de-Haen (Seelze, Germany). Amino acid standard kits were obtained from Pierce or Sigma (Deisenhofen, Germany). Additional amino acid and amine standards of highest purity available were obtained from Aldrich (Steinheim, Germany), Fluka, Merck, Sigma and Serva (Heidelberg, Germany). All glassware and polypropylene reaction vials were rinsed thoroughly with 70% ethanol and water and dried before use. Glass vials for protein/peptide hydrolysis were heated at 500°C for 3 h to remove any organic contaminants [5]. Highly purified water (Milli-Q, Millipore) was used throughout for preparation of all buffers and reagents.

Amino acid and amine standards

Composite amino acid and amine standards were prepared from stock solutions ($2.5\ \mu\text{mol}/\text{ml}$ 0.1 M HCl) to yield an overall concentration of 250 nmol/ml per component (except for physiological standards with varying concentrations). Norleucine or norvaline were used as internal standards at final concentration of 250 nmol/ml. TDPA (0.2%, w/v) was generally added to all standards as an antioxidant.

2.2. Protein/peptide hydrolysis [22]

An aliquot of protein or peptide solution in 0.1 mol/l HCl–0.2% TDPA containing 100 ng to 5 μg was transferred into micro glass-vials and dried in vacuo. Hydrolysis was carried out in the gas phase over 6 M HCl–0.2% TDPA at 110°C

for 24 h. Amino acids were redissolved in 50 to 200 μl of 0.1% HCl–0.2% TDPA and a 10- μl aliquot was submitted to derivatization.

2.3. Extraction of free amino acids and biogenic amines

Between 0.1 and 1.0 g of thoroughly homogenized solid samples, as food (cheese, meat, sausages, fish), tissue or plant material, or lyophilized samples (plasma, tissue) was dispersed with 10 ml of 0.1 mol/l hydrochloric acid solution containing 0.2% TDPA and the internal standard (250 nmol/ml) in a 25-ml centrifuge vial using an Ultra-Turrax homogenizer for 2 min at 20 000 rpm. The tube was covered with Parafilm and kept in an ultrasonic bath for maximal 30 min, centrifuged at 5000 g for 20 min, and any topping fat layer was removed. The supernatant was filtered through a 0.45- μm membrane and 3 ml of the filtrate was deproteinized by passing through ultrafiltration inserts (prewashed with 200 μl of the extraction medium prior to use) via centrifugation at maximal 3500 g for about 1 h. Membrane-filtrated liquid food samples were diluted with 0.1 mol/l HCl–0.2% TDPA–250 mmol/l internal standard and ultrafiltrated as described above.

Alternatively, 1 ml of supernatant or diluted liquid sample was deproteinized by mixing with 1 ml of 40% (w/v) trichloroacetic acid, and the mixture was kept for 10 min in an ice bath. After centrifugation (15 000 g, 15 min), a 100- μl aliquot of the supernatant was dried in a vacuum concentrator (Speed-Vac) and redissolved in 100 μl of reaction buffer immediately before derivatization.

2.4. Dabsylation procedure

Reagents

Reaction buffer (0.15 mol/l NaHCO_3 , pH 8.6) consisted of 630 mg sodium hydrogen carbonate, dissolved in 40 ml Milli-Q water, adjusted to pH 8.6 with diluted NaOH and made up to 50 ml with water.

Dilution buffer was a mixture of 50 ml acetoni-

trile, 25 ml ethanol and 25 ml elution buffer A (see HPLC section).

Dabsyl chloride reagent (12.4 mM in acetone) was prepared by dissolving 40 mg dabsyl chloride in 10 ml of acetone by ultrasonic treatment (10 min) and filtering through an ANOTOP filter into brown-glass vials, and was stored at -20°C .

Manual derivatization

Aliquots of 20 μl of amino acid and amine standards, containing 0.2–50 nmol per component, or deproteinized sample extracts—if necessary diluted with 0.1 mol/l HCl–0.2% TDPA according to the expected total free amino acid and amine content—were transferred into 1.8-ml screw-cap vials and diluted with 180 μl reaction buffer. After thorough mixing on a vortex-mixer, 200 μl of dabsyl chloride reagent was added and the vials were stoppered tightly and shortly mixed again. Samples were incubated at 70°C for 15 min with intermediate mixing at 1 min and 12 min. The reaction was stopped by placing the vials in an ice bath for 5 min. Subsequent to a short centrifugation step (10 s, 10 000 g), 400 μl of the dilution buffer was added, followed by thorough mixing and centrifugation (5 min, 15 000 g). The clear supernatants were directly set for injection or stored at -20°C until chromatography.

Automated derivatization

Using an automated pre-column dabsylation device for dabsylation (AS 3500, Thermo Separation Products, Darmstadt, Germany), 100 μl of dabsyl chloride reagent, 10 μl of amino acid–biogenic amine standards or appropriate diluted sample extracts and 90 μl of reaction buffer were subsequently loaded into a teflon loop. The content of the loop was then transferred to an empty vial, mixed and incubated at 70°C for 15 min. While heating, the vial was mixed during the first five minutes and during the last minute of the incubation period. After cooling to 12°C during 5 min, 200 μl of dilution buffer was added. The solution was mixed again for 0.5 min and kept at least 20 min at 12°C before submitting to injection.

2.5. High-performance liquid chromatography

HPLC equipment

The HPLC equipment (Waters, Eschborn, Germany) consisted of a WISP 712 autosampler, two Model 510 high-pressure pumps and an UV 486 variable-wavelength detector interfaced to a NEC APC computer via a SIM box. Maxima 820 software was used for system controlling and peak integration. For automatic derivatization, the WISP 712 autosampler was replaced by the AS 3500 pre-column derivatization unit/autosampler.

HPLC conditions

Dabsyl derivatives of amino acids and amines were separated either on a 150 × 4.6 mm I.D. stainless-steel column filled with 3 μm Spherisorb ODS-2 (Knauer, Berlin, Germany), including a 10 × 4 mm I.D. guard cartridge containing the same stationary phase, or on a 150 × 3.9 mm I.D. Novapak C₁₈ column, 4 μm (Waters, Eschborn, Germany), including a guard cartridge. The column was thermostated at 50°C. Usually 10 μl of the derivatized samples was injected.

Mobile phase A, consisting of 9 mM sodium dihydrogenphosphate, 4% dimethylformamide and 0.1–0.2% triethylamine (TEA), was titrated to pH 6.55 with phosphoric acid. Mobile phase B was 80% (v/v) aqueous acetonitrile.

Dabsylated amino acids and amines were eluted at a flow-rate of 1 ml/min using the gradient system listed in Table 1; detection was at 436 nm and the data acquisition rate was 5 Hz.

3. Results and discussion

3.1. Deproteination

Deproteination by ultrafiltration was found to be preferable compared to trichloroacetic acid (TCA) precipitation, as with a relative high concentration of residual TCA after drying in vacuo, the derivatization yield was sometimes observed to be decreased remarkably. In addition, the ultrafiltration procedure increased the shelf-life of the chromatography column (100–200 analyses). Recovery of amino acids from ultrafiltered amino acid standards (each 250 nmol/ml) was between 98 and 102% from batch to batch when prewashed filters were used. Similar results were reported by Cohen and Strydom [23].

3.2. Dabsylation

Preliminary experiments were performed with combined standards or extracts of free amino acids and biogenic amines at greatly varying concentration. Initial results indicated that the concentration of dabsyl chloride in the reaction mixture had to be increased to 6.2 mM in order to achieve optimal derivatization and stability of the bis-dabsyl derivatives of lysine, tyrosine, histidine and carnosine and of the biogenic amines histamine, tyramine, putrescine and cadaverine. Similar observations were reported by Vendrell and Avilés [12]. Although the derivatization yield (judged by corresponding peak response factors) of glutamic and aspartic acid decreased with increasing concentration of

Table 1
Scheme of elution gradient

	Time (min)									
	0.0	2.0	7.0	35.0	45.0	66.0	71.0	77.0	77.5	90.0
Solvent B (%)	8.0	8.0	20.0	35.0	50.0	100.0	100.0	100.0	8.0	8.0
Curve type ^a		6	5	7	6	6	6	6	6	6

^a 5 = convex, 6 = linear, 7 = concave according to Maxima 820 (Waters) gradient-controlling software.

dabsyl chloride in the reaction mixture, derivatization was found to be linear over a wide concentration range (see section 3.3., linearity). It was also observed that methionine was readily oxidized to methionine sulfone and methionine sulfoxide under these conditions, but oxidation could be completely inhibited by adding 0.2% of the antioxidant TDPA to sample and standard solutions. For the reaction buffer, a molarity of 0.15 mol/l and pH 8.6 was encountered to be most suitable with respect to the derivatization yield of the bis-dabsyl derivatives and the repeatability of derivatization for all amino acids and biogenic amines tested. However, Jansen et al. [17] did not report a significant difference of peak heights when varying the pH of the reaction mixture within pH 7.5 to 9.0, but their data were restricted to a limited number of amino acids (glutamic acid, alanine, valine, leucine, lysine). Furthermore, their contrary findings may result from the low buffering capacity of the reaction buffer (0.05 mol/l) not guaranteeing to maintain the pH of the reaction mixture at the desired level. The volume ratio of sample, dabsyl reagent and dilution buffer, as well as the composition of the dilution buffer, significantly influenced the yield of the derivatives and the linearity range of the derivatization procedure. These findings were in congruence with the results of Vendrell and Avilés [12]. In derivatized samples, which were diluted according to Knecht and Chang [8], crystallization of amino acid derivatives or dabsonate (see Table 2) occasionally occurred upon prolonged standing, resulting in a concomitant clearance of the peak area of hydrophobic and basic amino acids and some biogenic amines (histamine, tyramine). After replacing Chang's dilution buffer by a modified solvent mixture (see Experimental section), all derivatives were observed to be stable within 24 h (decrease of peak area below 4%). With extended storage of derivatized samples at room temperature, a decrease of the peak area of asparagine and tyramine was observed in deproteinated samples of free amino acids in biological fluids or food extracts. Nevertheless, 24 h stability is a reasonable period for manual day-to-day preparation of the samples and consecu-

tive chromatographic analysis. A general improvement of the repeatability of the peak area was achieved by using an automated derivatization unit (AS 3500), serving to maintain a constant standby period of the derivatized samples prior to injection and a more precise fully automated liquid handling.

3.3. Chromatographic separation

Qualitative results

Using the chromatographic parameters described in the Experimental section, the separation of the dabsyl derivatives of numerous amino acids including phosphorylated or carboxymethylated compounds as well as biogenic amines was investigated, most of them being separated simultaneously in one chromatographic run. The elution order and separation efficiency of 68 dabsyl derivatives tested on a 4- μ m NovaPak C₁₈ column at a TEA concentration of 0.16% are summarized in Table 2; the separation of a combined amino acid and biogenic amine standard is shown in Fig. 1.

We observed that elution order and separation efficiency were strongly depending on the TEA concentration in the elution buffer A, not confirming the findings of Jansen et al. [17], who reported that additives like TEA or dimethylformamide (DMF) had no substantial effect upon chromatographic separation. From repeated experiments with increasing concentration of TEA in elution buffer A titrated to pH 6.55, an obvious non-linear relationship between TEA concentration and retention time was observed for several amino acid derivatives eluting between 13 and 55 min, as shown in Figs. 2A–2E. Whereas in the last part of the gradient, little influence on retention time for the hydrophobic biogenic amines was observed (Fig. 2F). Retention of dabsyl derivatives of almost any amino acid and amine reached a maximum at 0.18% TEA. Critical pairs of closely eluting amino acid and amine derivatives (phosphothreonine/aspartic acid, glycine/arginine, alanine/ β -alanine, α - γ -aminobutyric acid, lanthionine/agmatine and histidine/carnosine) were sufficiently separated at 0.16% TEA. Except for glycine/arginine, the

Table 2
Elution order and retention time of dabsyl derivatives (0.16% TEA)

Compound	Abbreviation ^a	Incomplete separation	Co-elution	Retention time (min)	Compound	Abbreviation ^a	Incomplete separation	Co-elution	Retention time (min)
O-Phosphoserine	PS			13.95	Norleucine	NLE			40.90
Aspartic acid	D	PT		14.94	Phenylalanine	F			41.57
O-Phosphothreonine	PT	D		15.15	Ammonia	NH ₃			42.05
Glutamic acid	E			15.91	Lanthionine	LAN			43.62
Carboxymethylcysteine	CMC			16.39	Agmatine	RN			44.00
S-Sulfocysteine	SC			16.89	2-Aminoethanol	SN		CYT	44.76
β -Aminoadipic acid	AAA			17.10	Cystathionine	CYT		SN	44.76
Hydroxyproline	OHP			22.51	Cysteine	C			45.65
Asparagine	N			23.13	Homocystine	HCT			46.83
Glutamine	Q			24.72	1-Amino-2-propanol	TN			48.02
Citrulline	CIT			25.35	Hydroxylysine	OHK			50.04
Serine	S			26.17	Ornithine	ORN			51.02
Phosphoethanolamine	PSN		MESO	27.43	Lysine	K			51.58
Methionine sulfoxide	MESO		PSN	27.69	Histidine	H			52.10
(two diastereomers)	MESO		PSN	28.15	Carnosine	CAR	AN		52.38
Threonine	T			28.45	Ethylamine	AN	CAR		52.59
Glycine	G		MH	28.94	Tyrosine	Y			54.30
1- and 3-Methyl-histidine	MH		G	28.94	Pyroglutamine	PN		WN	57.22
Arginine	R			29.38	Tryptamine	WN		PN	57.22
Alanine	A	β A		30.65	Isobutylamine	VN			57.79
β -Alanine	β A	A		30.92	3,4-Dihydroxyphenylalanine	DOPA			58.34
Anserine	AS			31.52	Phenylethylamine	FN			59.20
Taurine	TAU			32.31	Methylbutylamine	IN			59.94
Sarcosine	SAR		AABA	32.58	Putrescine	PUT			62.16
α -Aminobutyric acid	AABA	GABA	SAR	32.75	Cadaverine	CAD			63.29
γ -Aminobutyric acid	GABA	AABA		33.27	Histamine	HN			63.87
Proline	P			33.99	Cystamine	CN			63.87
β -Aminoisobutyric acid	BAIBA			34.40	Serotonin	OHWN			65.00
Norvaline	NVA			35.06	Tyramine	YN			67.31
Valine	V			35.55	Spermidine	MN			67.98
Methionine	M			37.60	Noradrenaline	NADN			68.49
Isoleucine	I			39.35	Dopamine	DOPN			69.05
Leucine	L			40.03	Adrenaline	ADN			70.61
Tryptophan	W			40.51	Spermine	SPN			71.94

^a One-letter code was used for the nomenclature of proteinogenic amino acid; for most of their decarboxylated products (biogenic amines) a "N" ("amine") was added as a second letter except for those indicated in the table. Hydrolyzed dabsyl chloride (dabsonate) elutes as a broad peak at $t_R = 20$ min.

elution order of most of the "critical" pairs of dabsylated amino acid and amines was inverted when increasing the TEA concentration from 0.15 to 0.22%. Separation of the derivatives of the remaining amino acids and amines of Table 2, not illustrated in Fig. 2, was not deteriorated with varying TEA concentration, although they showed the same tendency of retention behaviour.

Lowering the initial concentration of solvent B

led to an improved separation of O-phosphoserine, O-phosphothreonine, aspartic acid, glutamic acid and α -aminoadipic acid, but also resulted in an increased total gradient time. A convex flattening of the gradient with an average slope of 0.5% B/min positively affected the separation of the dabsonate to proline group. Dimethylformamide, added to mobile phase A, was found to improve the separation efficiency remarkably [17].

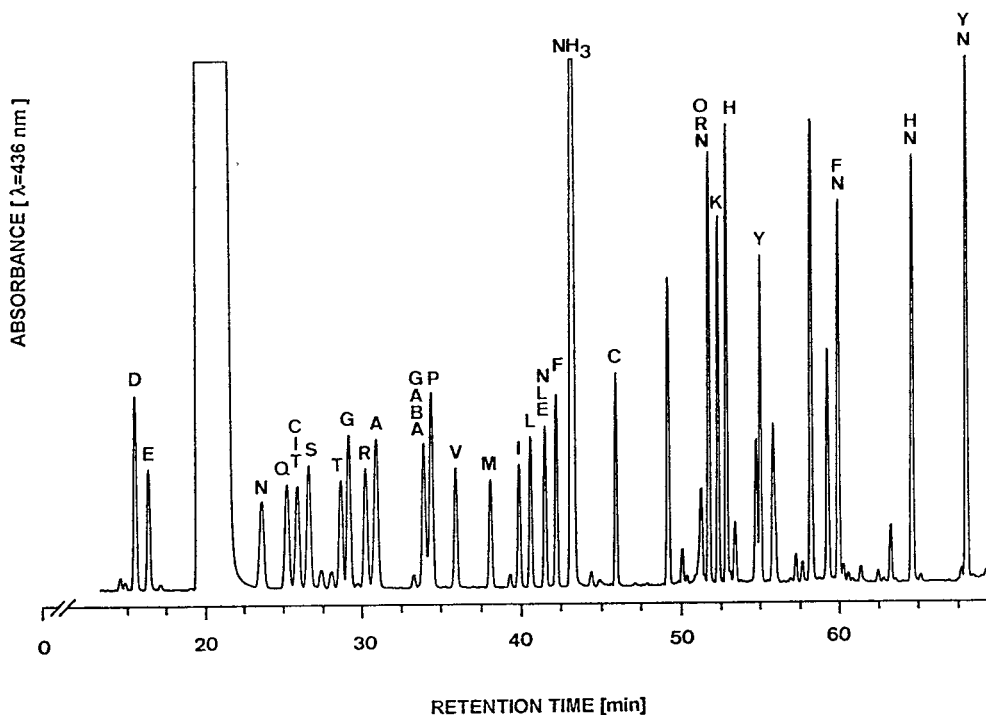


Fig. 1. RP-HPLC analysis of dabsyl derivatives from proteinogenic and physiological amino acids and selected biogenic amines, using elution buffer A containing 0.16% TEA, on a Novapak C_{18} column. For abbreviations of amino acids and biogenic amines see Table 2.

The elution system indicated in the Experimental section using an optimized TEA concentration for a 150-mm column with 3- μ m Spherisorb ODS-2 or 4- μ m NovaPAK C_{18} was most suitable for the simultaneous separation of a large number of components within a reasonable analysis time. Depending on the number and kind of amino acids and amines to be separated for an individual application, the gradient profile and, moreover, the appropriate TEA concentration, which may have to be adjusted according to type, batch and age of the chromatography column, has to be chosen carefully. Norleucine–eluting between leucine and phenylalanine–or norvaline–eluting between valine and methionine–proved to be suitable internal standards, which were included during the extraction of amino acids and biogenic amines or added to a protein/peptide prior to hydrolysis. By using a low molarity of phosphate and TEA as buffering additive in solvent A and aqueous

acetonitrile as solvent B the risk of salt precipitation during gradient formation was abandoned. The lifetime of the chromatography column usually was at least 200 runs.

Quantitative aspects

Linearity

A general, linear relationship between peak area and concentration, evaluated on a large number of samples ($n = 34$) of a combined standard of amino acids and biogenic amines, was observed over a range of 1.25 to 1250 pmol, provided that the samples were analyzed on the same day they had been derivatized. The correlation coefficients were greater than 0.999; data of regression analysis are compiled in Table 3.

Detection limit and determination limit [25]

According to Table 3, the detection limit of most of the dabsyl derivatives ranged between

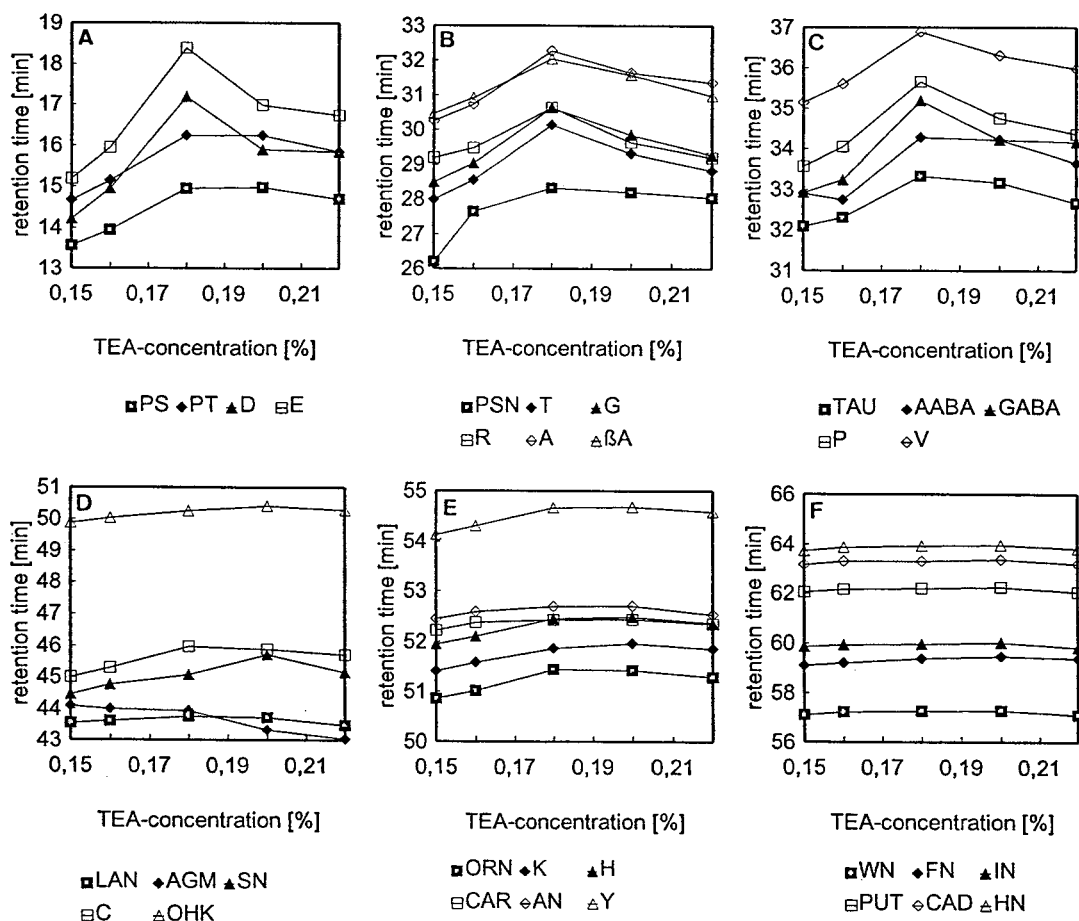


Fig. 2. Influence of the TEA concentration of elution buffer A on the elution behaviour of dabsylated amino acids and biogenic amines on a Spherisorb ODS-2 column. For abbreviations of amino acids and biogenic amines see Table 2.

0.12 and 0.52 pmol, with an average of approximately 0.3 pmol, a value being slightly lower than those reported by Chang and co-workers [6–8], Watanabe et al. [16] and Jansen et al. [17]. The determination limit ranged between 0.4 and 1.5 pmol. Nevertheless, when analyzing amino acids in the low picomole range, special attention has to be paid to avoid contamination of hydrochloric acid and glassware used for protein hydrolysis as well as of the derivatization buffer. Chang et al. [3,5,6] and Vendrell and Avilés [12] recommended that the starting amount of protein to be hydrolyzed and analyzed necessarily has to exceed 100 pmol in order to avoid extraneous contaminations of the sample and losses of

amino acids and derivatives. Consequently, the main clue for the amino acid analysis at the femtomole level is not the sensitivity of the method, but the sample handling.

Recovery

Recovery was evaluated for selected biogenic amines, which were spiked at two concentration levels onto a Parmesan cheese extract, in which these amines were either absent or present at a low level. Spiking was done prior to deproteination by ultrafiltration. Table 4 summarizes the recovery values for biogenic amines in Parmesan cheese, which were found to range between 98 and 104%. Recovery values usually exceeded

Table 3
Regression data, determination and detection limit of amino acid standards

Amino acid	Slope <i>m</i>	Intercept <i>y</i>	S.D. slope	S.D. intercept	Correlation coefficient	Detection limit (pmol)	Determination limit (pmol)
D	1.12	0.43	0.0023	1.47	0.999962	0.46	1.58
E	0.92	-2.01	0.0033	1.99	0.999875	0.51	1.76
N	0.80	1.21	0.021	1.52	0.999341	0.27	0.93
Q	1.04	-2.91	0.014	1.01	0.999828	0.28	0.97
CIT	1.12	-2.54	0.0076	0.56	0.999954	0.21	0.73
S	1.07	4.10	0.0075	5.56	0.999482	0.12	0.42
T	0.68	0.12	0.0020	1.30	0.999922	0.21	1.01
G	1.37	-0.055	0.000035	0.012	1.00	0.26	0.89
R	1.04	-0.43	0.0039	2.42	0.999858	0.33	1.15
A	1.38	0.62	0.0016	0.84	0.999992	0.17	0.61
GABA	1.12	2.92	0.0180	1.35	0.999735	0.26	0.93
P	1.41	0.011	0.000030	0.014	1.00	0.29	1.03
V	1.20	-9.29	0.0087	6.16	0.999274	0.52	1.80
M	1.17	-10.10	0.0090	6.63	0.999141	0.10	0.35
I	1.14	-13.59	0.0089	6.00	0.999275	0.41	1.40
L	1.25	-10.97	0.0086	6.02	0.999356	0.23	0.79
NLE	1.11	-1.91	0.029	2.12	0.99956	0.13	0.46
F	1.32	-9.21	0.0071	5.05	0.999592	0.31	1.09
C	0.99	-2.67	0.0041	2.56	0.999854	0.29	0.99
ORN	2.62	-8.04	0.027	1.97	0.999897	0.40	1.38
K	2.37	-13.17	0.020	14.69	0.998938	0.28	0.98
H	2.28	-2.38	0.0065	3.65	0.999919	0.30	1.05
Y	2.18	0.017	0.0021	1.27	0.999993	0.26	0.89
FN	1.75	1.07	0.027	1.99	0.999765	0.17	0.59
HN	2.26	-2.08	0.063	4.69	0.999219	0.31	1.07
YN	2.64	-4.33	0.025	1.88	0.999907	0.17	0.61

Relationship between peak area (*V_s*) and the amount of amino acids (pmol). Each 7 amino acid standards of 1250 and 1.25 pmol and each 5 samples of 1000, 50, 500 and 250 pmol, respectively, were analyzed. Claims of linearity are supported by regression data, which include slope, intercept, standard deviations of slope and intercept and correlation coefficients. The determination and detection limit was calculated in the range between 0 and 25 pmol according to DIN 32 645 [34].

Table 4
Recovery (%) of selected biogenic amines spiked onto an extract of a Parmesan cheese

Amino acid	Parmesan + 500 ppm amine (<i>n</i> = 5)	Parmesan + 1000 ppm amine (<i>n</i> = 5)
Tryptamine	103.15 ± 0.05	97.90 ± 0.48
Phenylethylamine	103.78 ± 0.18	97.57 ± 0.78
Putrescine	102.27 ± 0.57	100.37 ± 1.63
Cadaverine	102.32 ± 1.13	99.73 ± 1.43
Histamine	103.26 ± 0.30	99.39 ± 0.27
Tyramine	102.39 ± 0.85	102.31 ± 0.94

100% for spiking with 500 ppm biogenic amines as a consequence of single-point calibration.

Repeatability

The influence of the several steps of the method—extraction, automated derivatization and chromatographic separation—on its overall repeatability was investigated using Parmesan cheese sample (see Fig. 4), containing between 68 and 17 633 ppm of free amino acids and biogenic amines. When analyzing five subsamples of a single extract of free amino acids and biogenic amines after automated derivatization following a fixed time schedule, the repeatability was found to range between 0.2 and 3.3%, the average repeatability (1.3%) was merely influenced by chromatographic determination, including sample injection and automated peak integration. In a second series, five subsamples of the free amino acid extract were derivatized and analyzed separately. The average value of

repeatability was found to be slightly increased to 2.0%, due to an increased number of liquid-transferring steps during derivatization. As could be expected, a more pronounced increase of the average repeatability (3.1%) was observed when analyzing five separate samples of the Parmesan cheese submitted to extraction, deproteination and derivatization.

Furthermore, performance studies were extended using protein hydrolyzates, food samples as wine, meat, poultry meat conserves, ham, salami, Asian fish sauce, seasonings, and biological materials as plant and cortex extracts and lyophilized human plasma samples, giving similar results for repeatability and recovery values (data not shown). The repeatability values reported by several authors [12,14,16]—in some cases called “reproducibility” values—lie within the same range as described here, although some of the investigations were only performed on a limited number of amino acids, sometimes mere-

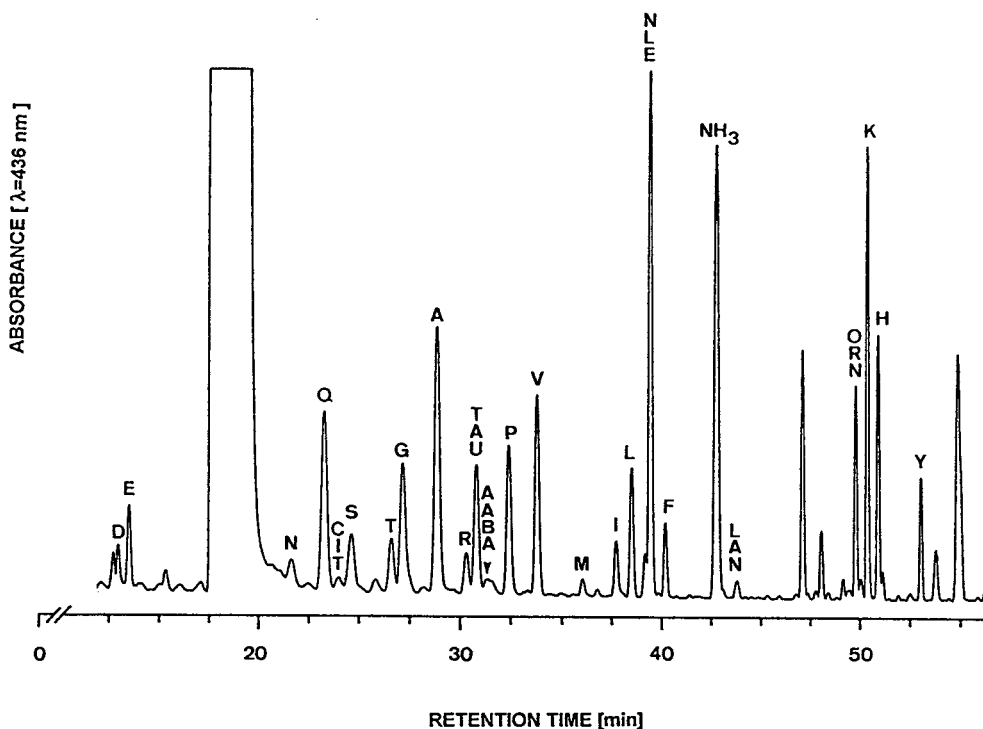


Fig. 3. RP-HPLC separation of dabsyl derivatives from human plasma, using elution buffer A containing 0.16% TEA, on a Spherisorb ODS-2 column. For abbreviations of amino acids and biogenic amines see Table 2.

ly using a single hydrolyzate standard sample or a protein hydrolyzate for controlling. In a collaborative study on the determination of free amino acids in cheese samples, the results of the dabsyl method were compared with those obtained by ion-exchange chromatography and RP-HPLC of FMOC/OPA derivatives and found to be in good accordance [26].

4. Applications

We have applied our method to the analysis of free amino acids and biogenic amines in human plasma (Fig. 3), cortex, Parmesan cheese (Fig. 4), ham (Fig. 5), seasonings and rice wine. As could be expected, amino acid and biogenic amine profiles are greatly varying within different types of individual samples, but no interference of the different matrices on the separation of the dabsyl derivatives was observed. With the possibility of obtaining data sets of usually more

than 30 components for a food sample like cheese, the method is valuable for quality (“identity”) control [24]. Furthermore, the complex information that can be obtained for numerous amino acids and amines in various biological materials may be helpful in clinical diagnosis or protein analysis.

5. Conclusion

The sample preparation and derivatization procedure was optimized to achieve an efficient sensitive and reliable simultaneous determination of free amino acids and biogenic amines over a wide range of concentration. For the chromatographic separation of the dabsyl derivatives of amino acids and amines, TEA has proved to be a very effective additive to the aqueous mobile phase. The use of an automated derivatization device clearly improves the performance of the method, additionally avoiding

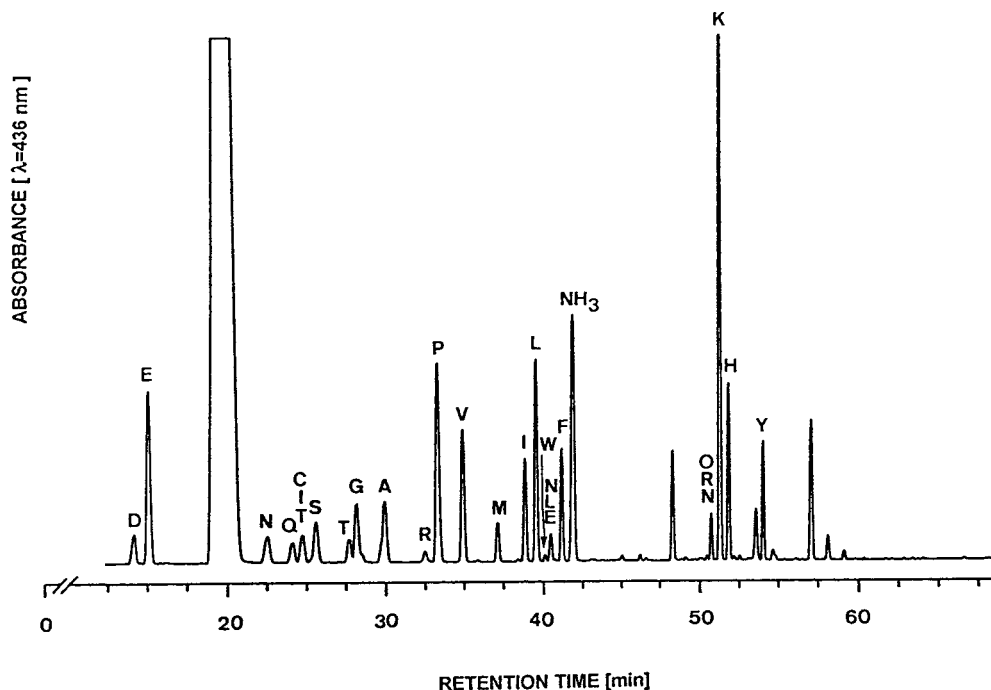


Fig. 4. RP-HPLC separation of amino acids extracted from Parmesan cheese. For chromatographic conditions and abbreviations see Fig. 3 and Table 2.

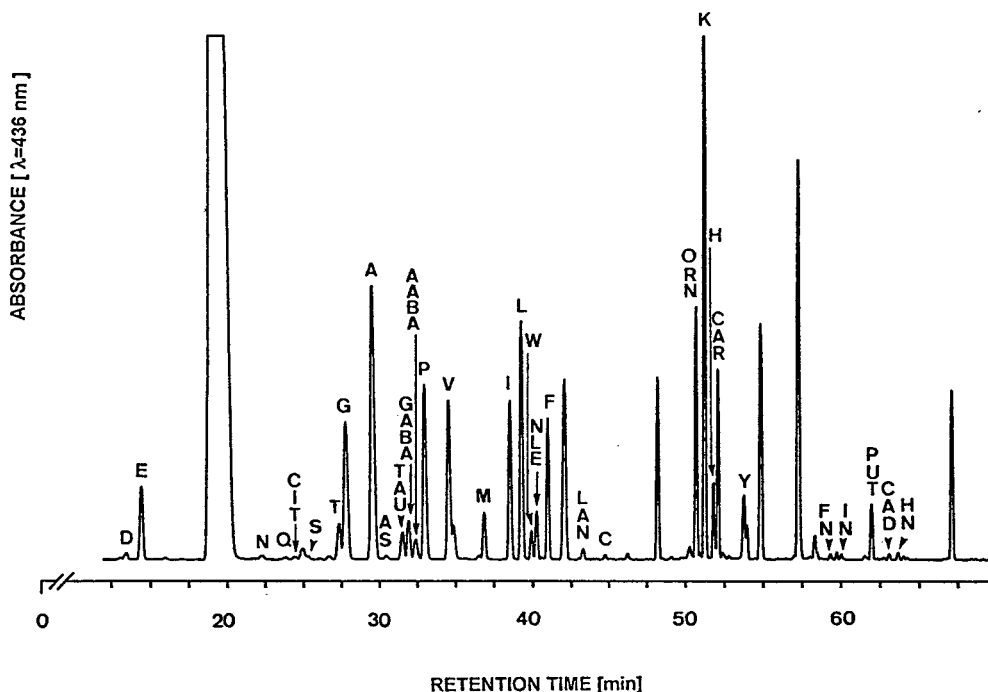


Fig. 5. Amino acid and biogenic amine profiles of ham. For chromatographic conditions and abbreviations see Fig. 3 and Table 2.

laboratory hazard from dabsyl chloride. Acceptable linearity, repeatability and recovery values in combination with feasible analysis time makes the method a serious alternative to conventional amino acid and amine analysis by the ion-exchange/ninhydrin or to RP-HPLC separation methods in combination with pre- or post-column derivatization procedures.

Acknowledgements

This work was kindly supported by the Bayerisches Staatsministerium für Ernährung, Landwirtschaft und Forsten – Sondervermögen der Milch- und Fettwirtschaft.

The authors thank Mrs. D. Luginger and Mrs. S. Ebert for excellent technical assistance.

References

- [1] J.K. Lin and J.Y. Chang, *Anal. Chem.*, 47 (1975) 1634.
- [2] J.K. Lin and C.C. Lai, *J. Chromatogr.*, 227 (1982) 369.
- [3] J.-Y. Chang, R. Knecht and D. Braun, *Biochem. J.*, 199 (1981) 547.
- [4] J.-Y. Chang, P. Martin, R. Bernasconi and D. Braun, *FEBS Lett.*, 132 (1981) 117.
- [5] J.-Y. Chang, R. Knecht and D. Braun, *Biochem. J.*, 203 (1982) 803.
- [6] J.-Y. Chang, R. Knecht and D. Braun, *Methods Enzymol.*, 91 (1983) 41.
- [7] J.-Y. Chang, *J. Chromatogr.*, 295 (1984) 193.
- [8] R. Knecht and J.Y. Chang, *Anal. Chem.*, 58 (1986) 2375.
- [9] J.Y. Chang, R. Knecht, P. Jenoe and S. Vekemans, in T.E. Hugli (Editor), *Techniques in Protein Chemistry*, Academic Press, San Diego, CA, 1989, p. 305.
- [10] V. Stocchi, L. Cucchiari, G. Piccoli and M. Magnani, *J. Chromatogr.*, 349 (1985) 77.
- [11] V. Stocchi, G. Piccoli, M. Magnani, F. Palma, B. Biagiarelli and L. Cucchiari, *Anal. Biochem.*, 178 (1989) 107.
- [12] J. Vendrell and F.X. Avilés, *J. Chromatogr.*, 358 (1986) 401.
- [13] M. Nieder, G.J. Hughes, S. Frutiger and E. Grom, *Labor Praxis*, 14 (1990) 26.
- [14] H.J. Schneider, *Chromatographia*, 28 (1989) 45.
- [15] D.A. Malencik, Z. Zhao and S.R. Anderson, *Anal. Chem.*, 184 (1990) 353.
- [16] A. Watanabe, J. Semba, A. Kurumaji, S. Kumashiro and M. Toru, *J. Chromatogr.*, 583 (1992) 241.

- [17] E.H.J.M. Jansen, R.H. van den Berg, R. Both-Miedema and L. Doorn, *J. Chromatogr.*, 553 (1991) 123.
- [18] D. Drnevich and T. Vary, *J. Chromatogr.*, 613 (1993) 137.
- [19] E. Mentasti, C. Sarzanini, O. Abollino and V. Porta, *Chromatographia*, 31 (1991) 41.
- [20] H. Treptow and A. Askar, *Ernährung*, 14 (1990) 9.
- [21] W.J. Hurst, *J. Liq. Chromatogr.*, 13 (1990) 1.
- [22] A. Otto, S. Kostka, A. Müller and G. Etzold, in B.J. Radola (Editor), *Elektrophorese Forum '91*, Bode, Freising, 1991, p. 351.
- [23] S.A. Cohen and D. Strydom, *Anal. Biochem.*, 174 (1988) 1.
- [24] I. Krause, A. Bockhardt, H. Neckermann and H. Klostermeyer, in preparation.
- [25] German Normative Institute, DIN 32 645, Beuth, Berlin, 1994.
- [26] U. Bütikofer, Evaluation of FLAIR/COST 902 collaborative test III, FAM Federal Dairy Research Institute Report, CH-Liebefeld, 25-8-1992.

Microcalorimetric characterization of the anion-exchange adsorption of recombinant cytochrome b_5 and its surface-charge mutants

Davinder S. Gill¹, David J. Roush², Kari A. Shick³, Richard C. Willson*

Department of Chemical Engineering, University of Houston, 4800 Calhoun Avenue, Houston TX 77204-4792, USA

First received 26 October 1994; revised manuscript received 22 March 1995; accepted 27 March 1995

Abstract

The adsorption of recombinant soluble tryptic fragment of rat cytochrome b_5 on the strong anion exchanger Mono Q was studied using isothermal titration calorimetry and differential scanning calorimetry (DSC). Titration calorimetry results obtained at low levels of adsorbed protein show increasingly endothermic (unfavorable) enthalpies of binding with increasing surface coverage, confirming the heterogeneous nature of binding. The enthalpy of adsorption declines toward zero at higher loadings. At low surface coverage, enthalpies increase linearly with temperature, giving rise to a positive value of ΔC_p . Enthalpies of adsorption depend strongly on the history of the adsorbent. DSC is used to show that cytochrome b_5 is stable in both free and adsorbed states at all temperatures used in the titration calorimetric experiments. Site-directed mutants of recombinant cytochrome b_5 carrying single charge-neutralizing substitutions are used to test the contributions of particular residues to the thermodynamics of adsorption. Like those derived from van 't Hoff analysis of equilibrium adsorption isotherms and HPLC retention data, calorimetric enthalpies of adsorption are positive, confirming the dominant role of entropic effects in ion-exchange adsorption in this system.

1. Introduction

The adsorption of proteins at solid–liquid interfaces has been the subject of active interest because of its biomedical and technological importance [1,2]. Much attention has been focused

on protein adsorption on hydrophobic surfaces [3–13], particularly those used in biomedical applications [1,2]. It is well established that protein molecules often undergo irreversible adsorption on hydrophobic surfaces, generally associated with conformational changes in the protein upon binding. The degree of conformational change increases with increasing hydrophobicity of the adsorbent and the protein [13–17].

The interactions of proteins with charged hydrophilic surfaces (e.g., ion-exchange adsorbents) have been less well characterized on a fundamental level. There is an extensive body of

* Corresponding author.

¹ Present address: Department of Surgery, Massachusetts General Hospital and Harvard Medical School, Boston, MA 02114, USA.

² Present address: Merck and Co., Bioprocess R&D, P.O. Box 2000, Rahway, NJ 07065, USA.

³ Present address: Tanox Biosystems, Houston, TX 77025, USA.

literature concerning the use of hydrophilic polyelectrolyte surfaces in the chromatographic separation of proteins, but equilibrium studies of the thermodynamics of protein adsorption on chromatographic adsorbents are uncommon. The resolution with which variations in thermodynamic behavior as a function of protein loading and temperature can be detected by batch equilibrium experiments is limited, and the indirect method of van 't Hoff analysis may be confounded by the presence of multiple sub-processes associated with adsorption. The recent advent of highly sensitive titration microcalorimeters has opened new opportunities for detailed investigation of the thermodynamics of adsorption.

Microcalorimetry has been previously used to examine the interfacial behavior of two human serum proteins— γ -globulin and fibrinogen—on silica surfaces [18,19], of human serum albumin and bovine pancreatic ribonuclease on negatively charged hydrophobic polystyrene lattices [5–7], and of human serum albumin on hematite [20]. Reported enthalpies of adsorption were negative for γ -globulin and fibrinogen (indicative of enthalpically promoted adsorption) and positive for adsorption of human serum albumin and bovine pancreatic ribonuclease on polystyrene and hematite (entropically driven adsorption). To our knowledge, only one report other than the present contains calorimetric data for protein adsorption on ion-exchange surfaces [21]. This work reported enthalpies of adsorption of bovine serum albumin on two kinds of strong anion exchangers—a cellulose-based fibrous material and a polyethyleneimine-based macroporous resin. Values of adsorption enthalpies were mostly positive (entropically driven adsorption) for the former and mostly negative (enthalpically driven adsorption) for the latter. In addition, the authors reported a characteristic, surface coverage dependent change in adsorption enthalpies which was also observed in the present work.

Our ongoing interest has been in characterizing the structural and thermodynamic contributions to adsorption of the well-characterized recombinant soluble tryptic fragment of rat cytochrome b_5 on the monodisperse, hydrophilic

quaternary amine-based strong anion exchanger, Mono Q. To this end, we have used site-directed surface-charge mutants and titration calorimetry as mutually complementary strategies. Our previous work on the cytochrome b_5 -Mono Q system [22–24] has established that adsorption on Mono Q is reversible (through exchange) and that batch and HPLC van 't Hoff enthalpies of adsorption are positive. Scatchard analyses of adsorption isotherms established that adsorption was heterogeneous, with the apparent adsorption affinity declining with protein loading. This result implied that enthalpies derived from van 't Hoff analysis of adsorption data might represent averages over a range of enthalpies associated with adsorption at different binding sites or different binding orientations. In the present work, we describe the use of isothermal titration microcalorimetry for direct quantitation of the enthalpy of adsorption at specific temperatures, as a function of loading. We complement these measurements with studies involving site-directed charge mutants of cytochrome b_5 .

2. Experimental

2.1. Sample preparation

A synthetic gene directing the expression of the soluble tryptic fragment of rat cytochrome b_5 in *Escherichia coli* was synthesized by von Bodman et al. [25]. Bacteria were grown in batches of 5 l, as described previously [26]. Cytochrome b_5 and its mutants were purified from *E. coli* lysates by ion-exchange and size exclusion chromatography, and were characterized as homogeneous preparations using SDS-PAGE, spectrophotometry, and HPLC as described previously [22–24]. Protein samples were concentrated to 5–10 mg/ml using Centriprep YM 10 cartridges (Amicon) in a Beckman J2-21 centrifuge (Beckman Instruments) at 3800 g at 4°C, in two steps of one hour each, using the same cartridge.

Mono Q (Pharmacia, average particle size $10 \pm 0.1 \mu\text{m}$, pore diameter approximately 1000 Å) is based on a hydrophobic, crosslinked, styrene divinyl benzene base derivatized with a

hydrophilic layer bearing quaternary amine groups. Mono Q used in this work was the generous gift of Prof. J.-C. Janson of Pharmacia LKB, and was supplied as a suspension in a 20% ethanol–water solution with sulfate as the counterion. The adsorbent was first equilibrated with 1 M NaCl to allow exchange of chloride for sulfate counterions, and then washed five times (15 min each at room temperature) with 10 mM Tris, pH 8.0 + 0.1 mM EDTA. The completeness of equilibration by this procedure was confirmed by a control experiment in which the conductivity of the supernatant liquid was found to be equal to that of 10 mM Tris buffer. Equilibrium adsorption isotherms for wild-type cytochrome b_5 on fresh Mono Q were measured as described previously [23] at 25°C, 10 mM Tris + 0.1 mM EDTA, pH 8.0. Mass balances calculated for each experiment routinely closed with recoveries of 90% or more, except where noted.

For calorimetric experiments the Mono Q bead density was adjusted to $5 \cdot 10^6 \text{ ml}^{-1}$ using a hemacytometer [23]. This adsorbent concentration was found to maintain a high signal-to-noise ratio (> 100) in the experiments. Careful sample preparation was required to eliminate any mismatch in pH or buffer concentration between the protein and Mono Q samples, both of which were adjusted to pH 8.0 at the experimental temperature. Small pH mismatches could potentially produce dilution or buffer titration enthalpy artifacts. The concentrated protein sample and the Mono Q suspension used in each experiment were codialyzed at 4°C against the same 10 l reservoir of 10 mM Tris + 0.1 mM EDTA, pH 8.0 buffer in separate dialysis tubes (molecular mass cutoff of 7000; Spectrum Industries) with constant stirring for at least 16 h.

2.2. Adsorption isotherm measurement

Equilibrium adsorption isotherms were measured as described previously [22]. Experiments were performed at a density of 10^7 ml^{-1} to match the Mono Q concentration used in the titration calorimetry experiments described

below. Isotherms were measured using fresh Mono Q.

2.3. Isothermal titration calorimetry

Calorimetric measurements were made on an Omega titration microcalorimeter (Microcal) interfaced with a 386/25 personal computer (IST, OH, USA) and equipped with a Keithley Model 181 nanovolt pre-amplifier. The instrument was protected from electrical noise by an on-line voltage conditioner (Tripp Lite) and a ferroresonant transformer (General Signal). Isothermal titration calorimetry has been reviewed by Friere et al. [27]. The design and operation of the Omega instrument have been described by Wiseman et al. [28]. The calorimeter was connected to a Haake A81 external water bath for temperature stabilization. For the measurements at 25°C, the external bath was set at 21.0°C and the sample cell warmed to 25°C before equilibration was initiated. Temperature was routinely controlled within $\pm 0.3^\circ\text{C}$ over the course of an experiment. The reaction cell and the loading and injection syringes were rinsed with dialysis buffer prior to filling them with the dialyzed protein or adsorbent. Samples were degassed by warming to room temperature prior to loading, and care was taken not to introduce air bubbles into the cell or the injection syringe. An amount of 2 ml (ca. 10^7) dialyzed Mono Q beads was placed in the reaction cell, which was agitated at 600 rpm to ensure efficient mixing. Protein samples (0.36–0.72 mM) were loaded into the 250 μl stirrer–syringe assembly, which was then installed into the calorimeter. A partial vacuum (residual pressure about 100 Torr) was applied to the compartment around the sample and reference cells to eliminate any condensation on the exterior walls of the cells, and the vacuum line was kept sealed until the end of the experiment. The instrument was regularly calibrated by filling the sample cell with buffer alone and measuring the response to standard heat pulses generated by electrical dissipation, as suggested by the manufacturer. Injection of pure buffer into the cell according to the injection schedule used in the experiments resulted in a flat baseline.

Equilibration typically required 30–60 min to reach a baseline rms noise of less than 15 ncal/s (often < 10 ncal/s). A 2- or 5- μ l pre-injection was made to account for any syringe leakage that might have occurred during equilibration, as recommended by the manufacturer. Power associated with such pre-injections was negligibly small compared to that observed for the experimental injections. For this reason, enthalpies of adsorption were calculated based on the experimental injections alone. Protein samples were titrated onto the adsorbent typically in twelve 10- μ l injections, each lasting 15 s. Mono Q was titrated with protein and not vice versa because the high affinity of adsorption in this system would cause the injected beads to be immediately loaded with a significant amount of protein. Incremental addition of limiting amounts of protein allowed study of the surface-coverage dependence of the enthalpy of adsorption. A 5-min interval was allowed between injections for equilibration of the adsorbed protein; this period was more than sufficient for complete return of the peaks to baseline. Data were collected and analyzed using Microcal's OMEGA and ORIGIN algorithms, respectively.

At the end of each experiment, the protein-loaded adsorbent particles were withdrawn from the calorimeter cell and centrifuged at 2700 g for 15 min in a centrifuge with a swinging-bucket-type rotor (PR-6000, IEC) to allow the supernatant to be accurately separated from the ion-exchange beads. The adsorbed protein was eluted from the recovered beads by incubation with 2 ml of a 0.5 M NaCl solution in 10 mM Tris, pH 8.0, followed by centrifugation. This procedure had been shown to give essentially complete recovery of the adsorbed protein, and not to alter its optical properties [23]. The absorbances of the original supernatant and of the liquid containing protein eluted from the beads were measured at 412 nm using a DU-64 spectrophotometer (Beckman). Cytochrome b_5 concentration was calculated using an extinction coefficient of 130 mM⁻¹ cm⁻¹ for the strong Soret band of the oxidized protein at this wavelength [25]. The spectra of protein samples were also measured from 240 to 700 nm. This allowed

for detection of any major change in the tertiary structure of the free or the desorbed protein, since the spectral properties of cytochrome b_5 are altered upon unfolding. Mass balances were calculated to control for any loss of protein by proteolysis, denaturation, or adsorption on the calorimeter cell surfaces, and these normally closed within 10%. Eluted protein was discarded at the end of each experiment; the cell was cleaned with 500 ml of an 0.2% solution of the surfactant Tween 20, followed by 2 l of deionized water. When required, the cell was also rinsed with 500 ml 1 M NaOH solution to hydrolyze any proteinaceous material deposited in the cell, followed by rinsing with deionized water until the pH returned to neutral.

2.4. Titration calorimetry data analysis

Experimental data were collected as power, P (μ cal s⁻¹) vs. time, and were integrated and scaled by the amount of protein adsorbed to give the apparent enthalpy of adsorption, ΔH_{ads} (kcal/mol) associated with each injection. Typically, several hundred micrograms of the protein were injected in 12 equal volumes. Since a negligible amount of protein (< 25 μ g) was found to remain unbound at the end of each experiment, it was assumed that all protein in each injection was adsorbed. Thus, the total amount of adsorbed protein divided by the number of injections made gave the amount adsorbed per injection. A correction for heat of dilution (ΔH_{dil}) of the protein was calculated from the results of control experiments, identical to the adsorption experiments but with the adsorbent omitted. Corrected heats of adsorption were calculated according to the relation $\Delta H_{\text{ads}} = \Delta H_{\text{obs}} - \Delta H_{\text{dil}}$. The variation in adsorption enthalpies with surface loading necessitated adoption of a standard protocol to obtain average values of ΔH_{ads} , so that data between different experiments could be directly compared. For this reason, it was decided to plot the cumulative heat of adsorption ($\sum[\Delta H_{\text{ads}}]_i$, where i is the injection number, $i = 1, 2, \dots, n$) against increasing adsorbed-protein concentration. A linear least squares regression of these data was used to

interpolate an average ΔH_{ads} for 500 μg (0.037 μmol) of protein adsorbed per 10^7 beads. The value of 500 μg per 10^7 beads represents relatively low surface loading, allowing the resulting data to be free from effects of lateral interactions. Also, this level of surface coverage approximates the loadings at which the adsorption isotherm measurements were made, allowing direct comparison with calorimetric results. A value of 13 603 was used as the relative molecular mass of recombinant soluble cytochrome b_5 [25].

2.5. Differential scanning calorimetry

Protein samples were prepared and concentrated as described above. Samples were extensively dialyzed against 10 l of 10 mM sodium phosphate, pH 8.0. DSC was performed on an MC-2 (MicroCal) instrument located in the Biochemical Laboratory, Baylor College of Medicine, Houston, TX, USA. The instrument was interfaced with an IBM AT computer running the Microcal DA-2 software package for data acquisition and analysis (for reviews of DSC, refer to Refs. [29,30]). The calorimeter was connected to a recirculating, refrigerated bath for optimal temperature control. Experiments were conducted at scan rates of 0.5°C/min under a nitrogen atmosphere of about 138 kPa to prevent sample outgassing at elevated temperatures. Only heating scans were recorded because irreversible denaturation was expected. As the purpose of these experiments was to establish the thermal stability of cytochrome b_5 under the conditions of the titration calorimetric experiments, no attempt was made to calculate the enthalpies of unfolding.

For DSC of the unbound protein, a baseline scan was first recorded by filling both the reference and the sample cells with dialysis buffer and scanning from 8 to 90°C. No transitions were observed on the baseline. The solution from the sample cell was then replaced with a 10 mg/ml solution of cytochrome b_5 and the scan repeated. For DSC of the bound protein, about 10^7 fresh Mono Q beads were loaded with a large excess (0.75 μmol) of cytochrome b_5 in 10 mM sodium

phosphate, pH 8.0. After equilibration with gentle agitation for one hour (a period found previously to be sufficient for adsorption equilibration) the supernatant containing unadsorbed protein was removed. Thereafter, the beads were washed once with 10 mM phosphate buffer and resuspended in 20% w/v dextran (Sigma, average molecular mass 168 000) to maintain them in suspension over the period of the experiment. For protection of the DSC cell, it was verified in advance that such a solution did not congeal when heated to 100°C. The stability of soluble cytochrome b_5 which had never contacted Mono Q was also measured separately in the presence and absence of 20% dextran. Control scans on Mono Q and dextran alone were also performed.

3. Results

3.1. Adsorption isotherms and Scatchard plots

Equilibrium isotherms for adsorption of wild-type cytochrome b_5 on fresh Mono Q at the low ionic strength used in the calorimeter experiments (10 mM Tris + 0.1 mM EDTA, pH 8.0) at 25°C are shown in Fig. 1. The different symbols represent the results of independent experiments. The inset emphasizes the high affinity of adsorption, as shown by the close proximity of the initial slope of the isotherm to the y-axis

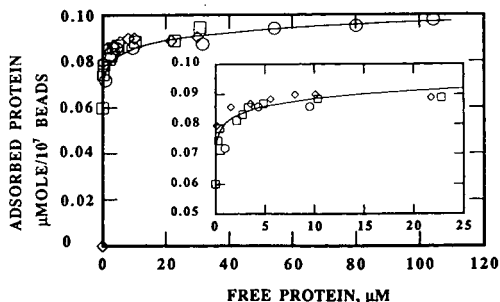


Fig. 1. Isotherms for adsorption of cytochrome b_5 on Mono Q, 25°C in 10mM Tris + 0.1 mM EDTA, pH 8.0 (three independent measurements). Inset shows data for lower surface coverage. Initial slopes virtually coincide with the y-axis depicting the high affinity of adsorption.

even at low free protein concentration. Because of such high affinity, nearly all protein injected into the calorimeter cell is adsorbed. A representative set of isotherm data from Fig. 1 is plotted in Scatchard form in Fig. 2 to illustrate the heterogeneous nature of adsorption. This result is in agreement with our previous observations of heterogeneity of adsorption at higher ionic strengths in this system [23,24].

3.2. Titration calorimetry

Fig. 3 shows isothermal titration calorimetric data for the adsorption of wild-type cytochrome b_5 on fresh Mono Q measured at 25°C in 10 mM Tris buffer + 0.1 mM EDTA, pH 8.0. The results shown are representative of multiple replicate experiments. Twelve 10- μ l injections of cytochrome b_5 (6 mg/ml) were made into a suspension of Mono Q. The top panel in Fig. 3 shows the raw power corresponding to the apparent heats of adsorption (upward peaks) as well as heats of dilution (smaller, downward peaks) derived from separate experiments, depicted as $\mu\text{cal s}^{-1}$ versus time (in minutes). Manual peak-by-peak determination of the resting baseline resulted in a better fit than the automatic estimation provided by the calorimeter software; the two procedures gave similar average results. Integrated heats of adsorption

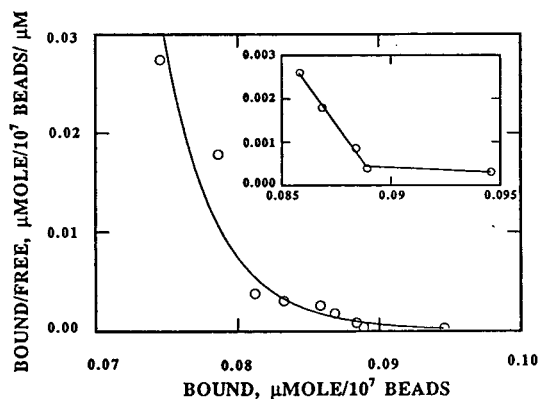


Fig. 2. Scatchard plot of a representative data set from Fig. 1. Concave upward plot suggests negative cooperativity or the presence of heterogeneous binding sites. Inset shows curvature for low surface coverage.

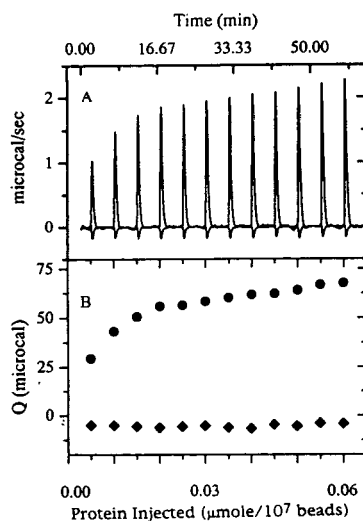


Fig. 3. Titration microcalorimetric data collected on a MicroCal Omega instrument for the adsorption of wild-type cytochrome b_5 on Mono Q at 25°C in 10 mM Tris + 0.1 mM EDTA, pH 8.0. Twelve 10- μ l injections were made into the cell containing a suspension of about 10^7 Mono Q beads in the same buffer. Panel A shows raw data; upward peaks correspond to apparent heats of adsorption, smaller, downward peaks are the heats of dilution measured in a separate experiment in which the adsorbent was omitted. Panel B shows the integrated heats of adsorption (\bullet) and heats of dilution (\blacklozenge) in microcalories as a function of injection number.

and dilution for each peak are shown in the lower panel of Fig. 3. The kinetics of heat evolution observed in the raw data suggest that adsorption is complete well within the time between injections (5 min). The effect of surface coverage on heat of adsorption was further studied by making a larger number of injections (25); the results obtained are shown in Fig. 4. The amount of protein adsorbed per injection was used to calculate the incremental heat of adsorption as a function of protein adsorbed, by dividing the integrated heats of adsorption by the moles of protein adsorbed in each injection (Fig. 4, lower panel). Because of the heterogeneous nature of the adsorbent surface no attempt was made to extract an equilibrium binding constant (or Gibbs free energy of binding, ΔG_{ads}) from the calorimetric data. In the past, attempts have been made to calculate the ΔG_{ads} from adsorption isotherm measurements [31–33]. Because of

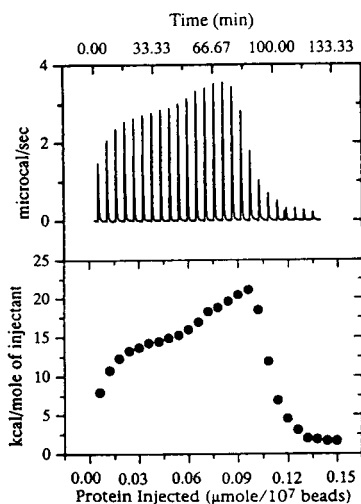


Fig. 4. Titration microcalorimetric data for the adsorption of wild-type cytochrome b_5 on Mono Q at 25°C in 10 mM Tris + 0.1 mM EDTA, pH 8.0. Twenty-five 10- μ l injections of the protein were made into a suspension of about 10^7 Mono Q beads in the same buffer. The top panel shows corrected data for adsorption and the bottom panel shows the integrated heats of adsorption in kcal/mol.

the uncertain validity of such calculations (primarily, lack of assured reversibility of adsorption), numbers derived for ΔG_{ads} through such analyses must be viewed with caution [34].

The majority of the fresh Mono Q used in this study was received as a liquid suspension. The average ΔH_{ads} (to a loading of 500 μ g protein/ 10^7 beads) for this material was 11.4 kcal/mol. We wished to compare the behavior of this material with that of Mono Q recovered from packed FPLC columns, which was used in our previous work [23,24]. The ΔH_{ads} value obtained with Mono Q extracted from a fresh FPLC column and prepared as described above was 10.4 kcal/mol, in reasonable agreement with the material received unpacked. Practical use of ion-exchange adsorbents involves many cycles of adsorption and regeneration, which could affect binding characteristics. We therefore examined the enthalpy of adsorption of cytochrome b_5 onto Mono Q that had been regenerated after isotherm measurements in which the adsorbent was loaded to 20–25% of its capacity [23] with cytochrome b_5 . Mono Q was regenerated by extensive elution with 1 M NaCl until the super-

natant A_{280} fell to values approximately equal to that of the buffer alone ($\ll 0.05$ AU), and then used in calorimetric experiments under conditions identical to those of Fig. 4. Adsorption of wild-type cytochrome b_5 on regenerated Mono Q gave an enthalpy of adsorption of only 0.3 kcal/mol (up to 500 μ g/ 10^7 beads) at 25°C in 10 mM Tris, pH 8.0, well below the values obtained with the two types of fresh Mono Q. In the presence of high ionic strength (> 200 mM NaCl), no detectable adsorption or enthalpic signal was observed for fresh or regenerated Mono Q. These results suggest that microcalorimetry may offer a particularly sensitive method of characterizing the surface properties of chromatographic media, as regenerated columns give similar chromatographic separation [35]. It is likely that traces of uneluted protein remain after regeneration, and/or that cycles of loading and elution change the character of the ion-exchange surface on Mono Q. This question is the subject of further investigation. For the present work, fresh Mono Q was used in all experiments reported hereafter.

As a check for potential contributions of buffer titration enthalpy to the observed heats of adsorption, a control experiment was performed with the use of sodium phosphate buffer instead of Tris. The heat of ionization (ΔH_{ion}) of sodium phosphate buffer at 25°C ($\Delta H_{\text{ion}} = 1.22$ kcal/mol) is one-tenth that of Tris ($\Delta H_{\text{ion}} = 11.51$ kcal/mol; Ref. [36]). The average value obtained for ΔH_{ads} in phosphate buffer was 0.5 kcal/mol, in agreement with results using Tris, allaying any concern of a buffer contribution to the observed enthalpies of adsorption. This result also establishes that the adsorption of cytochrome b_5 is not accompanied by significant proton uptake or liberation.

Experiments were also performed at 12 and 37°C to examine the temperature dependence of the adsorption enthalpy (Fig. 5). These experiments were conducted in 10 mM Tris adjusted to pH 8.0 at the experimental temperature. All samples were pre-equilibrated to the experimental temperature to allow for rapid equilibration of the calorimeter, and to avoid degassing of samples as temperature increased. Experiments

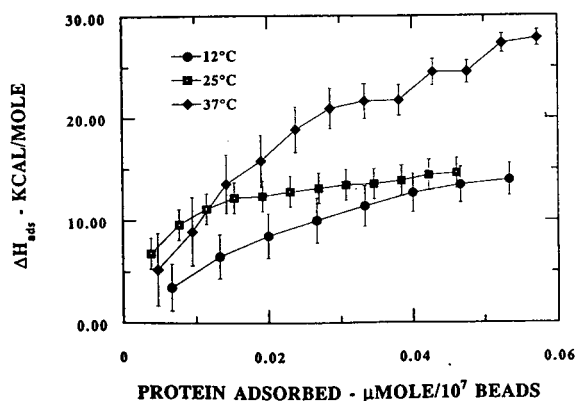


Fig. 5. Enthalpies of adsorption of cytochrome b_5 on Mono Q as a function of extent of surface coverage, at three different temperatures.

at subambient conditions required cooling of the reaction cell by an external water bath to well below the desired temperature combined with calorimeter-controlled warming. For this reason, the external bath circulator was set at 2.0°C for the 12°C experiment and 37.0°C for the 37°C experiment. For accurate quantitation of the extent of adsorption, the contents of the sample cell were recovered at the end of each experiment and promptly centrifuged to allow assessment of the extent of adsorption under the experimental conditions. These experiments were conducted under conditions of low surface coverage to allow for comparison with van 't Hoff enthalpies derived from measurements at similar loadings. Average ΔH_{ads} up to 500 μg of protein adsorbed per 10^7 Mono Q beads (0.037 $\mu\text{mol}/10^7$ beads) are plotted in Fig. 6. These values increase linearly with temperature from 12 to 37°C, giving a correlation coefficient of 0.99 and a positive ΔC_p at this loading of $286 \pm 27 \text{ cal mol}^{-1} \text{ }^\circ\text{C}^{-1}$ (Fig. 6). It is clear from the results presented above, however, that the magnitude (and even sign) of ΔC_p depends of the extent of loading. At higher loadings the dependence of ΔH_{ads} on temperature is no longer linear, suggesting a more complex relationship between the two.

Finally, enthalpies of adsorption were measured for three site-directed mutants of cyto-

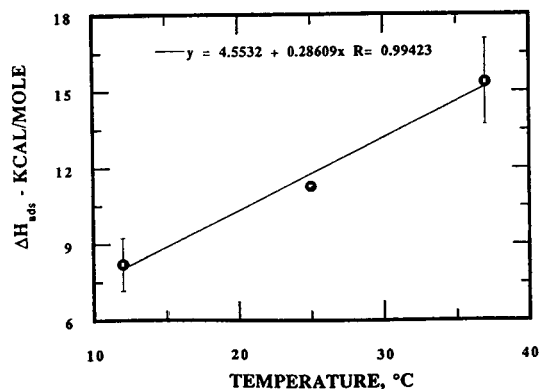


Fig. 6. ΔH_{ads} calculated for a loading of 500 μg protein adsorbed per 10^7 beads (see text for details) as a function of temperature, derived from averages of duplicate experiments. Line represents linear least squares fit with slope corresponding to $\Delta C_p = 286 \pm 27 \text{ cal } ^\circ\text{C}^{-1} \text{ mol}^{-1}$.

chrome b_5 with single amino-acid substitutions on different regions of the protein surface. We have previously identified [24] a preferred chromatographic contact region for the anion-exchange adsorption of cytochrome b_5 based on the pronounced effect of mutations in the dominant cluster of negatively charged groups on the protein surface (Glu 41, 47, 48, and 52) on the stoichiometry and affinity of binding. Mutant E48Q belongs to the preferred cluster of negative groups, D64N lies in the negatively charged domain opposite the E48Q cluster, and E15Q lies away from the dominant negative regions around the heme-binding cleft. Data for the enthalpies of adsorption as a function of surface coverage for the wild-type protein along with these three mutant forms are shown in Fig. 7.

3.3. Differential scanning calorimetry

The DSC thermograms of phosphate buffer or phosphate-buffered 20% dextran solution containing Mono Q alone were featureless. DSC of soluble wild-type cytochrome b_5 in phosphate buffer produced a single, rather broad transition around 75°C, while adsorption of cytochrome b_5 to Mono Q in the presence of 20% dextran reduced the protein's transition temperature to about 50°C (Fig. 8). In the presence of a phosphate-buffered 20% dextran solution, DSC of

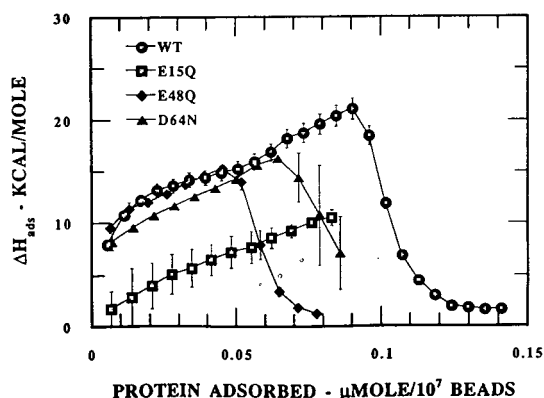


Fig. 7. ΔH_{ads} for adsorption of mutant forms of cytochrome b_5 listed in Table 1 onto Mono Q at 25°C in 10 mM Tris + 0.1 mM EDTA, pH 8.0. WT represents wild-type cytochrome b_5 , E15Q represents the mutation Glu15→Gln, E48Q the mutation Glu48→Gln, and D64N represents Asp64→Asn.

soluble cytochrome b_5 produced a major transition at 78°C. The need to include dextran in the DSC samples and its apparent effect on cytochrome b_5 stability prevents the DSC measurements from being conducted under conditions completely representative of those of the titration calorimetric experiments, but in all cases cytochrome b_5 is stable to temperatures significantly above the highest temperature used in our

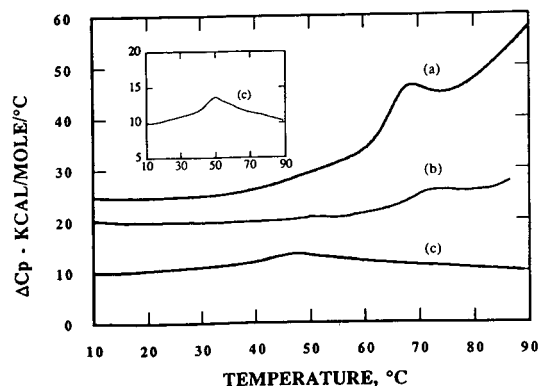


Fig. 8. Differential scanning calorimetric data for (a) free cytochrome b_5 in 10 mM phosphate buffer, (b) free cytochrome b_5 in 10 mM phosphate buffer + 20% dextran, and (c) cytochrome b_5 bound to Mono Q in the presence of 10 mM phosphate buffer + 20% dextran. Measurements were made on a MicroCal MC-2 scanning calorimeter using scan rates of 30°C/h. Inset shows the thermal transition for the bound protein (T_m ca. 50°C) in greater detail.

adsorption studies (37°C). It should also be noted that mass balances on the free and adsorbed protein after titration calorimetry closed within 2% for experiments at 12 and 25°C, and within 18% for experiments at 37°C, implying that significant irreversible denaturation may have occurred only at 37°C or above. Denaturation under such conditions could make some contribution to the observed enthalpy of adsorption. Reduced recoveries of cytochrome b_5 bound to Mono Q under conditions of low ionic strengths and high retention times have also been observed in our independent HPLC studies [22]. Further investigation of these issues is in progress.

4. Discussion

The high affinity of the adsorption isotherm even at significant loadings implies that ΔG_{ads} is negative under the conditions used. The heterogeneous nature of the adsorbent surface and the ill-characterized surface-charge density and distribution, however, preclude calculation of a meaningful value of ΔG_{ads} [34]. Furthermore, the van 't Hoff analysis often used for calculation of ΔH_{ads} is based on the assumption that a reversible equilibrium exists between the bound and the free protein. It lumps together all subprocesses accompanying protein adsorption and is therefore only a qualitative indicator of adsorption thermodynamics. Direct microcalorimetry does not resolve the difficulties in estimating ΔG_{ads} , but does allow for a more robust quantitation of the enthalpy of adsorption than is achievable by van 't Hoff analysis. It also allows for examination of the potential variation of ΔH_{ads} with loading and with temperature in a more direct manner than is possible by any other means.

Microcalorimetric characterization of the adsorption of cytochrome b_5 on fresh Mono Q shows endothermic heats of adsorption which, at low loadings, increase with the amount of protein adsorbed (Fig. 3). Heats of dilution, in contrast, are constant, exothermic, and much smaller (about -1 kcal/mol). Calorimetric mea-

surements made at higher surface coverages (Fig. 4) show rapidly declining enthalpies of adsorption after the initial linear increase. A transition in adsorption enthalpies occurs at a loading of about $0.09 \mu\text{mol}/10^7$ beads, closely corresponding to the higher-slope region of the adsorption isotherms (Fig. 1). However, mass balances performed after the last injection show that of the total protein recovered from the calorimeter cell, $>95\%$ is in the bound state. It is noteworthy that the adsorption enthalpy has a uniformly positive sign, implying an entropic driving force under these conditions. Positive values of ΔH_{ads} have also been calculated for this system from the results of HPLC and equilibrium adsorption experiments, as discussed below. The large increase in entropy may arise from liberation of bound ions from the adsorbent and protein surfaces, as well as waters of hydration from both surfaces.

Between 12 and 37°C , the average ΔH_{ads} (to $500 \mu\text{g}/10^7$ beads) increases from about 8 kcal/mol to 15 kcal/mol, giving ΔC_p ($=\partial(\Delta H_{\text{ads}}/\partial T)_p$) equal to $286 \pm 27 \text{ cal mol}^{-1} \text{ }^\circ\text{C}^{-1}$, relatively independent of temperature ($r=0.99$). A classical enthalpy–entropy compensation effect [37,38] does not seem to be active as both ΔG_{ads} [22–24] and ΔH_{ads} increase with temperature over the range of interest. Positive ΔC_p values are usually attributed to the transfer of nonpolar moieties from a hydrophobic to a more polar environment [39]. Also, the expected sign of ΔC_p for an increase in exposure of electrostatic charges is negative, implying that for the reverse case (creation of electrostatic links, as in ion-exchange adsorption) ΔC_p might be expected to be positive [40]. This is in agreement with arguments made by Norde [34] that in aqueous media changes in ΔC_p are largely due to changes in water structure around the interacting surfaces and transfer of ions from the binding interface to the bulk solvent.

The sign of ΔC_p , however, depends on the conditions under which it is measured. Van 't Hoff analyses of the equilibrium adsorption of cytochrome b_5 gave enthalpies of $+3.8 \text{ kcal/mol}$ at $4\text{--}25^\circ\text{C}$ and -0.7 kcal/mol at $25\text{--}37^\circ\text{C}$ [23]. The overall change in ΔH_{ads} from 4 to 37°C

corresponds to a negative average ΔC_p . In contrast, for HPLC, a small positive value of ΔC_p is implied by the linear van 't Hoff plots observed over temperatures ranging from 4 to 37°C [22]. A similar observation was made by Sigursjold and Bundle [41], who reported opposing signs of ΔC_p measured by van 't Hoff methods and by titration calorimetry. This difference was ascribed to factors such as release or uptake of ions, conformational change, or change in solvation upon association. As discussed above, the possibility of such subprocesses in the adsorption of cytochrome b_5 on Mono Q exists. It should also be noted that the characteristic times of the experimental methods differ significantly. Titration calorimetry reports the enthalpy of processes occurring on a time scale of $1\text{--}5 \text{ min}$, equilibrium adsorption experiments occupy $30\text{--}60 \text{ min}$, and isocratic HPLC retention times can range up to 900 min . The different protein loadings involved can also impair comparison of results obtained by different methods. The influence of loading on thermodynamic parameters is clearly illustrated in Figs. 4 and 5.

Both the bound and the free protein appear to be stable over the entire temperature range used in the titration calorimetry experiments, as shown by the absence of DSC transitions at these temperatures, the closure of mass balances for each experiment, and the results of previous work [42]. Although the observed destabilization upon adsorption requires further investigation, the present results suggest that the observed positive ΔC_p is not primarily due to a conformational-change dependent entropy increase. It may arise both from liberation of waters of hydration at elevated temperature and from partial exposure of buried hydrophobic side chains.

The enthalpy of adsorption varies quite strongly with the history of the adsorbent, although fresh and regenerated Mono Q produced the same chromatographic behavior. Adsorption measurements described in Ref. [23] show that the Z number (apparent number of contacts made by the protein with the adsorbent [48]) is virtually identical for fresh and regenerated Mono Q, and the apparent affinity constant (K)

is 5- to 10-fold higher for the fresh Mono Q. Titration calorimetry in 10 mM Tris buffer at 25°C gave ΔH_{ads} values of 11.4 and 0.3 kcal/mol for fresh and regenerated Mono Q, respectively. Van 't Hoff analysis of batch adsorption data (in 100 mM NaCl at 4–25°C) gave 9.0 kcal/mol for adsorption on the fresh material and 2.9 ± 0.3 kcal/mol for the regenerated material. An HPLC van 't Hoff ΔH_{ads} of 10.6 ± 0.4 kcal/mol was derived from data collected at 4–37°C at 150 mM NaCl on relatively fresh Mono Q; the van 't Hoff ΔH_{ads} fell with increasing ionic strength to 5.2 ± 0.4 kcal/mol at 400 mM NaCl [22]. Although the reproducibility of the HPLC experiments is excellent, the repeated injection of small amounts of protein relative to the total column capacity makes it uncertain at which point HPLC adsorbents should no longer be regarded as “fresh”. Another unique characteristic of the HPLC experiments is that their duration varies significantly with ionic strength, potentially allowing for greater energetic contributions from slower processes such as conformational rearrangement. Despite the differences among the experimental methods, all give a larger value of ΔH_{ads} for fresh than for regenerated Mono Q. The difference between the calorimetric and the van 't Hoff enthalpies is appreciable, nonetheless it is noteworthy that both methods confirm the entropic driving force under these conditions.

The calorimetric behavior of surface-charge mutants of cytochrome b_5 does not correlate in a direct way with their ion-exchange chromatographic properties. As described elsewhere, equilibrium adsorption and HPLC retention of the protein are dominated by a cluster of negatively charged residues lying around the heme-binding cleft, shown in Fig. 9 [24,53]. Structurally conservative mutations neutralizing charged amino acids in these clusters exert far greater influence on the affinity and apparent number of protein/adsorbent contacts than do mutations on the opposite end of the protein. There is independent 2D NMR evidence that the mutation does not induce large conformational changes in several of the proteins of interest [49]. The calorimetric behavior of the mutant proteins,

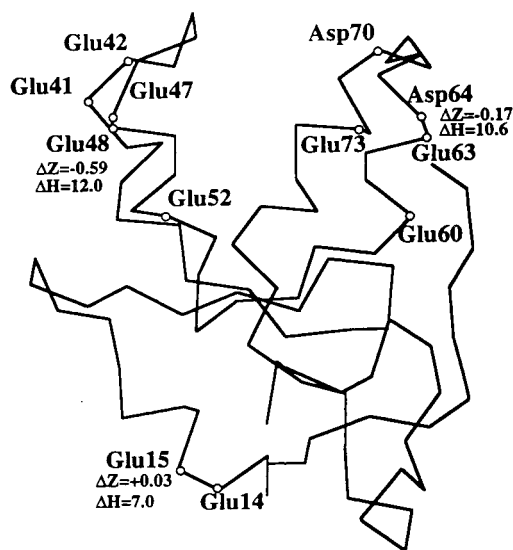


Fig. 9. Three-dimensional representation of tertiary structure of rat cytochrome b_5 [52] is shown; the C_α backbone atoms are connected by pseudo-bonds. Acidic groups which form clusters of negative charge are shown on either side of the heme-binding cleft (open pocket in the top-center of the diagram). The positions of the mutations calorimetrically characterized in this study are shown along with values of ΔH_{ads} and ΔZ , the change in the apparent number of contacts relative to the wild-type cytochrome b_5 .

however, does not reflect their retention behavior. As shown in Table 1 and Fig. 9, proteins altered in residues belonging to the dominant charge cluster (e.g., E48Q) show enthalpies of adsorption quite similar to that of the wild-type protein. Mutant E15Q, which is very little altered in its adsorption and HPLC retention behavior, shows a very different pattern of enthalpy of adsorption as a function of loading. This observation is particularly striking in view of the fact that calorimetric experiments were conducted at low ionic strength at which batch adsorption and HPLC retention differences among the mutants are greatest. This result suggests that the large enthalpies of adsorption on fresh adsorbent arise from different sources than do the lower (near-zero) enthalpies associated with adsorption on regenerated adsorbent.

One source of enthalpy which may be unique to fresh adsorbent is denaturation on high-affinity sites produced by local clusters of adsorbent

Table 1

Values of ΔH_{ads} at 25°C in 10 mM Tris, pH 8.0, for mutant forms of cytochrome b₅ calculated for low surface coverage (500 μg protein/10⁷ beads)

Protein	Q^{net}	Z^{Batch}	Z^{HPLC}	K^{Batch}	k^{HPLC}	ΔH_{ads} (kcal/mol)
Wild type	-9.5	2.92 ± 0.32	3.42 ± 0.01	0.081 ± 0.002	155.6 ± 21.2	11.4 ± 0.2
E48Q	-8.5	2.33 ± 0.34	2.76 ± 0.07	0.020 ± 0.000	40.1 ± 1.7	12.1 ± 0.3
D64N	-8.5	2.75 ± 0.33	ND	0.051 ± 0.000	ND	10.6 ± 0.2
E15Q	-8.5	2.95 ± 0.25	3.37 ± 0.04	0.100 ± 0.002	132.8 ± 5.5	6.9 ± 0.9

Q^{net} is the net charge of the proteins [51]. Z and K values are from Refs. [24,53]. Reported values of K^{Batch} were measured at 100 mM NaCl and those of k^{HPLC} were measured at 150 mM NaCl. The superscripts "Batch" and "HPLC" refer to equilibrium batch adsorption and isocratic, isothermal HPLC methods. ND represents not determined. Three-dimensional representation of the positions at which mutations were characterized using microcalorimetry are shown in Fig. 9.

charge, or by hydrophobic patches on the adsorbent surface. The possible role of hydrophobic interactions is supported by the fact that residue 15 lies near the two largest patches of hydrophobic surface on the cytochrome b₅ surface, in a region which we have shown to have a net positive charge [51] otherwise unfavorable for interaction with the cationic adsorbent surface. One hydrophobic patch (337 Å²; 1.4 Å probe radius using CHARMM v. 20.1, see also Ref. [50]) comprises atoms from residues Ile91, Pro94, and Leu98. Another (323 Å²) consists of residues Val8, Tyr10, Tyr11, His84, and Pro85. Together these patches comprise 11% of the total solvent-accessible surface area of the molecule and 50% of the hydrophobic surface area. The insensitivity of the enthalpy of adsorption to mutations which strongly affect adsorption and retention, together with insensitive van 't Hoff enthalpies of adsorption previously determined for a larger set of mutants [24], further support our conclusion that enthalpy does not play an important role in the selectivity of anion-exchange adsorption in this system. While the origins of the large enthalpies of adsorption on fresh Mono Q or of their surface-coverage dependence are not yet entirely clear, the calorimetric results support our previous conclusion that anion-exchange adsorption in this system is entropically driven, presumably by liberation of counterions or waters of hydration.

In conclusion, we have shown that titration calorimetry can be used as a sensitive probe to

test the energetics of ion-exchange adsorption. We have confirmed in a direct manner our previous conclusion that adsorption in this system is entropically driven. The character of adsorption on fresh and regenerated adsorbent is quite different, in ways which are demonstrated more directly by ITC than by any other available technique.

Acknowledgements

We would like to thank Dr. John Brandts, Sam Williston, and the late Tom Wiseman of MicroCal, Inc. for their indispensable help in designing the titration calorimetry experiments. We would also like to thank Dr. Jan-Christer Janson of Pharmacia LKB for the generous gift of Mono Q. *E. coli* strains producing cytochrome b₅ were the generous gift of Dr. Steve Sligar at the University of Illinois. Drs. Henry Pownall and Martha Mims of the Baylor College of Medicine, Houston, kindly allowed us use of their DSC equipment, and Dr. Barry McKeone provided valuable assistance in performing DSC experiments. The skillful assistance of Rene Ochoa, Colin Johnston, Henry Chang, Jerry Mulholland, and Don MacManus is gratefully acknowledged. Funding for this project was provided by NSF through CTS-8910087 and through a PYI award to R.C.W., and by the Welch Foundation.

References

- [1] J.D. Andrade, *Surface and Interfacial Aspects of Biomedical Polymers: Surface Chemistry and Physics*, Plenum Press, New York, NY, 1985.
- [2] J.D. Andrade, *Surface and Interfacial Aspects of Biomedical Polymers: Protein Adsorption*, Plenum Press, New York, NY, 1985.
- [3] J.L. Brash and T.A. Horbett, *Proteins at Interfaces: Physicochemical and Biochemical Studies*, American Chemical Society, Washington, DC, 1987.
- [4] J.L. Brash and Q.M. Samak, *J. Colloid Interface Sci.*, 65 (1978) 495.
- [5] W. Norde and J. Lyklema, *J. Colloid Interface Sci.*, 66 (1978) 257.
- [6] W. Norde and J. Lyklema, *J. Colloid Interface Sci.*, 66 (1978) 285.
- [7] W. Norde and J. Lyklema, *J. Colloid Interface Sci.*, 66 (1978) 295.
- [8] B.D. Fair and A.M. Jamieson, *J. Colloid Interface Sci.*, 77 (1980) 525.
- [9] A.B. Anderson, S.A. Darst and C.R. Robertson, in J.L. Brash and T.A. Horbett (Editors), *Proteins at Interfaces: Physicochemical and Biochemical Studies*, American Chemical Society, Washington, DC, 1987.
- [10] B.R. Young, W.G. Pitt and S.L. Cooper, *J. Colloid Interface Sci.*, 124 (1988) 28.
- [11] H. Shirahama, J. Lyklema and W. Norde, *J. Colloid Interface Sci.*, 139 (1990) 177.
- [12] A.V. Elgersma, R.L.J. Zsom, W. Norde and J. Lyklema, *Colloids Surfaces*, 54 (1991) 89.
- [13] D.S. Walker, M.D. Garrison and W.M. Reichert, *J. Colloid Interface Sci.*, 157 (1993) 41.
- [14] J. Lyklema, *Colloids Surfaces*, 10 (1984) 33.
- [15] J.D. Andrade and V. Hlady, *Adv. Polym. Sci.*, 79 (1986) 1.
- [16] R.L. Donghao and K. Park, *J. Colloid Interface Sci.*, 144 (1991) 271.
- [17] K. Matsuno, R.V. Lewis and C.R. Middaugh, *Arch. Biochem. Biophys.*, 291 (1991) 349.
- [18] E. Nyilas, T.H. Chiu and G.A. Herzlinger, *Trans. Am. Soc. Art. Int. Org.*, 20 (1974) 480.
- [19] T.H. Chiu, E. Nyilas and D.M. Lederman, *Trans. Am. Soc. Art. Int. Org.*, 22 (1976) 498.
- [20] P.G. Koutsoukos, W. Norde, J. Lyklema, *J. Colloid Interface Sci.*, 95 (1983) 385.
- [21] W.R. Bowen and D.T. Hughes, *J. Colloid Interface Sci.*, 158 (1993) 395.
- [22] D.J. Roush, D.S. Gill and R.C. Willson, *J. Chromatogr.*, 653 (1993) 207.
- [23] D.S. Gill, D.J. Roush and R.C. Willson, *J. Colloid Interface Sci.*, 167 (1994) 1.
- [24] D.S. Gill, D.J. Roush and R.C. Willson, *J. Chromatogr.*, 684 (1994) 55.
- [25] S.B. von Bodman, M.A. Schuler, D.R. Jollie and S.G. Sligar, *Proc. Natl. Acad. Sci. USA*, 83 (1986) 9443.
- [26] D.S. Gill, Ph.D. Thesis, University of Houston, 1993.
- [27] E. Friere, O.L. Mayorga and M. Straume, *Anal. Chem.*, 62 (1990) 950.
- [28] T. Wiseman, S. Williston, J.F. Brandts and L. Lungnan, *Anal. Biochem.*, 179 (1989) 131.
- [29] K.S. Krishnan and J.F. Brandts, *Meth. Enzymol.*, 49 (1978) 3.
- [30] P.L. Privalov, *Adv. Prot. Chem.*, 33 (1979) 167.
- [31] W.J. Dillman and I.F. Miller, *J. Colloid Interface Sci.*, 44 (1973) 221.
- [32] R.G. Lee and S.W. Kim, *J. Biomed. Mater. Res.*, 8 (1974) 251.
- [33] A. Schmitt, R. Varoqui, S. Uniyal, J.L. Brash and C. Pusineri, *J. Colloid Interface Sci.*, 92 (1983) 25.
- [34] W. Norde, *Adv. Colloid Interface Sci.*, 25 (1986) 267.
- [35] D.J. Roush, Ph.D. Thesis, University of Houston, 1994.
- [36] P.E. Morin and E. Friere, *Biochemistry*, 30 (1991) 8494.
- [37] R. Lumry and S. Rajender, *Biopolymers*, 9 (1970) 1125.
- [38] P.D. Ross and S. Subramaniam, *Biochemistry*, 20 (1980) 3096.
- [39] J.T. Edsall and H. Gutfreund, *Biothermodynamics: The Study of Biochemical Processes at Equilibrium*, John Wiley and Sons, Chichester, 1983.
- [40] J.M. Sturtevant, *Proc. Natl. Acad. Sci. USA.*, 74 (1977) 2236.
- [41] B.W. Sigursjold and D.R. Bundle, *J. Biol. Chem.*, 267 (1992) 8371.
- [42] R.D. Guiles, V.J. Basus, I.D. Kuntz and L. Waskell, *Biochemistry*, 31 (1992) 11365.
- [43] A. Kondo, S. Oku and K. Higashitani, *J. Colloid Interface Sci.*, 143 (1991) 214.
- [44] B.W. Morrissey and R.R. Stromberg, *J. Colloid Interface Sci.*, 46 (1974) 152.
- [45] T.J. Lenk, B.D. Ratner, R.M. Gendreau and K.K. Chittur, *J. Biomed. Mater. Res.*, 23 (1989) 549.
- [46] T.J. Lenk, T.A. Horbett, B.D. Ratner and K.K. Chittur, *Langmuir*, 7 (1991) 1755.
- [47] B.L. Steadman, K.C. Thompson, C.R. Middaugh, K. Matsuno, S. Vrona, E. Lawson and R.V. Lewis, *Biotechnol. Bioeng.*, 40 (1992) 8.
- [48] W. Kopaciewicz, M.A. Rounds and F.E. Regnier, *J. Chromatogr.*, 266 (1983) 3.
- [49] K.K. Rodgers, T.C. Pochapsky and S.G. Sligar, *Science*, 240 (1988) 1657.
- [50] F.S. Mathews, *Prog. Biophys. Molec. Biol.*, 45 (1985) 1.
- [51] D.J. Roush, D.S. Gill and R.C. Willson, *Biophys. J.*, 66 (1994) 1290.
- [52] D.S. Gill, D.J. Roush and R.C. Willson, *J. Biomol. Struct. Dyn.*, 11 (1994) 1.
- [53] D.J. Roush, D.S. Gill and R.C. Willson, *J. Chromatogr. A*, 704 (1995) 339.



ELSEVIER

Journal of Chromatography A, 715 (1995) 95–104

JOURNAL OF
CHROMATOGRAPHY A

Chromatographic and chemometric investigation of the chemical defence mechanism of poplar tree genotypes against a bark fungine parasite

C. Baiocchi^{a,*}, E. Marengo^a, M.A. Roggero^a, D. Giacosa^a, A. Giorcelli^b,
S. Toccori^b

^aDipartimento di Chimica Analitica, Università di Torino, 10125 Turin, Italy

^bIstituto di Sperimentazione per la Pioppicoltura, SAF Str. Frassineto 35, Casale Monferrato (AL), Italy

First received 14 October 1994; revised manuscript received 9 May 1995; accepted 16 May 1995

Abstract

Phenolic compounds in bark extracts of seven different clones of poplar trees were analysed by RP-HPLC with diode-array UV detection. The chromatographic results obtained were treated by means of chemometric methods to highlight any pattern in the data allowing one to discriminate poplars in terms of resistance to the fungus *Discosporium populeum*. The phenolic compounds turned out to be more related to the genetic origin of the clones than to their resistance.

1. Introduction

There is an increasing awareness that the phenolic constituents of plants are a key to understanding many plant–environment and, particularly, plant–parasite relationships. Poplar trees, like all plants, respond to various types of injuries with rather generalized metabolic responses. These frequently include the synthesis, oxidation and polymerization of phenolic compounds [1]. However, these substances probably represent only one of the many lines of defence that may be enforced by the plant. For this reason, it may be difficult to separate the defensive role of phenolics from that of alkaloids, terpenoids, coumarins or flavonoids. Anyway,

considering phenolics as indicators of disease resistance may be justified on the grounds that the two principal routes for the formation of aromatic compounds from aliphatic precursors, the shikimate and the polyketide pathways, each contribute to the formation of phenolic compounds. The shikimate pathway gives the phenylpropanoid nucleus while the polyketide pathway yields the A-ring of flavonoids [2]. In practice, phenolics may be considered as a crossroads of different biosynthetic pathways, many of which are activated by a range of stress factors such as wounding, infection and low-temperature stress. The central role of phenolic compounds in the resistance of poplar trees to infection by the fungus *Discosporium populeum*, the main topic of this paper, has been suggested by many workers [3–5]. Even in the case where the

* Corresponding author.

studies involved non-phenolic bark components such as the phenylalanine ammonia-lyase enzyme (PAL) [6], cytokinin [7] and β -glucosidase [8], these were related to phenolic substances and confirmed their importance.

In two previous papers [9,10], we tried to relate the qualitative and quantitative distributions of phenolics contained in bark extracts of poplar trees to their resistance to the fungus. Two clones of different genetic origin, one known, as a result of a biological test, to be resistant and the other susceptible to the fungal attack, were studied. The experimental data obtained were treated chemometrically so as to obtain the maximum information. As a final result it was possible to link the two clones to different classes of phenolics.

This paper constitutes an extension of the study to seven poplar clones belonging either to different species or to different genotypes of the same hybrid species. RP-HPLC with diode-array UV detection was used to analyse the bark extracts. Principal component analysis was applied to the chromatographic data in order to explore their structure. Subsequently KNN, a multivariate classification method, was used to investigate the kind and amount of information discriminating among the clones obtainable from the variation of the phenolic content of bark extracts.

2. Experimental

2.1. Instrumentation

The bark extracts were analysed using a Varian Star 9010 ternary gradient HPLC pump

equipped with a Varian Star 9065 diode-array spectrophotometric detector. System control and data acquisition and processing were performed utilising the multi-task program Varian Star 9000 on an Epson 386 (33 MHz) PC.

The chromatographic column was Lichrosphere RP-18 (250 × 4.6 mm I.D.), 5 μ m particle size (Merck, Darmstadt, Germany). The injection volume was 10 μ l and the flow-rate was 1.0 ml/min.

2.2. Reagents

HPLC-grade methanol and acetonitrile and a 0.57% solution of acetic acid in water purified in a Milli-Q system (Millipore) were used as mobile phase constituents.

2.3. Chromatographic conditions

A ternary gradient programme was used involving (A) acetonitrile, (B) 0.57% acetic acid and (C) methanol. The starting conditions were 6% A–88% B–6% C and after 40 min the mobile phase composition was 6% A–48% B–46% C.

2.4. Sampling

The bark of seven clones known to differ in resistance to *D. populeum* was sampled. The sampling programme was scheduled in December, January, February and March. Several samples of each clone, for each period, were collected to give a total of 216 samples. The detailed structure of the data is given in Table 1.

Table 1
Description of data set

Total number of objects	216
Number of different clones	7 (A, B, C, D, E, F and G)
Number of samples collected for each clone	A = 29, B = 32, C = 30, D = 32, E = 31, F = 30, G = 32
Number of sample periods	4 (1 = December, 2 = January, 3 = February, 4 = March)
Number of samples collected for each period	1 = 55, 2 = 56, 3 = 53, 4 = 52
Number of resistance groups	4 (A, B, C, resistant, class 1; D, moderately resistant, class 2; E, F, moderately susceptible, class 3; G, very susceptible, class 4)

2.5. Sample preparation

About 30 mg of previously lyophilized bark were added to 2.0 ml of 1.0 M sodium hydroxide solution in a filter tube. The air was removed from the tube by flushing with nitrogen and the stopper secured. The suspension was shaken at 20°C for 20 h and subsequently filtered. The residue was washed with water (total volume of filtrate ca. 2.0 ml). The filtrate was acidified to pH 2.5 with 6.0 M hydrochloric acid and diluted with water to a final volume of 5.0 ml [9,10].

2.6. Standards

The standard substances 1,2,3-trihydroxybenzene, 3,4-dihydroxybenzoic acid, 1,2-dihydroxybenzene, 4-hydroxybenzoic acid, 4-hydroxy-3-methoxybenzoic acid, 4-hydroxybenzaldehyde, 3,5-dimethoxy-4-hydroxybenzoic acid, 4-hydroxy-3-methoxybenzaldehyde, 4-hydroxy-3,5-dimethoxybenzaldehyde, 4-hydroxycinnamic acid, 4-hydroxy-3-methoxycinnamic acid, 2-hydroxybenzoic acid, benzoic acid and 4-methoxybenzoic acid were purchased from Aldrich Chimica (Milan, Italy).

2.7. Chemometrics

Principal component analysis (PCA) is a well known technique which provides a significant insight into the structure of any numerical data matrix [11,12]. It generates a set of new orthogonal variables, the principal components (PCs), a linear combination of the original ones, so that the maximum possible amount of variance contained in the starting data matrix is concentrated in as few PCs as possible. These new variables can be used in place of the original ones for successive treatment.

The coefficients of the original variables defining each PC are called "loadings" and the projections of the experimental points on the new variables are called "scores". Since PCA effectively concentrates the variance of the data matrix in a smaller number of new variables, it is suitable to reduce the dimensionality of large data matrices by eliminating the non-significant

PCs and facilitating successive treatments on the reduced data. PCA was computed through the diagonalization of the variance-covariance matrix by means of the Jacobi algorithm. The data were autoscaled before PC computation in order to assign the same numerical weight to each variable.

3. Results and discussion

Various bark samples of seven different poplar clones sampled in four different periods (December, January, February and March) were analysed. A detailed description of the samples (216 in total) is given in Table 1. The seven poplar clones were assigned to four different classes of resistance, determined by a biological test: LUX, DVINA (*P. deltoides*) and GHY (*P. × euroamericana*) class 1, very resistant; B.L. COSTANZO (*P. × euroamericana*) class 2, resistant; BOCCALARI and FARSI (*P. × euroamericana*) class 3, moderately susceptible; and J. POURTET (*P. nigra*) class 4, very susceptible. In the following discussion these clones will be identified by the letters A, B, C, D, E, F and G, respectively.

Chromatographic results for the seven clones sampled in winter are reported in Fig. 1. The peaks were identified by comparing the retention times and UV spectra monitored between 220 and 330 nm with those for a standard mixture of sixteen phenolic substances (listed in Table 2). There are differences in the chromatographic profiles, but considering they account, in a complex way, for differences among clones, resistance and sample collection periods, it is evident that there is the need for a data treatment allowing one to separate the different sources of information and to organize them in a convincing pattern. For this purpose suitable statistical treatments were applied to a set of experimental data made up of 16 variables (peak areas) and 216 objects (all collected samples), giving a total number of 3456 data.

First a PCA was performed for a synthetic and informative visualization of the data. Table 3 shows the values of the variance explained by the

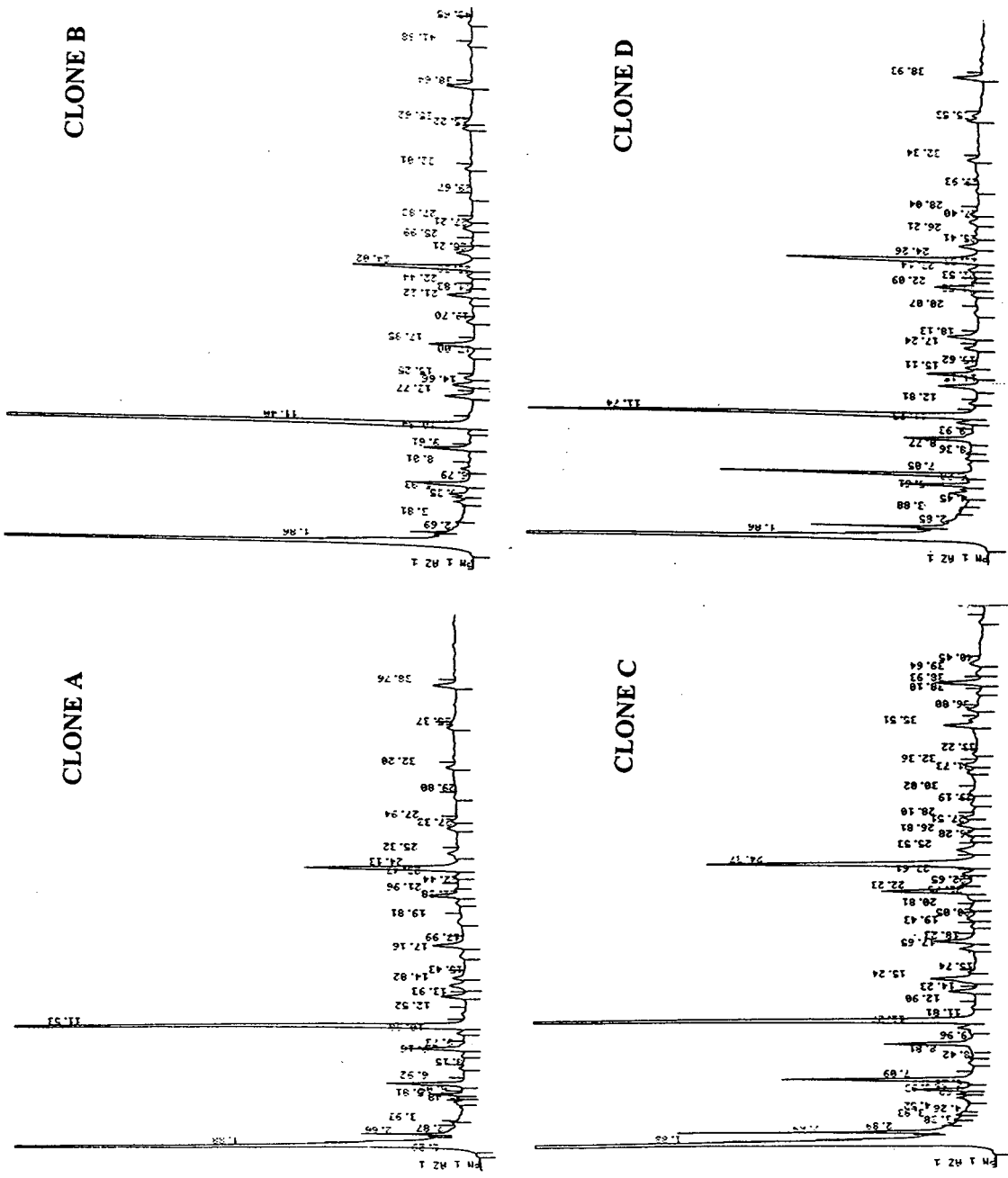


Fig. 1.

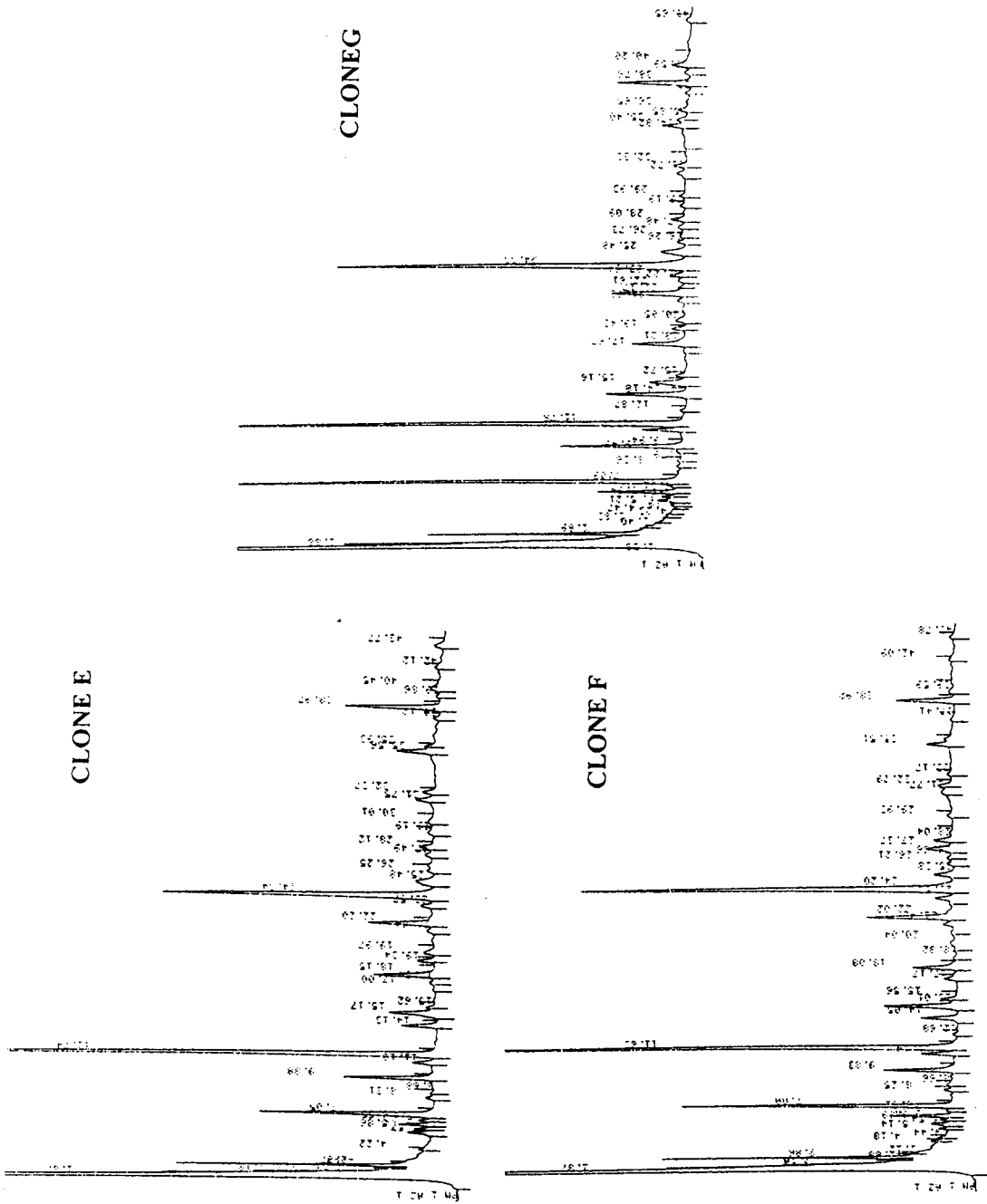


Fig. 1. Chromatographic results for the bark extracts of the seven different clones sampled in winter.

Table 2
Variables taken into consideration in the chromatographic and chemometric analysis

Variable	Compound
1	1,2,3-Trihydroxybenzene
2	3,4-Dihydroxybenzoic acid
3	1,2-Dihydroxybenzene
4	4-Hydroxybenzoic acid
5	4-Hydroxy-3-methoxybenzoic acid
6	4-Hydroxybenzaldehyde
7	3,5-Dimethoxy-4-hydroxybenzoic acid
8	4-Hydroxy-3-methoxybenzaldehyde
9	4-Hydroxy-3,5-dimethoxybenzaldehyde
10	4-Hydroxycinnamic acid
11	Degradation product of 10
12	4-Hydroxy-3-methoxycinnamic acid
13	Degradation product of 12
14	2-Hydroxybenzoic acid
15	Benzoic acid
16	4-Methoxybenzoic acid

more significant principal components and Table 4 lists the loadings of the sixteen variables on the first three PCs. Fig. 2 shows a plot of the scores of PC1 vs. PC2 for all the objects. In spite of the complexity due to the large number of classes present, it is evident that the clusters of clones A, B and G are separated, whereas all the others are more or less in a cluster lying between the previous ones. In fact the distinction of the clones belonging to pure species. (*P. deltoides*, clones A and B, *P. Nigra*, clone G) is very sharp. The discrimination among the hybrids (*P. × euroamaricana*, clones C, D, E and F) which are sensitive to a more or less genetic proximity to their parents is instead more difficult. PC1 mainly discriminates clones A and B with respect to

Table 3
Variance explained by the PCs with eigenvalue greater than 1.0

PC	Variance explained	Cumulative variance
1	28.7	28.7
2	15.2	43.9
3	13.9	57.8
4	8.6	66.4
5	6.7	73.1

the others. As the list of loadings reported in Table 4 shows, the variables contributing substantially to the PC1 definition are variables 2 (3,4-dihydroxybenzoic acid) 4 (4-hydroxybenzoic acid) and 12 (4-hydroxy-3-methoxycinnamic acid). Variables 5 (4-hydroxy-3-methoxybenzoic acid) and 8 (4-hydroxy-3-methoxybenzaldehyde), the main constituents of PC2, seem instead effective in the separation of clones G and D from the group of clones B, E and F. Given that, from the resistance point of view, the expected classification ought to be A, B, C–D–E, F–G, there is evidence of a clear decrease in the contribution of this kind of information to the discrimination of the objects in favour of one related to the genetic diversity of the clones. PC3 does not provide any further contribution in this direction, but seems rather to contain some information about the possible influence of seasonal factors.

Fig. 3 shows the plot of the scores of PC2 and PC3, defining a trend to discriminate winter samples (1 and 2) from early spring samples (3 and 4). The variables which seem to exert the most discriminating effect are 1 (1,2,3-trihydroxybenzene), 3 (1,2-dihydroxybenzene), 6 (4-hydroxybenzaldehyde), 8 (4-hydroxy-3-methoxybenzaldehyde) and 11 (degradation product of 4-hydroxycinnamic acid). These variables are different from those discriminating the clones, so there is no apparent mixing between the information related to clone classification and to the sample collection period classification.

From the variance–covariance matrix (not reported) used to perform PCA calculations, it is also possible to visualize the complete pattern of correlations among the variables important for this study. A positive correlation among the variables may be interpreted in terms of a strict link characterizing the presence of the substances that they represent in the poplar bark. For instance, they may be final products of correlated biosynthetic pathways, or even of an individual pathway, and may contribute to define the same sample features. This is the case with the variables 2 (3,4-dihydroxybenzoic acid) and 12 (4-hydroxy-3-methoxycinnamic acid), important constituents of PC1. A negative correlation

Table 4
Loadings of the original variables on the first three PCs

Variable	PC1	PC2	PC3
1. 1,2,3-Trihydroxybenzene	-0.18	-0.11	-0.11
2. 3,4-Dihydroxybenzoic acid	-0.38	0.34	-0.21
3. 1,2-Dihydroxybenzene	-0.15	-0.31	-0.38
4. 4-Hydroxybenzoic acid	0.50	-0.07	0.06
5. 4-Hydroxy-3-methoxybenzoic acid	-0.24	0.40	-0.32
6. 4-Hydroxybenzaldehyde	-0.31	-0.22	-0.10
7. 3,5-Dimethoxy-4-hydroxybenzoic acid	0.08	0.22	0.11
8. 4-Hydroxy-3-methoxybenzaldehyde	0.12	-0.44	-0.31
9. 4-Hydroxy-3,5-dimethoxybenzaldehyde	0.05	-0.34	-0.17
10. 4-Hydroxycinnamic acid	-0.32	-0.03	0.32
11. Degradation product of 10	-0.03	0.05	0.29
12. 4-Hydroxy-3-methoxycinnamic acid	-0.43	-0.12	0.05
13. Degradation product of 12	-0.05	-0.09	-0.11
14. 2-Hydroxybenzoic acid	-0.19	-0.13	0.34
15. Benzoic acid	-0.13	-0.26	0.48
16. 4-Methoxybenzoic acid	-0.15	-0.30	0.03

may instead be interpreted in terms of a reciprocal transformation of the substances involved, as if one or more of them were key compounds in the biosynthesis of the others (this may be the case with variables 5 and 8, relevant in the PC2 definition). A variable negatively correlated with the majority of the others is variable 4 (4-hydroxybenzoic acid). In previous papers [9,10], the role of this substance in defining the data structure was found to be extremely important.

At this stage, a classification study was performed in order to check thoroughly the possibility of discriminating the clones as species or even as genotypes.

A *K*th nearest neighbours (KNN) classification study was performed. This method determines for each object the *k*th nearest ones, and assigns it to the most represented class among the *K* nearest samples. In the case of an equal population of two or more classes, the sample is assigned to the nearest among them. It would be

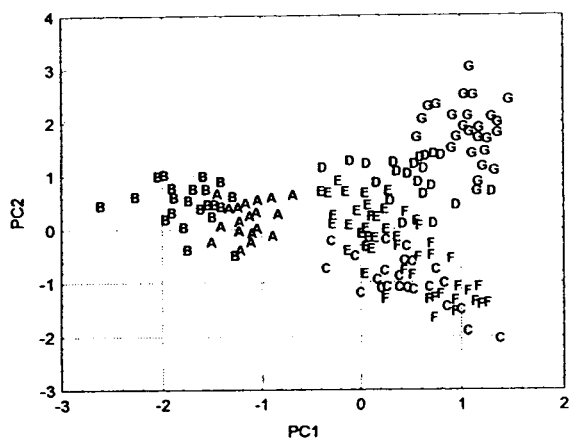


Fig. 2. Scatter plot of samples vs. PC1 and PC2.

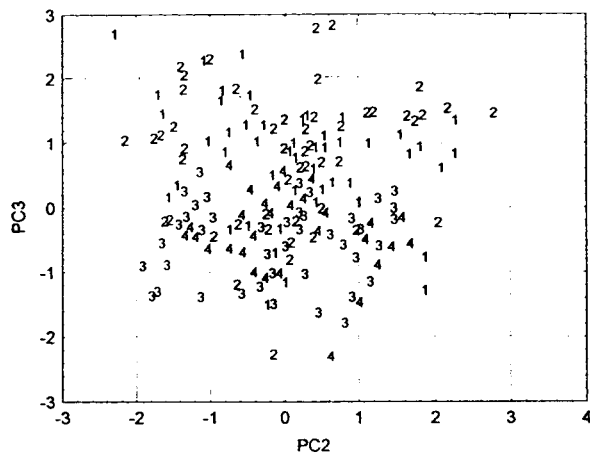


Fig. 3. Scatter plot of samples vs. PC2 and PC3.

desirable to eliminate from the data the information related to the sample collection period and to non-discriminant variables, but any procedure we can use for this purpose may have some side-effect on the KNN method, which is based on the calculation of distances. However, since the presence of non-discriminant information may introduce confusion in the results, we introduced two correction mechanisms. A stepwise algorithm of selection of the discriminant variables, after autoscaling, searching iteratively for the best set of variables by adding or deleting one variable at a time, repeated until no further improvement of the percentage non-error rate (%NER), defined as the percentage of the correctly classified objects, was achieved. A further variable scaling operation, centred on sample collection time, was performed in order to "clean up" the data from this kind of information. Hence the following four different data sets were defined: set 1 (all original variables, autoscaled), set 2 (all original variables, centred on sample collection period), set 3 (selected variables 2, 4, 5, 7, 8, 10, 12 and 15, autoscaled) and set 4 (selected variables 2, 5, 6, 10, 12, 13 and 15, autoscaled and centred on sample collection period). Calculations were then performed and the results were compared.

The results obtained using $K = 5$, summarized in Table 5, show that the best set of variables

Table 5

KNN results for: set 1, all autoscaled variables; set 2, all variables centred on the sample collection time after autoscaling; set 3, variables 2, 4, 5, 7, 8, 10, 12 and 15, autoscaled; set 4, variables 2, 5, 6, 10, 12, 13 and 15, centred on the sample collection time after autoscaling

Clone	%NER			
	Set 1	Set 2	Set 3	Set 4
A	82.7	86.2	96.5	89.7
B	84.4	87.5	84.4	93.7
C	73.3	73.3	90.0	93.3
D	65.6	68.7	93.7	90.6
E	80.6	90.3	87.1	96.7
F	86.7	76.7	93.3	93.3
G	100.0	100.0	100.0	100.0
Overall	81.9	83.3	92.1	94.0

corresponds to set 4. In particular, the results obtained using all the variables (untreated or class centred) are markedly worse than those obtained with the stepwise refinement algorithm. This confirms that the variables which do not contain information on the clone discrimination introduce a lot of confusion (noise) in the pattern of distances, which makes the KNN classification much less effective.

The differences between the class-centred and the untreated variables are smaller. It is interesting that the variables which emerged from the PCA treatment are present among the selected variables of sets 3 and 4, with the noteworthy exception of variable 4 in the case of the data set centred on the sample collection period. This variable was eliminated during the last step of the stepwise procedure because its elimination does not change the %NER. This can be easily justified if we remember the mentioned high and negative correlation of this variable with all other variables and particularly with variables 2 (a possible hydroxylation product) and 10 (a possible precursor). Variable 4 may be considered no longer necessary since its information is already present.

The remaining variables, i.e., 6 and 13, or 7 and 8, increase the %NER in both cases by about 2% and are added only during the last refinement steps. Their statistical significance is dubious.

The %NER values for the clones show that the best results are achieved by performing the calculation with the reduced dataset, after eliminating the information about the sample collection time. The consideration of the confusion matrix for this calculation (Table 6) better describes the pattern of the classification results. This is a matrix containing categorical classification results. The rows of the matrix correspond to true classes and the columns to predicted classes. The number of correctly classified objects in each class appears on the main diagonal, while the number of misclassified objects are the off-diagonal elements. From Table 6, it can be concluded that the classification can be effectively performed and that the highest number of errors is due to exchanges between clones 1 and

Table 6
Confusion matrix for the KNN classification of clones, using set 3

Class	A	B	C	D	E	F	G
A	26	3	0	0	0	0	0
B	2	30	0	0	0	0	0
C	0	0	28	0	0	2	0
D	0	0	0	29	1	0	2
E	0	0	1	0	30	0	0
F	1	0	1	0	0	28	0
G	0	0	0	0	0	0	32

2 (belonging to the same species and not mixed with the others). This means that the selected variables are effectively responsible for the discrimination between the clones.

An analogous study by means of the KNN method was performed on the classification of the samples on the basis of their different collection times. Only the best results are reported (Table 7) obtained with autoscaled variables, selected using the stepwise procedure.

The overall and partial %NER are not as large as in the previous case. Anyway, it should be noted that most of the wrong assignments are due to exchanges between sampling periods 1 and 2 on one side and 3 and 4 on the other. This means that the four sampling periods can be grouped into two main behaviours: winter and early spring, as already suggested by the PCA results. Also, the fact that the selected variables are partially different from those found by PCA is due to the fact that KNN tries a priori to discriminate period 1 from period 2 samples and period 3 from period 4 samples, while during the

Table 7
Confusion matrix for the KNN classification on the basis of the sample collection periods, variables selected 2, 3, 6, 9 and 12

Class	1	2	3	4	%NER ^a
1	49	9	3	0	78.2
2	9	37	4	6	66.1
3	2	1	35	15	66.0
4	1	0	10	41	78.8

^a Overall %NER: 72.2.

principal component analysis the similarity between the two couples has been accepted a posteriori after the analysis of the results. If the four sample collection periods are grouped together into two couples, winter (W) and spring (S) samples, the best results obtained by the stepwise KNN will consist of an overall %NER of 93.5. The corresponding confusion matrix is reported in Table 8. The classification is highly satisfactory. Several variables among those selected contribute very poorly to the improvement of the classification; their statistical significance is small. The most important variables seem to be 3 (1,2-dihydroxybenzene), 6 (4-hydroxybenzaldehyde) and 9 (4-hydroxy-3,5-dimethoxybenzaldehyde), which alone leads to an overall %NER of about 90.

Reporting all the information obtained to a phytochemical basis, we can draw important and maybe definitive considerations about the possibility of using phenolics as indicators of poplar tree resistance towards *D. populeum* infection. The statistical methods adopted constituted different approaches to the analysis of data, so all possible, if any, underlying structures were highlighted. It is then clear that the analysis of phenolics provides information not about the plant resistance, but about the genetic origin of clones. In our previous work [9,10] we attributed resistance discrimination ability to phenolic compounds only because there occurred a fortuitous coincidence of the two features. In fact, these substances seem to account also for seasonal effects and the variables responsible are different from those discriminating among the clones. This confirms that phenolics are involved in many ways in the biochemical production of poplars,

Table 8
Confusion matrix for the KNN classification on the basis of the sample collection periods, variables selected 2, 3, 4, 6, 9, 12, 13 and 15

Class	W	S	%NER ^a
1	99	12	89.2
2	2	103	98.1

^a Overall %NER: 93.5.

maybe also as pre-infection factors, but that they can be better defined as multi-purpose compounds and are not easily related to the defence mechanism against *D. populeum*.

Further developments in this direction must take into account new data and new substances in the attempt to characterize the mechanism of defence. Work of this kind is in progress.

References

- [1] M.J.C. Rhodes and L.S.C. Woollorton, in G. Kahl (Editor), *The Biochemistry of Wounded Plant Tissues*, Walter de Gruyter, Berlin, 1978, pp. 243–246.
- [2] K. Hahlbrock and H. Grisebach, *Annu. Rev. Plant. Physiol.*, 30 (1979) 105.
- [3] S. Pucacka, *Arbor. Kornickie*, 20 (1975) 227.
- [4] S. Pucacka, *Arbor. Kornickie*, 25 (1980) 257.
- [5] Y. Chuanhe, Y. Wang and Z. Zhongming, presented at International Poplar Commission, XVIIIth Session, Beijing, September 5–8, 1988.
- [6] S. Pucacka, *Arbor. Kornickie*, 24 (1979) 209.
- [7] M. Rudawska, *Annual Reports, Institute of Dendrology, Kornik, Poland*, 1980, p. 195.
- [8] B. Kieliszewska-Rokicka, *Annual Reports, Institute of Dendrology, Kornik, Poland*, 1980, p. 203.
- [9] C. Baiocchi, E. Marengo, G. Saini, M.A. Roggero and D. Giacosa, *J. Chromatogr.*, 644 (1993) 259.
- [10] C. Baiocchi, E. Marengo, M.A. Roggero, D. Giacosa, L. Vietto and S. Toccari, *Chromatographia*, 39 (1994) 7.
- [11] E.R. Malinowski and D.G. Howery, *Factor Analysis in Chemistry*, Wiley, New York, 1978.
- [12] S. Wold, *Pattern Recognition*, 8 (1976) 127.



ELSEVIER

Journal of Chromatography A, 715 (1995) 105–115

JOURNAL OF
CHROMATOGRAPHY A

Ion-exchange mechanisms of some transition metals on a mixed-bed resin with a complexing eluent

P. Janvion, S. Motellier*, H. Pitsch

Commissariat à l'Energie Atomique, DCC/DESD/SESD/SGC, B.P. 6, 92265 Fontenay-aux-Roses Cedex, France

First received 16 January 1995; revised manuscript received 2 May 1995; accepted 15 May 1995

Abstract

Ion-exchange chromatography was used for the simultaneous elution of transition metals. The mobile phase consisted of an acetate buffer with pyridine-2,6-dicarboxylic acid (PDCA) as a chelating agent; the stationary phase was a mixed-bed resin that displays both anion- and cation-exchange properties. Under the selected conditions, the only species of the analyte that occur in solution are the anionic chelates $M(\text{PDCA})_2$ while both the free cations and the chelates may be present in the resin. The mechanisms involved in this complex chromatographic pattern are described, considering either cation or anion exchange. It was found that the chromatographic behaviour of the transition metals can be explained by electrostatic interactions, the prevailing mechanism being pure anion exchange. Selectivity coefficients between the eluted species and either PDCA or acetate were derived from the experiments. The results were compared with those obtained after replacement of the mixed-bed resin by a low capacity anion-exchange resin. In this case, additional mechanisms such as adsorption had to be taken into account in the explanation of the retention behaviour of the transition metals.

1. Introduction

The chromatography of transition metals is a challenge concerning both their separation and detection. Their similar affinities for most common cation exchangers make it difficult to separate them by standard cation-exchange chromatography. In addition, chemically suppressed conductivity cannot be used for the detection of transition metals since the pH increase inherent in the method precipitates them as their hydroxides [1].

The latter problem can be overcome by post-column addition of a chelating agent that converts the metals into coloured complexes to be

detected by visible spectrometry [1,2]. An alternative to the former problem consists in adding an anionic chelating agent such as tartrate, oxalate or citrate to the mobile phase and to carry out the separation of the resulting complexes on cation [3] or anion exchangers [4], or using reversed-phase chromatography [3,5,6]. The principles and applications of the different methods have been described [7]. The chromatographic performances of various sulfonated substrates, viz., silica gel, poly(styrene-divinylbenzene) [8] and methacrylate [9], have been compared. They showed a strong influence of non-specific interactions and poor efficiencies were reported for polymer-based stationary phases. However, even silica-based exchangers lack selectivity and show relatively low efficiencies.

* Corresponding author.

Some workers have suggested the use of a mixed-bed resin that features both anion- and cation-exchange sites to achieve a better separation [10,11]. The mobile phase contains a complexing agent for transition metals [pyridine-2,6-dicarboxylic acid (PDCA)] that accounts for chromatographic selectivity while another chelant [pyridyl-2-azo-4-resorcinol (PAR)] is used as a postcolumn reagent. The metal–PDCA complexes successively eluted from the column are readily dissociated and recomplexation occurs to yield metal–PAR complexes, which are detected spectrophotometrically. This method was applied to the determination of transition metals in the primary coolants of light water nuclear reactors [12] and is compatible with on-line preconcentration to achieve limits of detection lower than 1 ppb [13]. It was assumed that anion exchange is the dominant retention mechanism [14], although no evidence was given.

The purpose of this work was to determine the chromatographic behaviour of some transition metals, Fe(III), Ni(II), Co(II), Cu(II) and Zn(II), when determined by this complex method. Mathematical models were developed to evaluate the relative contributions of the cation- and anion-exchange mechanisms to their retention.

2. Experimental

PDCA was purchased from Fluka and PAR from Merck. All other chemicals were of Suprapur grade from Merck. Standard solutions of metals were prepared by dilution of Specpure standard solutions from Johnson Matthey (1 g l⁻¹). They were acidified to pH 2 with HNO₃. The water used throughout these experiments was purified with a Milli-Q system (Millipore).

The chromatographic set-up consisted of an ActIon Analyser (Waters) including an inert Model 625 pump driven by a Model 600E controller unit. The built-in injector (Waters Model 125) was equipped with a 100- μ l loop. A reagent delivery module (RDM) (Waters) was connected to the flow stream at the column outlet via a T-shaped connector; the postcolumn reagent was

delivered by argon pressure. Detection was performed with a diode-array detector (Waters Model 990) set at 520 nm unless stated otherwise.

The experiments were carried out on a CG5 (guard) + CS5 (analytical) set of columns (Dionex). In this type of resin, quaternary ammonium and sulfonate functional groups co-exist in the pellicular layer located on the core of the bead [15,16]. The cation- and anion-exchange capacities are 0.071 and 0.033 mequiv./ml resin, respectively. A MFC-1 column (Dionex) was inserted upstream from the injector for eluent purification. The purely anion-exchange set of columns was an AG4A (guard) + AS4A (analytical), of quaternary ammonium type (Dionex).

The determination of the transition metals was carried out with the following optimized mobile phase (denoted E₀): 6 · 10⁻³ M PDCA – 5 · 10⁻² M CH₃COOH – 5 · 10⁻² M CH₃COONa pumped at a flow-rate of 1 ml min⁻¹. Various eluent compositions were used to test for the models and will be stated when needed. The postcolumn reagent was delivered at a flow-rate of 0.4 ml min⁻¹. It consisted of 4 · 10⁻⁴ M PAR – 3 M NH₃ – 1 M CH₃COOH (pH 9.7). The transition metal cations were injected in a single run at a concentration of 100 μ g l⁻¹ each.

3. Results and discussion

In the following AcO⁻ denotes acetate and HA⁻ and A²⁻ the two ionic forms of PDCA. Charges will be omitted in formulae for ease of reading.

3.1. Mobile and stationary phase compositions

PDCA is a diacid, pK₂ = 2.10 and pK₁ = 4.68 at 20°C, for an ionic strength *I* = 0.1 M [17]. The pK_A of acetic acid under the same conditions [18], 4.65, was checked experimentally. From these data, the equilibrium composition of the eluent E₀ can be deduced (Table 1). In this medium, all the investigated transition metals are predominantly in the form of the anionic

Table 1

Composition of the mobile and stationary phases in the determination of transition metals by ion chromatography on the CS5 column

Species	Eluent E_0	Resin
[Na]	$5.00 \cdot 10^{-2} M = 5.00 \cdot 10^{-2}$ mequiv. ml $^{-1}$	0.0710 mequiv. ml $^{-1}$ (100%)
[HA]	$3.96 \cdot 10^{-3} M = 3.96 \cdot 10^{-3}$ mequiv. ml $^{-1}$	
[A]	$2.04 \cdot 10^{-3} M = 4.08 \cdot 10^{-3}$ mequiv. ml $^{-1}$	0.0245 mequiv. ml $^{-1}$ (74%)
[AcOH]	$5.86 \cdot 10^{-2} M$	
[AcO]	$4.15 \cdot 10^{-2} M = 4.15 \cdot 10^{-2}$ mequiv. ml $^{-1}$	0.0085 mequiv. ml $^{-1}$ (26%)

complexes MA_2^{2-} (divalent cations) and FeA_2^- [Fe(III)].

The only cationic species in the eluent E_0 are Na^+ and H^+ . According to their respective concentrations in solution ($[Na]_s = 5 \cdot 10^{-2} M$ and $[H]_s = 3.2 \cdot 10^{-5} M$) and orders of affinity versus most sulfonated resins ($Na^+ > H^+$), sodium is likely to be the only cation involved in a cation-exchange mechanism with metals. This will be true for every eluent where $[Na]_s$ is at least ten times $[H]_s$. As a consequence,

$$[Na]_r = Ce_c = 0.071 \text{ mequiv. ml}^{-1}$$

where the subscript r represents the resin and Ce_c is the cation-exchange capacity of the mixed-bed stationary phase.

There are three competing exchangeable anions in the eluent: AcO^- , HA^- and A^{2-} . In order to determine the selectivity coefficients between these species, a $10^{-5} M$ solution of PDCA was injected on to the column and eluted with acetate buffer at different pH values. In this mobile phase, the concentration of AcO^- was maintained constant at $0.1 M$ and the pH was adjusted by adding increasing concentrations of AcOH. Spectrophotometric detection at 270 nm was applied. The distribution coefficient of the eluted species was measured.

If both HA^- and A^{2-} are involved in an exchange mechanism, the conditional distribution coefficient D_A of PDCA must take into account its two ionic species:

$$D_A = \frac{[HA]_r + [A]_r}{[H_2A]_s + [HA]_s + [A]_s}$$

Fig. 1 shows the evolution of the logarithm of the distribution coefficient of PDCA as a function of the eluent pH. When A^{2-} is largely predominant in the aqueous phase, i.e., for pH values higher than 6, a plateau is observed; this is evidence for the predominance of the dianionic form of PDCA in the resin. In this pH range, D_A may be simplified to

$$D_A = \frac{[A]_r}{[A]_s}$$

From the mean value of D_A for $pH > 6$ and knowing that $[AcO]_s = 0.1 M$, and $[AcO]_r = Ce_a = 0.033 \text{ mequiv. ml}^{-1}$, where Ce_a is the anion-exchange capacity of the resin, the selectivity coefficient between A^{2-} and AcO^- , K_{2AcO}^A , can be deduced:

$$K_{2AcO}^A = \frac{[A]_r [AcO]_s^2}{[A]_s [AcO]_r^2} = 135 \pm 25$$

When the pH value is decreased to below 4.7, A^{2-} is transformed into HA^- in the mobile phase. Owing to the higher affinity of the resin for A^{2-} than for HA^- , protonation in the stationary phase does not occur: a plateau that would similarly correspond to the predominance of HA^- in both phases is not observed in Fig. 1. Between pH 3.3 and 4.3, A^{2-} remains the unique PDCA species in the resin.

The composition of the stationary phase in contact with the eluent E_0 used for transition metal determination can then be deduced (Table 1).

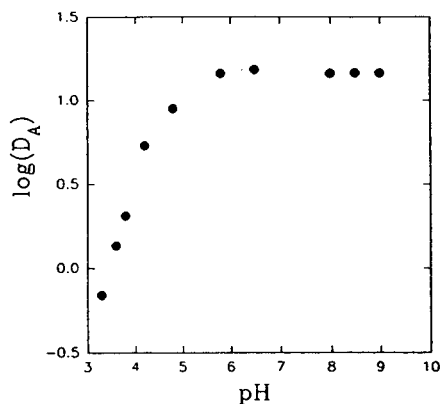


Fig. 1. Influence of the pH on the distribution coefficient of PDCA. Chromatographic conditions: column, CG5 + CS5; mobile phase, 0.1 M AcONa (pH adjusted with AcOH or NaOH); flow-rate, 1.0 ml min⁻¹; detection, UV at 270 nm; injection loop, 100 μl; PDCA, 10⁻⁵ M.

3.2. Retention models for transition metals

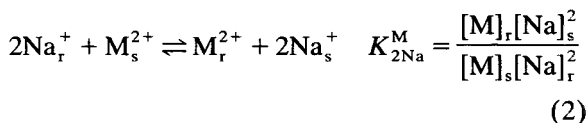
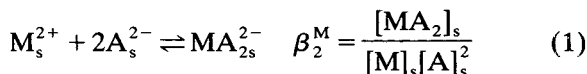
Under the conditions chosen for their analytical separation, the transition metals occur exclusively as their MA₂²⁻ complexes [FeA₂⁻ for Fe(III)] in the mobile phase. Since both anion- and cation-exchange sites co-exist on the resin, the metals may be retained as M²⁺, Fe³⁺ or FeA⁺, or as their anionic complexed form, considering that, for a pellicular resin, the distribution of the neutral form MA may be neglected. For both hypotheses, a model was developed and tested. The validation experiments consisted in selected alterations of the mobile phase and quantification of the subsequent effects on the retention of the transition metals. Models will be exposed first, followed by a description of the experiments and a discussion of the fitting results.

Hypothesis of cation exchange

The model developed here compares with that proposed by Haddad and Foley [19] for divalent cations eluted from a cation-exchange column with an eluent containing a single competing cation and a complexing ligand. This model was recently adapted to a more complex elution pattern, taking into account multiple ionic eluents [20].

Here, Na⁺ is the exchangeable competing ion

in the resin. Given a divalent metal, M²⁺, the equilibria involved are



Following the hypothesis of a cation-exchange mechanism, M²⁺ is the only metal species allowed to enter the resin while MA₂²⁻ is the predominant species in solution, by at least three orders of magnitude under the conditions of our experiments. The distribution coefficient of the metal is

$$D_M = \frac{[M]_r}{[MA_2]_s} \quad (3)$$

Substitution of Eqs. 1 and 2 in Eq. 3 yields

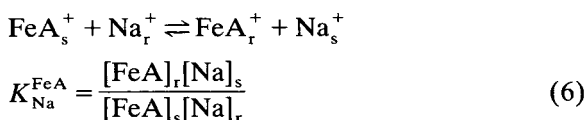
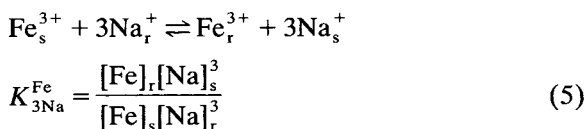
$$D_M = K_{2Na}^M \cdot \frac{[Na]_r^2}{[Na]_s^2} \cdot \frac{1}{\beta_2^M[A]_s^2} \quad (4)$$

Since [Na]_r is equal to the cation-exchange capacity *Ce_c*, we obtain from Eq. 4

$$\log D_M = \log K_{2Na}^M + 2 \log Ce_c - 2 \log [Na]_s - \log \beta_2^M - 2 \log [A]_s \quad (I)$$

The distribution coefficient of the metal is a function of the concentration of the competing cation and that of the complexing agent in the mobile phase.

In the case of Fe(III), two cationic species may be retained on the resin:



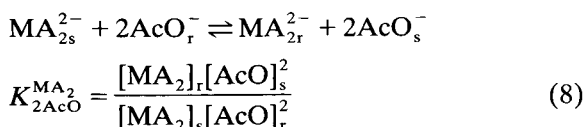
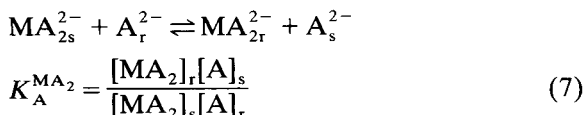
Combining the expression of the corresponding distribution coefficient, $D_{Fe} = ([Fe]_r + [FeA]_r) / [FeA_2]_s$ with Eqs. 5 and 6 and the complexation

constants in the solution ($K_1^{\text{Fe}} = [\text{FeA}]_s / [\text{Fe}]_s [\text{A}]_s$ and $\beta_2^{\text{Fe}} = [\text{FeA}_2]_s / [\text{Fe}]_s [\text{A}]_s^2$), and still assuming that $[\text{Na}]_r$ is equal to the cation-exchange capacity Ce_c , the following equation is obtained:

$$D_{\text{Fe}} = K_{3\text{Na}}^{\text{Fe}} \cdot \frac{Ce_c^3}{[\text{Na}]_s^3} \cdot \frac{1}{\beta_2^{\text{Fe}} [\text{A}]_s^2} + K_{\text{Na}}^{\text{FeA}} Ce_c \cdot \frac{K_1^{\text{Fe}}}{\beta_2^{\text{Fe}} [\text{A}]_s [\text{Na}]_s} \quad (\text{II})$$

Hypothesis of anion exchange

As determined previously, both AcO^- and A^{2-} potentially participate in an anion-exchange mechanism. In this case, the elution of a divalent metal is governed by the following two equilibria:



The distribution coefficient of a metal, in its complexed form, is given by

$$D_M = \frac{[\text{MA}_2]_r}{[\text{MA}_2]_s} \quad (9)$$

Since

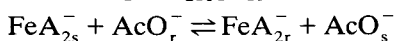
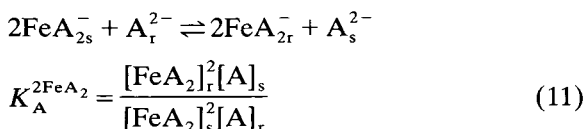
$$Ce_a = [\text{A}]_r + [\text{MA}_2]_r + [\text{AcO}]_r \quad (10)$$

where $[\text{MA}_2]_r$ is negligible, substitution of Eqs. 7, 8 and 9 in Eq. 10 gives

$$Ce_a = \frac{[\text{A}]_s}{K_A^{\text{MA}_2}} \cdot D_M + \frac{[\text{AcO}]_s}{(K_{2\text{AcO}}^{\text{MA}_2})^{1/2}} \cdot \sqrt{D_M} \quad (\text{III})$$

The distribution coefficient depends on the concentrations of both competing anions.

In the case of Fe(III), the only difference is in the charge of the complex:



$$K_{\text{AcO}}^{\text{FeA}_2} = \frac{[\text{FeA}_2]_r [\text{AcO}]_s}{[\text{FeA}_2]_s [\text{AcO}]_r} \quad (12)$$

Hence an equivalent expression to Eq. 10 may be written:

$$Ce_a = \frac{[\text{A}]_s}{K_A^{2\text{FeA}_2}} \cdot (D_{\text{Fe}})^2 + \frac{[\text{AcO}]_s}{K_{\text{AcO}}^{\text{FeA}_2}} \cdot D_{\text{Fe}} \quad (\text{IV})$$

Supposing either cation or anion exchange, the concentration of the PDCA and that of the acetate buffer in the mobile phase are independent parameters that determine the value of the distribution coefficient of each metal ion. The form of the dependence will be the discriminating factor that allows one to decide which mechanism is actually governing the retention.

3.3. Variation of the distribution coefficient of the metal ions with the eluent composition

The experimental verification of these models was performed by measurements of the retention time of the investigated metals with different eluting phases. The corresponding distribution coefficients were deduced in the usual way. In the first series of experiments, the concentration of the acetate buffer was varied, all other parameters remaining constant, while in the second series the concentration of the PDCA was the investigated parameter. Initially, interpretations will concern divalent metals only; the behaviour of Fe(III) will be analysed separately.

Influence of concentration of acetate buffer

Each eluent contained a constant concentration of PDCA, $6 \cdot 10^{-3} M$. The concentration of acetate was varied from $4 \cdot 10^{-3}$ to $0.25 M$ and the pH was adjusted to 4.5 by addition of acetic acid. Under these conditions the speciation of PDCA was constant all over the experiments.

Considering a purely cation-exchange mechanism, only $[\text{Na}]_s$ varies in Eq. I. $\log D_M$ versus $\log[\text{Na}]_s$ is expected to be linear with a slope of -2 . Fig. 2 shows that such is not the case, and, particularly, the existence of a plateau cannot be explained by the cation-exchange model.

A similar profile is observed (Fig. 3) when \log

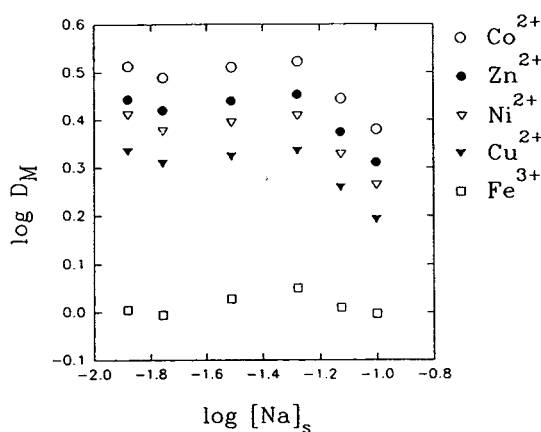


Fig. 2. Variation of the distribution coefficient of the transition metals with $[Na]_s$. Chromatographic conditions: column, CG5 + CS5; mobile phase, $6 \cdot 10^{-3} M$ PDCA with AcOH and AcONa at various concentrations (pH 4.5); flow-rate, 1.0 ml min^{-1} ; postcolumn reagent, $4 \cdot 10^{-4} M$ PAR– $3 M$ NH_3 – $1 M$ CH_3COOH (pH 9.7); flow-rate, 0.4 ml min^{-1} ; detection, visible at 520 nm; injection loop, 100 μl .

D_M is plotted versus $\log[AcO]_s$, but this may be explained quantitatively in the frame of an anion-exchange model by the modification of the resin phase. The concentrations of AcO^- and

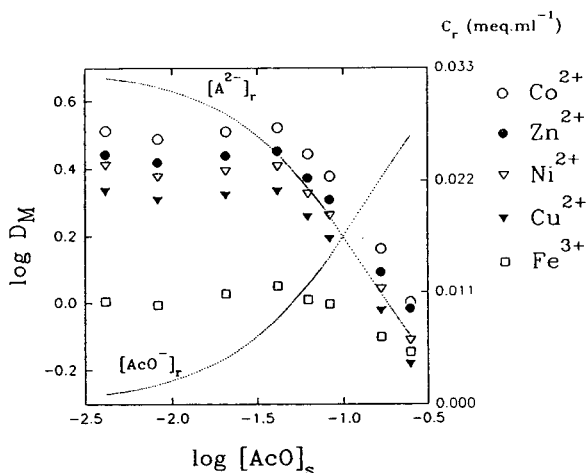


Fig. 3. Variation of the distribution coefficient of the transition metals with $\log[AcO]_s$. Dotted lines: concentrations in the resin of the anionic species of the eluent. Chromatographic conditions as in Fig. 2.

A^{2-} in the resin phase are also displayed (dotted lines).

First, the existence of a plateau is evidence for the steady elution behaviour of the analytes as long as $[A]_r$ is the prevailing species ($[A]_r > \frac{3}{4} Ce_a$). In this domain, the retention is governed by the exchange between MA_2^{2-} and A^{2-} , and Eq. III may be simplified to

$$Ce_a = \frac{[A]_s}{K_A^{MA_2}} \cdot D_M$$

where $[A]_s$ has a known constant value of $4.51 \cdot 10^{-3}$ mequiv. ml^{-1} . D_M is constant, and the selectivity coefficients between A^{2-} and each divalent metal cation can be deduced (Table 2).

Second, when $[AcO]_s$ increases, the composition of the stationary phase is modified and $[AcO]_r$ is no longer negligible; a ternary exchange takes place, $[A]_r$ decreases and so does D_M . Eq. III can be rewritten as

$$D_M = - \frac{K_A^{MA_2}}{[A]_s (K_{2AcO}^{MA_2})^{1/2}} \cdot [AcO]_s \sqrt{D_M} + \frac{K_A^{MA_2}}{[A]_s} \cdot Ce_a$$

If D_M is plotted versus $[AcO]_s \sqrt{D_M}$, straight lines are expected with an intercept $K_A^{MA_2} Ce_a / [A]_s$ and a slope $-[K_A^{MA_2} / (K_{2AcO}^{MA_2})^{1/2} [A]_s]$. Fig. 4 shows that linearity is achieved for the highest concentrations of acetate ions in solution, above $3 \cdot 10^{-2} M$, when the acetate ions occupy over 20% of the anion-exchange sites of the resin.

Table 2
Selectivity coefficients between A^{2-} and the PDCA complexes of the divalent metals

Experiment	Cu	Ni	Zn	Co
I	0.34	0.40	0.44	0.52
II	0.36	0.42	0.46	0.55
III	0.34	0.40	0.44	0.52
Mean	0.35 ± 0.03	0.41 ± 0.04	0.45 ± 0.05	0.53 ± 0.05

Values deduced from different experiments: I = variation of $[AcO]_s$, exchange with A^{2-} only; II = variation of $[AcO]_s$, exchange with A^{2-} and AcO^- ; III = variation of $[PDCA]_s$.

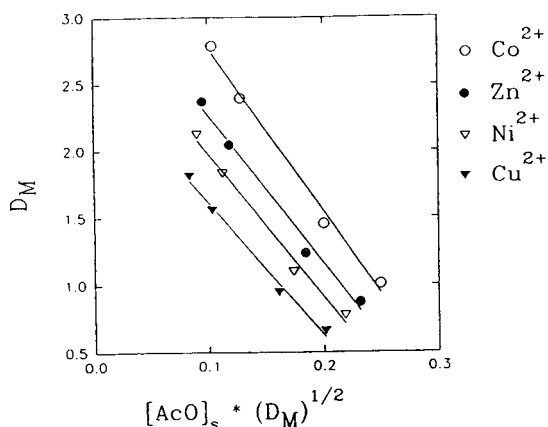


Fig. 4. Variation of the distribution coefficient of the transition metals with $[AcO]_s(D_M)^{1/2}$. Validation of the anion-exchange model for the divalent cations. Chromatographic conditions as in Fig. 2.

The linear part of the curves was fitted to obtain estimates of both $K_A^{MA_2}$ and $K_{2AcO}^{MA_2}$ (Tables 2 and 3); Table 4 gives the values of the selectivity coefficient K_{2AcO}^A , as calculated by the ratio of the two former coefficients. $K_A^{MA_2}$ values are in good agreement with those determined from the plateau but the K_{2AcO}^A values are larger by ca. 25% than the values determined in the first part of this work.

Influence of concentration of PDCA

In this series of experiments, $[AcOH] = 5 \cdot 10^{-2} M$, $[AcONa] = 5 \cdot 10^{-2} M$ and the concentration of PDCA in the eluent was varied from $1.6 \cdot 10^{-3}$ to $1.6 \cdot 10^{-2} M$; the final pH was

Table 3
Selectivity coefficients between AcO^- and the PDCA complexes of the divalent metals

Experiment	Cu	Ni	Zn	Co
II	65	75	84	97
III	59	71	84	96
Mean	62 ± 6	73 ± 7	84 ± 8	96 ± 9

Values deduced from different experiments: II = variation of $[AcO]_s$; III = variation of $[PDCA]_s$. See text for details.

Table 4
Selectivity coefficients between AcO^- and A^{2-}

Experiment	Cu	Ni	Zn	Co
II	181	179	183	176
III	174	178	191	185
Mean	181 ± 15			

Values deduced from the retention behaviour of the divalent metals in different experiments: II = variation of $[AcO]_s$; III = variation of $[PDCA]_s$. See text for details.

adjusted to 4.5 with NaOH. Under such conditions, $[AcO]_s$ was constant and equal to $4.15 \cdot 10^{-2} M$, but $[Na]_s$ varied and its variations were taken into account in the calculations to come.

If the exchange mechanism were of the cation-exchange type for the divalent metals, straight lines with a slope of -2 would be expected on plotting $\log D_M + 2 \log[Na]_s$ versus $\log[A]_s$ (Eq. 1). In Fig. 5, straight lines are observed but with a slope of -0.6 . This result confirms that cation

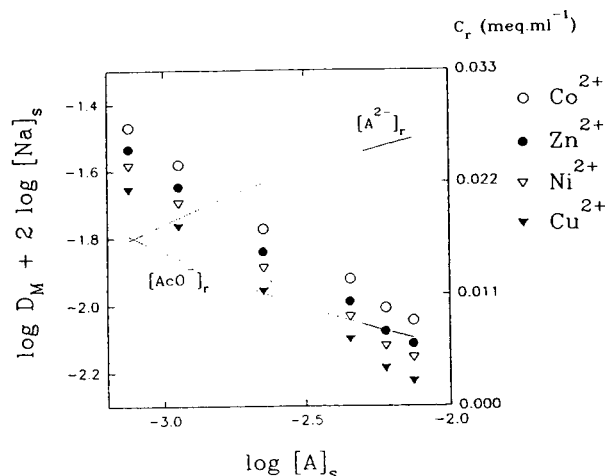


Fig. 5. Variation of $\log D_M + 2 \log[Na]_s$ versus $\log[A]_s$ for the divalent cations. Chromatographic conditions: column, CG5 + CS5; mobile phase, $5 \cdot 10^{-2} M$ -AcOH, $5 \cdot 10^{-2} M$ AcONa with PDCA at various concentrations (pH 4.5, adjusted with NaOH); flow-rate, 1.0 ml min^{-1} ; postcolumn reagent, $4 \cdot 10^{-4} M$ PAR-3 M NH_3 - $1 M$ CH_3COOH (pH 9.7); flow-rate, 0.4 ml min^{-1} ; detection, visible at 520 nm; injection loop, $100 \mu\text{l}$.

exchange cannot account for the retention behaviour of divalent metals.

On plotting $\log D_M$ as a function of $\log[A]_s$ (Fig. 6), a steady decrease can be observed with a slope reaching -1 in the region where A^{2-} prevails in the resin ($[A]_r > \frac{3}{4} Ce_a$). In this region, the exchange with acetate can be omitted and Eq. III can be simplified to

$$Ce_a = \frac{[A]_s}{K_A^{MA_2}} \cdot D_M$$

$$\log D_M = \log K_A^{MA_2} + \log Ce_a - \log[A]_s$$

The observed linear relationship between $\log D_M$ and $\log[A]_s$ confirms the theoretical model.

The rest of the plot can be represented according to the following expression of Eq. III:

$$[A]_s D_M = - \frac{K_A^{MA_2} [AcO]_s}{(K_{2AcO}^{MA_2})^{1/2}} \cdot \sqrt{D_M} + Ce_a K_A^{MA_2}$$

Fig. 7 shows that $[A]_s D_M$ does not vary with $\sqrt{D_M}$ over the first three points (no exchange with AcO). The remaining points for each cation lie on a straight line that corresponds to anion exchange of MA_2^{2-} with both AcO^- and A^{2-} . Estimates of $K_A^{MA_2}$ and $K_{2AcO}^{MA_2}$ can be deduced from regression analysis (Tables 2, 3 and 4) and

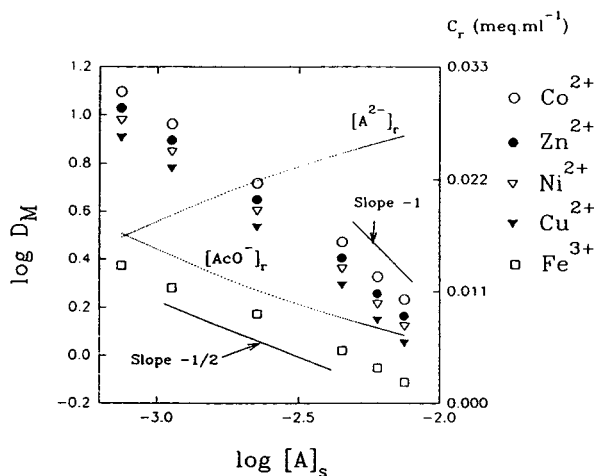


Fig. 6. Variation of the distribution coefficient of the transition metals with $\log[A]_s$. Dotted lines: concentrations in the resin of the anionic species of the eluent. Chromatographic conditions as in Fig. 5.

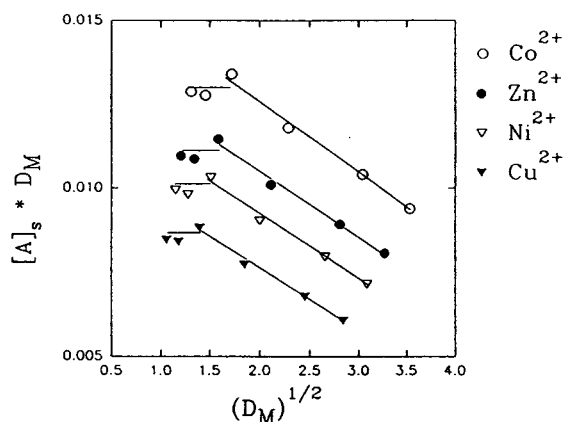


Fig. 7. Variation of $[A]_s D_M$ with $(D_M)^{1/2}$. Validation of the anion-exchange model for the divalent cations. Chromatic conditions as in Fig. 5.

the calculated values are in good agreement with those obtained from the previous series of experiments. Proposed mean values for the selectivity coefficients are also given in the corresponding tables.

From both series of experiments, it appears that the divalent cation complexes undergo an anion-exchange process in the column, the competing anions being AcO^- and A^{2-} .

Retention of Fe(III)

The behaviour of Fe(III) was studied separately, according to the models developed previously. Fig. 2 shows that, in the first series of experiments, D_{Fe} is almost constant when $[Na]_s$ varies over nearly one decade. This is not compatible with the cation-exchange model, which shows a strong dependence of the distribution coefficient on the concentration of the competing cation (Eq. II). Therefore, cation exchange can be excluded as the unique retention mechanism.

As far as the anion-exchange model is concerned, the variation of the distribution coefficient D_{Fe} with the concentration of the acetate in the eluent may be interpreted in the same way as for divalent metals: at low concentrations of acetate, D_{Fe} is constant because of single exchange with A^{2-} ; at higher AcO^- concentrations, D_{Fe} decreases owing to the possible additional exchange with acetate ions (Fig. 3). In

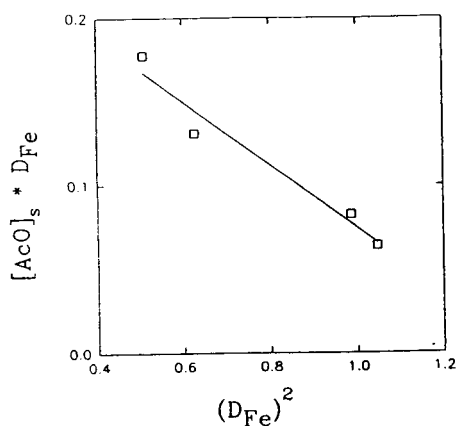


Fig. 8. Variation of $[\text{AcO}]_s D_{\text{Fe}}$ with $(D_{\text{Fe}})^2$. Validation of the anion-exchange model for iron(III). Chromatographic conditions as in Fig. 2.

this region, as suggested by Eq. IV, $[\text{AcO}]_s D_{\text{Fe}}$ is a linear function of $(D_{\text{Fe}})^2$ (Fig. 8). From the slope and intercept, the two selectivity constants were deduced: $K_A^{2\text{FeA}_2} = 0.19$ and $K_{\text{AcO}}^{\text{FeA}_2} = 7.9$.

In the second series of experiments, a linear dependence of $\log D_{\text{Fe}}$ on $\log[\text{A}]_s$ with a slope of $-1/2$ (Fig. 6) is observed over the investigated concentration range of PDCA in the eluent. Considering Eq. IV, it can be concluded that the term describing the exchange with AcO^- must be omitted to allow proper fitting of the data. In this instance, only A^{2-} is involved in an anion-exchange mechanism with the Fe(III)–PDCA complexes and Eq. (IV) is reduced to

$$C_{e_a} = \frac{[\text{A}]_s}{K_A^{2\text{FeA}_2}} \cdot (D_{\text{Fe}})^2$$

This allows one to calculate the value of the selectivity coefficient between FeA_2^- and A^{2-} :

$$K_A^{2\text{FeA}_2} = \frac{[\text{A}]_s}{C_{e_a}} \cdot (D_{\text{Fe}})^2 = 0.21$$

which is close to the value determined from the first series of experiments.

It can be observed that the selectivity coefficient between acetate and PDCA calculated from these constants ($K_{2\text{AcO}}^{\text{A}} = 318$) is higher than the value deduced from the retention data for divalent cations. Although this may be attrib-

uted to imprecision of the determination, it is more likely the existence of additional interactions that contribute to the retention of Fe(III) together with the probably prevailing anion-exchange mechanism.

3.4. Comparison with a purely anion-exchange stationary phase

Anion exchange seems to be the prevailing retention mechanism for all the metals investigated. To confirm this result, a mixture of $100 \mu\text{g l}^{-1}$ of each investigated cation was injected on to the mixed-bed column and on to a purely anion-exchange column (Dionex AS4A, an aminated styrene–divilbybenzene resin), using the same eluent E_0 in both cases (Fig. 9). For the four divalent species, the elution order is the same and the ratio of the distribution coefficient on the AS4A versus that on the CS5 for each metal is constant: $D_M(\text{AS4A})/D_M(\text{CS5}) = 1.06 \pm 0.05$. As the anion-exchange sites on both phases are of the same chemical nature, this result is a good indication of a similar behaviour of the

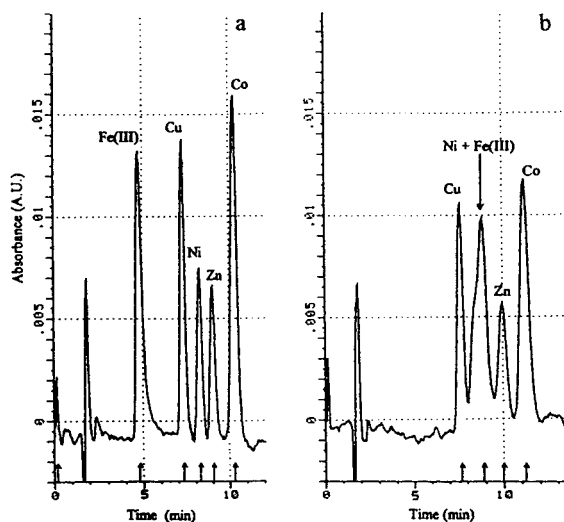


Fig. 9. Comparison of the retention of some transition metals ($100 \mu\text{g l}^{-1}$) on (a) the CS5 and (b) the AS4A column. Chromatographic conditions: mobile phase, $5 \cdot 10^{-2} \text{ M AcOH} - 5 \cdot 10^{-2} \text{ M AcONa} - 6 \cdot 10^{-3} \text{ M PDCA}$ (pH 4.5); flow-rate, 1.0 ml min^{-1} ; postcolumn reagent, $4 \cdot 10^{-4} \text{ M PAR} - 3 \text{ M NH}_3 - 1 \text{ M CH}_3\text{COOH}$ (pH 9.7); flow-rate, 0.4 ml min^{-1} ; detection, visible at 520 nm; injection loop, $100 \mu\text{l}$.

divalent cations in both chromatographic systems.

Fe(III) is much more retained on the purely anion-exchange resin than on the mixed-bed resin [$D_{\text{Fe}}(\text{AS4A})/D_{\text{Fe}}(\text{CS5}) = 2.14$], and co-elution with Ni is observed. Complete separation of all the metals is not achieved with this type of resin.

The CS5 column, with a total anion-exchange capacity of 70 $\mu\text{equiv.}$, should retain the anionic chelates more strongly than the AS4A column (20 $\mu\text{equiv.}$). The calculated distribution coefficient ratios show that such is not the case. Two other interactions can superimpose on ion exchange: (1) electrostatic repulsion between the anionic chelates and the sulfonate groups of the CS5 column (cation-exchange capacity 150 $\mu\text{equiv.}$) and (2) hydrophobic interactions which are stronger on the low capacity AS4A, and would specially affect the iron chelate, which is less polar than the divalent metal chelates because of its lower charge. Table 5 summarizes the separate contributions of these two interactions to the retention of the Fe(III) and of the divalent metals chelates. It can be inferred from this qualitative analysis that the resulting effect is a severe repulsion for divalent cation chelates on the CS5 column (electrostatic repulsion) that forces their early elution while they tend to undergo a slight additional retention on the AS4A column. Such additional contributions can explain the similar distribution coefficients on both columns, despite the different anion-exchange capacities. For this series of divalent metals, the CS5 column displays what could be

termed a “reduced apparent affinity” towards the anion-exchange sites.

Similarly, the odd behavior of the iron chelate may be the result of an increased affinity for the AS4A stationary phase (hydrophobic interactions), while both effects tend to neutralize each other on the CS5 column. Given the similar distribution coefficients of iron and the divalent metals on the AS4A column, hydrophobic interactions certainly play an important part in the retention.

Such a complex behaviour induced by hydrophobic affinity has been observed by other workers [7].

4. Conclusion

It can reasonably be concluded that on the CS5 mixed-bed column, the retention of transition metal cations is governed by electrostatic forces. Under the conditions of the recommended procedure (eluent E_0), the divalent metals and iron(III) follow an anion-exchange process involving their anionic PDCA chelates and the free divalent ligand. However, electrostatic repulsion between the cation-exchange sites and the chelates tends to decrease their “apparent affinity” for the resin, particularly for the divalent metal chelates. On a purely anion-exchange low-capacity phase, the contribution of hydrophobic adsorption is significant: the iron chelate is strongly retained and interferes with the divalent metal chelates, leading to an incomplete separation.

Table 5

Contribution of possible additional interactions to the retention of the transition metals

	Electrostatic repulsion		Hydrophobic interaction		Global effect	
	CS5	AS4A	CS5	AS4A	CS5	AS4A
MA_2^{2-}	--	~0	~0	+	--	+
FeA_2^-	-	~0	+	++	~0	++

-- = Decreased retention; + = increased retention; ~0 = little influence on the retention.

References

- [1] R.E. Smith, *Ion Chromatography Applications*, CRC Press, Boca Raton, FL, 1988, p. 76.
- [2] R.C. Foley and P.R. Haddad, *Chem. Aust.*, 54 (1987) 414.
- [3] D.T. Gjerde, *J. Chromatogr.*, 439 (1988) 49.
- [4] R.E. Smith, *Ion Chromatography Applications*, CRC Press, Boca Raton, FL, 1988, p. 144.
- [5] H. Sirén and M.-L. Riekkola, *J. Chromatogr.*, 590 (1992) 263.

- [6] P.N. Nesterenko, G. Zh. Amirova and T.A. Bol'shova, *Anal. Chim. Acta*, 285 (1994) 161.
- [7] A.R. Timerbaev, O.M. Petrukhin, I.P. Alimarin and T.A. Bol'shova, *Talanta*, 38 (1991) 467.
- [8] A. Klingenberg and A. Seubert, *J. Chromatogr.*, 640 (1993) 167.
- [9] J. Hradil, F. Svec, A.A. Aratskova, L.D. Belyakova and V.I. Orlov, *J. Chromatogr.*, 509 (1990) 369.
- [10] S.S. Heberling and J.M. Riviello, *Res. Dev.*, Sept. (1987) 74.
- [11] R.B. Rubin and S.S. Heberling, *Int. Lab.*, Sept. (1987) 54.
- [12] M.D.H. Amey and D.A. Bridle, *J. Chromatogr.*, 640 (1993) 323.
- [13] V. Cheam, *J. Chromatogr.*, 450 (1988) 361.
- [14] P.R. Haddad and P.E. Jackson, *Ion Chromatography Principles and Applications (Journal of Chromatography Library, Vol. 46)*, Elsevier, Amsterdam, 1990, p. 105.
- [15] R.E. Smith, *Ion Chromatography Applications*, CRC Press, Boca Raton, FL, 1988, pp. 78–82.
- [16] P.R. Haddad and P.E. Jackson, *Ion Chromatography Principles and Applications (Journal of Chromatography Library, Vol. 46)*, Elsevier, Amsterdam, 1990, pp. 56–66.
- [17] L.G. Sillen, *Stability Constants of Metal-Ion Complexes (Special Publication No. 17)*, Chemical Society, London, 1964, p. 545.
- [18] L.G. Sillen, *Stability Constants of Metal-Ion Complexes (Special Publication No. 17)*, Chemical Society, London, 1964, p. 364.
- [19] P.R. Haddad and R.C. Foley, *J. Chromatogr.*, 500 (1990) 301.
- [20] P. Hajos, G. Revesz, C. Sarzanini, G. Sacchero and E. Mentasti, *J. Chromatogr.*, 640 (1993) 15.



ELSEVIER

Journal of Chromatography A, 715 (1995) 117–126

JOURNAL OF
CHROMATOGRAPHY A

Influence of bulk and surface composition on the retention of colloidal particles in thermal field-flow fractionation

Paul M. Shiundu¹, J. Calvin Giddings*

Field-Flow Fractionation Research Center, Department of Chemistry, University of Utah, Salt Lake City, UT 84112, USA

First received 18 November 1994; revised manuscript received 9 May 1995; accepted 12 May 1995

Abstract

In this paper we report a wide range of cases in which the retention of colloidal particles in thermal field-flow fractionation (FFF) shows a strong dependence on the chemical composition of the particles or of the particle surfaces. These results are observed among similar particles (such as different latexes) or between dissimilar particles (including latexes as well as inorganic and metallic colloids). These compositional effects are observed for particles suspended in both aqueous and nonaqueous carrier liquids. The dependence of retention on composition is complementary to its dependence on particle size, which has been amply demonstrated in previous studies. The compositional effect is attributed to the dependence of the thermal diffusion coefficient on compositional factors.

A number of cases are presented here where compositional effects are significant. Examples include the baseline resolution of 0.30- μm silica particles and 0.300- μm polystyrene (PS) particles and a large difference in retention times between 0.232- μm PS and 0.229- μm polymethylmethacrylate (PMMA) latexes in aqueous suspensions. Also, metallic particles (e.g., palladium) were less retained than silica particles, with latex particles most retained. The resolution of equal-size particles in the nonaqueous carrier liquid acetonitrile is also demonstrated.

Surface compositional effects have also been found in this study. These effects suggest the possibility of colloidal surface analysis by thermal FFF. The potential for performing both bulk and surface compositional analysis of particles by thermal FFF makes this FFF technique complementary to both sedimentation FFF and flow FFF techniques for the analysis of complex particulate materials.

1. Introduction

The capabilities of the field-flow fractionation (FFF) family of techniques to separate and characterize a broad range of macromolecular, colloidal, and particulate materials has now been well established [1]. For over two decades one of the FFF techniques, thermal field-flow fractiona-

tion (ThFFF), was used exclusively for the separation and characterization of synthetic polymers [2–16]. The molecular mass range studied has been wide, extending to ultra-high molecular mass polymers of mass ca. $20 \cdot 10^6$ [17]. Recently, however, the applications of ThFFF have expanded to include the retention and fractionation of particulate materials suspended in both aqueous and nonaqueous carrier liquids [18–20]. The technique has been applied both to colloidal particles (those under 1 μm diameter) and micrometer-size particles up to 20 μm diameter.

* Corresponding author.

¹ Present address: Department of Chemistry, University of Nairobi, PO Box 30197, Nairobi, Kenya.

Particles are separated selectively according to size in both diameter ranges. However, these initial studies have demonstrated that retention also depends on the composition of the particles. The compositional dependence of retention is the focus of this study. If compositional effects are found to be sufficiently selective, ThFFF could become a valuable tool for the compositional analysis of particulate materials.

By examining the theory of ThFFF, it can be shown that compositional effects derived from the compositional dependence of the thermal diffusion coefficient D_T , a basic transport coefficient describing the movement of matter under an applied temperature gradient. In order to understand compositional effects in ThFFF, the compositional dependence of D_T must be known. Unfortunately, the fundamental basis of D_T is not well understood. However, ThFFF can be used to rapidly accumulate data on the compositional dependence of D_T . Accordingly, D_T measurements of several types of latex particles as well as silica particles have been made using ThFFF [18,19].

The compositional dependence of the retention of particles in ThFFF appears to be analogous to compositional effects for polymers. Many studies have shown that polymer retention depends on the chemical nature of the polymer as well as on its molecular mass [21–24]. The possibility for using ThFFF for the analysis of polymer composition as well as molecular mass has been under consideration for some time [21].

According to theory, the retention of sample materials (either polymeric or particulate) in ThFFF is controlled by two transport processes: ordinary concentration diffusion, coefficient D , and thermal diffusion, coefficient D_T [21]. Of the two parameters, only D is well understood. According to the Stokes–Einstein expression ($D = kT/3\pi\eta d$, where k = Boltzmann's constant, T = absolute temperature, η = solvent viscosity, and d = hydrodynamic diameter), D can be readily calculated if the hydrodynamic diameter d of the polymeric molecule or particle is known. Because the use of sample materials with well-characterized D values simplifies the examination of D_T , standard spherical particles of known

sizes were used in our experiments in order to improve the measurement process and eventually arrive at a better understanding of the thermal diffusion phenomenon in ThFFF.

Specific factors that influence D_T (and thus control retention) are not yet fully understood. However, some interesting characteristics of D_T have been determined that are applicable to both polymeric and particulate sample materials. For instance, D_T has been found to be sensitive not only to the chemical nature of the retained components but also to the solvent used [19,22]. However, it has been established that D_T for specific polymer classes is essentially constant, independent of both the molecular mass and the form of branching of the polymer molecule [23]. This is in sharp contrast with the behavior of particles in which D_T shows a significant dependence on diameter d [18]. In a recent publication, we reported opposite trends in the dependence of D_T on d for aqueous and nonaqueous carrier liquids (i.e., positive and negative slopes in the plots of D_T versus d , respectively), with the latter media showing a relatively smaller dependence [19].

The dual size–composition dependence of retention in ThFFF has the potential to provide particle compositional analysis, thereby making ThFFF a technique that could complement both sedimentation FFF and flow FFF for the characterization of complex sample materials. The possibility of doing a composition-based separation and analysis of particles was first suggested in an earlier publication [18]. However, in order to realize this goal, a better understanding of the influence of particle composition on D_T is required. For instance, we need to know whether the observed compositional effects are surface- or bulk-driven phenomena.

In this paper, we demonstrate that ThFFF can separate various particles of the same or similar size (or size distribution) that have different chemical compositions. We also report that modifying the surface of submicron particles has an effect on retention behavior, hence showing the influence of surface properties on observed compositional effects. Thus, based on the apparent sensitivity of the retention of colloidal par-

ticles on the particle surface, we demonstrate the potential of ThFFF to determine the chemical composition of particle surfaces.

2. Theory

According to the standard retention theory for normal-mode FFF, retention time t_R is related to the dimensionless retention parameter λ of a retained component by the expression [25,26]

$$\frac{t_R}{t^o} = \frac{1}{6\lambda[\coth(1/2\lambda) - 2\lambda]} \quad (1)$$

where t^o is the void time (the time needed to elute a nonretained component) and $\lambda = l/w$, where w is the channel thickness or distance between the hot and cold walls and l is the distance from the cold wall to the center of gravity of the component zone. The parameter λ is a measure of the extent of interaction between the external field or gradient and the sample component. From Eq. 1, it is clear that each experimental measurement of t_R yields a unique value of λ . Eq. 1 is, however, an approximation for ThFFF since it is based on a parabolic flow profile model which assumes uniform viscosity across the channel. Therefore, this expression needs to be corrected to account for distortions due to viscosity changes caused by the temperature gradient applied across the channel [27]. Such corrections have been made for all the calculated results provided in this paper.

For purposes of better understanding the relationships among t_R , λ , and the underlying transport coefficient D_T , we use several approximations that result in simple, but still reasonably accurate, mathematical forms. First of all, we begin with Eq. 1 despite perturbations caused by viscosity gradients. Second, for highly retained species (i.e., $\lambda \rightarrow 0$), we use the limiting form of Eq. 1

$$\frac{t_R}{t^o} = \frac{1}{6\lambda} \quad (2)$$

We next need the relationship between the retention parameter λ and the coefficients D and D_T . This dependence is expressed by

$$\frac{1}{\lambda} = \frac{wD_T dT}{D dx} \quad (3)$$

where dT/dx is the temperature gradient applied across the component band in the channel. By assuming a linear temperature gradient across the channel thickness, the product $w dT/dx$ can be approximated as the temperature drop ΔT applied between the cold and hot walls. Thus, Eq. 3 is approximated by

$$\frac{1}{\lambda} = \frac{D_T \Delta T}{D} \quad (4)$$

Combining Eqs. 2 and 4, we get

$$\frac{t_R}{t^o} = \frac{D_T \Delta T}{6D} \quad (5)$$

From Eq. 5 it is evident that at constant ΔT , variations in t_R for different particles suspended in the same carrier solution can be attributed to differences in both D and D_T . Using the Stokes–Einstein expression ($D = kT/3\pi\eta d$), we can obtain the value of D for particles of known d . By substituting the Stokes–Einstein expression for D into Eq. 5, we get

$$\frac{t_R}{t^o} = \frac{\pi\eta d D_T \Delta T}{2kT} \quad (6)$$

Because particles having the same size distribution are expected to have equivalent values of d and D , this equation shows that significant differences in their retention times can only be attributed to variations in D_T .

3. Experimental

The ThFFF system used for this work is similar in design to the Model T100 polymer fractionator from FFFractionation (Salt Lake City, UT, USA). Details are provided elsewhere [18]. The channel spacer was confined between two chrome-plated copper bars, with the top bar heated using rods controlled by relay switches with cycle times activated by a microprocessor. The cold wall was cooled using continuously flowing tap water. The temperatures of the hot and cold walls were monitored through three

thermal sensors that were inserted (two in the hot and one in the cold wall) into wells drilled into both the top and bottom bars.

The thickness of the mylar channel spacer used here was 76 μm , unless stated otherwise. The channel had a breadth of 2.0 cm and a tip-to-tip length of 46 cm. The ΔT used was 45 K unless indicated otherwise. Both acetonitrile (ACN) and aqueous carrier liquids were used in this study. They were delivered using a Model M-6000A pump from Waters Associates (Milford, MA, USA). The spectrograde ACN was obtained from EM Science (Cherry Hill, NJ, USA); its ionic strength was modified by 0.10 mM tetrabutylammonium perchlorate (TBAP). The aqueous carriers were either a phosphate buffer of ionic strength 0.01 M and pH 4.52 (or 9.68) or consisted of doubly distilled water containing 0.1% FL-70 surfactant plus 0.02% sodium azide. The flow-rate used was 0.20 ml/min unless noted otherwise. A Model UV-106 detector from Cole Scientific (Calabasas, CA, USA) operating at 254 nm wavelength was used to detect particles eluting from the ThFFF channel. Data acquisition of the detector signal was accomplished using a PC-AT compatible computer. The detector signal was also recorded using an OmniScribe chart recorder from Houston Instruments (Austin, TX, USA). Samples were injected via a 20- μl loop injection valve.

Several types of particles from different sources were used in this work. Silica particles of nominal diameters 0.15 and 0.25 μm were obtained from E. Merck (Darmstadt, Germany) while particles of 0.30 μm were obtained from Bangs Laboratories (Carmel, IN, USA). Polybutadiene (PB) and polystyrene (PS) latex particles were obtained from Dow Chemical (Midland, NJ, USA) and Duke Scientific (Palo Alto, CA, USA), respectively. Polymethylmethacrylate (PMMA) and 0.230- μm polystyrene-polymethylmethacrylate (PS/PMMA) core-shell latex particles were obtained from Seradyn (Indianapolis, IN, USA) and Bangs Laboratories. The core-shell latex particles consist of a PS core and a PMMA shell. Also obtained from Bangs Laboratories were 0.210- μm PS/acrylamide + hydrazine particles (containing 10 $\mu\text{eq/g}$ of

particles with-NHNH₂ surface functional groups), 0.091- μm styrene-14% vinylbenzylchloride (VBC) having-CH₂Cl surface groups, and 0.098- μm styrene-34% vinylbenzylchloride (VBC) copolymer latex particles.

The surface of the 0.30- μm silica particles was modified by derivatization of the silanol groups using the process reported by Little et al. [28]. The silanization reagent used was octadecyl trichlorosilane and some of the unreacted silanol groups were "capped" using trimethylchlorosilane.

4. Results and discussion

Fig. 1a shows plots of t_R/t^0 (retention time relative to void time) versus d for PS, PB, PMMA, and silica particles suspended in ACN carrier liquid. The concentration of tetrabutylammonium perchlorate (TBAP) used was 0.10 mM. (The importance of using a salt in nonaqueous carrier liquids was established in a previous publication [3].) Other experimental conditions entailed a channel flow-rate of 0.30 ml/min, a ΔT of 30 K, and a corresponding cold wall temperature of 287 K. It is evident from the figure that retention in ThFFF is not only dependent on particle size but also on the particle chemical composition. The dependence of particle retention on composition is reflected in the different retention levels for the various particle types. The figure shows that silica particles are the least retained compared to the three types of latex particles and that the retention levels varied between the different latexes. This variation among latexes is also found in aqueous carrier suspensions, as shown in Fig. 1b. The carrier liquid in this case was doubly distilled water containing 0.10 mM concentration of TBAP, with the other experimental conditions the same as in Fig. 1a. These results show that latex particles are retained somewhat longer in an aqueous carrier suspension than in the nonaqueous carrier liquid. It is also significant to note that the order of retention of the PMMA particles has been reversed in the two carrier

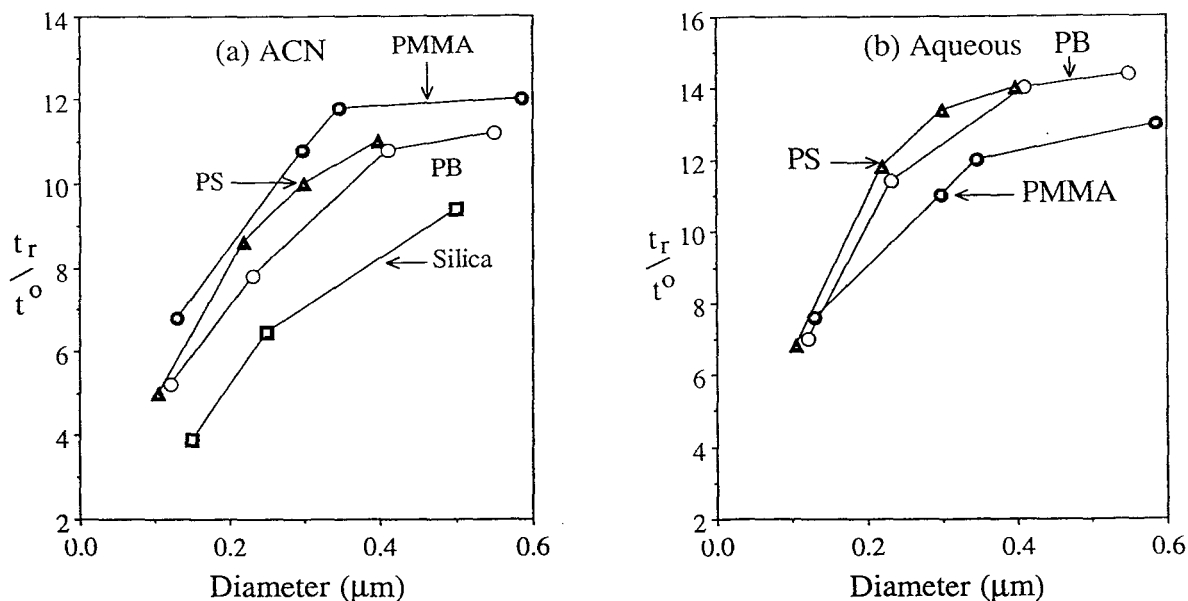


Fig. 1. Plots of retention time t_r (relative to void time t^0) versus particle diameter for (a) PS, PB, PMMA, and silica particles suspended in ACN, and (b) PS, PB, and PMMA particles suspended in an aqueous medium. Experimental conditions: flow-rate = 0.30 ml/min, [TBAP] = 0.10 mM, $\Delta T = 30$ K, $T_c = 287$ K.

liquids relative to both PS and PB (i.e., PMMA is the most retained latex in ACN and least retained in the aqueous carrier liquid). These observations further illustrate the dependence of particle retention in ThFFF on the composition of both the particle and the carrier solution.

Additional results showing compositional effects on latex particle retention in an aqueous carrier suspension are shown in Fig. 2. The figure shows elution profiles of different types of latexes of similar size distributions suspended in a phosphate buffer of pH 9.68 and ionic strength of 0.01 M. It is clear that the 0.232- μm PS particles are retained the most, followed by 0.230- μm PB latex beads. The 0.229- μm PMMA shows comparable retention with the 0.230- μm PS/PMMA core-shell latex particles. Two interesting observations can be made from this figure: (1) It is possible to separate equal sizes of PS from PB or PS from PS/PMMA, and (2) modification of the surface of latex particles can have a dramatic effect on retention behavior. For instance, despite the similar size distribution of the core-shell PS/PMMA and the PS latexes,

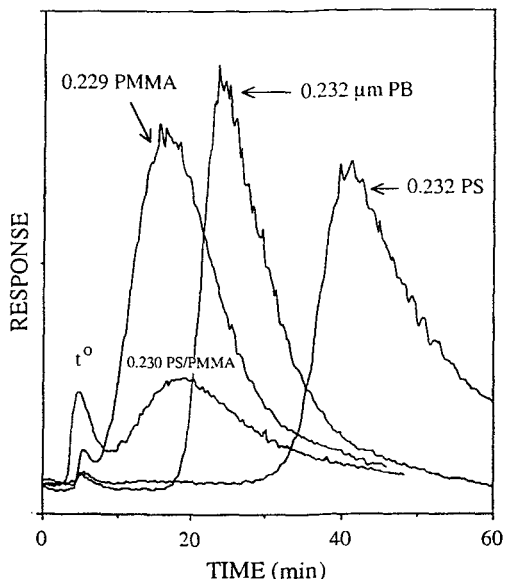


Fig. 2. Superimposed elution profiles of 0.229- μm PMMA, 0.230- μm PS/PMMA (core-shell), 0.232- μm PB, and 0.232- μm PS latex beads in a 0.01 M ionic strength phosphate buffer at pH 9.68. Experimental conditions: flow-rate = 0.20 ml/min, $\Delta T = 45$ K, and $T_c = 288$ K.

different retention times were observed for these samples. This illustrates the potential influence of surface properties on particle retention behavior in ThFFF. Of additional significance is the order and magnitude of the elution times for the PS and PB particles in the phosphate buffer carrier liquid. The elution order is similar to that reported for ACN in Fig. 1; however, the degree of separation is much higher in an aqueous carrier medium than was previously reported with ACN as a carrier liquid [19].

As mentioned earlier, the contribution of D to retention time in ThFFF should be the same for particles having the same or comparable size distributions. Thus, the observed differences in the retention times shown in Fig. 2 are attributable to the differences in their thermal diffusion coefficients, reflecting the dependence of D_T on particle chemical composition. This explanation is consistent with Eqs. 5 and 6.

The dual dependence of retention on both size and chemical composition promises to make ThFFF complementary to both sedimentation FFF, which separates samples according to den-

sity and size, and flow FFF, which separates sample materials only according to their hydrodynamic size (and hence would not distinguish between chemically unlike samples having similar size distributions).

Retention dependence on chemical composition between dissimilar types of particles (e.g., latexes versus inorganic or metallic particles) is widely observed. Such compositional effects are shown clearly in Fig. 3. Fig. 3a shows the separation of 0.25- μm silica particles from 0.232- μm PS latex particles in an aqueous carrier solution containing 0.1% FL-70 surfactant plus 0.02% sodium azide (as electrolyte and bactericide). In spite of the somewhat larger mean size of silica particles compared to PS particles, the silica particles are much less retained. This observation is consistent with the results shown in Fig. 1a. Fig. 3b similarly shows the near-baseline resolution between 0.30- μm silica particles and 0.300- μm PS latex beads. The experimental conditions were similar to those reported for Fig. 3a, except that the flow-rate was 0.30 instead of 0.20 ml/min.

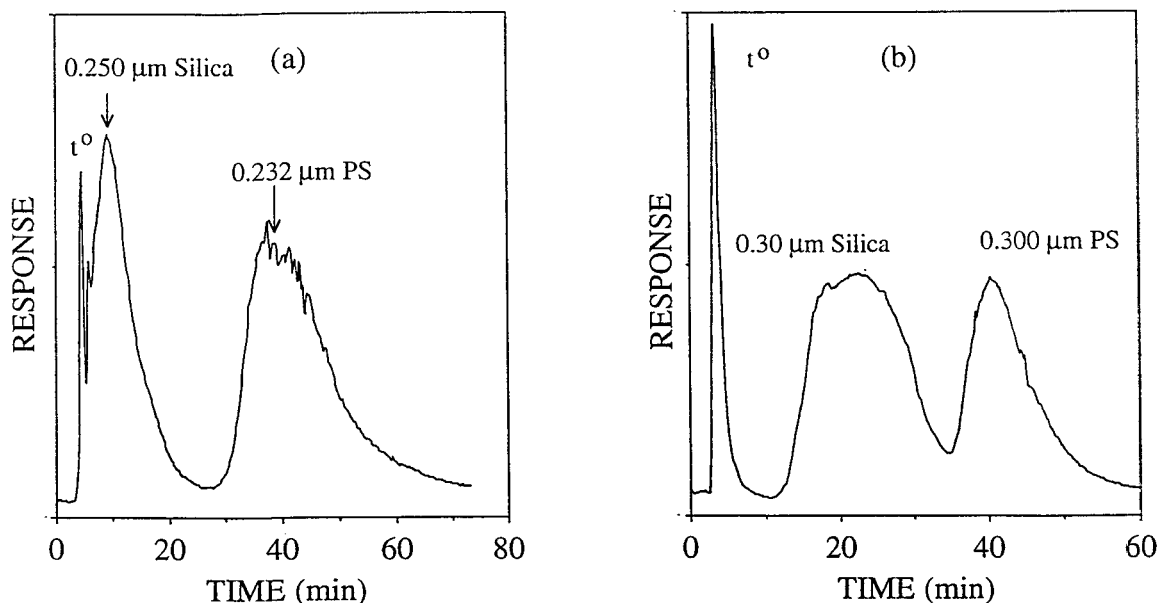


Fig. 3. Separation of submicrometer populations of silica and PS particles suspended in an aqueous carrier medium: (a) 0.25- μm silica and 0.232- μm PS particles and (b) 0.30- μm silica and 0.300- μm PS particles. Experimental conditions: flow-rate = 0.20 ml/min for (a) and 0.30 ml/min for (b), and $\Delta T = 45$ K, and $T_c = 288$ K.

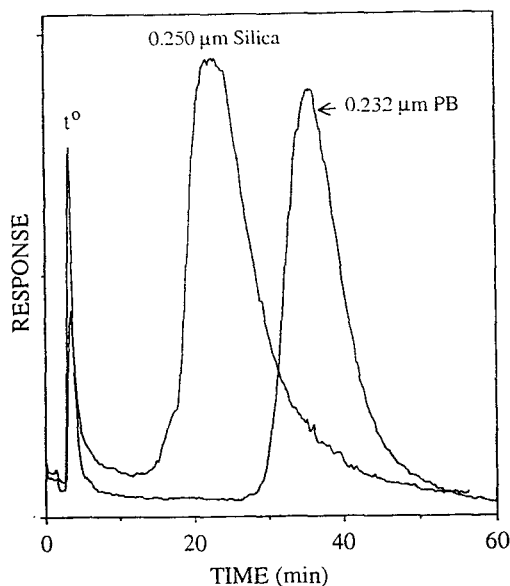


Fig. 4. Superimposed elution profiles of 0.232- μm PB and 0.250- μm silica particles suspended in ACN. Experimental conditions: flow-rate = 0.30 ml/min, [TBAP] = 0.10 mM, $\Delta T = 45$ K, and $T_c = 288.5$ K.

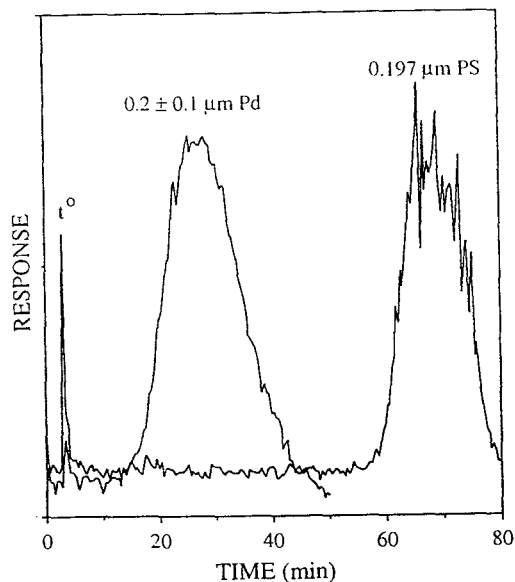


Fig. 5. Superimposed elution profiles of 0.198- μm PS and 0.2 \pm 0.1- μm Pd metal particles suspended in ACN. Experimental conditions: flow-rate = 0.70 ml/min, [TBAP] = 0.10 mM, $\Delta T = 40$ K, and $T_c = 286$ K.

Similar compositional effects are observed in nonaqueous carrier suspensions. Fig. 4 shows superimposed elution profiles of 0.232- μm PB and 0.25- μm silica particles obtained with ACN as the carrier liquid in a channel with a flow-rate of 0.30 ml/min, a ΔT of 20 K, and a cold wall temperature T_c of 288.5 K. The 0.25- μm silica particles were retained less than the PB latex beads, demonstrating the weaker thermal diffusivity of silica particles.

Fig. 5 shows superimposed elution profiles of 0.197- μm PS particles and 0.2 \pm 0.1- μm palladium (Pd) metal particles obtained using ACN as carrier liquid in a channel with a flow-rate of 0.50 ml/min, a ΔT of 40 K, a cold wall temperature of 286 K, and a concentration of TBAP of 0.10 mM. (The channel thickness in this case was 127 μm .) Here again the retention time (measured at peak maxima) of the smaller PS latex particles is over twice as long as that of the Pd particles, showing the much weaker thermal diffusivity of metal particles relative to latexes. This is the first report on the use of ThFFF to retain metal particles.

Despite the accumulation of evidence that D_T has a dependence on the chemical composition of particulate materials, most data do not indicate whether surface or bulk properties dominate these compositional effects. However, one of the retention experiments reported above suggests that surface composition effects are dominant in determining retention. This suggestion arises from Fig. 2, which shows that the retention of the PS/PMMA core-shell latex (in which the shell is composed of PMMA) is very close to that of equal-sized PMMA particles but substantially less than the observed retention of PS latex particles. This provocative result requires further substantiation.

In an attempt to further determine the relative contributions of bulk and surface composition, experiments were conducted using particles whose surfaces were either modified chemically or that had different compositions. First, we examine 0.30- μm silica particles, some untreated and some of whose surfaces were chemically derivatized by silanization using octadecyl trichlorosilane reagent. Fig. 6 shows the elution

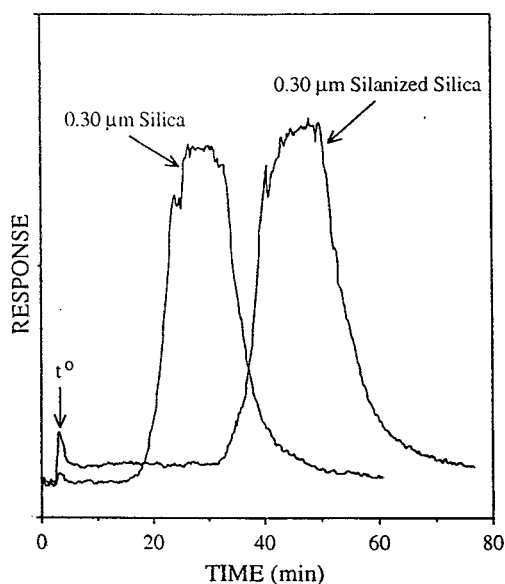


Fig. 6. Superimposed elution profiles of equal-size ($0.30\text{-}\mu\text{m}$) silanized and unsilanized silica particles in an aqueous carrier liquid. Experimental conditions: flow-rate = 0.30 ml/min , $\Delta T = 45\text{ K}$, and $T_c = 289\text{ K}$.

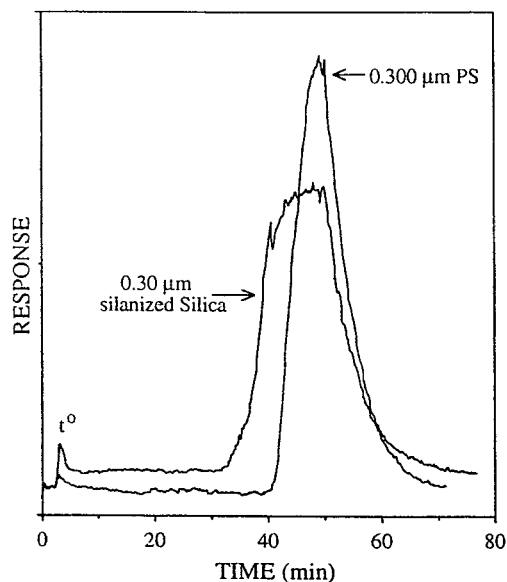


Fig. 7. Superimposed elution profiles of $0.300\text{-}\mu\text{m}$ PS latex beads and $0.30\text{-}\mu\text{m}$ silanized silica particles in an aqueous carrier liquid. Experimental conditions: flow-rate = 0.30 ml/min , $\Delta T = 45\text{ K}$, and $T_c = 289\text{ K}$.

profiles of the two forms of silica particles obtained under identical experimental conditions. The aqueous carrier contained 0.1% FL-70 and 0.02% sodium azide, the flow-rate was 0.30 ml/min , and ΔT was 45 K . From the two profiles, it is evident that the surface-derivatized silica particles were retained much longer than their underivatized counterparts, despite their equal size distributions. (It should be possible to baseline resolve any two monodisperse components.)

The above results further illustrate the sensitivity of particle retention in ThFFF to the chemical composition of the particle surface. While our understanding of the nature of this dependence is still limited, it may be related in part to the hydrophobicity or hydrophilicity of the particle surface. This hypothesis is substantiated by Fig. 7, which shows superimposed elution profiles of $0.300\text{-}\mu\text{m}$ PS latex particles and the $0.30\text{-}\mu\text{m}$ silanized silica particles. The two profiles almost coelute, in contrast with the earlier results shown in Fig. 3b where the unsilanized $0.30\text{-}\mu\text{m}$ silica was nearly baseline re-

solved from the $0.300\text{-}\mu\text{m}$ PS particles. The transformation of the silica surface from a hydrophilic surface (containing predominantly silanol groups) to a more hydrophobic surface comprised of long-chain hydrocarbons may account for the similarity in retention behavior of the silanized silica and the PS latex particles. (We assume that the relatively low-density coverage of the PS surface by sulfonate groups and the presence of some nonderivatized silanol groups on the silica surface only weakly affect retention.)

Additional experiments performed using PS latexes having comparable or equal size distributions and having different surface functional groups (generally at low density) such as carboxylates, sulfonates, hydroxylates, and so on, showed no significant differences in retention times. These results are omitted here for reasons of brevity. However, a significant difference in retention times was observed between the $0.198\text{-}\mu\text{m}$ PS and $0.210\text{-}\mu\text{m}$ PS/acrylamide + hydrazine particles. These results are shown in Fig. 8a. An aqueous carrier solution made up of

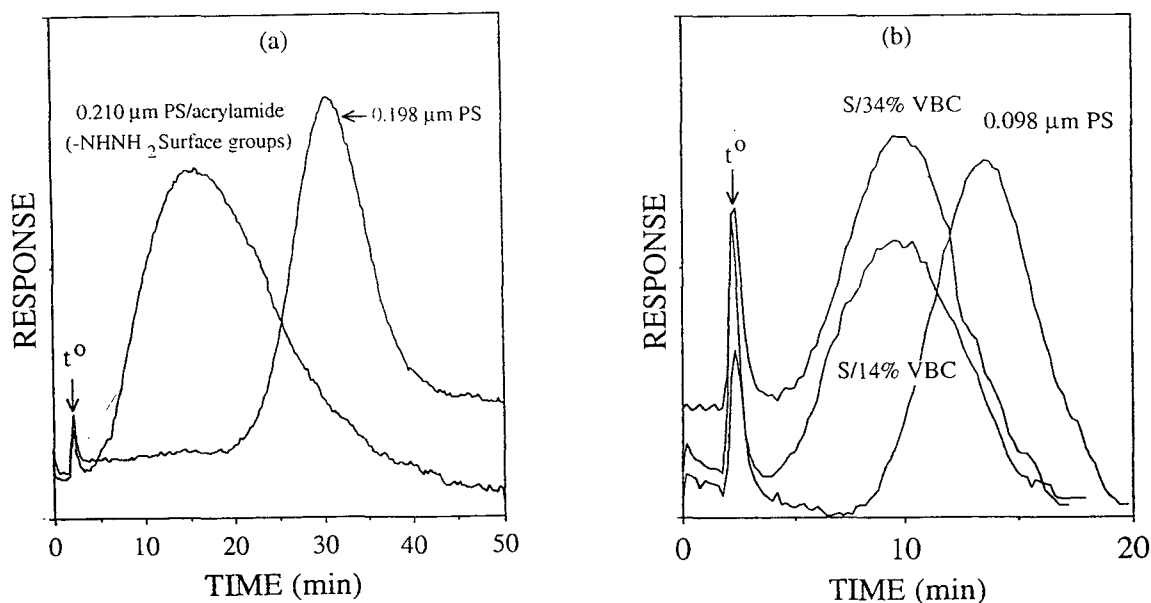


Fig. 8. (a) Elution profiles of 0.198- μm PS particles and 0.210- μm PS/acrylamide + hydrazine ($-\text{NHNH}_2$ surface groups) suspended in an aqueous carrier liquid containing 0.1% FL-70 surfactant and 0.02% sodium azide. Experimental conditions: flow-rate = 0.30 ml/min, $\Delta T = 40$ K, and $T_c = 286$ K. (b) Elution profiles of 0.098- μm PS particles, 0.098- μm S/34% VBC ($-\text{CH}_2\text{Cl}$ surface groups), and 0.091- μm S/14% VBC ($-\text{CH}_2\text{Cl}$ surface groups). The carrier solution and experimental conditions are the same as in (a).

0.1% FL-70 surfactant and 0.02% sodium azide (as a bactericide) was used. The channel flow-rate was 0.30 ml/min and ΔT was 40 K with a corresponding cold wall temperature of 311 K. These results further illustrate a tendency toward a weaker retention for the more hydrophilic surface.

In Fig. 8b, the retention profile of 0.098- μm PS is compared with the profiles of both 0.091- μm S/14% VBC and 0.098- μm S/34% VBC, both having $-\text{CH}_2\text{Cl}$ surface groups. The retention times of the two S/VBC copolymer particles appear to be independent of the ratio of styrene (S) to vinylbenzylchloride (VBC), but neither is retained as long as the 0.098- μm PS particles. Unfortunately, it is not clear whether the difference in retention time between the PS and the S/VBC particles is due to their different surface groups or to the fact that S/VBC is a copolymer whereas PS is not. Additional latex samples with well-defined bulk and surface properties would have to be studied to resolve this question.

5. Conclusions

In this paper we demonstrate that the effects of chemical composition on retention are sufficiently strong that the separation of equal-size particles in a variety of compositional classes (latex, inorganic, metallic) can be readily achieved. We thereby open up possibilities for compositional separations and analysis by ThFFF. This prospect is intriguing because field-flow fractionation techniques are generally considered to be physical separation methods that have only a secondary dependence on chemical composition. The results of this study show that the effects of composition might be quite subtle. Furthermore, the prospect that colloidal materials can be differentiated according to their surface composition not only has significant implications in utilizing ThFFF as a new surface analysis tool but is also suggestive of the enormous complexity of the chemical composition effects that underlie ThFFF retention.

Although this study has primarily focused on the intricate effects of changes in particle composition, the potential role of the carrier liquid composition is similarly promising. Once the thermal diffusion process is better understood, it may be possible to alter the composition of the carrier liquid in order to generate differential retention shifts. These shifts might be engineered to enhance resolution based on particle compositional factors of interest while suppressing resolution based on unimportant compositional differences. A great deal more work is needed to define and exploit these intricate compositional effects.

Acknowledgements

This work was supported by Grant CHE-932 2472 from the National Science Foundation. We would like to thank Dr. Grant Von Wald of Dow Chemical for providing polybutadiene latexes and Dr. J.N. Kinkel of E. Merck who supplied us with the silica particles.

Symbols

d	particle diameter
dT/dx	temperature gradient in channel
D	ordinary diffusion coefficient
D_T	thermal diffusion coefficient
k	Boltzmann's constant
l	mean thickness of sample zone
R	retention ratio
t_R	retention time
t°	channel void time
T	absolute temperature
T_c	cold wall temperature
w	channel thickness
ΔT	temperature drop across channel
η	viscosity
λ	dimensionless retention parameter

References

[1] J.C. Giddings, *Science*, 260 (1993) 1456–1465.

- [2] G.H. Thompson, M.N. Myers and J.C. Giddings, *Sep. Sci.*, 2 (1967) 797–800.
- [3] G.H. Thompson, M.N. Myers and J.C. Giddings, *Anal. Chem.*, 41 (1969) 1219–1222.
- [4] J.C. Giddings, M.E. Hovingh and G.H. Thompson, *J. Phys. Chem.*, 74 (1970) 4291–4294.
- [5] J.C. Giddings, Y.H. Yoon and M.N. Myers, *Anal. Chem.*, 47 (1975) 126–131.
- [6] J.C. Giddings, K.D. Caldwell and M.N. Myers, *Macromolecules*, 9 (1976) 106–112.
- [7] J.C. Giddings, M.N. Myers, G.C. Lin and M. Martin, *J. Chromatogr.*, 142 (1977) 23–38.
- [8] M. Martin and P. Reynaud, *Anal. Chem.*, 52 (1980) 2293–2298.
- [9] J. Janca and K. Kleparnik, *Sep. Sci. Technol.*, 16 (1981) 657–670.
- [10] M. Martin, *Chromatographia*, 15 (1982) 426.
- [11] M. Martin and J. Hes, *Sep. Sci. Technol.*, 19 (1984) 685.
- [12] J.J. Kirkland, S.W. Rementer and W.W. Yau, *J. Appl. Polym. Sci.*, 38 (1989) 1383–1395.
- [13] M.E. Schimpf, *J. Chromatogr.*, 517 (1990) 405–421.
- [14] Y. Gao and X. Chen, *J. Appl. Polym. Sci.*, 45 (1992) 887–892.
- [15] J.J. Kirkland and S.W. Rementer, *Anal. Chem.*, 64 (1992) 904–913.
- [16] A.C. van Asten, E. Venema, W.Th. Kok and H. Poppe, *J. Chromatogr.*, 644 (1993) 83–94.
- [17] Y.S. Gao, K.D. Caldwell, M.N. Myers and J.C. Giddings, *Macromolecules*, 18 (1985) 1272–1277.
- [18] G. Liu and J.C. Giddings, *Chromatographia*, 34 (1992) 483–492.
- [19] P.M. Shiundu, G. Liu and J.C. Giddings, *Anal. Chem.*, in press.
- [20] G. Liu and J.C. Giddings, *Anal. Chem.*, 63 (1991) 296–299.
- [21] J.J. Gunderson and J.C. Giddings, *Macromolecules*, 19 (1986) 2618–2621.
- [22] M.E. Schimpf and J.C. Giddings, *J. Polym. Sci. Polym. Phys. Ed.*, 27 (1989) 1317–1332.
- [23] M.E. Schimpf and J.C. Giddings, *Macromolecules*, 20 (1987) 1561–1563.
- [24] M.E. Schimpf, L.M. Wheeler and P.F. Romeo, in T. Provder (Editor), *Chromatography of Polymers: Characterization by SEC and FFF*, ACS Symp. Series Vol. 521, American Chemical Society, Washington, DC, 1993, pp. 63–76.
- [25] J.C. Giddings, *Sep. Sci. Technol.*, 19 (1984) 831–847.
- [26] J.C. Giddings, *Chem. Eng. News*, 66 (1988) 34–45.
- [27] J.J. Gunderson, K.D. Caldwell and J.C. Giddings, *Sep. Sci. Technol.*, 19 (1984) 667–683.
- [28] C.J. Little, J.A. Whatley, A.D. Dale and M.B. Evans, *J. Chromatogr.*, 171 (1979) 435–438.

Solution properties of amorphous co- and terpolymers of styrene as examined by inverse gas chromatography

Vladimir I. Bogillo^a, Adam Voelkel^{b,*}

^a*Institute of Surface Chemistry of Ukrainian National Academy of Sciences, Prospekt Nauki 31, 252022 Kiev, Ukraine*

^b*Poznań University of Technology, Institute of Chemical Technology and Engineering, Pl. M. Skłodowskiej-Curie 2, 60-965 Poznań, Poland*

First received 17 November 1994; revised manuscript received 8 May 1995; accepted 16 May 1995

Abstract

Inverse gas chromatography was used for determination of thermodynamic functions of solution of C₇–C₁₀ *n*-alkanes, *n*-butanol, di-*n*-butyl ether and 1,4-dioxane in amorphous polystyrene and its copolymers [styrene–nonyl methacrylate (4:1), styrene–maleic anhydride–methacrylic acid (1:1:1) and styrene–nonyl methacrylate (4:1) with addition of 2% (w/w) *p*-phthalimidinoxymethacrylic acid] at infinite dilution and also the glass transition temperatures of these polymers. The influence of modification of the polymer structure on the glass transition temperature and on ability of the polymer functional groups to interact with non-polar, donor or acceptor sorbates was established.

1. Introduction

Inverse gas chromatography (GC) is extensively used in investigations of the thermodynamics of polymer solutions at infinite dilution [1–26]. A knowledge of the thermodynamic functions of solution of test organic compounds in polymers [12–25], glass transition temperatures of amorphous polymers [1–11] and their dependence on the molecular structure of sorbates gives an insight into the physico-chemical properties of new polymers.

In this work, inverse GC was used for the determination of thermodynamic functions of solution at infinite dilution and the glass transition temperatures for the following amorphous polymers: polystyrene (PS), styrene–nonyl

methacrylate (4:1) (SNM), styrene–maleic anhydride–methacrylic acid (1:1:1) (SMAM) and styrene–nonyl methacrylate (4:1) with 2% (w/w) *p*-phthalimidinoxymethacrylic acid (SNMP). These copolymers are widely used in, e.g., the manufacture of photoresists.

The aim of this work was to determine the influence of modification of the polymer structure on the glass transition temperature and on the ability of copolymer functional groups to interact with non-polar, donor or acceptor molecules.

2. Experimental

2.1. Materials

Polystyrene was synthesized by radical poly-

* Corresponding author.

merization of styrene with benzoyl peroxide as initiator in the ethyl acetate solution at 84°C for 10 h. This polymer was purified by precipitation from acetone solution into methanol. The molecular mass is 14 500.

The copolymer of styrene with nonyl methacrylate was synthesized by the radical polymerization of mixture of styrene and nonyl methacrylate in a 4:1 ratio in the presence of benzoyl peroxide in ethyl acetate solution at 84°C for 10 h. Purification was performed by precipitating the copolymer obtained into 2-propanol with addition of 10% (w/w) water. The molecular mass is 29 000.

The terpolymer styrene–nonyl methacrylate (4:1) plus 2% (w/w) *p*-phthalimidinoxymethacrylic acid was synthesized by radical polymerization of a mixture of these reagents at 80°C for 10 h. Purification was performed by precipitating the copolymer into 2-propanol followed by drying under vacuum at 50°C. The molecular mass is 8100.

The terpolymer styrene–maleic anhydride–methacrylic acid (1:1:1) was synthesized by addition of 0.15 M styrene to 400 ml of a toluene solution of 0.15 M maleic anhydride, 0.15 M methacrylic acid and dinitroazobutyrate as polymerization initiator [2% (w/w) of monomers mixture], followed by heating and stirring at 80°C for 10 h. The molecular mass is 28 000.

The composition of the co- and terpolymers was confirmed from their ¹H NMR spectra in perdeuterated dimethyl sulfoxide solvent (Bruker WP-100 SU high-resolution NMR spectrometer). The molecular masses of the polymers were determined by viscosimetry and calculated from the Mark–Houwink equation. We used benzene as the solvent for PS at 283 K and acetone for SNM and SNMP and ethyl acetate for SMAM at 303 K. The molecular volumes of the polymers were calculated on the basis of their density from dilatometric data above their glass transition temperature.

2.2. IGC experiments

The test compounds used were non-polar *n*-heptane, *n*-octane, *n*-nonane and *n*-decane, ac-

ceptor *n*-butanol (BuOH) and donor di-*n*-butyl ether (DBE) and 1,4-dioxane (DO). All the compounds were of chromatographic or analytical-reagent grade and were used as received.

Polymers were deposited on Chromosorb W AW DMCS (80–100 mesh) from a chloroform or acetone solution by continuous stirring and slow evaporation of the solvent. The coated support was dried under vacuum at 293 K to remove traces of solvent. The fillings were packed into a stainless-steel column (1 m × 4 mm I.D.). The column loading was 10% (w/w) for SMAM and 20% (w/w) for the other polymers.

GC measurements were carried out with the use of an LHM-80 modification 6 gas chromatograph equipped with a katharometer as detector. The column temperature was controlled to ±0.2 K over the measured temperature range. Helium was used as the carrier gas. Air, as a non-interacting marker, was used to measure the dead volume of the column. Injection of the test sorbates was repeated at least three times. The pressures at the inlet and outlet of the column were used to compute corrected retention volumes by the usual procedures. The flow-rate was measured at the end of the column with a bubble flow meter and its value was maintained at 15 ml/min. The molecular probes were injected manually with a 1-μl Hamilton syringe. The volume of liquid probe injected was 0.1–0.3 μl. The columns were conditioned at 150–200°C for 12 h under helium before the measurements.

The net retention volume was calculated with the following equation [2]:

$$V_N = F_{\text{corr}} J(t_R - t_0) \quad (1)$$

where

$$J = \frac{3}{2} \left[\frac{(P_i/P_o)^2 - 1}{(P_i/P_o)^3 - 1} \right]$$

and

$$F_{\text{corr}} = F_{\text{meas}} T(1 - P_{\text{H}_2\text{O}}/P_o)/T_{\text{room}} \quad (2)$$

$P_{\text{H}_2\text{O}}$ is the water-saturated vapour pressure at the temperature of the chromatographic column T (K), T_{room} is room temperature (K), P_i is the inlet pressure of the carrier gas (atm), P_o is the

outlet pressure of the carrier gas (atm), t_0 is the retention time of non-sorbed gas (air) (s), t_R is the retention time of the probe at temperature T (s), F_{meas} is the flow-rate of the carrier gas measured at room temperature (cm^3/s) and J is the James–Martin correction factor for gas compressibility.

The specific retention volume, i.e., the net retention volume of a probe at column temperature T , per gram of polymer, adjusted to a standard state of 273.13 K, was calculated from the well known equation [2]

$$V_g^\circ = V_N \times 273.15/wT \quad (3)$$

The first step in our experiments was to determine the glass transition temperature of the polymers (T_g) using retention diagrams. Further measurements and calculations of bulk properties of polymers and their solutions were carried out above these T_g values.

3. Results and discussion

The relationships $\ln V_g^\circ$ vs. $1/T$ (retention diagrams) for the test compounds are presented in Fig. 1. Similar relationships were obtained for all polymers studied.

The T_g value is located at the maximum point of the plot $\ln V_g^\circ$ vs. $1/T$. It is well established that sigmoidal-type retention diagrams are related to a transition from surface to bulk retention mechanism in the vicinity of T_g in polymers [1–11]. The values of the apparent glass transition temperatures determined by using different test molecules are presented in Table 1. Thus, inverse GC allows the determination of apparent glass transition temperatures for the copolymers studied. The observed dependence of T_g on the structure of the test molecules in the case of SNM and SMAM copolymers is due to the fact that their diffusion coefficient is a strong function of the chemical potentials of the diffusant and polymer. Hence it is obvious that the introduction of maleic anhydride into polystyrene copolymer, in the case of SMAM, causes a significant increase in its glass transition tem-

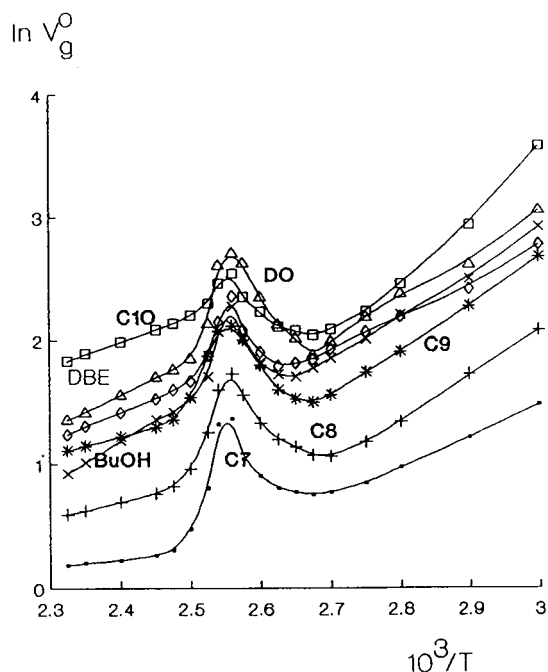


Fig. 1. Relationships $\ln V_g^\circ$ vs. $1/T$ (retention diagrams) for test compounds on styrene-nonyl methacrylate (4:1) copolymer.

perature in comparison with the other polymers studied.

Flory–Huggins parameters characterizing the interaction of a solute with the polymer at infinite dilution were determined from the following expression [2]:

Table 1
Glass transition temperatures (K) for the polymers studied, determined with the use of different test compounds

Test solute	Polymer			
	PS	SNM	SNMP	SMAM
<i>n</i> -Heptane	392	333	331	504
<i>n</i> -Octane	392	337	332	506
<i>n</i> -Nonane	391	341	332	508
<i>n</i> -Decane	391	341	—	510
<i>n</i> -Butanol	391	340	332	508
Di- <i>n</i> -butyl ether	391	343	332	513
1,4-Dioxane	391	337	331	509

$$\kappa_{12}^{\infty} = \ln\left(\frac{273.15R}{P_1^{\circ}V_g M_1}\right) - \frac{P_1^{\circ}}{RT}(B_{11} - V_1^{\circ}) + \ln\left(\frac{\rho_1}{\rho_2}\right) - \left(1 - \frac{V_1^{\circ}}{V_2^{\circ}}\right) \quad (4)$$

where M_1 , P_1° , B_{11} , V_1° , ρ_1 and V_g° are the molecular mass, saturated vapour pressure, second virial coefficient, molar volume and specific retention volume of the solute, respectively, ρ_2 and V_2° are the density and molar volume of the stationary phase, T is the column temperature and R is the gas constant. The P_1 value was calculated from Antoine's equation [27]. The B_{11} values for polar test molecules were calculated from the following equations [27]:

$$B_{11} = (RT_c/P_c)(g_0 + \omega g_1 + \omega_p g_2) \quad (5)$$

where

$$g_0 = 0.1145 - 0.330/T_r - 0.1385/T_r^2 - 0.0121/T_r^3$$

$$g_1 = 0.073 + 0.46/T_r - 0.50/T_r^2 - 0.097/T_r^3 - 0.0073/T_r^8$$

$$g_2 = 0.1042 - 0.2717/T_r + 0.2388/T_r^2 - 0.0716/T_r^3 + 0.0001502/T_r^8$$

$$T_r = T/T_c$$

and the acentric factor (ω) was calculated from [27]

$$\omega = T_b^{1.72}/M_1 - 263 \quad (6)$$

where T_c and T_b are the critical and boiling temperatures of the test solute, respectively, and P_c is the critical pressure. If ω_{calc} was lower than 0, then ω was rounded up to zero.

The solubility parameter of a test molecule was determined from the following equation [1,2]:

$$\delta_1 = \left(\frac{H_v - RT}{V_1}\right)^{1/2} \quad (7)$$

The solubility parameter δ_2 for the polymers examined was calculated from the slope of the linear relationship for a series of test solutes having different δ_1 values:

$$\frac{\delta_1^2}{RT} - \frac{\kappa_{12}^{\infty}}{V_1} = \frac{2\delta_2}{RT} \cdot \delta_1 - \left(\frac{\delta_2^2}{RT} + \frac{\kappa_s^{\infty}}{V_1}\right) \quad (8)$$

where κ_{12}^{∞} is the Flory–Huggins interaction parameter [1].

The solubility parameter of a polymer may be also calculated from the partial molar free energy of mixing at infinite dilution (above the glass transition temperature of the polymer). The partial molar free energy of a probe (G_1^E) was determined from the mass fraction activity coefficient (a_1/w_1) at infinite dilution [2]:

$$\ln\left(\frac{a_1}{w_1}\right) = \ln\left(\frac{273.15R}{P_1^{\circ}V_g M_1}\right) - \frac{P_1^{\circ}}{RT}(B_{11} - V_1^{\circ}) - 1 \quad (9)$$

where M_1 is the molecular mass of the solute.

The relationships between the G_1^E , a_1/w_1 and δ values at infinite dilution are [1]

$$G_1^E = RT \ln(a_1/w_1) \quad (10)$$

$$G_1^E = V_1(\delta_1 - \delta_2)^2 \quad (11)$$

Plotting $\delta_1^2 - G_1^E/V_1$ value versus δ_1 gives a straight line with a slope equal to $2\delta_2$ and intercept $-\delta_2^2$.

A high value of the Flory–Huggins interaction parameter denotes a poor solvent used for the polymer examined, whereas a low value reflects a good solubility capacity. The κ_{12}^{∞} values for polymer–solute systems studies are presented in Table 2. The solubility parameters of polymers calculated from Eqs. 8 and 11 are compared in Table 3. A polymer and solute having equal solubility parameters should be mutually soluble owing to the negative entropy factor. As the difference between δ_{solute} and δ_{polymer} increases, the tendency towards dissolution decreases. This is in accordance with the general rule that chemical and structural similarity favours solubility. The high values of κ_{12}^{∞} for the solutes in Table 2 indicate that the compounds studied are poor solvents for polystyrene. The negative κ_{12}^{∞} values found for the SMAM–*n*-alkane and SNMP–dioxane systems indicate good mutual solubility of the component. The results presented also indicate that these solute–polymer

Table 2

Specific retention volumes (V_g°), excess free energies of solution at infinite dilution (G_1^E) and Flory–Huggins residual free energy of interaction between solute and polymer (κ_{12}^∞) at 526.6 K for test compounds in the polymer solutions

Polymer	Test solute	V_g° (ml/g)	G_1^E (kJ/mol)	κ_{12}^∞
PS	<i>n</i> -Heptane	0.9	9.3	1.6
	<i>n</i> -Octane	1.1	9.8	1.7
	<i>n</i> -Nonane	1.6	9.6	1.7
	<i>n</i> -Decane	2.7	8.6	1.5
	<i>n</i> -Butanol	0.8	11.0	2.1
	Di- <i>n</i> -butyl ether	1.6	8.6	1.5
	1,4-Dioxane	1.7	6.1	1.2
SMAM	<i>n</i> -Heptane	4.1	2.6	0.0
	<i>n</i> -Octane	7.5	1.5	-0.2
	<i>n</i> -Nonane	12.4	0.6	-0.4
	<i>n</i> -Decane	18.4	0.3	-0.4
	<i>n</i> -Butanol	4.2	3.8	0.0
	Di- <i>n</i> -butyl ether	7.4	2.0	0.0
	1,4-Dioxane	4.9	1.3	0.2
SNM	<i>n</i> -Heptane	3.2	3.7	0.3
	<i>n</i> -Octane	4.5	3.8	0.3
	<i>n</i> -Butanol	1.5	8.4	1.5
	Di- <i>n</i> -butyl ether	1.6	8.5	1.5
	1,4-Dioxane	1.9	5.4	1.1
SNMP	<i>n</i> -Heptane	1.8	6.3	0.9
	<i>n</i> -Octane	2.9	5.7	0.8
	<i>n</i> -Nonane	4.9	4.8	0.6
	<i>n</i> -Butanol	1.8	7.6	1.4
	Di- <i>n</i> -butyl ether	1.8	8.4	1.5
	1,4-Dioxane	7.4	-0.5	-0.2

interaction parameters decrease with increase in temperature (Fig. 2a–d). The values of the Flory–Huggins interaction parameter vary from

Table 3

Hildebrand–Scatchard solubility parameters (at 526.6 K) for the polymers studied

Polymer	Solubility parameter [10^3 (J/m) $^{1/2}$]	
	δ_2^a	δ_2^b
SNM	13.1	13.2
PS	13.5	13.4
SMAM	15.2	15.1
SNMP	16.3	16.3

^a Calculated from Eq. 8.

^b Calculated from Eq. 11.

2.2 to -0.4. In order to attain good polymer–solute miscibility, κ_{12}^∞ must be lower than the critical value of 0.5. It is apparent from comparison of the κ_{12}^∞ values that *n*-butanol, and in some cases di-*n*-butyl ether, are slightly less soluble in the polymers studied than 1,4-dioxane and *n*-alkanes.

We also calculated thermodynamic functions of solution of the test compounds in the polymers at infinite dilution and the excess thermodynamic functions of the solutions on the basis of the dependences of logarithms of specific retention volumes and activity coefficients on the inverse temperature [2]. The enthalpy (H_1^S) and entropy (S_1^S) values of test compounds solutions in the polymers at infinite dilution are presented in Table 4.

Linear relationships were obtained between H_1^S and the number of carbon atoms in the homologous alkane series used as solutes. The contribution of the methylene group to the H_1^S values was attributed to Van der Waals dispersive forces between the alkane molecule and the polymer.

The enthalpy and entropy of mixing of test solutes with polymers at infinite dilution are presented in Table 5. There is no significant variation of H_1^E for the *n*-alkane series in PS solution. In the case of other polymer solutions the H_1^E values decrease with increase in carbon number in the *n*-alkane molecule.

The molar solution enthalpy at infinite dilution (H_1^S) is the most representative parameter for the interaction energies of test molecules with polymer groups in the solutions. It represents the combination of contributions of non-specific and specific interactions [6]:

$$-H_1^S = H_{1(\text{nsp})}^S + H_{1(\text{sp})}^S - A \quad (12)$$

where A is the work of hole formation in the volume of polymer. This value varies proportionally with the molar volume of the test solute (V_1). The contribution of non-specific interactions (mainly dispersive interactions) is proportional to the solute molar deformation polarization (RN), and the contribution of specific interactions is proportional to the electron-donor and

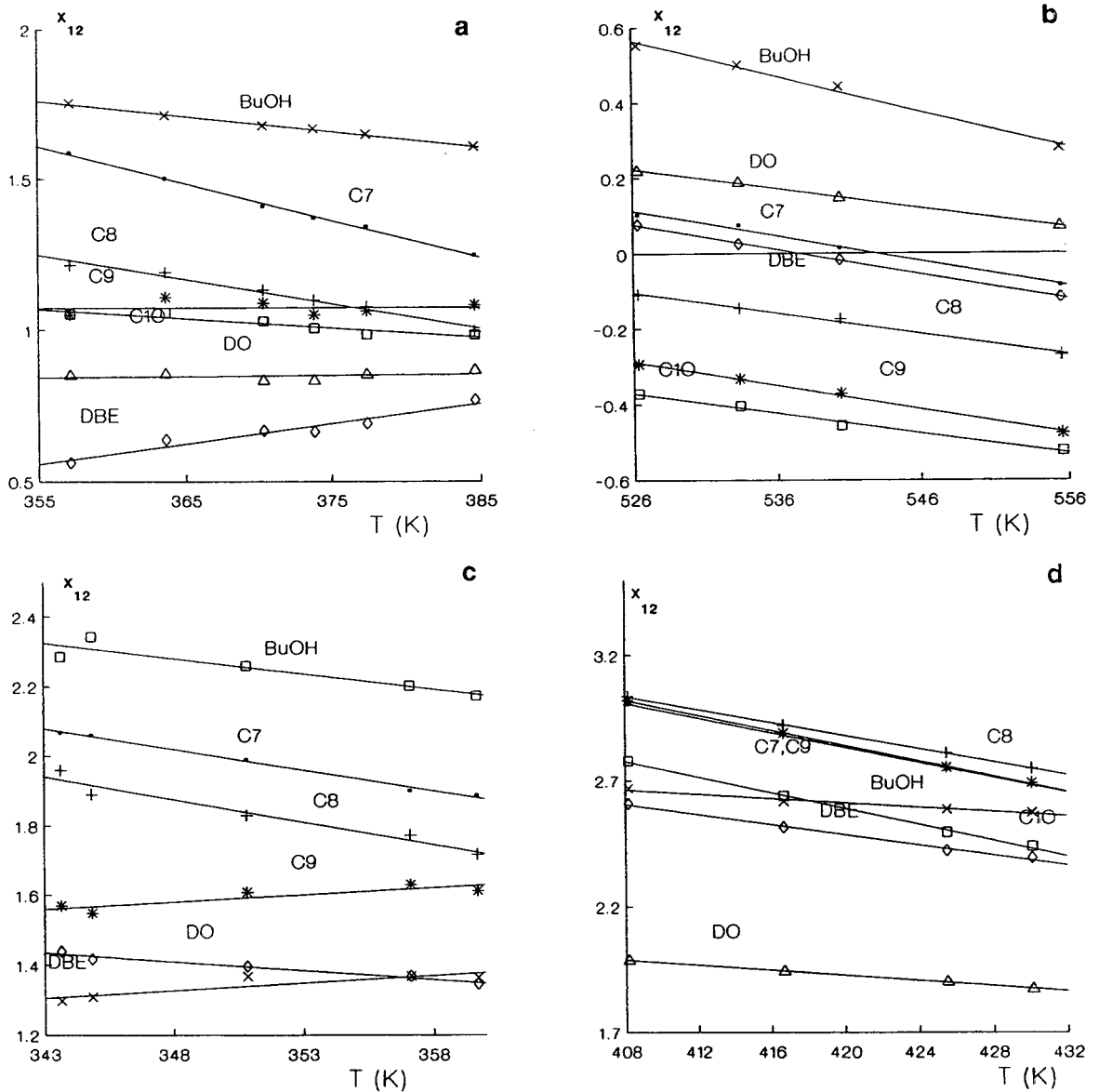


Fig. 2. Dependence of Flory-Huggins interaction parameter on temperature for the test solutes and polymers examined: (a) SNM; (b) SNAM; (c) SNMP; (d) PS.

electron-acceptor abilities of the molecule, i.e., its donor (DN) and acceptor (AN) numbers. Rewriting Eq. 12 in these terms, we obtain

$$-H_1^S = (RN)_{ps}RN + (AN)_{ps}DN + (DN)_{ps}AN + V_{ps}V_1 + S_S \quad (13)$$

where $(RN)_{ps}$, $(AN)_{ps}$ and $(DN)_{ps}$ are the parameters reflecting the ability of the polymer to interact with non-polar, electron-donor and electron-acceptor solutes, respectively, V_{ps} accounts for the cohesive ability of the polymer and S_S is a constant for the solutes studied. The coefficients

Table 4
Enthalpy (H_1^S , kJ/mol) and entropy (S_1^S , J mol \cdot K) of test compounds in polymer solution at infinite dilution

Test solute	Polymer							
	PS		SNMP		SMAM		SNM	
	$-H_1^S$	S_1^S	$-H_1^S$	S_1^S	$-H_1^S$	S_1^S	$-H_1^S$	S_1^S
<i>n</i> -Heptane	5	9	19	31	15	15	16	20
<i>n</i> -Octane	11	21	27	44	17	14	25	37
<i>n</i> -Nonane	13	19	46	91	15	7	40	69
<i>n</i> -Decane	16	21	—	—	18	9	41	67
<i>n</i> -Butanol	29	59	35	66	11	8	38	71
Di- <i>n</i> -butyl ether	19	33	44	87	15	11	46	94
1,4-Dioxane	23	41	30	51	15	14	34	59

Table 5
Enthalpy (H_1^E , kJ/mol) and entropy (S_1^E , J mol \cdot K) of test compounds and polymer mixing at infinite dilution

Test solute	Polymer							
	PS		SNMP		SMAM		SNM	
	$-H_1^S$	S_1^S	$-H_1^S$	S_1^S	$-H_1^S$	S_1^S	$-H_1^S$	S_1^S
<i>n</i> -Heptane	22	24	12	14	16	25	14	22
<i>n</i> -Octane	19	17	11	9	13	22	9	12
<i>n</i> -Nonane	22	25	-4	-29	15	28	0	-13
<i>n</i> -Decane	23	29	—	—	13	24	4	-2
<i>n</i> -Butanol	6	-10	12	13	23	36	5	-1
Di- <i>n</i> -butyl ether	15	11	-5	-27	16	26	-8	-29
1,4-Dioxane	8	1	5	3	13	21	0	-9

of Eq. 13 calculated for the polymers studied are presented in Table 6. The polarization contribution (RN_{ps}) decrease in the order SNMP > SNM > PS > SMAM.

Table 6
Parameters reflecting the ability of polymers to interact with non-polar (RN_{ps}), electron-donor (AN_{ps}) and electron-acceptor (DN_{ps}) solutes, parameter accounting for cohesive ability of polymer (V_{ps}) and constant for solutes studied (S_{ps}), calculated from Eq. 13

Polymer	RN_{ps}	AN_{ps}	DN_{ps}	S_{ps}	V_{ps}
PS	0.08	0.78	0.69	-20.0	-0.005
SNM	0.19	1.45	0.60	-48.3	-0.005
SMAM	0.03	0.06	0.07	6.3	-0.001
SNMP	0.30	1.31	1.33	-88.0	-0.011

SNMP exhibits the highest donor ability (DN_{ps}), whereas the highest acceptor ability (AN_{ps}) was found for SNM. Thus, the introduction of *p*-phthalimidinoxymethacrylic acid into the polystyrene matrix causes a dramatic increase in the polarization and electron-donor ability of the terpolymer functional groups.

4. Conclusions

Inverse GC was used for the determination of the thermodynamic functions of C₇–C₁₀ *n*-alkanes, *n*-butanol, di-*n*-butyl ether and 1,4-dioxane in solutions of polystyrene and its co- and terpolymers: styrene–nonyl methacrylate (4:1), styrene–maleic anhydride–methacrylic acid (1:1:1) and styrene–nonyl methacrylate (4:1)

with 2% (w/w) of *p*-phthalimidinoxymethacrylic acid at infinite dilution and also the glass transition temperatures of these amorphous polymers. The dependence of the apparent glass transition temperature on the structure of the test molecules is due to the fact that their diffusion coefficients are a function of the chemical potentials of the diffusant and polymer. The introduction of maleic anhydride into polystyrene copolymer, in the case of SMAM, causes a large increase in its glass transition temperature in comparison with other polymers. Values of the Flory–Huggins interaction parameter for the polymer–solute systems studied range from 2.2 to -0.4 . The influence of modification of the polymer structure on the glass transition temperature and on the ability of the polymer functional groups to interact with non-polar, donor or acceptor molecules of solutes was established. The introduction of 2% of *p*-phthalimidinoxymethacrylic acid into the polystyrene matrix causes a dramatic increase in the polarization and electron-donor ability of the terpolymer functional groups.

Acknowledgements

The authors thank Sharwin-Williams (Ohio, USA) (V.I.B.) and acknowledge DS grant 32/220/95 (A.V.) for financial support of this work. They also thank Professor V.G. Syromyatnikov (Chemical Faculty of Taras Shevchenko University, Kiev, Ukraine) for supplying the samples of polymers and providing copolymer structures and molecular mass analyses.

References

- [1] A. Voelkel, *CRC Crit. Rev. Anal. Chem.*, 22 (1991) 411.
- [2] J.R. Conder and C.L. Young, *Physicochemical Measurements in Gas Chromatography*, Wiley-Interscience, New York, 1979.
- [3] J.E. Guillet and M. Galin, *J. Polym. Sci., Polym. Lett. Ed.*, 11 (1973) 233.
- [4] A. Lavoie and J.E. Guillet, *Macromolecules*, 2 (1969) 443.
- [5] D.G. Gray and J.E. Guillet, *Macromolecules*, 7 (1974) 244.
- [6] G.J. Courval and D.G. Gray, *Macromolecules*, 8 (1975) 328.
- [7] G.J. Courval and D.G. Gray, *Macromolecules*, 8 (1975) 916.
- [8] J.M. Braun and J.E. Guillet, *Macromolecules*, 9 (1976) 340.
- [9] J.M. Braun and J.E. Guillet, *Macromolecules*, 9 (1976) 617.
- [10] G.J. Courval and J.E. Guillet, *Can. J. Chem.*, 54 (1976) 3496.
- [11] C. Beldie, O. Auo, G. Borceanu and J.C. Poinescu, *Eur. Polym. J.*, 21 (1985) 443.
- [12] R.D. Newman and J.M. Prausnitz, *J. Phys. Chem.*, 76 (1972) 1492.
- [13] F.H. Covitz and J.W. King, *J. Polym. Sci., Part A-1*, 10 (1972) 689.
- [14] L.J. Stiel and D.F. Harnish, *AIChE J.*, 22 (1976) 117.
- [15] Y. Jwai, M. Nagatuiji and Y. Arai, *J. Jpn. Pet. Inst.*, 23 (1980) 215.
- [16] M.T. Ratzsch, G. Jlling and Ch. Wohlfatrth, *Acta Polym.*, 33 (1982) 89.
- [17] S. Gunduz and S. Dincer, *Polymer*, 21 (1980) 1041.
- [18] P.J.T. Tait and A.M. Abushihada, *Polymer*, 18 (1977) 810.
- [19] P.J.T. Tait and A.M. Abushihada, *Macromolecules*, 11 (1978) 918.
- [20] M. Galin and M.S. Ruprecht, *Polymer*, 19 (1978) 506.
- [21] O. Olabisi, *Macromolecules*, 8 (1975) 316.
- [22] R.H. Schuster, H. Grater and H.J. Cautow, *Macromolecules*, 17 (1984) 619.
- [23] L. Bonifaci and G.P. Ravanetti, *J. Chromatogr.*, 641 (1993) 301.
- [24] M. Castun, I. Kaya and E. Ozdemir, *J. Macromol. Sci., Pure Appl. Chem.*, A30, Suppl. 5 (1993) 425.
- [25] E. Ozdemir, Z. Ilter, M. Castun and S. Celik, *J. Macromol. Sci., Pure Appl. Chem.*, A30, Suppl. 5 (1993) 391.
- [26] J.I. Irrebarren, M. Iriarte and J.J. Iruin, *J. Appl. Polym. Sci.*, 37 (1989) 3459.
- [27] R.C. Reid, J.M. Prausnitz and T.K. Sherwood, *The Properties of Gases and Liquids*, McGraw-Hill, New York, 1977.



ELSEVIER

Journal of Chromatography A, 715 (1995) 135-141

JOURNAL OF
CHROMATOGRAPHY A

Double-chain surfactants with two sulfonate groups as micelle-forming reagents in micellar electrokinetic chromatography of naphthalene derivatives

Hiroya Harino^a, Minoru Tanaka^{b,*}, Takashi Araki^b, Yuta Yasaka^b, Araki Masuyama^c, Yohji Nakatsuji^c, Isao Ikeda^c, Koichi Funazo^d, Shigeru Terabe^e

^aOsaka City Institute of Public Health and Environmental Science, Tennoji, Osaka 543, Japan

^bResearch Center for Environmental Preservation, Osaka University, Yamada-oka, Suita, Osaka 565, Japan

^cDepartment of Applied Chemistry, Faculty of Engineering, Osaka University, Yamada-oka, Suita, Osaka 565, Japan

^dDepartment of Chemistry, Osaka Prefectural College of Technology, Neyagawa, Osaka 572, Japan

^eDepartment of Material Science, Faculty of Science, Himeji Institute of Technology, Kamigori, Hyogo 678-12, Japan

First received 14 February 1995; revised manuscript received 8 May 1995; accepted 12 May 1995

Abstract

Three surfactants having two sulfonate groups and two lipophilic chains, disodium 5,12-bis(dodecyloxymethyl)-4,7,10,13-tetraoxa-1-16-hexadecanedisulfonate (DBTHX), 5,13-bis(dodecyloxymethyl)-4,7,11,14-tetraoxa-1-17-heptadecanedisulfonate (DBTHP) and 5,13-bis(dodecyloxymethyl)-4,7,11,14-tetraoxa-9,9-dimethyl-1-17-heptadecanedisulfonate (DBTDMHP), were used in micellar electrokinetic chromatography (MEKC) to separate eight naphthalene derivatives as model analytes. Their capacity factors linearly increased as the concentration of each surfactant increased from 1 to 10 mM at pH 7.0. These double-chain surfactants exhibited different selectivity and wider migration time windows when compared with sodium dodecyl sulfate (SDS), which is used widely in MEKC. The eight naphthalene derivatives were baseline separated at 5 mM DBTHX and 2.5 mM DBTHP, respectively, and nearly baseline separated at 2.5 mM DBTDMHP. However, SDS at 60 mM could not completely resolve three of the analytes.

1. Introduction

Micellar electrokinetic chromatography (MEKC) [1] has been developed for the separation of electrically neutral analytes by electrophoresis with an ionic micellar solution as the separation solution, and has attracted much attention in various fields. Since the MEKC

separation principle is based on differential partitioning of the analyte between the micelle and the surrounding aqueous phase, the choice of surfactant significantly affects MEKC selectivity. Therefore, the introduction of new types of surfactants for MEKC is of great interest and is expected to be useful in modulating its selectivity.

Recently, one of the authors has shown that amphipathic compounds with two sulfate or sulfonate groups and two long alkyl chains, which are derived from glycol diglycidyl ethers,

* Corresponding author.

have good water solubility and excellent surface active properties in water [2,3]. In particular, disodium 5,12-bis(dodecyloxymethyl)-4,7,10,13-tetraoxa-1-16-hexadecanedisulfonate (DBTHX) had a very low critical micelle concentration (CMC) (0.014 mM) and a low Krafft point (below 0°C). In a previous paper [4], we applied this double-chain surfactant in MEKC for the first time and compared it with sodium dodecyl sulfate (SDS), a widely used surfactant with one ionic group and one lipophilic chain. For several benzene and naphthalene derivatives, DBTHX exhibited promising results (i.e., different selectivity and a wider migration time window).

In the present paper, we describe the synthesis of new double-chain surfactants such as disodium 5,13-bis(dodecyloxymethyl)-4,7,11,14-tetraoxa-1,17-heptadecanedisulfonate (DBTHP) and 5,13-bis(dodecyloxymethyl)-4,7,11,14-tetraoxa-9,9-dimethyl-1,17-heptadecanedisulfonate (DBTDMHP), which differ from DBTHX in the structure of the linkage between the two lipophilic chains. These three double-chain surfactants are compared with SDS, a typical single-chain surfactant, as micelle-forming reagents in the MEKC of naphthalene derivatives.

2. Experimental

2.1. Apparatus

MEKC was carried out using an Applied Biosystems Model 270A capillary electrophoresis system (CA, USA) with a fused-silica capillary tube (72 cm × 50 μm I.D., 50 cm from inlet to detector). The temperature and applied voltage for separation were held constant at 30°C and 15 kV, respectively. UV detection was at 210 nm. A Hitachi D-2500 Chromato-Integrator (Hitachi, Japan) was used for data processing.

Sample solutions (1.0 · 10⁻²% in 10% methanol) were injected using a vacuum technique (12.7 cmHg pressure difference for 0.5 s). All experiments were performed in duplicate to ensure reproducibility.

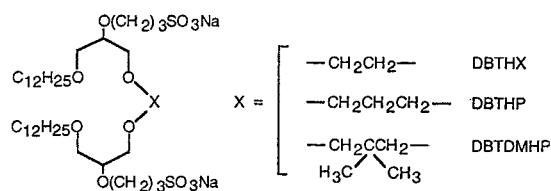


Fig. 1. Structures of double-chain surfactants.

2.2. Reagents

The structures of the double-chain surfactants are shown in Fig. 1. DBTHP and DBTDMHP were synthesized using 1,3-propanediol diglycidyl ether and 2,2-dimethyl-1,3-propanediol diglycidyl ether, respectively, instead of ethylene glycol diglycidyl ether for DBTHX as previously reported [2]. 1,3-Propanediol diglycidyl ether and 2,2-dimethyl-1,3-propanediol diglycidyl ether were obtained by the reaction of epichlorohydrin with 1,3-propanediol and 2,2-dimethyl-1,3-propanediol, respectively. The isolated double-chain surfactants were identified by MS and NMR spectra and elemental analysis. The purity of the surfactants was more than 99%. Several physico-chemical properties of the surfactants are given in Table 1, together with their yields based on the corresponding diols treated with propanesulfone. All other reagents were of analytical-reagent grade and used as received.

Separation solutions were prepared by dissolving the double-chain surfactants in a buffer solution of 0.1 M sodium dihydrogenphosphate–

Table 1
Several physico-chemical properties of double-chain surfactants

	Surfactant		
	DBTHX	DBTHP	DBTDMHP
Molecular mass	823.111	837.146	865.200
CMC (mM)	0.014	0.017	0.0043
Krafft point (°C)	<0	<0	<0
Yield ^a (%)	68	83	48

^a Based on diols.

0.05 M sodium borate at pH 7.0. Methanol was used as a marker of the electroosmotic flow and Sudan III was used as the micelle tracer.

3. Results and discussion

3.1. Separation of model analytes

The structures of the eight monosubstituted naphthalene derivatives used as analytes in this study are shown in Fig. 2. Their migration times were measured at five double-chain surfactant concentrations between 1.0 and 10.0 mM in 0.1 M phosphate–0.05 M borate buffer at pH 7.0. All the analytes were baseline separated with DBTHX and DBTHP at concentrations above 5.0 and 2.5 mM, respectively, and almost baseline separated with DBTDMHP above 2.5 mM. In the DBTDMHP system, the complete baseline separation of 1-naphthalenemethanol and 1-naphthylamine could not be attained even at 10.0 mM DBTDMHP. Typical chromatograms for the separation of the analytes using these double-chain surfactants are shown in Fig. 3.

MEKC with SDS was also performed in a concentration range of 10–60 mM. In this case, 1-naphthalenemethanol, 1-naphthol and 2-

naphthol could not be baseline separated even at 60 mM SDS (chromatogram not shown).

3.2. Comparison of surfactants

The capacity factor of a neutral analyte in MEKC can be calculated using the following equation [1].

$$k' = \frac{t_R - t_o}{t_o(1 - t_R/t_{mc})} \quad (1)$$

where t_R , t_o and t_{mc} are the migration times of the analyte, the solute which does not interact with the micelle (methanol peak) and the micelle (Sudan III peak), respectively. When the micellar concentrations are low, k' is approximately related to the surfactant concentration using Eq. 2 [5].

$$k' = Kv(C_{sf} - CMC) \quad (2)$$

where K is the distribution coefficient of the analyte, and v and C_{sf} are the partial specific volume of the micelle and the surfactant concentration, respectively.

The plots of calculated k' for the eight naphthalene derivatives vs. concentration of each surfactant are shown in Fig. 4. The capacity

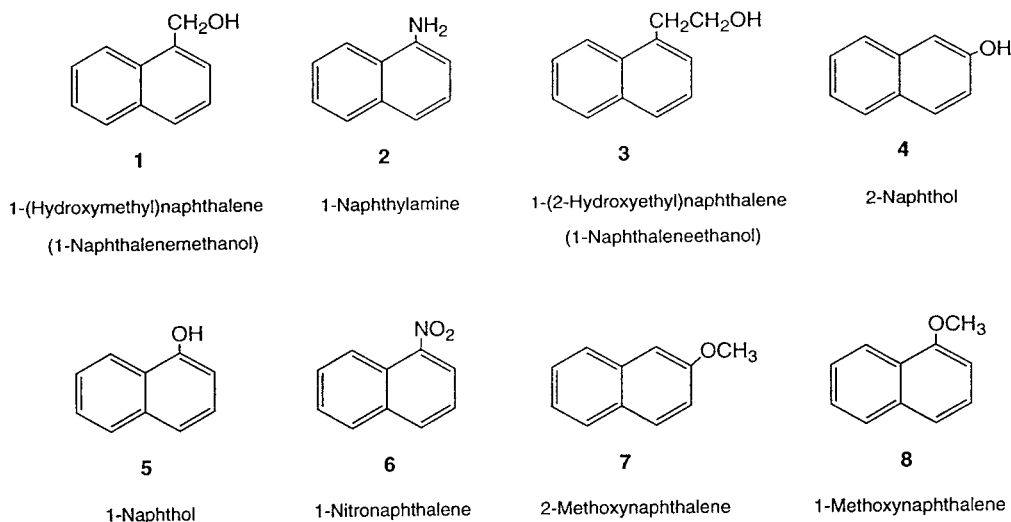


Fig. 2. Structures of naphthalene derivatives used as model analytes.

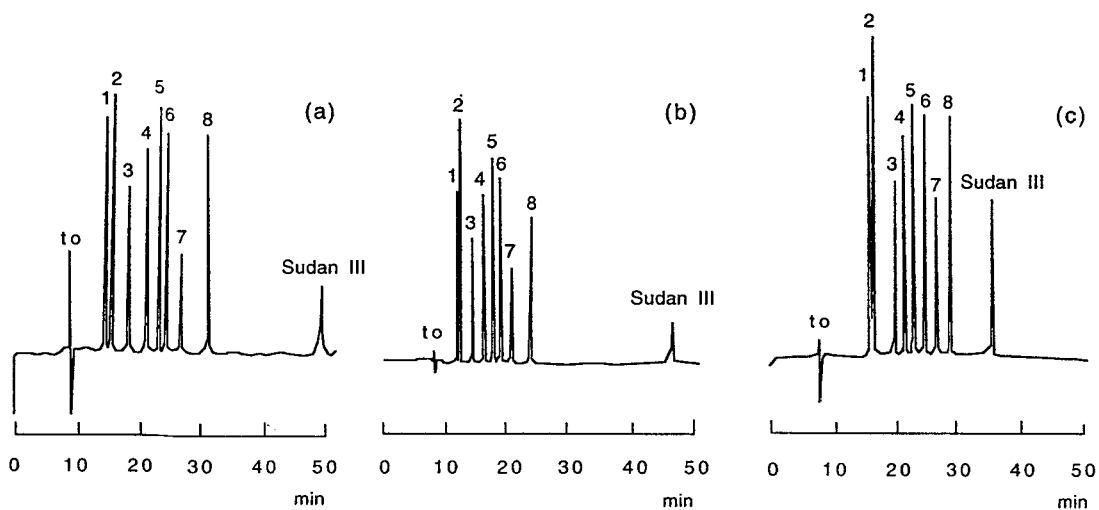


Fig. 3. Separations of naphthalene derivatives with (a) 5.0 mM DBTHX, (b) 2.5 mM DBTHP and (c) 2.5 mM DBTDMHP. Peak numbers same as in Fig. 2.

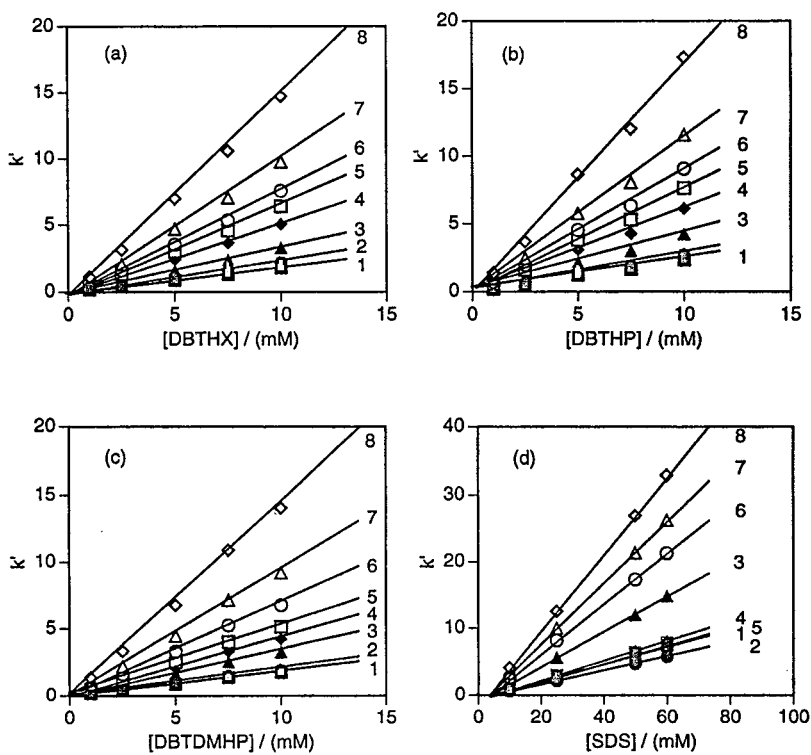


Fig. 4. Dependence of calculated capacity factor (k') of naphthalene derivatives on concentration of (a) DBTHX, (b) DBTHP, (c) DBTDMHP and (d) SDS. Analyte numbers same as in Fig. 2.

factors of the analytes increased linearly with an increase in the concentration of each surfactant (1.0–10 mM for DBTHX, DBTHP or DBTDMHP and 10–60 mM for SDS). For DBTHX, DBTHP and DBTDMHP, the current only increased from 26 to 28 μA with an increase of the surfactant concentration from 1.0 to 10 mM. For SDS, on the other hand, a current increase from 25 (10 mM) to 33 μA (60 mM) was observed. Table 2 gives the results of the regression analyses for the double-chain surfactants. Good linear relationships (correlation coefficient range: more than 0.993) were obtained for each analyte, which suggests that the distribution coefficients remain constant at least in

the measured concentration range. Similar linear plots were also obtained for SDS.

From Eq. 2, the intercepts of the plots in Fig. 4 extrapolated to $k' = 0$ can be interpreted to be the CMC of the surfactant under the MEKC conditions used. The averaged CMC values estimated for DBTHX, DBTHP and DBTDMHP are 0.283, 0.325 and 0.058 mM, respectively. Their CMC values in pure water were also determined from the break points of the surface tension (measured with a Wilhelmy tensiometer at 20°C) vs. concentration plots. The resulting CMC values are 0.014, 0.017 and 0.0043 mM for DBTHX, DBTHP and DBTDMHP, respectively (Table 1). The CMC

Table 2
Correlation between concentration of surfactant and capacity factor

Analyte	Surfactant	Regression equation	Correlation coefficient
1-Naphthalenemethanol	DBTHX	$y = 0.182x - 0.037$	0.999
	DBTHP	$y = 0.240x - 0.093$	0.993
	DBTDMHP	$y = 0.177x + 0.003$	0.998
1-Naphthylamine	DBTHX	$y = 0.223x - 0.063$	0.998
	DBTHP	$y = 0.281x - 0.116$	0.994
	DBTDMHP	$y = 0.194x - 0.015$	0.998
1-Naphthaleneethanol	DBTHX	$y = 0.337x - 0.007$	0.999
	DBTHP	$y = 0.436x - 0.129$	0.994
	DBTDMHP	$y = 0.328x + 0.011$	0.999
2-Naphthol	DBTHX	$y = 0.520x - 0.169$	0.999
	DBTHP	$y = 0.627x - 0.202$	0.995
	DBTDMHP	$y = 0.426x - 0.017$	0.998
1-Naphthol	DBTHX	$y = 0.657x - 0.234$	0.998
	DBTHP	$y = 0.778x - 0.254$	0.995
	DBTDMHP	$y = 0.520x - 0.035$	0.998
1-Nitronaphthalene	DBTHX	$y = 0.773x - 0.283$	0.998
	DBTHP	$y = 0.920x - 0.265$	0.995
	DBTDMHP	$y = 0.685x - 0.053$	0.998
2-Methoxynaphthalene	DBTHX	$y = 1.01x - 0.358$	0.999
	DBTHP	$y = 1.17x - 0.333$	0.995
	DBTDMHP	$y = 0.938x - 0.105$	0.998
1-Methoxynaphthalene	DBTHX	$y = 1.51x - 0.533$	0.999
	DBTHP	$y = 1.75x - 0.490$	0.994
	DBTDMHP	$y = 1.44x - 0.201$	0.998

value decreases in the order DBTHP > DBTHX > DBTDMHP in both cases. However, the CMC values obtained from the surface-tension plots are about one order of magnitude smaller compared to those estimated from the MEKC plots. The reason for this discrepancy is not clear at present but is speculated as follows. In general, it is unlikely that the discrepancy comes from temperature differences in the tension and MEKC measurements. The presence of salts usually reduces CMC, but the results obtained are not consistent. Since the surfactant molecules in water are partitioned between the bulk phase and the interface, the CMC values are affected by the property of the interface. The surface tension and the MEKC methods are related with the gas–liquid and the solid–liquid interfaces, respectively. In the latter case, adsorption should result in an increased total amount of molecules required to aggregate in the bulk phase as compared with the case of the surface-tension method. Thus, the above-mentioned discrepancy in the CMC values may be ascribed to differences in measurement environment.

The elution order of the analytes in MEKC with the double-chain surfactants is identical, i.e., 1-naphthalenemethanol < 1-naphthylamine < 1-naphthaleneethanol < 2-naphthol < 1-naphthol < 1-nitronaphthalene < 2-methoxynaphthalene < 1-methoxynaphthalene. This elution order is clearly different from that found with SDS, i.e., 1-naphthylamine < 1-naphthalenemethanol < 1-naphthol < 2-naphthol < 1-naphthaleneethanol < 1-nitronaphthalene < 2-methoxynaphthalene < 1-methoxynaphthalene. Namely, the elution order of 1-naphthalenemethanol and 1-naphthylamine as well as that of 1-naphthaleneethanol, 2-naphthol and 1-naphthol was reversed in the SDS system. As already mentioned, 1-naphthalenemethanol, 2-naphthol and 1-naphthol could not be baseline separated in the SDS system, though this was readily done in the double-chain surfactant systems. In HPLC analysis, the elution order of the analytes on an ODS column eluted with water–acetonitrile (45:55) is 1-naphthalenemethanol < 1-naphthaleneethanol < 2-naphthol < 1-naph-

thylamine < 1-naphthol < 1-nitronaphthalene < 2-methoxynaphthalene < 1-methoxynaphthalene. This order is identical with that found in the double-chain surfactant systems, except that 1-naphthylamine eluted between 2- and 1-naphthol.

A wide migration-time window between t_o and t_{mc} is favorable for high resolution, although a long analysis time may be required. The t_{mc}/t_o value is directly related to the width of the migration-time window. The larger the value of t_{mc}/t_o , the wider the migration-time window. The t_{mc}/t_o values of DBTHX, DBTHP and DBTDMHP at 10 mM were 6.0, 5.8 and 4.5, respectively. On the other hand, the value was 4.1 for SDS at 10 mM. The double-chain surfactants produced larger t_{mc}/t_o values than SDS at the same concentration. The t_{mc}/t_o value is smaller than 5 for most ionic micelles at pHs greater than 6.0. This is in favor of the use of double-chain surfactants, DBTHX and DBTHP in particular, as micelle-forming reagents in MEKC.

Compared with SDS, the three double-chain surfactants, DBTHX, DBTHP and DBTDMHP, exhibited a remarkably different selectivity of the substituted naphthalene derivatives in MEKC; their MEKC separation could be performed with the double-chain surfactants at concentrations at least one order of magnitude lower. The performance of MEKC separations at low surfactant concentration enables the use of the separation solutions at low ionic strength (low current). This results in a decrease in Joule heating and in a high column efficiency. Moreover, the double-chain surfactants, DBTHX and DBTHP, gave significantly wider migration-time windows. These results suggest that the introduction of double-chain surfactants is promising for MEKC performance. Quite recently, capillary electrophoresis including MEKC has become competitive in trace analysis and the door has been opened to environmental applications in real matrices. The application of double-chain surfactants to the determination of pollutants such as aromatic hydrocarbons in waste gases is of great interest.

Acknowledgement

This work was partially supported by a Grant-in-Aid for Scientific Research (No. 06650934) from the Ministry of Education, Science and Culture of Japan.

References

[1] S. Terabe, K. Otsuka, K. Ichikawa, A. Tsuchiya and T. Ando, *Anal. Chem.*, 56 (1984) 111–113.

- [2] Y.-P. Zhu, A. Masuyama, T. Nagata and M. Okahara, *J. Jpn. Oil. Chem. Soc. (Yukagaku)*, 40 (1991) 473–477.
- [3] Y.-P. Zhu, A. Masuyama and M. Okahara, *J. Am. Oil. Chem. Soc.*, 67 (1990) 459–463.
- [4] M. Tanaka, T. Ishida, T. Araki, A. Masuyama, Y. Nakatsuji, M. Okahara and S. Terabe, *J. Chromatogr.*, 648 (1993) 469–473.
- [5] S. Terabe, K. Otsuka and T. Ando, *Anal. Chem.*, 57 (1985) 834–841.

Determination of the enantiomeric purity of 5,6-dihydroxy-2-aminotetralin by high-performance capillary electrophoresis with crown ether as chiral selector

Pierfrancesco Castelnovo*, Carlo Albanesi

Medicinal Chemistry Analytical Laboratory, Zambon Group, via del Duca 10, 20092 Bresso (Milan), Italy

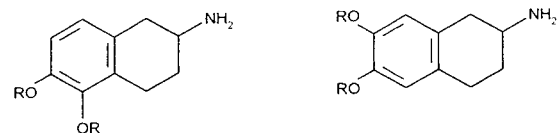
First received 15 December 1994; revised manuscript received 8 May 1995; accepted 12 May 1995

Abstract

5,6-Dihydroxy-2-aminotetralin was resolved into its enantiomers by high-performance capillary electrophoresis. The separation was performed with a background electrolyte containing 18-crown-6 tetracarboxylic acid as chiral selector. The chiral recognition is based on a primary interaction between the hydrogens of the amino group and the oxygens of the crown ether and a secondary interaction between the catechol and the carboxylates of the crown ether. The resolution factor was 1.42 and the detection limit of the enantiomer present as impurity was 0.3%. Data on the optimization and the validation of the assay are also reported.

1. Introduction

Dihydroxy-2-aminotetralins (ADTNs) (Fig. 1) are racemic dopamine receptor agonists of high potency. Their pharmacological dopaminergic



R = H 5,6-ADTN

R = OCH₃ 5,6-ADMTN

R = H 6,7-ADTN

R = OCH₃ 6,7-ADMTN

Fig. 1. Structures of 5,6- and 6,7-dihydroxy-2-aminotetralin (ADTN) and of 5,6- and 6,7-dimethoxy-2-aminotetralin (ADMTN).

* Corresponding author.

activity resides on the *R*-enantiomer for 5,6-ADTN and on the *S*-enantiomer for 6,7-ADTN. The fact that the active enantiomers have opposite configuration has raised some speculation on the structural features required for the interactions of these agonist with the dopamine receptor [1–3]. Thus an analytical assay which can determine their enantiomeric purity is highly desirable for both the ADTN isomers and the corresponding 5,6- and 6,7-dimethoxy precursors.

We have recently developed a direct chiral HPLC assay for the enantiomers of 5,6- and 6,7-ADTN [4]. The high resolution allowed small amounts (<0.1%) of the diastomer present as impurity in the eutomer to be determined, the only drawback being the high cost of the HPLC column.

High-performance capillary electrophoresis (HPCE) is an attractive alternative for chiral

separations compared to the direct chiral HPLC assay, which is the most effective of the HPLC approaches. In fact many different types of expensive chiral phases are needed for the separation of a relatively narrow range of racemic compounds, while one single inexpensive silica capillary can be subsequently filled with background electrolytes containing different chiral selectors. In addition the small volume of a capillary electrophoresis system, which requires only few milliliters of electrolyte for multiple runs, allows the use of expensive or commercially unavailable chiral selectors.

Many examples of chiral separations by HPCE have been published over the last few years, most of them employing cyclodextrins and their derivatives. Fanali and co-workers reported the optical isomer resolution of epinephrine and related compounds [5], tryptophan and derivatives [6,7] and propranolol and terbutaline [8]. Novotny and coworkers showed the enantioseparation of basic drugs such as verapamil, fluoxetine, bupivacaine and some β -blockers [9] and other pharmaceuticals [10]. Another set of racemic basic drugs, most of them belonging to the cardiovascular or CNS-active compounds, was separated by Nielsen [11], while Peterson [12,13], Francotte et al. [14] and Rawjee et al. [15] reported the enantioseparation of ophthalmic drugs, non-steroidal aromatase inhibitors and barbiturates, and non-steroidal antiinflammatory drugs, respectively. Other examples of chiral selectors used in HPCE are bile acids [16,17], chiral surfactants [18], cyclodextrins incorporated into a gel matrix [19,20], cyclodextrins coated on a capillary wall [21], chiral functionalized micelles [22] and maltodextrins [23].

A more recent approach is the use of crown ethers, first reported by Kuhn and co-workers [24,25]. Since the chiral HPLC assay for the ADTNs was based on a column filled with a chiral crown ether stationary phase coated on silica gel, we investigated the addition of 18-crown-6 tetracarboxylic acid ($18C_6H_4$) as a chiral selector to the background electrolyte for the separation of the enantiomers of 5,6-ADTN and of their dimethoxy precursors 5,6-

and 6,7-ADMTN. This approach was recently reported also by Walbroehl and Wagner [26] for the enantioseparation of unsubstituted and monosubstituted aminotetralins. The present paper describes the results of the investigation and optimization of the parameters influencing the resolution between the enantiomers of 5,6-ADTN as well as the validation of the quantitative analysis.

2. Experimental

2.1. Chemicals

18-Crown-6 tetracarboxylic acid and tris(hydroxymethyl)-aminomethane (Tris) were of analytical grade and obtained from Merck (Darmstadt, Germany). Citric acid (RPE-ACS grade) was from Carlo Erba (Milan, Italy). All solutions were prepared in Milli-Q water (Millipore, Bedford, MA, USA), filtered through a 0.22- μ m cellulose filter from Hewlett-Packard (Cernusco S/N, Italy) and degassed by sonication.

2.2. Instrumentation

A Beckman P/ACE 2100 capillary electrophoresis system equipped with a filter UV detector set at 280 nm was used. Separations were performed in unmodified silica capillary (57 cm \times 75 μ m I.D., 50 cm to detector) mounted on a liquid-cooled cartridge (Beckman). Data acquisition and processing was performed using the Beckman System Gold software installed on a Hewlett-Packard Vectra QS/20 personal computer.

2.3. Running conditions

Injections were made at the anodic site using the electrokinetic technique applying a 5 kV potential for 15 s. Separations were carried out at 25°C using the constant voltage mode in the range 5–15 kV; the observed current at 10 kV was 40 A.

Running buffer was prepared by dissolving 10

mM Tris-base in water, adjusting the pH to 2.2 with citric acid and adding the desired amount (10–50 mM) of 18C6H₄. The sample solutions were prepared by dissolving each solute in running buffer without the addition of 18C6H₄ at a concentration of approx. 0.5 mg/ml.

Conditioning for each experiment was done by rinsing the capillary with running buffer for 2 min while the daily conditioning before the beginning of a set of experiments was with 0.1 M sodium hydroxide, water and hydrochloric acid (2 min each).

2.4. Calculation of the resolution parameters

The resolution parameters were calculated as follows:

$$\text{separationfactor}(\alpha) = \text{MT}_2/\text{MT}_1 \quad (1)$$

$$\text{resolutionfactor}(R) = (\text{MT}_2 - \text{MT}_1)/0.88(W_2 + W_1) \quad (2)$$

where MT_1 , MT_2 , W_1 and W_2 are the migration times and the bandwidths at half-height of the chromatographic peaks. The suffixes 1 and 2 refer to the first and the last eluting enantiomer, respectively.

3. Results and discussion

18-Crown-6 tetracarboxylic acid is a macrocyclic polyether ring consisting of six oxygen atoms joined by methylene bridges. According to Kuhn and co-workers [24,25,27], the primary interaction between 18C6H₄ and 5,6-ADTN is

by hydrogen bonding between the hydrogens of the primary amine group attached to the chiral centre and the oxygens of the ring system. This interaction occurs also for 6,7-ADTN and for their dimethoxy precursors 5,6- and 6,7-ADMTN. In fact, the addition of 18C6H₄ as chiral selector to the carrier electrolyte increased the migration time of both the ADTNs and the ADMTNs (Table 1) because the electrophoretic mobility of the analyte–chiral selector complex is lower than that of the plain analyte. This is due to the higher mass and the less positive charge of the complex, since at the pH of the buffer electrolyte 18C6H₄ is slightly negatively charged and hence migrates to the anodic site. The measured $\text{p}K_a$ is 3.6 which corresponds to a 4% ionization at pH 2.2.

In addition a secondary lateral interaction, which is responsible for the chiral discrimination, takes place. This enantio-recognition was postulated to occur by either a steric hindrance mechanism or by electrostatic interaction between the carboxylate groups of 18C6H₄ and the guest molecule [25,27] and is very sensitive to the type and the position of the substituents on the tetralin ring [26]. In fact 5,6-ADTN, but not its positional isomer 6,7-ADTN or the dimethoxy analogues, could be resolved into its enantiomers: only for 5,6-ADTN did the spatial arrangement lead to a difference in the stability constant of the analyte–ligand complex of the individual enantiomers large enough to obtain enantio-recognition.

A kinetic model for chiral recognition in HPCE was described by Wren and Rowe [28–31]. According to this model, an optimum chiral

Table 1
Effect of the addition of 18-crown-6 tetracarboxylic acid on the migration time of 2-aminotetralins

18C6H ₄ Concentration (mM)	Migration time ^a			
	5,6-ADTN	6,7-ADTN	5,6-ADMTN	6,7ADMTN
0	9.27	9.56	9.50	10.18
30	32.50	34.68	45.39	48.57

Applied potential = 10 kV. See Experimental for the other running conditions.

^a Migration times are in min.

selector concentration exists that depends on the affinity of the analyte for the chiral selector and hence varies from case to case. The influence of the amount of 18C6H₄ on the resolution at fixed applied potentials was therefore investigated. The results are shown in Table 2 and, as predicted by the model, we found an initial increase in resolution from 10 to 30 mM followed by a decrease when the chiral selector concentration was further increased to 50 mM. We also found an increase in resolution raising the applied voltage up to 10 kV. At higher values, the increase in peak efficiency of the enantiomers that is obtained by increasing the electric field across the capillary is overwhelmed by the decreased separation.

All experiments were carried out at pH 2.2, as recommended in the fundamental work by Kuhn et al. [25]. Since a more recent work showed the influence of pH on the resolution of D,L-histidine [27], we also investigated this parameter. At pH 2.0, a dramatic loss of resolution ($R_s < 0.4$) was observed, while slightly increasing the pH to 2.5 the migration time of both enantiomers shifted to more than 40 min with an increase in the separation factor and resolution. This favourable result was unfortunately associated with a severe distortion in peak shape which prevented its use for trace analysis. The reason of this distortion is unclear.

Temperature is another parameter which greatly influences resolution in capillary electrophoresis using a crown ether as chiral selector [24]. The result of the dependence of migration times and resolution on capillary temperature is

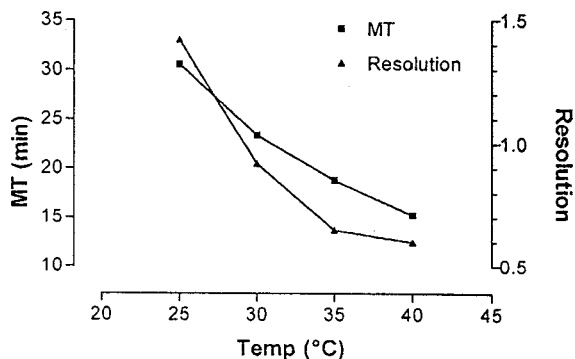


Fig. 2. Dependence of the migration time (MT) and resolution of the enantiomers of 5,6-ADTN on capillary temperature (voltage = 10 kV, [18C6H₄] = 30 mM). See Experimental for other electrophoretic conditions.

shown in Fig. 2. As expected retention times and resolution decreased when temperature was increased, the former due to the lower viscosity of the electrolyte, and the latter to the enhanced band broadening resulting from higher diffusion. Therefore a strict control of the temperature is essential in order to obtain high resolution.

An electropherogram of a racemic mixture under optimized conditions is shown in Fig. 3. The enantiomeric migration order was determined by HPCE runs of the individual enantiomers under similar conditions. Thus, the peak with lower migration time was identified as the *R*-enantiomer.

Most papers about chiral separations by HPCE include chromatograms of a racemic mixture showing the resolution between the two

Table 2

Resolution parameters for the separation of 5,6-ADTN as a function of the amount of the chiral selector

Applied voltage (kV)	10 mM			30 mM			50 mM		
	R_s	MT ^a	α	R	MT	α	R	MT	α
5.0	0.966	49.3	1.025	1.382	76.1	1.025	1.059	80.7	1.024
7.5	0.967	29.8	1.022	1.382	45.0	1.024	1.136	55.5	1.021
10	1.136	23.8	1.023	1.420	32.5	1.025	1.263	39.9	1.020
15	1.003	14.7	1.022	1.308	19.1	1.021	0.941	21.4	1.019

Applied potential = 10 kV. See Experimental for the other running conditions.

^a Migration time in min. of the first eluting enantiomer.

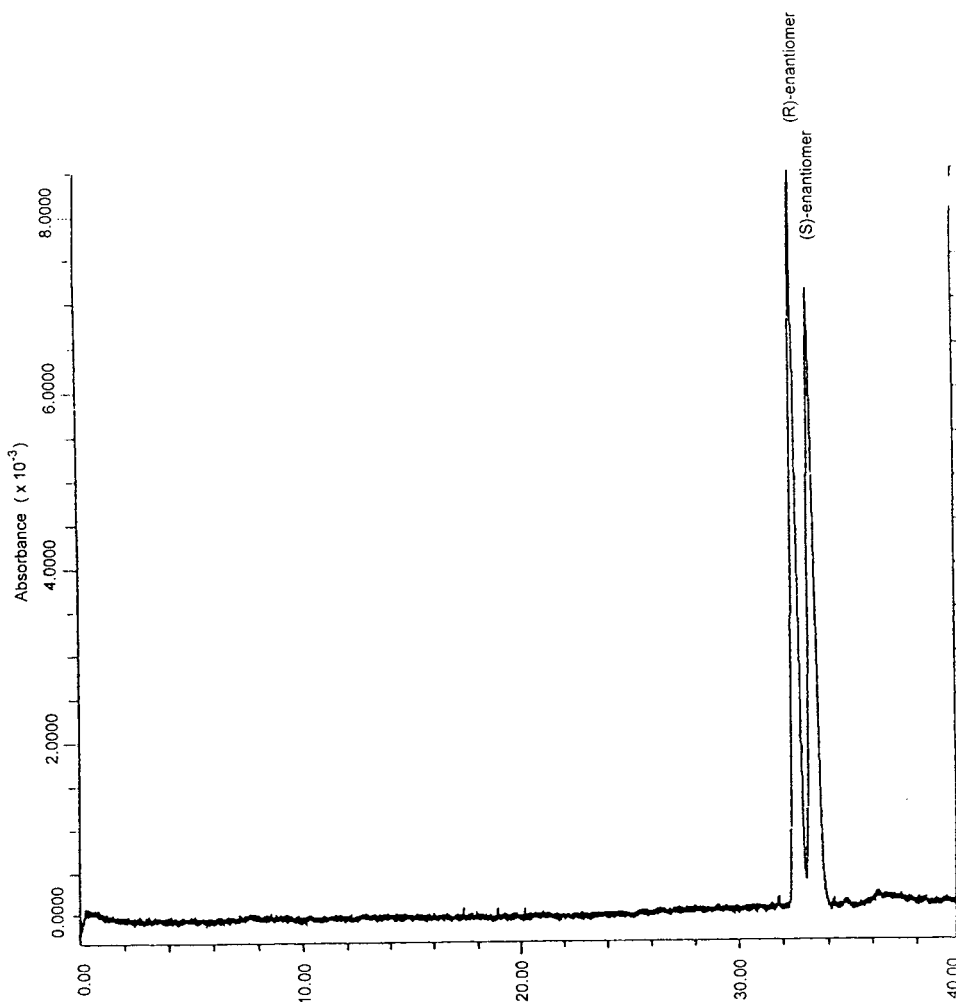


Fig. 3. Separation of the enantiomers of 5,6-ADTN under optimized conditions (voltage = 10 kV, $[18C6H_4] = 30$ mM, $T = 25^\circ\text{C}$). See Experimental for other electrophoretic conditions. Time scale in min.

enantiomers, but only few show quantitative data on the determination of the enantiomer present as impurity [32–34].

Since we were interested not only in good resolution but also in the accurate determination of a small amount of diastomer in the eutomer, we validated the method for both enantiomers by spiking one enantiomer with increasing amounts (range 0.5–5.0%) of the other present as impurity. The results are reported in Table 3 showing the good accuracy (expressed as bias, %) and precision (from the C.V. value) of the

assay that allows quantitation down to 0.5% of the enantiomer present as impurity.

Quantitation was determined from peak areas (normalized to their respective migration times) of the enantiomers since there was no difference in their response factor. This assumption was experimentally verified from the fact that the normalized peak-area ratio of an authentic racemic mixture was 1.002 (R/S ratio, C.V. = 2%, $n = 12$). In addition the linearity of the response for both enantiomers was checked in the same range (0.5–5.0%) in the presence of

Table 3

Validation data for the determination of the enantiomeric purity of 5,6-ADTN

Concentration added (%)	<i>R</i> (+) in <i>S</i> (-)			<i>S</i> (-) in <i>R</i> (+)		
	Found ^a (%)	Bias (%)	C.V. (%)	Found ^a (%)	Bias (%)	C.V. (%)
0.5	0.39 ± 0.03	-22.0	6.7	0.58 ± 0.02	+16.0	3.8
1.0	1.00 ± 0.08	0.0	7.8	1.01 ± 0.07	+1.0	6.8
2.0	2.05 ± 0.14	+2.5	6.7	2.12 ± 0.07	+5.8	3.1
5.0	4.70 ± 0.13	-6.0	2.7	5.10 ± 0.06	+1.9	1.2

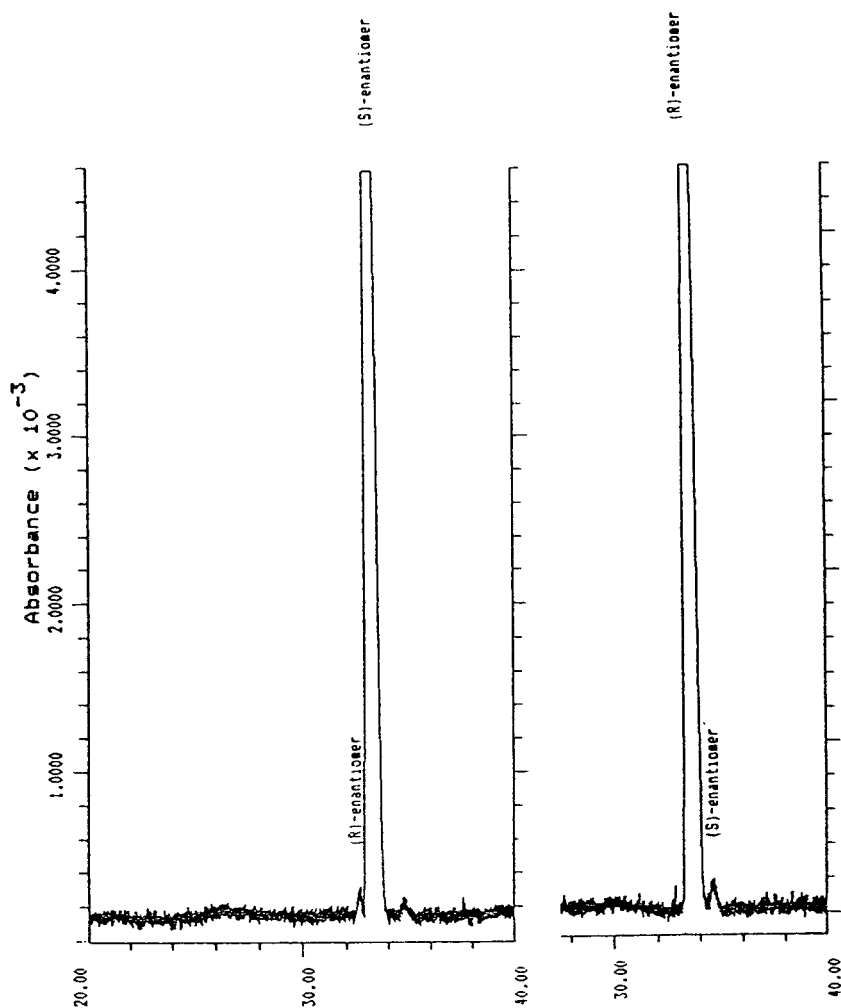
^a Mean ± standard deviation ($n = 4$).

Fig. 4. Separation and trace amount analysis of (*S*)-5,6-ADTN (0.5%) in (*R*)-5,6-ADTN (left electropherogram) and of (*R*)-5,6-ADTN (0.6%) in (*S*)-5,6-ADTN (right electropherogram) under optimized conditions (voltage = 10 kV, $[18C6H_4] = 30$ mM, $T = 25^\circ\text{C}$). See Experimental for other electrophoretic conditions. Time scale in min.

the corresponding amount (99.5–95.0%) of the other enantiomer. The regression analysis gave straight lines with slope 0.0506 ($r = 0.9991$) for the *R*-enantiomer and slope 0.0503 ($r = 0.9996$) for the *S*-enantiomer thus confirming their equal detector response.

This assay has been successfully employed for the determination of the enantiomeric purity of synthetic batches of both (*R*)- and (*S*)-5,6-ADTN. The electropherograms of a batch of a *R*-enantiomer containing 0.5% of the *S*-enantiomer and of a batch of *S*-enantiomer containing 0.6% of the *R*-enantiomer are shown in Fig. 4 showing a detection limit of about 0.3% (at a signal-to-noise ratio of 2).

Since we were involved in a research project where both ADTNs and ADMTNs are used as chiral building blocks for the synthesis of *N,N*-disubstituted aminotetralins acting on the dopaminergic system, we evaluated the use of other chiral selectors that could be able to perform the enantioseparation of 6,7-ADTN and of 5,6- and 6,7-ADMTN, which was unsuccessful using the system described here. The result of that study will be published elsewhere [35].

References

- [1] J.D. McDermed, H.S. Freeman and R.M. Ferris, in E. Usdin, J.I. Kopin and J. Barchas (Editors), *Catecholamines: Basic and Clinical Frontiers*, Pergamon Press, Oxford, 1979, p. 568.
- [2] H.S. Freeman and J.D. McDermed, in A.M. Creighton and S. Turner (Editors), *The Chemical Regulation of Biological Mechanisms*, Royal Society of Chemistry, London, 1982, p. 154.
- [3] J.D. McDermed and H.S. Freeman, *Adv. Bioscience*, 37 (1982) 179.
- [4] P. Castelnovo, *Chirality*, 5 (1993) 181.
- [5] S. Fanali, *J. Chromatogr.*, 474 (1989) 441.
- [6] S. Fanali and P. Bocek, *Electrophoresis*, 11 (1990) 757.
- [7] A. Nardi, L. Ossicini and S. Fanali, *Chirality*, 4 (1992) 56.
- [8] S. Fanali, *J. Chromatogr.*, 545 (1991) 437.
- [9] H. Soini, M. Riekkola and M.V. Novotny, *J. Chromatogr.*, 608 (1991) 265.
- [10] J. Snopek, H. Soini, M. Novotny, E. Smolkova-Keulemansova and I. Jelinek, *J. Chromatogr.*, 559 (1991) 215.
- [11] M.W.F. Nielsen, *Anal. Chem.*, 65 (1993) 885.
- [12] T.E. Peterson and D. Trowbridge, *J. Chromatogr.*, 603 (1992) 298.
- [13] T.E. Peterson, *J. Chromatogr.*, 630 (1993) 353.
- [14] E. Francotte, S. Cherkaoui and M. Faupel, *Chirality*, 5 (1993) 516.
- [15] Y.Y. Rawjee, D.U. Staerk and G. Vigh, *J. Chromatogr.*, 635 (1993) 291.
- [16] H. Nishi, T. Fukuyama, M. Matsuo and S. Terabe, *J. Microcolumn Sep.*, 1 (1989) 234.
- [17] H. Nishi, T. Fukuyama, M. Matsuo and S. Terabe, *J. Chromatogr.*, 515 (1990) 233.
- [18] R.O. Cole, M. Sepaniak and W.L. Hinze, *J. High Resolut. Chromatogr.*, 13 (1990) 579.
- [19] K. Otsuba and S. Terabe, *J. Chromatogr.*, 515 (1990) 221.
- [20] A. Guttman, A. Paulus, A.S. Cohen, N. Grinsberg and B.L. Karger, *J. Chromatogr.*, 448 (1988) 41.
- [21] I.D. Crusado and G. Vigh, *J. Chromatogr.*, 608 (1992) 421.
- [22] A. Dobashi, T. Hono, S. Hara and J. Yamaguchi, *J. Chromatogr.*, 480 (1989) 413.
- [23] A. D'Hulst and N. Verbeke, *J. Chromatogr.*, 608 (1992) 275.
- [24] R. Kuhn, F. Stoecklin and F. Erni, *Chromatographia*, 33 (1992) 32.
- [25] R. Kuhn, F. Erni, T. Bereuter and J. Hausler, *Anal. Chem.*, 64 (1992) 2815.
- [26] Y. Walbroehl and J. Wagner, *J. Chromatogr. A*, 680 (1994) 253.
- [27] R. Kuhn, J. Wagner, Y. Walbroehl and T. Bereuter, *Electrophoresis*, 15 (1994) 828.
- [28] S.A.C. Wren and R.C. Rowe, *J. Chromatogr.*, 603 (1992) 235.
- [29] S.A.C. Wren and R.C. Rowe, *J. Chromatogr.*, 609 (1992) 363.
- [30] S.A.C. Wren and R.C. Rowe, *J. Chromatogr.*, 635 (1993) 113.
- [31] S.A.C. Wren, *J. Chromatogr.*, 636 (1993) 57.
- [32] K.D. Altria, A.R. Walsh and N.W. Smith, *J. Chromatogr.*, 645 (1993) 193.
- [33] K.D. Altria, D.M. Goodall and M.M. Rogan, *Electrophoresis*, 15 (1994) 824.
- [34] E.C. Rickard and R.J. Bopp, *J. Chromatogr. A*, 680 (1994) 609.
- [35] P. Castelnovo, C. Albanesi, *Chirality*, in press.



ELSEVIER

Journal of Chromatography A, 715 (1995) 151–158

JOURNAL OF
CHROMATOGRAPHY A

Determination of chiral reagent purity by capillary electrophoresis

A. Engström, H. Wan, P.E. Andersson, B. Josefsson*

Department of Analytical Chemistry, The Arrhenius Laboratories for Natural Sciences, Stockholm University, S-106 91 Stockholm, Sweden

First received 14 March 1995; revised manuscript received 17 May 1995; accepted 17 May 1995

Abstract

A method for the determination of the enantiomeric purity of the chiral reagent 1-(9-fluorenyl)ethyl chloroformate (FLEC) has been developed. The reagent is reacted with glycine, an achiral compound, and separated by capillary electrophoresis using β - or γ -cyclodextrin as chiral selectors. A general equation for the recalculation of the measured values with respect to the chiral reagent purity is presented. The suitability of this approach is practised on the peptide D-Arginine–Glycine to determine trace amounts of the enantiomeric contaminant, the L-form.

1. Introduction

The determination of enantiomeric purity is of increasing importance in the pharmaceutical industry where the concentration of an enantiomeric impurity often may not exceed 0.1%. Chiral impurity quantitation below 0.1% will most probably be enforced by regulatory agencies in most countries [1]. Regulations in this area are enforced because of the different biological activities of the enantiomers.

Enantiomeric vasopressin peptides sometimes show quite different biological activities. Essential differences in this respect have been observed in blood pressure activity of the natural hormone 8-Arg-vasopressin. The change of the amino acid residue in position 8 from the L- to the D-form resulted in a decrease in the blood pressure activity from 450 IU/mg to 4 IU/mg

[2]. In liquid phase synthesis, the peptides are generated from the C-terminal (amide function) by fragment condensation. In order to control the biological activity during production of the active substance, it is important to determine any contamination of the corresponding enantiomer in the D-Arginine–Glycine (D-Arg–Gly) fragment at an early stage in the synthesis.

Enantiomeric determination of dipeptides in capillary electrophoresis (CE) has only been described by Tran et al. [3]. Their work concerns the separation of diastereomers after derivatisation with Marfey's reagent. The impurity of commercial Marfey's reagent has been reported to be approximately 0.25% of the opposite enantiomer [4]. When using chiral derivatising agents the enantiomeric purity of the reagent has to be exactly known, or the reagent has to be sufficiently pure in order to obtain an accurate determination of the enantiomeric ratio [5]. However, no published work on chromatograph-

* Corresponding author.

ic determination of chiral reagent impurity is known to the authors.

The drawback of reagent purity is eliminated in direct chiral separation. In a recently published paper, a comparison was made between direct and indirect chiral separation of amino acids by CE [6]. A large number of amino acids could be separated in both modes. The indirect method generally provided higher separation efficiencies than the direct method. The slow kinetics, generally connected with the direct chiral separation mechanisms, resulted in decreased chromatographic efficiency. Moreover, the screening procedure, which is necessary in order to find selectivity, was simplified by using the indirect approach.

The 1-(9-fluorenyl)ethyl chloroformate (FLEC) reagent has been briefly discussed as a versatile reagent in connection with micellar electrokinetic chromatography (MEKC) [7]. The advantages of the reagent have been discussed previously [6,8,9]. The commercially available FLEC reagent has a specified enantiomeric ratio of >99.5:0.5. High demands are made on a method for the exact determination of enantiomeric trace impurity. There are only a few papers dealing with the application of CE for the determination of enantiomeric trace impurity. Houben et al. [10] showed that such determinations are dependent on the detection sensitivity while the amount of sample to be introduced is limited. In addition, some different approaches in connection with pharmaceutical products have been investigated by Altria and co-workers [11–13]. Enantiomeric trace impurity determination of amino acids was reported by Ruyters and Van der Wal [14]. They developed a method for direct chiral separation of amino acids, derivatised with 4-fluoro-7-nitrobenz-2,1,3-oxadiazole, using β -cyclodextrin (β -CD) as chiral selector.

The aim of this work was to determine the enantiomeric purity of the chiral reagent FLEC in order to assure the enantiomeric quality of the hormone 8-D-Arg-vasopressin at trace levels. In this study emphasis is directed to find optimal CE separation conditions by statistical techniques. Then it is practicable to locate a specific

position of a local optimum condition with full factorial design in combination with response surface modelling [15,16]. Experimental designs have previously been used for MEKC method developments [17,18].

2. Experimental

2.1. Chemicals

The (+)- and (-)-FLEC reagent was a gift from EKA Nobel AB (Bohus, Sweden). The Arg-Gly dipeptide was from Ferring Pharmaceuticals (Malmö, Sweden). Boric acid, phosphoric acid and 2-propanol were from E. Merck (Darmstadt, Germany). Sodium dodecyl sulphate (SDS) from Fluka Chemie AG (Buchs, Switzerland). Glycine, β -, and γ -cyclodextrin (β -, and γ -CD) were from Sigma (St. Louis, MO, USA). All buffer solutions were made with water from an Elgastat UHQII (Elga, High Wycombe, UK).

2.2. Apparatus

The separations were carried out using a Prince autosampler (Lauerlabs, Emmen, Netherlands). An ISCO CV⁴ UV detector (ISCO, Lincoln, NE, USA) was used at 256 nm for the detection. The separation capillaries (25 and 50 μ m I.D.) were from Polymicro Technologies (Phoenix, AZ, USA). Data collection was made with ELDS 900 (Chromatography Data System, Kungshög, Sweden).

2.3. Derivatisation procedure

A solution of 10 mM Arg-Gly in 200 mM borate buffer (pH 9.2) was prepared. From this solution 400 μ l was mixed with 400 μ l of 30 mM FLEC reagent solution in acetone. After 10 min the reaction mixture was extracted with 0.5 ml pentane to terminate the reaction by removing excess reagent. The aqueous phase was diluted 10 \times with water and thereby ready for injection. The derivatisation of glycine was performed in the same way.

2.4. Separation conditions

The capillary was rinsed with five column volumes of 0.1 M NaOH and water, then equilibrated with ten column volumes of buffer prior to each run. For other separation conditions see figure legends. Buffer concentration, SDS concentration, CD concentration and pH are given as they were before the addition of organic modifiers. All injections were made by pressure.

2.5. Optimisation

Calculations and figures concerning optimisation were performed using the CODEX program (AP Scientific Service, Sollentuna, Sweden). The starting point for the optimisation of dipeptide MEKC separation was identical to separation conditions found for FLEC derivatised D- and L-arginine [6]. The test experiments were made by varying pH, buffer composition, SDS concentration, type of organic modifier and organic modifier concentration. When selectivity was found, a central composite design with three variables in two levels was used in order to optimise the separation system.

For the direct chiral separations, type of CD, CD concentration, pH, buffer composition, type and amount of organic modifier were varied in the scouting experiments. Optimisation was performed in the same way as for MEKC, except that only two variables were used.

The fit of the models to experimental data was evaluated by making five runs in the centre point of the models. The experimental noise was thereby determined. In addition to the response surfaces, the 95% confidence interval is represented as the interval over the regression coefficient. If the interval exceeds the regression coefficient, the variable is not significant to the model.

The functional relation between the experimental variables and the obtained results is approximated to fit a Taylor expansion

$$y = \beta_0 + \sum \beta_i x_i + \sum \sum \beta_{ij} x_i x_j + \beta_{ii} x_i^2 + e$$

where the coefficients β are the parameters of

the model and e is the overall error term [16]. The estimation of the parameters is done using multiple linear regression and a polynomial model is fitted to the experimental results. The linear coefficient for the experimental variables, β_i , describes their quantitative influence of the model. The cross-product, β_{ij} will measure the interaction effect between the variables, and the square term $\beta_{ii} x_i^2$ will describe the non-linear effect of the response.

3. Results and discussion

3.1. Determination of enantiomeric purity of (+)- and (-)-FLEC by reaction with glycine

When diastereomers are formed, reagent enantiomeric impurity will contribute to errors in the analytical results. This is due to the fact that the impurity will react and form enantiomeric pairs with the main products. The enantiomers will coelute and affect the impurity peak more than they do the main peak [5]. However, if the purity of the chiral reagent is known, the enantiomeric purity of the compound of interest can be calculated by:

$$y = \frac{1}{2} \left[\frac{M_A - I_A}{(2x - 1)(M_A + I_A)} + 1 \right] \quad (1)$$

where y is defined as the molar fraction of one enantiomer [$y = R/(R + S)$] of the compound to be investigated, and x is defined in the same way as the molar fraction of one form of the reagent [$x = R/(R + S)$]. M_A and I_A are the peak areas (i.e. corrected peak areas) of the main and impurity peak, respectively.

In the case where $x = 1$ (100% enantiomeric purity of the reagent) Eq. 1 is reduced to:

$$y = \frac{1}{2} \left[\frac{M_A - I_A}{M_A + I_A} + 1 \right] = \frac{M_A}{M_A + I_A} \quad (2)$$

In order to develop an accurate method for the enantiomeric trace-impurity determination utilising the benefits of the diastereomeric approach, the (+)- and (-)-FLEC reagent was reacted with glycine, an amino acid without a

chiral centre, thus producing (+)- and (-)-FLEC-glycine (FLEC-Gly) enantiomers. No differences in reaction speed can occur since the products possess the same physicochemical properties.

In the separation of the reagent it was found that the selectivity changed with β - and γ -CD. However, the presence of 2-propanol in the buffers was necessary for selectivity. The elution order of the FLEC-Gly enantiomers changed completely with the different cyclodextrins.

The separations were optimised with a factorial design including the 2-propanol and β - or γ -CD concentration, respectively. The pH was not included since the test runs did not show a significant effect of the pH in the range 5.5–7.0. Fig. 1 shows the response surfaces for β -CD (A) and γ -CD (B) as a function of the 2-propanol concentration with the resolution as the response. The optimisation for the β -CD concentration in Fig. 1A showed that the resolution increased with increasing β -CD concentration and that an optimum 2-propanol percentage existed. Since a concentration of β -CD above 15 mM resulted in increased noise, 14 mM β -CD and 18% 2-propanol were chosen for running conditions. A separation under these conditions is presented in Fig. 2A.

The elution order of (+)- and (-)-FLEC-Gly was altered when β -CD was changed to γ -CD. The best resolution was found with 12% 2-propanol and 10 mM γ -CD (Fig. 2B). The change in the elution order of (+)- and (-)-FLEC is important in order to determine the purity of both (+)- and (-)-forms, since it allows for the small impurity peak to be eluted before the main peak. With γ -CD as the chiral selector, the enantiomeric purity of 1.0 mM (+)-FLEC-Gly was investigated. Under these conditions no impurity peak was observed. However, after standard addition of 0.01% (-)-FLEC-Gly, a peak was observed, (Fig. 3). Since the purpose was to show the presence of (-)-FLEC-Gly a signal-to-noise ratio of 2/1 was used.

With β -CD as chiral selector, the (+)-FLEC-Gly was eluted first. The purity of 1.0 mM (-)-FLEC-Gly was investigated. Under these conditions no impurity peak was observed. How-

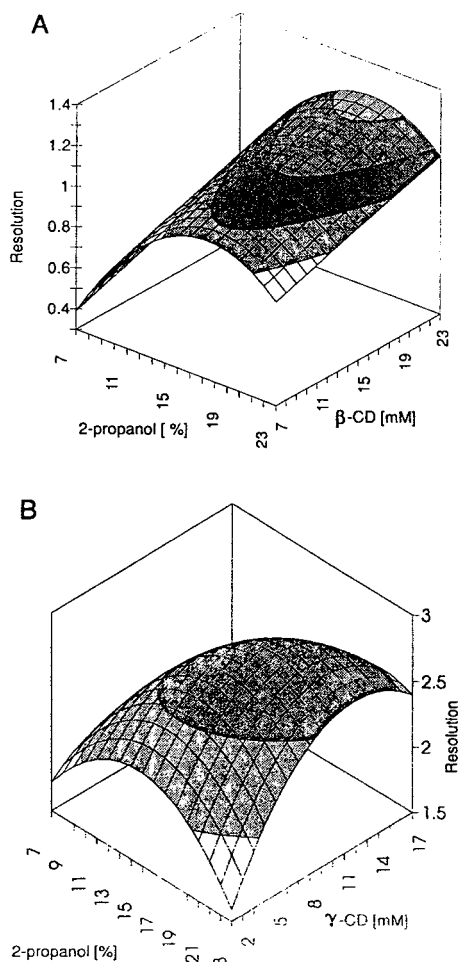


Fig. 1. Optimisation of separation of (\pm)-FLEC-Gly. Separation column: 50 μ m I.D. \times 65 cm (45 cm to detector); Voltage: 25 kV; Buffer: 50 mM phosphate, pH 6.0; 2-propanol and CD concentrations are varied. (A) β -Cyclodextrin used as chiral selector, (B) γ -cyclodextrin used as chiral selector.

ever, after standard addition of 0.1% (+)-FLEC-Gly, a peak was observed (Fig. 4). Determination below 0.1% was not successful. This is mainly caused by the lower resolution obtained with β -CD than with γ -CD. The lower resolution led to a partial overlap of the peaks.

The relative standard deviations of the repeatability of the determination of two (-)-FLEC-Gly spiked samples, were 14.6 and 5.8 for 0.1% and 0.5%, respectively ($n = 6$).

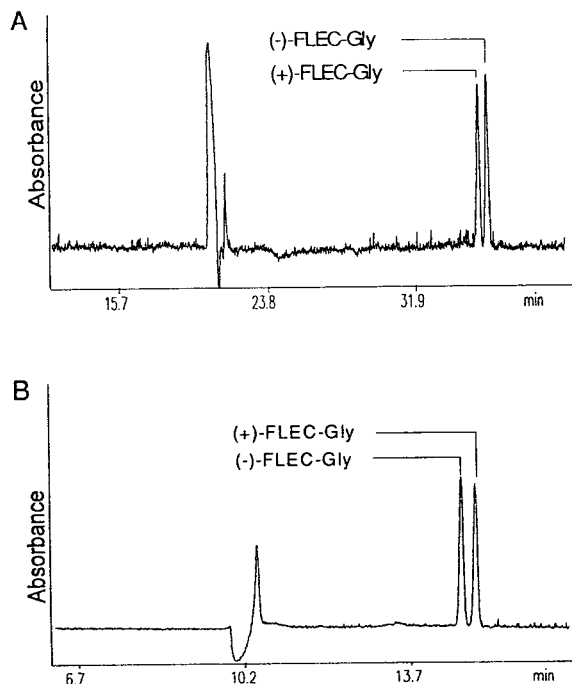


Fig. 2. Separation of (\pm)-FLEC-Gly. Column: 50 μ m I.D. \times 65 cm (45 cm to detector). (A) Buffer: 100 mM acetate, pH 6.0, 14 mM β -CD, 18% 2-propanol; 20 kV, 18 μ A. (B) Buffer: 50 mM phosphate, pH 6.0, 10 mM γ -CD, 12% 2-propanol; 20 kV, 16 μ A.

3.2. Diastereomeric separation of dipeptide

In order to obtain the optimum separation conditions, an experiment was performed by

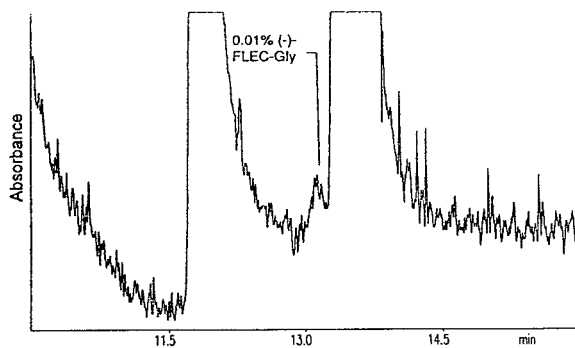


Fig. 3. Determination of 0.01% ($-$)-FLEC-Gly added to a ($+$)-FLEC-Gly sample. Buffer: 50 mM phosphate, pH 6.0, 10 mM γ -CD, 12% 2-propanol; 20 kV, 16 μ A. Column: 50 μ m I.D. \times 65 cm (45 cm to detector).

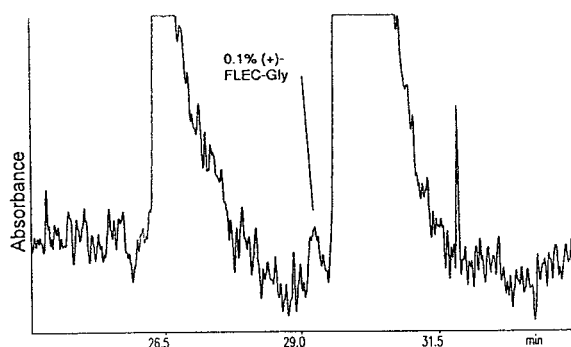


Fig. 4. Determination of 0.1% ($+$)-FLEC-Gly added to a ($-$)-FLEC-Gly sample. Buffer: 50 mM phosphate, pH 6.0, 14 mM β -CD, 18% 2-propanol; Separation column: 25 μ m I.D. \times 65 cm (45 cm to detector); 30 kV; 6 μ A.

factorial design. According to the test runs the most important factors were the SDS, buffer and 2-propanol concentrations. These three factors were therefore chosen as the variables in the optimisation experiment.

Three different response surfaces from this experimental design are presented in Fig. 5. The calculated responses were: selectivity (A, calculated without micellar elution time, see Ref. [6]), efficiency (B, theoretical plate number), and resolution (C, calculated according to conventional methods). From the response surfaces the effects of the different buffer parameters are determined. The main effect of 2-propanol was found for the selectivity response (Fig. 5A). Although a high SDS concentration gave an increased selectivity, the main effect was that low SDS concentrations resulted in higher selectivity, (Fig. 5A). High efficiency was obtained with high concentration of SDS (Fig. 5B). The 2-propanol square term showed that an optimum existed for efficiency and a minimum for selectivity. The resolution response surface shown in Fig. 5C was mainly dependent on the 2-propanol and buffer concentrations. The separation of D- and L-Arg-Gly-FLEC under optimum conditions is shown in Fig. 6.

Determination of the chiral dipeptide impurity was performed from the chromatogram in Fig. 7. The amount of L-form in the D-Arg-Gly sample was found to be 0.013%, with a standard devia-

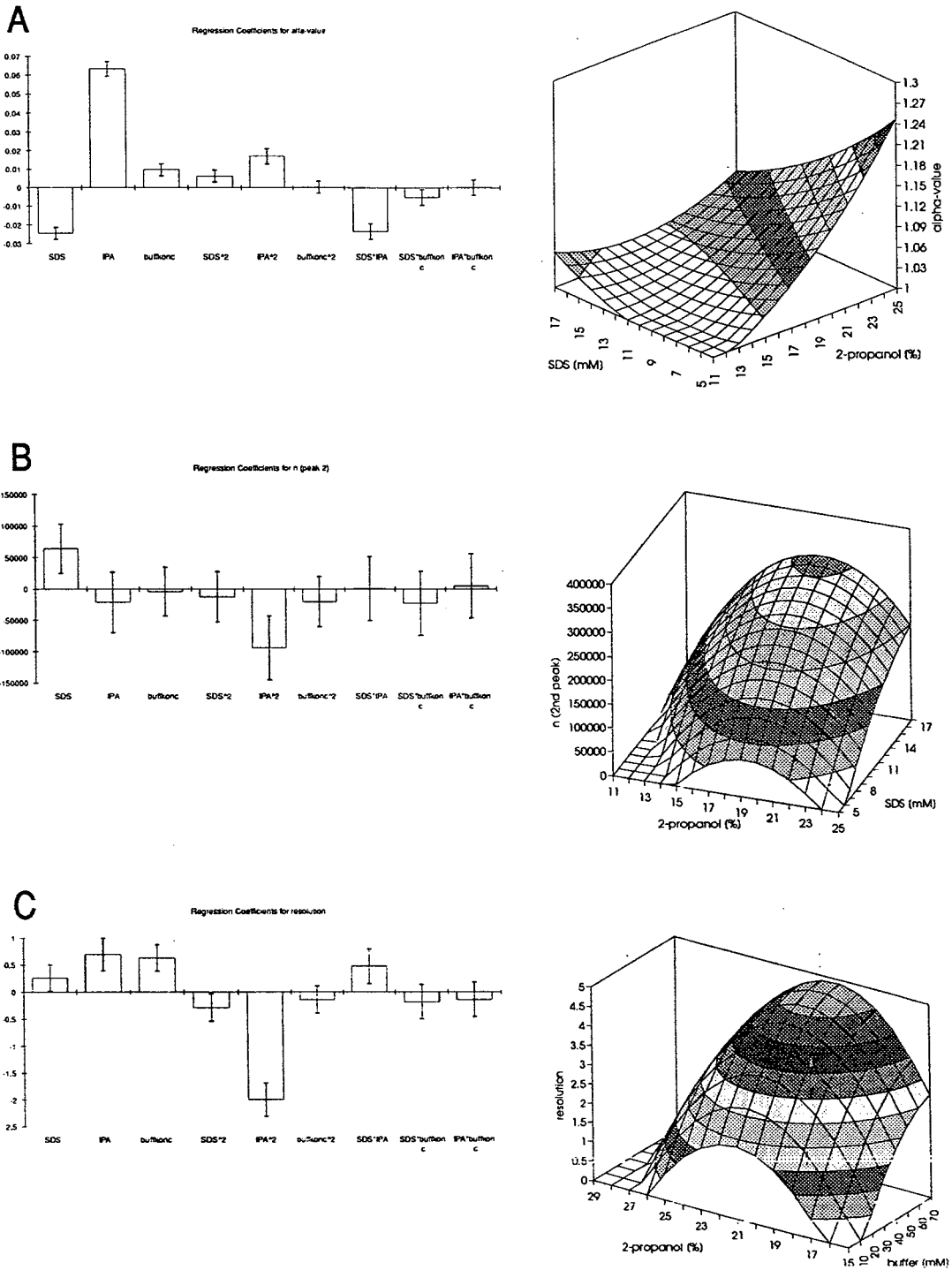


Fig. 5. Optimisation of FLEC-D,L-Arg-Gly separation. Separation column: 25 μ m I.D. \times 56 cm (40 cm to detector); pH 9.2; SDS, 2-propanol and buffer concentrations are varied.

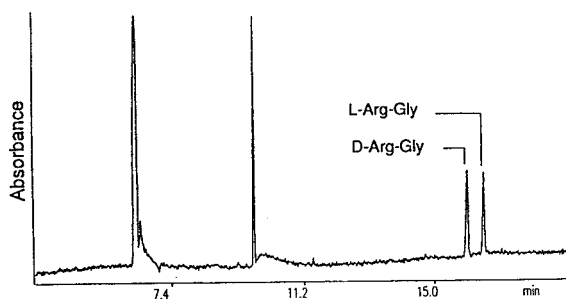


Fig. 6. MEKC separation of (–)-FLEC-D,L-Arg-Gly. Buffer: 20 mM borate–15 mM phosphate, pH 9.20, 10 mM SDS, 18% 2-propanol; Column: 25 μ m I.D. \times 56 cm (40 cm to detector); Voltage: 30 kV, 7.8 μ A.

tion of 0.002%. The determination was carried out by the standard addition method using 4 points. The percentages added were: 0.024, 0.047 and 0.094, the regression coefficient was $r^2 = 0.9966$.

If the (+)-FLEC would contain an impurity of 0.01% (–)-FLEC, the impurity of L-Arg-Gly in the D-Arg-Gly would be 0.003% according to Eq. 1. However, the amount of (–)-FLEC could only be determined to be less than 0.01%; thus, in this case it is better to use Eq. 2 since the value for the dipeptide impurity will otherwise be too low.

The detection limit for FLEC-Gly and FLEC-Arg-Gly was 0.1 μ M. This is ten times lower than the results reported earlier for the analogues non-chiral derivatisation reagent FMOC

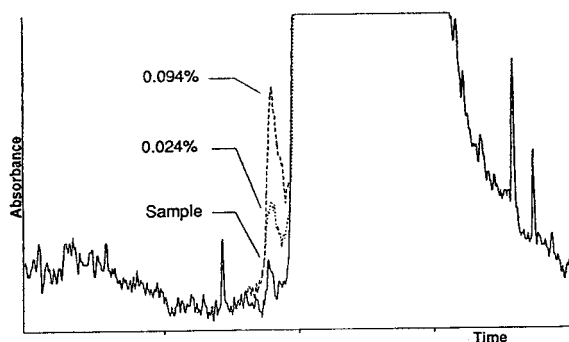


Fig. 7. Determination of L-Arg-Gly in a D-Arg-Gly sample by standard addition. Buffer: 20 mM borate–15 mM phosphate, pH 9.20, 10 mM SDS, 18% 2-propanol. Separation column: 50 μ m I.D. \times 65 cm (45 to detector); Voltage: 30 kV.

[19]. The sample plug injected was calculated to be 2.3 cm, which is one order of magnitude longer than what is generally recommended [20]. Stacking conditions were obtained without any desalting or pH adjustment of the sample prior to the injection. The buffer concentration in the sample was higher than in previously reported work [19]. In this work the higher buffer concentration remained from the derivatisation process.

4. Conclusions

The enantiomeric purity of chiral reagents at trace levels can be established by efficient separation systems. Capillary electrophoresis with chiral selectors such as cyclodextrins has been shown useful to separate (+)- and (–)-FLEC after reaction with achiral glycine.

By using the stacking principle a large amount of sample can be applied in the capillary; thus the (\pm)-enantiomers can be determined in a ratio of 1:10 000. Enantiomeric trace analyses are facilitated by a combination of efficient separation of the diastereomers and high detection sensitivity, which can be accomplished by incorporating a strong chromophore in the derivatising reagents. The FLEC reagent is available in both enantiomeric forms and thus the elution order of the derivatisation products can be arranged in a way that the small peak elutes in front of the large peak.

The indirect chiral separation with (+)- or (–)-FLEC reagents is demonstrated to be favourable to verify the enantiomeric purity of peptides at trace levels when the reagent enantiomeric purity is assured.

Acknowledgements

The authors would like to thank Krister Larsson (Ferring Pharmaceuticals) for financial support and also for providing the Arg-Gly peptide. Per Möller (EKA Nobel) kindly provided the FLEC reagent. Stig Allenmark and

Lars Blomberg are acknowledged for valuable discussions.

References

- [1] M. Novotny, H. Stefansson and S. Soini, *Anal. Chem.*, 66 (1994) 641A.
- [2] M. Zaoral, J. Kolc and F. Sorm, *Collection Czech Chem. Commun.*, 31 (1966) 382.
- [3] A.D. Tran, T. Blanc and E.J. Leopold, *J. Chromatogr.*, 516 (1990) 241.
- [4] L. Hansson and R. Isaksson, *J. Chromatogr. A*, 653 (1993) 9.
- [5] S.G. Allenmark, *Chromatographic Enantioseparation: methods and applications*, Ellis Horwood Limited, Chichester, 1988.
- [6] H. Wan, P.E. Andersson, A. Engström and L.G. Blomberg, *J. Chromatogr. A*, 704 (1995) 179.
- [7] R. Weinberger, *Practical Capillary Electrophoresis*, Academic Press, San Diego, CA, 1993, p. 184.
- [8] S. Einarsson, B. Josefsson, P. Möller and D. Sanchez, *Anal. Chem.*, 59 (1987) 1191.
- [9] C.W. Demarest, E.A. Monnot-Chase, J. Jiu and R. Weinberger, in P.D. Grossman and J. Colburn (Editors), *Capillary Electrophoresis: Theory and Practice*, Academic Press, San Diego, CA, 1992, Ch. 11, p. 336.
- [10] R.J.H. Houben, H. Gielen and S.J. van der Wal, *J. Chromatogr.*, 634 (1993) 317.
- [11] K.D. Altria, *Chromatographia*, 35 (1993) 177.
- [12] K.D. Altria, *Chromatographia*, 35 (1993) 493.
- [13] M.M. Rogan, K.D. Altria and D.M. Goodall, *Chromatographia*, 38 (1994) 723.
- [14] H. Ruyters and S.J. van der Wal, *J. Liq. Chromatogr.*, 17 (1994) 1883.
- [15] S.F.Y. Li, *Capillary Electrophoresis*, *J. Chromatogr. Library Ser.*, Vol. 52, Elsevier, Amsterdam, 1992.
- [16] R. Carlson, *Design and Optimisation in Organic Synthesis*, Elsevier, Amsterdam, 1992.
- [17] J. Vindevogel and P. Sandra, *Anal. Chem.*, 63 (1991) 1530.
- [18] J.H. Jumppanen, S.K. Wiedmer, H. Siren, M.L. Riekola and H. Haario, *Electrophoresis*, 15 (1994) 1267.
- [19] A. Engström, P.E. Andersson, W.D. Pfeffer and B. Josefsson, *Anal. Chem.*, (1995) in press.
- [20] S.L. Delinger and J.M. Davis, *Anal. Chem.*, 64 (1992) 1947.



ELSEVIER

Journal of Chromatography A, 715 (1995) 159–165

JOURNAL OF
CHROMATOGRAPHY A

Separation of formoterol enantiomers and detection of zeptomolar amounts by capillary electrophoresis using laser-induced fluorescence

Samir Cherkaoui, Michel Faupel, Eric Francotte*

Pharmaceutical Research, Ciba-Geigy, K-122.P.25, CH-4002 Basel, Switzerland

First received 7 September 1994; revised manuscript received 17 May 1995; accepted 17 May 1995

Abstract

A sensitive and rapid high-performance capillary electrophoresis (HPCE) method combined with laser-induced fluorescence (LIF) detection is described, which is suitable for the analysis of racemic formoterol and formoterol enantiomers after derivatization with fluorescein isothiocyanate (FITC). The limit of detection is 1 pg/ml in the case of FITC-derivatized racemic formoterol in the absence of chiral selector. Upon injection of 5 nl, it corresponds to an amount of not more than 120 molecules. The chiral recognition occurs in the presence of heptakis(2,3,6-tri-O-methyl- β -cyclodextrin) as a chiral selector in the buffer electrolyte and yields a detection limit of $10 \cdot 10^{-12}$ g/ml for each enantiomer.

1. Introduction

Most of the chiral drugs available on the market are administered as racemates [1]. However, the great difference in pharmacological effects and pharmacokinetics between the two enantiomeric forms of many drugs is also well known [2,3]. Therefore, the pharmaceutical industry increasingly needs new analytical and preparative procedures capable of resolving and quantitating drug enantiomers, and the resolution of racemic mixtures is becoming a highly challenging area of separation technology.

High-performance capillary electrophoresis (HPCE) is a relatively new mode of analytical separation with great potential and is already applied to a wide variety of molecules, ranging

from simple ions to larger particles, and for ionized as well as neutral compounds [4]. This technique has already attracted a considerable amount of attention in different areas such as analytical biochemistry, molecular biology, analytical chemistry, and medical biology. One particularly important application of HPCE is the chiral separation, where the technique offers new alternatives to the already existing methods. This application has already been the subject of different reviews [5–9]. Cyclodextrins and their derivatives are the most commonly used chiral selectors in HPCE due to their capacity to include a wide range of compounds and the generally high degree of chiral recognition they afford. We have already shown that HPCE is a very suitable enantioselective analytical tool for resolving chiral pharmaceuticals in terms of high speed, high resolving power, short optimization

* Corresponding author.

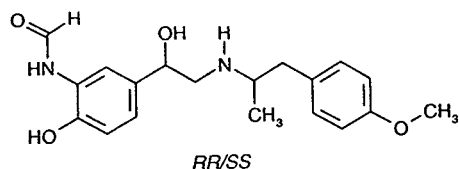


Fig. 1. Chemical structure of racemic formoterol (*RR/SS*).

time, and low cost [10]. Formoterol (Fig. 1), a relatively new and extremely potent oral β_2 -adrenoreceptor agonist with a long-lasting bronchodilator action, is administered as a racemate. The very low dosage required (usually 15 μg per inhalation) results in low plasma concentrations (generally < 50 pg/ml). Consequently, the development of an enantioselective analytical method allowing the separation and the detection of the enantiomer at very low concentrations constituted a real challenge.

In this work, we describe two rapid and sensitive analytical methods using HPCE in combination with laser-induced fluorescence detection (1) for the determination of racemic formoterol that has been derivatized with FITC and (2) for the enantiomeric separation of FITC-derivatized formoterol.

2. Experimental

2.1. Chemicals

All the cyclodextrins used, α -CD, β -CD, γ -CD, heptakis(2,6-di-O-methyl- β -CD) and heptakis(2,3,6-tri-O-methyl- β -CD) were purchased from Sigma Chemical (Buchs, Switzerland). Fluorescein isothiocyanate isomer I (FITC) and 1-octane sulfonic acid sodium salt monohydrate were from Fluka Chemicals (Buchs, Switzerland). The racemic formoterol was from Ciba Pharma (Basel, Switzerland). All other reagents and solvents were of analytical grade. It should be pointed out that special demands must be placed on the purity of the solvents used in fluorescence measurements since

considerable quenching can be caused by impurities.

2.2. Formoterol derivatization

A solution of 0.1285 g (0.33 mM) of fluorescein isothiocyanate dissolved in 15 ml of absolute ethanol is added dropwise and at room temperature to a mixture of 0.103 g (0.3 mM) of racemic formoterol and 0.5 ml of triethylamine dissolved in 15 ml of absolute ethanol. After addition, the mixture is stirred for 4 h at 40°C. The solvent is evaporated and the residue is purified by chromatography on silica gel (eluent: chloroform-ethylacetate-methanol, 4:6:6). The fractions containing the desired compound are collected and yield, after evaporation, 188 mg of the pure formoterol derivative (yield 85.5%). The NMR, elemental analysis, and mass spectroscopy data are in accordance with the expected structure.

2.3. Instrumentation

The experiments were carried out on a Beckman PACE 2100 capillary electrophoresis system equipped with a LIF detector and a power supply capable of delivering up to 30 kV. The excitation light from a 4-mW argon-ion laser was focused on the capillary window by means of a fiber-optic connection. Excitation was performed at 488 nm and a 520-nm band-pass filter was used for emission. A fused-silica capillary (Supelco, Gland, Switzerland), with 75 μm I.D., 57 cm total length, and 50 cm from the point of sample introduction to the detector window, was used in all the experiments. Data acquisition was performed using the Gold chromatography software package system.

Injections were made using the pressure mode (ca. 0.3 psi) for 5 s each. In all the experiments a constant voltage was applied and the temperature of the separation system was kept at 25°C during the run. In all cases the migration direction was toward the cathode.

The fluorescence measurements for determination of excitation and emission maxima of the FITC-derivatized formoterol were performed with a Perkin-Elmer MPF 66 spectrofluorimeter.

2.4. Running conditions

For the analysis of FITC-derivatized formoterol, the following mixed buffer was used: 10 mM borate buffer (pH 9) with 10% methanol. For the enantiomeric resolution of the FITC-derivatized formoterol, a buffer mixture of 10% methanol, 67 mM phosphate buffer (pH 8) was prepared and the appropriate amount of cyclodextrin was added. Prior to analysis, the capillary was rinsed with 0.1 M NaOH for 2 min and then filled with the electrophoretic buffer. All the buffer solutions were filtered through a membrane filter (Skan, Basel, Switzerland) of 0.2- μ m pore size prior to use. Stock solution of FITC-derivatized formoterol for LIF detection was prepared in methanol and diluted 10^9 times by steps of 10.

3. Results and discussion

Formoterol is administrated as a racemic mixture of both *RR*- and *SS*-enantiomers. Various methods were previously developed to detect the racemic drug, and the lowest limit of detection (20 pg/ml) has recently been obtained using HPLC and electrochemical detection with a signal-to-noise ratio of 3:1 [11]. However, in a recent report it has been shown that the therapeutic activity of formoterol probably resides only in the *RR*-enantiomer [12]. The enantioselective analysis of the samples was performed on a Chiral-AGP column using UV detection [13]. But, owing to the low plasma concentration, a more sensitive and reproducible analytical method is required to determine the enantiomeric composition of samples to evaluate the pharmacokinetic profile of both enantiomers.

HPCE with γ -cyclodextrin as a chiral selector has already been used as a means to analyze the enantiomeric composition of formoterol samples [14]. This chiral separation was achieved using a phosphate buffer (pH 3) containing 40 mM γ -cyclodextrin and 40 mM of the sodium salt of 1-octane sulfonic acid monohydrate. However, the on-line UV detection is not capable of attaining the sensitivity needed to perform

studies in the desired concentration range (ca. 10 pg/ml). This limitation is essentially due to the short path-length provided by the capillary tubing.

To date, the most sensitive detector for capillary electrophoresis is based on laser-induced fluorescence (LIF) [15] and it has already been used for various applications [16,17], including enantiomeric separations [18,19]. For example, with suitable tags, mass sensitivities on the zeptomolar level (10^{-21} moles or hundreds of molecules) have been obtained for amino acids by using capillary laser-induced fluorescence [20,21]. Unfortunately, the fundamental limitation of fluorescence detection is that relatively few molecules fluoresce. Then, most of the analytes have to be derivatized (pre- or post-column derivatization) with a fluorescence reagent.

3.1. Formoterol derivatization

To ensure the detection of fluorescence, formoterol has to be derivatized. This derivatization has been accomplished using fluorescein isothiocyanate isomer I. Isothiocyanates are known to react selectively with the amino group of amino alcohols and of amino phenols [22]. It consists of pre-column off-line derivatization; the reaction is carried out prior to injection of the sample into the capillary. This procedure does not impose any restrictions on the CE system. Reaction of racemic formoterol with 1.1 equivalent of fluorescein isothiocyanate in the presence of triethylamine in ethanol affords the desired derivative (Fig. 2), which has been subsequently purified by chromatography on silica gel. The reaction occurs regioselectively on the secondary amine, as indicated by the strong displacement observed in NMR spectroscopy for the protons of the $-\text{CH}_2\text{NCH}$ group, which are shifted respectively of about 2.7 ppm (CH) and 1 ppm (CH_2) to lower field. The derivative is very stable and can be stored as a stock solution for several weeks in methanol without observing any decomposition.

As can be seen from Fig. 3, the emission spectrum shows a maximum at wavelength 519

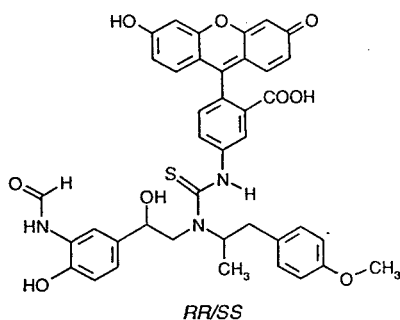


Fig. 2. Chemical structure of FITC-derivatized formoterol (RR/SS).

nm following excitation at 488 nm. The excitation spectrum gives a maximum at 499 nm with emission at 520 nm. This observed excitation maximum conveniently matches the argon-ion laser 488 nm line, and the emitted light can be measured near 520 nm.

3.2. FITC-derivatized formoterol analysis (achiral conditions)

As already mentioned above, chiral separation of formoterol using CE has been carried out under acidic conditions (pH 3) [14]. But, as formoterol has to be derivatized to enhance detection, we had to develop a new separation scheme for FITC-derivatized formoterol. It must be noted that each molecule of FITC coupled to formoterol incorporates a negative charge into

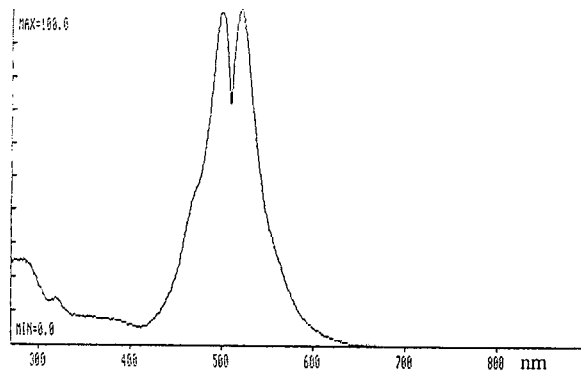


Fig. 3. Fluorescence spectra of FITC-derivatized formoterol.

the adduct, due to the presence of the carboxylic group on the label.

After optimization of the buffer conditions, a 10 mM borate buffer (pH 9) containing 10% methanol as organic modifier was selected for the analysis of the FITC-derivatized formoterol. Under those alkaline conditions, the electroosmotic flow is high enough to permit the elution of the compound within 7 min. The presence of 10% methanol in the running buffer contributes to band sharpness. The theoretical plate value is about 200 000 per m, which demonstrates the high resolving power of the method. The electropherogram (Fig. 4) shows that a concentration of 1 pg/ml of racemic FITC-derivatized formoterol is still detectable with a signal-to-noise ratio of about 10.

3.3. Chiral separation

To obtain chiral separation of the enantiomers of racemic FITC-derivatized formoterol, we evaluated different cyclodextrins and cyclodextrin (CD) derivatives as possible chiral selectors. Among the different cyclodextrins used for this

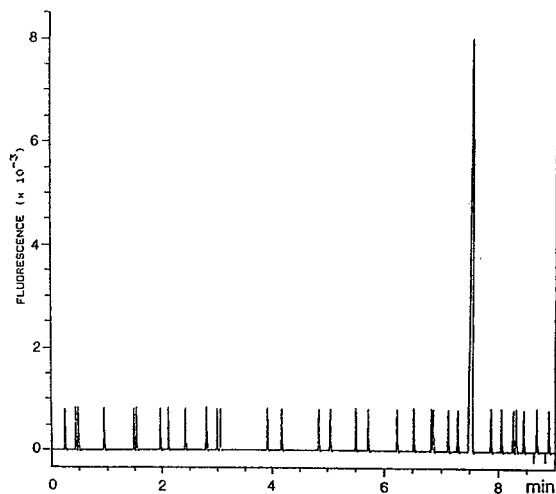


Fig. 4. Analysis of racemic FITC-derivatized formoterol. Sample: 1 pg/ml injected by the pressure mode for 5 s (ca. 5 nl). The electrophoresis was performed in pH 9 borate buffer containing 10% methanol. Applied voltage: 20 kV; LIF detection (argon-ion laser, excitation: 488 nm; emission: 520 nm).

study, α -CD, β -CD, γ -CD, heptakis(2,6-di-O-methyl- β -CD) and heptakis(2,3,6-tri-O-methyl- β -CD), only the latter compound was effective in achieving optical resolution of the FITC-derivatized formoterol. The type of CD as well as the structural features of the molecule play an important role in resolution. The β -CD derivative consists of seven glucopyranose units in which the three OH groups in positions 2, 3, and 6 of every unit are converted into methoxyl groups.

The effects of buffer pH, methanol percentage, and CD concentration on the enantiomeric resolution of FITC-derivatized formoterol were investigated to determine the optimum separation conditions. According to the results obtained above, our investigations were made at alkaline pH 7–9. In this pH range, the resolution improves as the pH of the running buffer decreases. Therefore, we select pH 8, which affords a good compromise for good resolution, short migration time, and high sensitivity.

We also studied the influence of the percentage of methanol used as an organic modifier. The methanol content in the electrophoretic buffer was first increased by adding 10% methanol. At higher percentages of methanol, no further improvement in resolution was observed, and the analysis time was dramatically lengthened due to the decrease in electroosmotic velocity (Table 1).

The influence of concentration of the added heptakis(2,3,6-tri-O-methyl- β -CD) (TM- β -CD) in the running buffer on the resolution (R_s) was

also investigated. The resolution increases rapidly from 5 mM TM- β -CD ($R_s = 1.02$) to 20 mM TM- β -CD ($R_s = 1.12$). Higher CD concentrations do not markedly further improve the resolution and have the disadvantage of increasing the retention time of the enantiomers.

A phosphate buffer (pH 8) containing 10% methanol and 20 mM TM- β -CD was the most appropriate to achieve both high enantiomeric resolution and high sensitivity. At a concentration of 10 pg/ml, the enantiomers are still well detectable (Fig. 5a). The very low detection limits obtained in this study are essentially due to the use of a suitable fluorogenic label, FITC isomer I, that is compatible with the spectral characteristics of the argon-ion laser.

We also investigated the possibility of enantiomeric resolution in the micellar electrokinetic capillary chromatography (MECC) mode. As already mentioned, separation of formoterol enantiomers with on-line UV detection has been achieved under acidic conditions and in the presence of the sodium salt of 1-octane sulfonic acid monohydrate. By adding 40 mM octane sulfonic acid Na salt to the buffer, FITC-derivatized formoterol was optically resolved as shown in Fig. 5b. The result is almost similar to that obtained in the capillary zone electrophoresis (CZE) mode. The migration time is slightly longer, which is certainly due to the presence of the micelles.

The MECC mode has some advantages over the CZE mode, because it is possible to modulate the migration time and the capacity factor by modifying both the CD and the micellar concentration, resulting in easier optimization of the separation. In addition, we have already demonstrated the possibility of directly determining hexobarbital enantiomers in rat plasma using CD-MECC [10]. In this case, the plasma proteins were solubilized by the micelle [sodium dodecyl sulfate (SDS)], and the migration times were selectively manipulated to avoid any interference with drug enantiomers. CD-MECC has the merit of allowing direct and rapid analysis of drug enantiomers in biological samples without any pretreatment such as deproteinization or extraction.

Table 1
Influence of methanol percentage on the enantiomeric resolution

Methanol (vol%)	Migration time (min)	Resolution R_s
0	14.32	1.16
10	19.70	1.26
20	26.55	1.22

Buffer electrolyte: phosphate buffer, pH 8, containing 20 mM TM- β -CD and different amounts of methanol. Applied voltage: 10 kV.

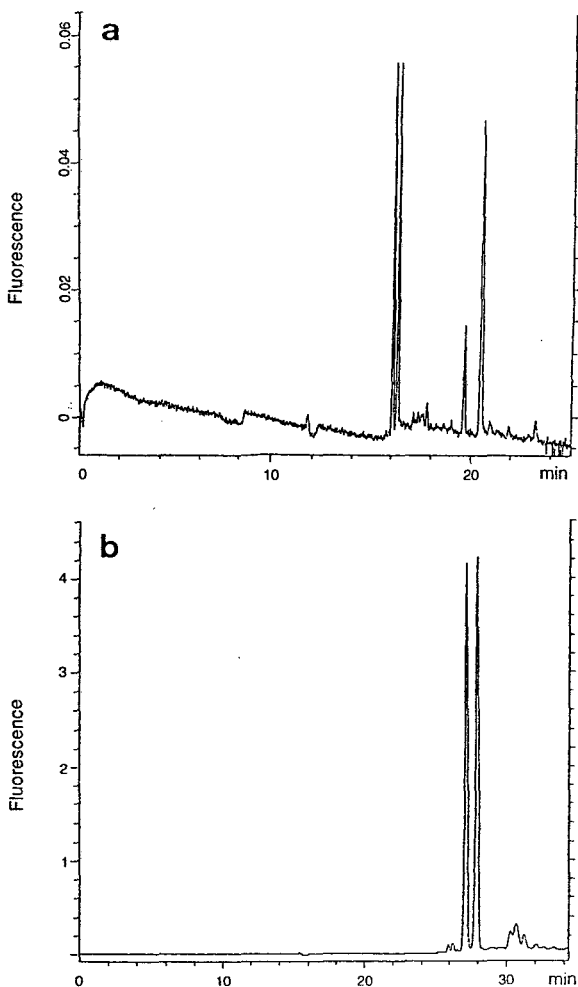


Fig. 5. Enantiomeric resolution of FITC-derivatized formoterol. LIF detection (argon-ion laser, excitation: 488 nm; emission: 520 nm). Injection by the pressure mode for 5 s (ca. 5 nl). (a) CZE resolution: sample, 10 pg/ml; buffer electrolyte, phosphate buffer (pH 8) containing 20 mM TM- β -CD and 10% methanol. Applied voltage: 12 kV. (b) MECC resolution: sample, 0.1 ng/ml; buffer electrolyte, phosphate buffer (pH 8) containing 20 mM TM- β -CD, 40 mM octane sulfonic acid, and 10% methanol. Applied voltage: 11 kV.

4. Conclusion

The combination of capillary electrophoresis with laser-induced fluorescence detection permits the analysis of samples containing very low concentrations of analytes. This technique is particularly suitable for highly potent drugs ac-

tive at extremely low doses, such as formoterol, a relatively new oral β 2-adrenoreceptor agonist. The high sensitivity of the method has been clearly demonstrated by the reported application to formoterol, which, after derivatization with fluorescein isothiocyanate, could be detected at a concentration of $1 \cdot 10^{-12}$ g/ml. Using an appropriate chiral selector in the buffer electrolyte, it is possible to simultaneously separate the enantiomers of formoterol detected in the $10 \cdot 10^{-12}$ g/ml concentration range. This application to the separation and detection of the enantiomers of a chiral drug at such a low concentration demonstrates the promising potential of the technique.

References

- [1] S.C. Stinson, Chem. Eng. News, September (1992) 46–79.
- [2] K. Williams and E. Lee, Drugs, 30 (1985) 333.
- [3] G.T. Tucker and M.S. Lennard, Pharmacol. Ther., 45 (1990) 309.
- [4] S.F.Y. Li, Capillary Electrophoresis, J. Chromatogr. Library, Vol. 52, Elsevier, Amsterdam, 1992.
- [5] R. Kuhn and S. Hoffstetter-Kuhn, Chromatographia, 34 (1992) 505–512.
- [6] J. Snopek, I. Jelinek and E. Smolkova-Keulemansova, J. Chromatogr., 609 (1992) 1–17.
- [7] M.M. Rogan, K.D. Altria and D.M. Goodall, Chirality, 6 (1994) 25.
- [8] T.L. Bereuter, LC·GC Int., 7 (1994) 78.
- [9] S. Terabe, K. Otsuka and H. Nishi, J. Chromatogr. A, 666 (1994) 295.
- [10] E. Francotte, S. Cherkaoui and M. Faupel, Chirality, 5 (1993) 516.
- [11] B.T.J. van den Berg, E.J.G. Portier, M. van den Berg, M.C.P. Braat and C.J. van Boxtel, Ther. Drug Monitoring, 16 (1994) 196.
- [12] B. Waldeck, Chirality, 5 (1993) 350.
- [13] J. Trofast, K. Österberg, B.-L. Källström and B. Waldeck, Chirality, 3 (1991) 443.
- [14] E. Fröch and M. Bloch, Ciba (Basel), personal communication.
- [15] E.S. Yeung, P. Wang, W. Li and R.W. Giese, J. Chromatogr., 608 (1992) 73.
- [16] T. Ueda, R. Mitchell, F. Kitamura, T. Metcalf, T. Kuwana and A. Nakamoto, J. Chromatogr., 593 (1992) 265.
- [17] S.R. Rabel, R. Trueworthy and J.F. Stobaugh, J. High Resolut. Chromatogr., 16 (1993) 326.

- [18] T. Toyooka, M. Ishibashi and T. Terao, *J. Chromatogr.*, 625 (1992) 357.
- [19] J. Kondo, T. Imaoka, T. Kawasaki, A. Nakanishi and Y. Kawahara, *J. Chromatogr.*, 645 (1993) 75.
- [20] C. Toulas and L. Hernandez, *LC · GC Int.*, 5 (1992) 27.
- [21] J.-Y. Zhao, D.-Y. Chen and N.J. Dovichi, *J. Chromatogr.*, 608 (1992) 117.
- [22] U. Kraatz, in H. Hagemann (Editor), *Methoden der Organischen Chemie (Houben-Weyl)*, Vol. E4, Georg Thieme Verlag, Stuttgart, 1983, pp. 439, 486.

Pre-column derivatization of proteins to enhance detection sensitivity for sodium dodecyl sulfate non-gel sieving capillary electrophoresis

Edwin L. Gump, Curtis A. Monnig*

Department of Chemistry, University of California, Riverside, CA 92521-0403, USA

First received 15 February 1995; revised manuscript received 17 May 1995; accepted 17 May 1995

Abstract

Pre-column derivatization of proteins with fluorescamine, naphthalene-2,3-dicarboxyaldehyde, and *o*-phthaldialdehyde was used to enhance absorption and fluorescence detection after separation by SDS non-gel sieving capillary electrophoresis. When compared with underivatized proteins, absorption sensitivity increased by as much as a factor of 22 at 280 nm, and 1.74 and 4.71 at 200 and 220 nm, respectively. Under favorable conditions, absorption detection limits with the labeled proteins at 280 nm were approximately equivalent to the detection limits of underivatized proteins at 200 nm. Fluorescence detection provided attomole detection limits with the best results being obtained with high-molecular-mass proteins. Pre-column labeling decreased the efficiency of the separation, but did not give rise to multiple peaks from heterogeneous labeling. The migration velocity of labeled proteins was slightly different from the unlabeled molecules, but did not significantly degrade molecular mass determinations. Pre-column derivatization with fluorescence detection allowed the proteins in a fertilization membrane isolated from a single amphibian embryo to be easily characterized.

1. Introduction

Sodium dodecyl sulfate polyacrylamide gel electrophoresis (SDS-PAGE) is a popular method for the separation of biopolymer mixtures. When SDS-protein complexes electromigrate in a sieving medium (e.g., gel), the mobility of the complex is proportional to the log of the effective molecular radius and thus to the molecular mass [1,2]. Performing these analyses in acrylamide gel-filled capillaries decreases the analysis time and enhances quantitation capabilities with on-column detection [3–5]. Despite these advan-

tages, capillary gel electrophoresis suffers from several significant problems. These include defect formation during gel polymerization, the break down of the gels in high electric fields, and fouling of the matrix with “dirty” samples [3,6,7]. However, replacing the gel with a solution containing a sieving linear polymer [6,8–20] provides a size-based separation media that easily adapts to high potential field environments and can be easily replaced between analyses [6,14,18].

One problem associated with SDS non-gel sieving capillary electrophoresis (NGSCE) is detecting analyte zones isolated in the capillary. Absorption detection is most commonly used

* Corresponding author.

with capillary electrophoresis, but demonstrates relatively poor sensitivity due to the short optical pathlengths in the capillary. When used with SDS-NGSCE, absorption detection demonstrates comparable if not superior mass detection limits, but inferior concentration detection limits relative to SDS-PAGE utilizing silver or coomassie blue stains. One means of enhancing detection sensitivity is to react the analyte with a reagent to form a product which is more easily detected. Previous attempts to increase absorption sensitivity for free zone capillary electrophoresis by pre-column derivatization have met with some success [21], but can also have detrimental effects on the separation. Specifically, the availability of multiple reaction sites on the analyte can give rise to a multiplicity of labeled states that diminishes separation efficiency, or in extreme cases produces multiple peaks in the electropherogram [5,22]. For these reasons, pre-column derivatization reactions are not commonly utilized to enhance absorption detection in capillary zone electrophoresis, and are only used for detection for techniques in which the detector sensitivity would normally be very low (i.e., fluorescence) [5,23–26].

Pre-column derivatization of proteins may ultimately prove more useful when used in conjunction with SDS-NGSCE. These gel-based separations isolate molecules based on their physical dimensions, and so the addition of a low-molecular-mass label to the large protein molecule should not dramatically alter its migration velocity. Furthermore, low-molecular-mass impurities and excess labeling reagent should be easily separated from the analyte because of the large difference in size, as has been previously noted for labeled proteins separation by SDS-PAGE [27,28].

This paper investigates the use of pre-column labels to enhance absorption and fluorescence detection sensitivity for SDS non-gel sieving capillary electrophoresis of proteins. Three derivatizing agents will be examined with respect to their ability to enhance this detection and for their influence on separation efficiency and the mass determinations. Finally, the utility of these pre-column labeling techniques will be demon-

strated by analyzing the proteins in a single fertilization membrane isolated from the embryo of the frog *Lepidobatrachus laevis*.

2. Experimental

2.1. Instrumentation

Capillary electrophoresis separations utilizing UV absorbance detection were performed with a BioFocus 3000 capillary electrophoresis system (Bio-Rad Laboratories, Hercules, CA, USA) controlled with a MS-DOS computer running BioFocus 3000 control software (version 3.10, Bio-Rad Laboratories). Separations were performed in 24-cm long capillaries (19.4 cm inlet to detector) with an inner diameter of 50 μm and an outer diameter of 360 μm (Polymicro Technologies, Phoenix, AZ, USA). The electric field was maintained at -774 V cm^{-1} for all experiments. Forced liquid cooling was used to maintain the capillary at 20°C, while the sample carousel and the buffer reservoirs were maintained at 10°C.

Capillary electrophoresis with laser-induced fluorescence detection was performed on an instrument constructed in our laboratory. A regulated high-voltage DC power supply (Model EH50R02, Glassman High Voltage, White House Station, NJ, USA) generated an electric field of -486 V cm^{-1} in the separation capillary. Platinum wire electrodes were used to establish electrical contact between the high-voltage supply and the 0.4-ml inlet buffer reservoir, and the outlet reservoir and ground. The inlet reservoir and high-voltage end of the capillary were enclosed in a Plexiglass box to protect the operator from accidental shock. The outlet buffer reservoir was placed in a stainless-steel bomb so that the polymer solution could be forced through the capillary with nitrogen gas under a pressure of 700 kPa. Current passing through the separation capillary was measured by grounding the outlet buffer reservoir through a 1 k Ω resistor and monitoring the voltage developed across this resistor. Separations were performed in fused-silica capillaries (50 μm I.D., 360 μm O.D.,

Polymicro Technologies) which had a total length of 37 cm and an inlet to detector distance of 25 cm. The capillary and buffer reservoirs were maintained at ambient temperature (approximately 20°C) by natural radiative processes.

A schematic of the fluorescence detector used in these studies is shown in Fig. 1. The excitation beam for the fluorophore was provided by an argon-ion laser (Innova 90-5, Coherent, Palo Alto, CA, USA) operating at 457.9 nm for naphthalene-2,3-dicarboxyaldehyde (NDA), 363.8 nm for fluorescamine, and 351.1 nm for *o*-phthaldialdehyde (OPA). When ultraviolet excitation was used to excite fluorescence, a bandpass filter centered at 330 nm and a spectral bandpass of 80 nm (330WB80, Omega Optical, Brattleboro, VT, USA) was used to remove the broadband emission signal from the plasma tube in the spectral regions corresponding to fluorescence emission. A fused-silica lens (100-mm focal length, Newport Research Corporation, Irvine, CA, USA) was used to focus the 20-mW excitation laser beam into the separation capillary through a window formed by removal of the polyimide coating. The fluorescence emission from the capillary was collimated with an aluminum parabolic reflector (24 mm diameter, 5 mm focal length) and imaged onto a bandpass filter positioned approximately 30 cm away. Specular reflection of the excitation beam from the walls of the capillary was blocked by a thin

strip of metal mounted across the front face of the parabolic reflector. For OPA and fluorescamine fluorescence measurements, a filter with a central pass wavelength of 450 nm and spectral bandpass of 100 nm (400EFLP with cutoff at 500 nm, Omega Optical) isolated the analytical signal. For NDA labeled proteins, a band pass filter centered at 500 nm and a bandpass of 40 nm (500DF40, Omega Optical) was used in conjunction with a 490-nm long-pass filter (490EFLP, Omega Optical) to select for the fluorescence signal. This signal was converted to a photocurrent with a photomultiplier tube (R1527-03, Hamamatsu Corp., Bridgewater, NJ, USA) biased at values between 650 and 1000 V, amplified with a current-to-voltage amplifier (Model 428, Keithley Instruments, Cleveland, OH, USA), and digitized with a 16-bit analog-to-digital converter (Model XL-1900 mainframe with XL-ADC2 ADC, Elexor Associates, Morris Plains, NJ, USA). An Objective C program developed in our laboratory and running on a NeXTstation computer (NeXT computer, Redwood City, CA, USA) recorded the data from the analog-to-digital converter and displayed the resulting electropherogram.

2.2. Data processing

Peak areas and peak heights for data collected on the BioFocus 3000 instrument were determined with commercial integration software (BioFocus 3000 Integrator, Version 3.01, Bio-Rad Laboratories). Data collected with the NeXTstation computer were digitally low-pass filtered (Fourier filter, cutoff frequency of 0.55 Hz) with the program SciPlot (version 3.9; M. Wesemann; Berlin, Germany) to enhance the signal-to-noise characteristics of the electropherogram. The separation efficiency (N , expressed as theoretical plates) was estimated with the following formula:

$$N = 5.54(t_m/w_{1/2})^2$$

where t_m is migration time and $w_{1/2}$ is the peak width at half height.

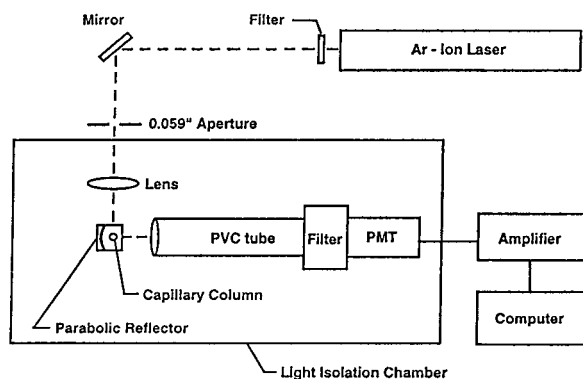


Fig. 1. Schematic of the laser-induced fluorescence detector used with non-gel sieving experiments.

2.3. Reagents

Horse heart myoglobin, α -chymotrypsinogen A type II (from bovine pancreas), conalbumin type I (from chicken egg white), fluorescamine, tris(hydroxymethyl)aminomethane (Tris) and dithiothreitol (DTT) were purchased from Sigma (St. Louis, MO, USA). Sodium dodecyl sulfate (SDS), 2-mercaptoethanol, and *o*-phthaldialdehyde in the form of phthalic dicarboxaldehyde were obtained from the Aldrich (Milwaukee, WI, USA). Certified A.C.S. grade sodium hydroxide, boric acid, and HPLC grade acetone and methanol were purchased from Fisher Scientific (Fair Lawn, NJ, USA). Protein molecular mass standards, SDS sieving buffer and SDS sample buffer were obtained from Bio-Rad Laboratories (Hercules, CA, USA), while naphthalene-2,3-dicarboxaldehyde (NDA) was purchased from Molecular Probes (Eugene, OR, USA).

Stock solutions containing 2 mg ml^{-1} of protein were prepared in doubly deionized filtered water and 100 mM sodium borate buffer (pH 9.0) as appropriate. Dithiothreitol solutions were prepared by mixing 5.7 mg DTT, $6.2 \mu\text{l}$ of 3 M NaOH, and $118 \mu\text{l}$ of water. Solutions of the derivatizing reagents were prepared just prior to use by dissolving the reagent in an appropriate solvent to achieve the desired concentration. Specifically, fluorescamine (5.0 mg ml^{-1}) was dissolved in acetone, NDA (4.0 mg ml^{-1}) was dissolved in methanol, and OPA (5.0 mg ml^{-1}) was prepared in a solution composed of $75 \mu\text{l}$ of methanol, $924 \mu\text{l}$ of water and $5 \mu\text{l}$ of 2-mercaptoethanol.

2.4. Procedures

Capillary preparation

Prior to each analysis on the BioFocus 3000, and at the beginning of each day for the fluorescence detection experiments, the capillary was sequentially purged with 0.1 M NaOH for 90 s, 0.1 M HCl for 60 s, and Bio-Rad CE SDS run buffer for a minimum of 120 s. To insure that all the run buffer had been washed from the outside

surface of the capillary prior to injection, the capillary inlet was dipped into two reservoirs containing a solution of 0.4 M boric acid, 0.4 M Tris, and 0.1% SDS.

Protein derivatization

Prior to analysis, protein samples were suspended in a 1:1 (v:v) solution containing Bio-Rad CE SDS sample buffer and 15 mM DTT, and boiled for 10 min to denature the protein. To react the sample with OPA, $40\text{-}\mu\text{l}$ aliquots of the denatured protein mixture were mixed with $4 \mu\text{l}$ of 5 mg ml^{-1} OPA solution and allowed to react for at least 5 min. For NDA derivatization, $35 \mu\text{l}$ of protein stock solutions (pH 9) were mixed with $2 \mu\text{l}$ of 0.1 M sodium cyanide and $5 \mu\text{l}$ of 4 mg ml^{-1} NDA solution. After approximately 3 min, the solution was mixed with $5 \mu\text{l}$ of DTT solution (15 mM) and $50 \mu\text{l}$ of Bio-Rad CE SDS sample buffer. Fluorescamine-labeled samples were prepared by mixing $85 \mu\text{l}$ of protein stock solutions (pH 9) with $5 \mu\text{l}$ of 5 mg ml^{-1} fluorescamine reagent. After 5 min, $10 \mu\text{l}$ of DTT stock solution and $100 \mu\text{l}$ of Bio-Rad CE SDS sample buffer were added to the mixture. These procedures utilized a large molar excess of the derivatizing reagent to simulate realistic analysis conditions and exhaustively label the analyte. Just prior to analysis, the solutions containing the labeled proteins were centrifuged for 2 min at $16\,000 \text{ g}$ to remove any particulates.

Preparation of molecular mass standards

Molecular mass standards were prepared by combining $10 \mu\text{l}$ of concentrated Bio-Rad SDS-PAGE standards, $40 \mu\text{l}$ of water, and $50 \mu\text{l}$ of Bio-Rad CE SDS sample buffer. After denaturing the mixture in a boiling water bath for 10 min, the sample was diluted to the desired concentration with a solution of 55% Bio-Rad CE SDS sample buffer and 45% water. Aliquots of this mixture were derivatized as previously described. The aprotinin standard was ignored for these experiments and was not used for molecular mass calibration.

Preparation of fertilization envelopes

Large quantities of fertilization envelopes from the frog *Lepidobatrachus laevis* were isolated by a previously described procedure [29], then individual membranes manually selected under a microscope with watchmakers forceps. This structure was suspended in 20 μ l of a 1:1 (v:v) mixture of Bio-Rad CE SDS sample buffer and a 15 mM DTT solution and boiled in a water bath for 10 min. After allowing the sample to cool to room temperature, aliquots from this mixture were derivatized as previously described.

3. Results and discussion

3.1. Absorption sensitivity enhancement

OPA, NDA and fluorescamine were evaluated for their utility as pre-column derivatization reagents to enhance absorption detection by measuring the enhancement factor, the ratio of the peak area (or height) of the derivatized molecule to the unlabeled molecule, for proteins separated by capillary electrophoresis. Table 1 summarizes this enhancement as a function of detection wavelength for two representative proteins, myoglobin and conalbumin. Although all

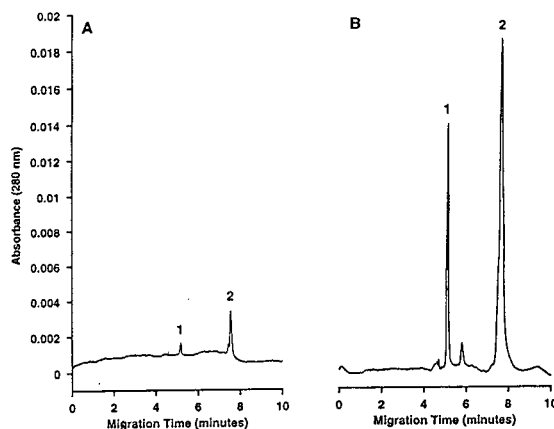


Fig. 2. Separation of (A) unlabeled and (B) NDA-labeled proteins. The peaks have been identified as follows: 1 = myoglobin (90 femtomoles), and 2 = conalbumin (48 femtomoles). Electrophoresis conditions: capillary length, 24 cm (19.4 cm from the inlet to the detector); electrokinetic injection, -10 kV for 10 s; detection, 280 nm; capillary temperature, 20°C ; carousel temperature, 10°C ; running buffer, Bio-Rad CE SDS sample buffer.

labels provided strong signal enhancement at 280 nm, the greatest signal enhancement and migration time reproducibility were observed for NDA labeled proteins. Typical %R.S.D. values observed for peak areas and heights for these measurements ranged between 5 and 10% for the three derivatizing agents. Fig. 2 shows the

Table 1
Enhancement of UV absorption by pre-column derivatization^a

Labeling reagent	Absorption					
	200 nm		220 nm		280 nm	
	Area	Height	Area	Height	Area	Height
<i>Myoglobin</i>						
NDA	1.57	1.36	2.69	2.36	22.5	19.5
OPA	1.71	0.79	4.71	2.16	4.14	2.03
Fluorescamine	1.74	0.93	2.16	1.14	14.6	7.88
<i>Conalbumin</i>						
NDA	1.21	0.82	2.09	1.23	12.0	7.24
OPA	1.52	0.70	3.48	1.56	3.03	1.41
Fluorescamine	1.48	0.77	1.64	0.84	7.51	3.80

^a These data represent the average of six or more independent measurements. Peak areas and peak heights are expressed in arbitrary units.

electrophoretic separation of labeled and unlabeled myoglobin and conalbumin. Although a dramatic enhancement of signal intensity is evident from these data, it is also important to note that the retention time and peak efficiency are not greatly altered by the presence of the derivatizing reagent. This suggests that significant gains in detection sensitivity are possible without significantly altering analysis time. It is also interesting to note that the signal enhancement for myoglobin is nearly twice that observed for conalbumin. This difference may result from the greater preponderance of accessible derivatization sites on myoglobin relative to conalbumin [30].

The data in Table 1 also suggests a trend toward smaller signal enhancements as the detection wavelength is decreased. For the underivatized proteins, only the aromatic amino acids exhibit a significant absorbance at 280 nm, whereas the entire peptide backbone contributes to the signal at shorter wavelengths. Since the initial signal is much stronger at the shorter wavelengths, the enhancements are smaller. Even greater enhancements were recorded in spectral regions in which no significant protein adsorption was observed. For example, NDA-labeled myoglobin and conalbumin demonstrated excellent sensitivity at 320 nm. By choosing protein labels with specific spectral characteristics, the absorption signal can be tailored to wavelength regions where few sample concomitants absorb, and thus obtain greater signal discrimination.

Although peak area and peak heights were both observed to increase with the derivatized

molecules, this enhancement is not necessarily consistent for both myoglobin and conalbumin. In general, when measurements were made at lower wavelengths, large increases in peak area were observed in good agreement with observations made for fluorescamine labeling of proteins in free-zone capillary electrophoresis [21]. However, peak heights were sometimes greater for the unlabeled molecules. At 200 nm, proteins derivatized with all three reagents showed a decrease in the peak heights of both proteins, while at 220 nm only fluorescamine-labeled proteins demonstrated this reduction. The signal improvement is small at the lower wavelengths because the increase in signal intensity is not able to compensate for the reduction in peak height caused by the reduced separation efficiency. At 280 nm, large enhancements of the absorbance signal resulted in peak heights greater than observed for the unlabeled species.

The separation efficiency for labeled and unlabeled conalbumin and myoglobin are summarized in Table 2. These data clearly indicate that pre-column derivatization of the proteins introduces additional zone broadening, but that the extent of this broadening is dependent on the reagent. NDA labeled proteins consistently demonstrated the highest efficiency of the reagents investigated. Fluorescamine and OPA produced nearly equivalent reductions in efficiency.

Electrophoretic analysis of proteins treated with SDS is typically used to estimate the mass of the molecule. To determine what impact pre-column labeling might have on molecular mass estimates, NDA-labeled and unlabeled solutions containing myoglobin, α -chymotrypsinogen A,

Table 2
Separation efficiency of labeled and unlabeled proteins^a

Labeling reagent	Myoglobin		Conalbumin	
	Labeled	Unlabeled	Labeled	Unlabeled
NDA	20.6	25.6	11.0	30.7
OPA	6.9	31.0	6.0	36.4
Fluorescamine	9.3	28.0	7.3	35.7

^a Efficiencies are expressed as thousands of theoretical plates.

ovalbumin, and conalbumin were analyzed by SDS-NGSCE. Unlabeled protein molecular mass standards were analyzed immediately preceding and following these samples. The logarithm of the molecular mass of each standard was plotted against its averaged migration time to construct a mass calibration plot to estimate the mass of both labeled and unlabeled proteins. These data are summarized in Table 3 along with the accepted mass of these molecules. Errors in molecular mass estimates were approximately equivalent for both samples, with the unlabeled proteins having a maximum error of 5.6% whereas the NDA-labeled species had a maximum error of 6.8%. While slightly poorer mass accuracy was observed for the labeled proteins, these errors are still within the 10% accuracy usually quoted for SDS sieving analysis [2,31].

With the data from Table 3, it is interesting to note that all of the molecular mass estimates for the derivatized proteins were lower than the actual molecular mass. This is surprising since the addition of the derivatizing reagent should increase the molecular mass of the protein SDS complex. There may be several explanations for these observations. The addition of hydrophobic label groups to the protein may have caused increased SDS binding to the protein, and therefore increased the negative charge on the complex. This would result in faster migration through the capillary and an apparent decrease in molecular mass. Similarly, the reaction of positively charged amine groups on the protein with the labeling reagent could reduce the positive charge intrinsic to the protein. Again, the

more negative charge on the complex would give rise to lower molecular mass estimates. Whether one or both effects are responsible for this change in migration velocity has not been determined.

Our observations indicate that detection limits for derivatized molecules detected at 280 nm are similar to those for underivatized molecules at 200 nm. For the reagents studied, derivatization is unlikely to provide significant improvement in detection limits. The most useful application of these reagents is to shift the region of detection to avoid spectral interferences from buffer components and sample concomitants. In favorable cases, very dramatic shifts in detection wavelengths can be observed with a minimum penalty in absorption sensitivity or separation efficiency. Even though enhanced absorptivities are observed for derivatized proteins at the 200 to 220 nm range, these improvements are usually not sufficient to justify the loss of separation efficiency and the additional complexity associated with the sample preparation. New reagents that demonstrate enhanced extinction coefficients in this spectral region, or which simplify sample preparation may overcome these limitations.

3.2. Fluorescence detection

Analyte derivatization can be used to improve the absorption signal for the detection of proteins, but even greater sensitivity enhancements can be obtained using fluorescence detection. While this mode of detection has been used for both SDS-PAGE and capillary zone electropho-

Table 3
Molecular mass determinations for labeled and unlabeled proteins

Protein	Actual M_r^a	Unlabeled proteins		NDA-labeled proteins	
		Estimated M_r ($\times 10^{-3}$)	Percent error	Estimated M_r ($\times 10^{-3}$)	Percent error
Myoglobin	16 950	17.9	5.6	15.9	6.2
α -Chymotrypsinogen A	25 656	24.8	3.3	23.9	6.8
Ovalbumin	43 300	44.0	1.6	42.9	0.9
Conalbumin	77 500	77.2	0.4	72.3	6.7

^a Molecular masses obtained from Ref. [36].

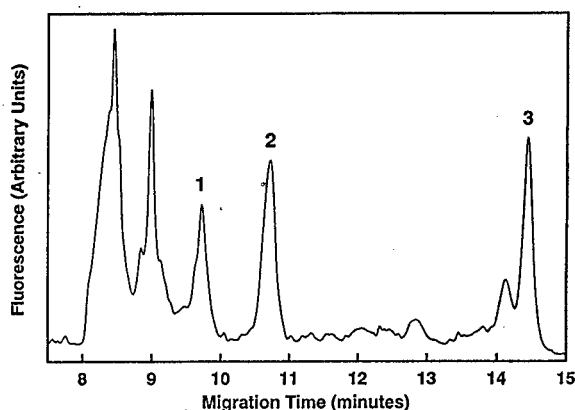


Fig. 3. Separation of fluorescamine-labeled: 1 = myoglobin (3.2 femtomole), 2 = α -chymotrypsinogen A (2.9 femtomole), and 3 = conalbumin (2.1 femtomole). Detection was by monitoring the laser-induced fluorescence signal. Electrophoresis conditions: capillary length, 37 cm (25 cm from the inlet to the detector); electrokinetic injection, -5 kV for 27 s; temperature, 20°C ; running buffer, Bio-Rad CE SDS sample buffer.

resis, fluorescence detection may prove better suited to NGSCE. On-column detection provides improved quantitation and detection limits when compared with SDS-PAGE. In addition, SDS sieving separations minimize multiple peak formation from heterogeneous labeling of single protein species. Furthermore, low-molecular-mass impurities and excess labeling reagents are easily separated from the proteins of interest.

Fig. 3 shows the separation of a 500 nM mixture of fluorescamine-labeled myoglobin (3.2 femtomole), α -chymotrypsinogen A (2.9 femtomole), and conalbumin (2.1 femtomole) monitored by laser-induced fluorescence detection. The large broad peak from 8 to 8.5 min results from excess labeling reagent and unidentified

low-molecular-mass species present in the sample and analysis buffer. The peak at 9 min is also an impurity and was present in blank samples. Impurity peaks in this region were common for all of the fluorophores. The numbers of these peaks and their position in the electropherogram are dependent on the derivatization reagent. Also noticeable are noise spikes throughout the electropherogram. These spikes were identified as small particulates generated by aggregation of material in the analysis buffer. The high viscosity of this buffer prevented these particles from being removed by filtration or centrifugation, but their presence could be minimized by heating the mixture in a boiling water bath for several minutes at the start of each day. The signal contribution of any particles remaining in the sieving buffer was suppressed with a digital low-pass filter. NDA-labeled protein solutions generated fewer artifacts in the electropherogram, but also caused a noticeable shift in the baseline approximately 10 to 12 min after the analysis was initiated.

Table 4 summarizes the limits of detection for myoglobin, conalbumin and α -chymotrypsinogen A labeled with the three fluorophores. OPA provided the lowest limit of detection for conalbumin ($3.0 \cdot 10^{-18}$ moles) but NDA provided nearly equivalent results. NDA provided better sensitivity than OPA for both myoglobin and α -chymotrypsinogen A, and both reagents provided consistently superior detection limits when compared with fluorescamine. As with absorption detection, there was a very significant reduction in detection limits with increasing mass of the analyte.

Labeling conditions for proteins were chosen to provide good detection limits and for their

Table 4
Fluorescence detection limits of pre-column labeled proteins^a

Protein	NDA	OPA	Fluorescamine
Myoglobin	27	57	190
α -chymotrypsinogen A	59	100	160
Conalbumin	9.5	3.0	96

^a Defined as a signal-to-noise of 3. Detection limits are expressed in attomoles.

ease of derivatization. While an attempt was made to use consistent conditions, the reaction characteristics of individual labels often dictated procedural changes. NDA and fluorescamine were used to derivatize protein samples prior to complexation of proteins with SDS. The NDA derivatization reaction is favored above pH 9, whereas the SDS sample buffer used in these studies was pH 8.3. Protein solutions were adjusted to pH 9.0 to insure good derivatization conditions, with the subsequent addition of the SDS buffer only after labeling had occurred. This was particularly important for fluorescamine as derivatization of proteins after SDS complexation was very difficult and resulted in low signal intensity. Fluorescamine hydrolyzes with a reaction half-time of only a few seconds [32], so we hypothesize that a large fraction of the fluorescamine is destroyed before it can interact with the SDS–protein complexes. Similarly, the slow change in color associated with the formation of the NDA–amine reaction product suggests that the NDA reaction is also slowed by the presence of SDS on the target molecule. It is possible that the SDS sterically hinders access to the derivatization sites on the protein or can interact with the labeling reagent to limit the accessibility of its reactive site. The OPA reagent was only reacted with the analyte after SDS complexation because the reaction product is relatively labile and would not tolerate the extreme conditions used for SDS complexation.

One advantage of SDS non-gel sieving CE is the ability to obtain molecular mass estimates of separated components. Fig. 4 shows the separation of commercial molecular mass standards derivatized with OPA. Detection limits for the protein molecular mass standards were determined to be 270 attomoles for lysozyme, 320 attomoles for trypsin inhibitor, 41 attomoles for carbonic anhydrase, 130 attomoles for ovalbumin, 240 attomoles for serum albumin, 51 attomoles for phosphorylase b, 39 attomoles for β -galactosidase, and 8.3 attomoles for myosin. Molecular mass calibration plots generated for labeled standards with fluorescence detection were nearly identical to similar plots generated with unlabeled standards and absorption detec-

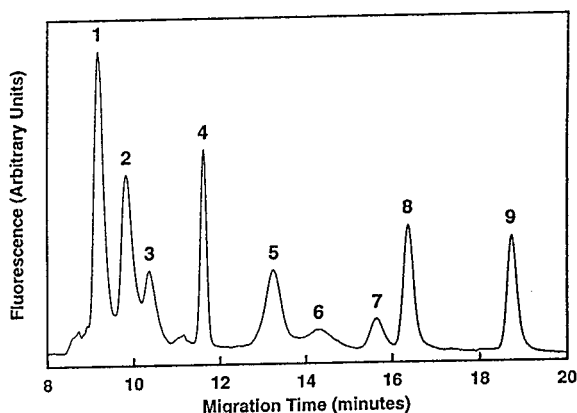


Fig. 4. Separation of molecular mass standards by non-gel sieving capillary electrophoresis. The peaks have been identified as follows: 1 = aprotinin, 2 = lysozyme, 3 = trypsin inhibitor, 4 = carbonic anhydrase, 5 = ovalbumin, 6 = bovine serum albumin, 7 = phosphorylase b, 8 = β -galactosidase, 9 = myosin. The amount of each protein injected on column was 25, 8.6, 5.8, 2.8, 2.9, 0.83, 0.57, 1.6, and 0.38 femtomoles, respectively. Electrophoresis conditions: capillary length, 37 cm (25 cm from the inlet to the detector); electrokinetic injection, -5 kV for 27 s; temperature, 20°C ; running buffer, Bio-Rad CE SDS sample buffer.

tion. Even for separations of molecular mass standards near the detection limit (signal-to-noise ratio ≈ 5), linear regression provided a correlation coefficient (r) of 0.994, suggesting that effective mass calibration can be carried out at very low concentrations.

3.3. Analysis of membrane proteins

To demonstrate the utility of pre-column derivatization techniques for the analysis of complex samples, the fertilization envelope from a single *Lepidobatrachus laevis* embryo was subjected to analysis by SDS-NGSCE with fluorescence detection. The resulting electropherogram of the OPA modified proteins is shown in Fig. 5. Previous investigations of this structure by SDS-PAGE required isolation of multiple envelopes for each analysis [29]. The detection sensitivity afforded by the pre-column derivatization reaction allowed a single fertilization envelope to be diluted in $21 \mu\text{l}$ of solution and still provides data with excellent signal-to-noise characteristics. This larger volume also simplifies sample hand-

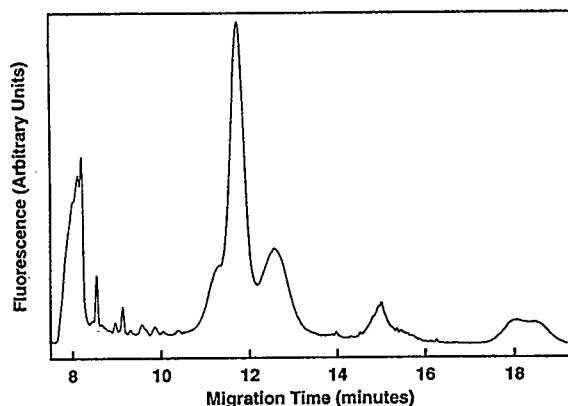


Fig. 5. Non-gel sieving capillary electrophoresis separation of a fertilization envelope from a single *Lepidobatrachus laevis* embryo. Electrophoresis conditions: capillary length, 37 cm (25 cm from the inlet to the detector); electrokinetic injection, -5 kV for 27 s; temperature, 20°C ; running buffer, Bio-Rad CE SDS sample buffer.

ling and is sufficient for more than two thousand analyses by SDS non-gel sieving capillary electrophoresis.

The molecular masses of the protein and glycoproteins separated by SDS non-gel sieving CE are comparable to data obtained from the previous SDS-PAGE study. The peak at 11.7 min in Fig. 5 was estimated to have a mass of 44 600, as compared with 39 900 by SDS-PAGE [29]. Similarly, SDS non-gel sieving molecular masses were larger than those observed by SDS-PAGE for other membrane components. This discrepancy in molecular mass may have resulted because glycosylated proteins tend to bind lower quantities of SDS, which causes them to migrate anomalously. Higher sieving gel concentrations minimize these errors [33]. Since polyacrylamide gels have a greater effective gel concentration than sieving polymer solutions, it is logical to assume that these two mass estimates might be different. Fortunately, these errors in mass assignment can be partly compensated with Ferguson analysis [34]. Ferguson analysis by SDS-NGSCE can be automated and completed in approximately the same amount of time required for one SDS-PAGE analysis, and so provide even more accurate mass estimates [19,35].

4. Conclusions

Pre-column labeling of proteins prior to separation by SDS non-gel sieving capillary electrophoresis provides an effective means of enhancing sensitivity for absorption and fluorescence detection. The greatest absorption sensitivity enhancements were observed at 280 nm with NDA as the derivatizing reagent although enhancements were also observed at 200 and 220 nm. Derivatized molecules monitored at 280 nm provided similar limits of detection as those measured for unlabeled proteins at 200 nm and 220 nm. This would allow detection to be shifted to longer wavelengths, thus avoiding spectral interferences from buffer components and sample concomitants without significant loss of sensitivity. Derivatization of the analyte produces a small but measurable reduction in separation efficiency, but this had a minimal impact on the accuracy of the molecular mass determinations. Formation of multiple peaks from single analytes due to derivatization was not observed with either UV absorbance or fluorescence detection, which suggests that pre-column derivatization of macromolecules may be more routinely applicable to this separation technique. When pre-column derivatization was utilized with fluorescence detection, the resulting detection limits were comparable to those observed for free zone capillary electrophoresis and allowed the analysis of microscopic samples.

It may be possible to further enhance detection sensitivity by developing labeling reagents which more readily react with target analytes, and which have enhanced absorptivity in specific spectral regions. Continued improvements in sieving polymer matrices which generate smaller background signals should also decrease detection limits. The high sensitivities provided by fluorescence detection coupled with the effectiveness of SDS electrophoresis techniques for separation of complex mixtures promises to be extremely useful for many applications of biological analysis. As previously demonstrated, the ability to characterize sub-cellular structures from individual cells may be advantageous when these structures cannot be isolated in larger quantities.

Acknowledgements

We would like to thank Dr. Edward J. Carroll, Jr. and Thomas R. Peavy for their assistance in acquiring fertilization envelopes from *Lepidobatrachus laevis* embryos, and to Bio-Rad Laboratories for donating the non-gel sieving polymer solutions. Financial support for this work was provided by the Arnold and Mabel Beckman Foundation and Eli Lilly and Company.

References

- [1] A.L. Shapiro, E. Viñuela and J.V. Maizel, *Biochem. Biophys. Res. Commun.*, 28 (1967) 815–820.
- [2] M. Osborn and K. Weber, *J. Biol. Chem.*, 244 (1969) 4406–4412.
- [3] A.S. Cohen and B.L. Karger, *J. Chromatogr.*, 397 (1987) 409–417.
- [4] K. Tsuji, *J. Chromatogr.*, 550 (1991) 823–830.
- [5] J.W. Jorgenson and K.D. Lukacs, *Science*, 222 (1983) 266–272.
- [6] K. Ganzler, K.S. Greve, A.S. Cohen, B.L. Karger, A. Guttman and N.C. Cooke, *Anal. Chem.*, 64 (1992) 2665–2671.
- [7] V. Dolnik, K.A. Cobb and M. Novotny, *J. Microcol. Sep.*, 3 (1991) 155–159.
- [8] A. Widhalm, C. Schwer, D. Blaas and E. Kenndler, *J. Chromatogr.*, 549 (1991) 446–451.
- [9] D. Wu and F.E. Regnier, *J. Chromatogr.*, 608 (1992) 349–56.
- [10] A. Guttman, J.A. Nolan and N. Cooke, *J. Chromatogr.*, 632 (1993) 171–175.
- [11] M. Zhu, V. Levi and T. Wehr, *Am. Biotech. Lab.*, 11 (1993) 26.
- [12] W.E. Werner, D.M. Demorest, J. Stevens and J.E. Wiktorowicz, *Anal. Biochem.*, 212 (1993) 253–258.
- [13] A. Guttman, J. Horváth and N. Cooke, *Anal. Chem.*, 65 (1993) 199–203.
- [14] M. Nakatani, A. Shibukawa and T. Nakagawa, *Biol. Pharm. Bull.*, 16 (1993) 1185–1188.
- [15] A. Guttman, P. Shieh, D. Hoang, J. Horváth and N. Cooke, *Electrophoresis*, 15 (1994) 221–224.
- [16] M. Nakatani, A. Shibukawa and T. Nakagawa, *J. Chromatogr. A*, 672 (1994) 213–218.
- [17] K. Benedek and S. Thiede, *J. Chromatogr. A*, 676 (1994) 209–217.
- [18] P. Shieh, D. Hoang, A. Guttman and N. Cooke, *J. Chromatogr. A*, 676 (1994) 219–226.
- [19] A. Guttman, P. Shieh, J. Lindahl and N. Cooke, *J. Chromatogr. A*, 676 (1994) 227–231.
- [20] K. Benedek and A. Guttman, *J. Chromatogr. A*, 680 (1994) 375–381.
- [21] N.A. Guzman, J. Moschera, C.A. Bailey, K. Iqbal and A.W. Malick, *J. Chromatogr.*, 598 (1992) 123–131.
- [22] B. Nickerson and J.W. Jorgenson, *J. Chromatogr.*, 480 (1989) 157–168.
- [23] J.W. Jorgenson and K.D. Lukacs, *J. Chromatogr.*, 218 (1981) 209–216.
- [24] B. Nickerson and J.W. Jorgenson, *J. High Resolut. Chromatogr. Chromatogr. Commun.*, 11 (1988) 878–881.
- [25] S. Wu and N.J. Dovichi, *Talanta*, 39 (1992) 173–178.
- [26] C. Toulas and L. Hernandez, *Analisis*, 20 (1992) 583–585.
- [27] J.M. Strottmann, J.B.J. Robinson and E. Stellwagen, *Anal. Biochem.*, 132 (1983) 334–337.
- [28] K. Muramoto, H. Meguro and K. Tuzimura, *Agric. Biol. Chem.*, 41 (1977) 2059–2062.
- [29] T.R. Peavy and E.J. Carroll, *Develop. Growth and Differ.*, 35 (1993) 447–460.
- [30] M.O. Dayhoff (Editor), *Atlas of Protein Sequence and Structure*, Vol. 5, 1972, The National Biomedical Research Foundation, Washington, DC.
- [31] A. Guttman and J. Nolan, *Anal. Biochem.*, 221 (1994) 285–289.
- [32] S. Udenfriend, S. Stein, P. Bohlen, W. Dairman, W. Leimgruber and M. Weigele, *Science*, 178 (1972) 871–2.
- [33] D. Tietz, *Adv. Electrophoresis*, 2 (1989) 109–169.
- [34] K.A. Ferguson, *Metabolism*, 13 (1964) 985–1002.
- [35] W.E. Werner, D.M. Demorest and J.E. Wiktorowicz, *Electrophoresis*, 14 (1993) 759–763.
- [36] R.D. Smith, J.A. Loo, C.G. Edmonds, C.J. Barinaga and H.R. Udseth, *Anal. Chem.*, 62 (1990) 882–899.



ELSEVIER

Journal of Chromatography A, 715 (1995) 179–188

JOURNAL OF
CHROMATOGRAPHY A

Improvement in the determination of food additive dyestuffs by capillary electrophoresis using β -cyclodextrin

Saeid Razee, Atsushi Tamura, Tsutomu Masujima*

Institute of Pharmaceutical Sciences, Hiroshima University, School of Medicine, Kasumi 1-2-3, Minami-ku, Hiroshima 734, Japan

Received 3 March 1995; accepted 16 May 1995

Abstract

The determination of seven food additive dyestuffs was investigated by capillary electrophoresis. When β -cyclodextrin was introduced into the carrier electrolyte, the apparent mobility was increased, leading to 9.5–39% lower migration times due to the increase in the solute's mass after inclusion complex formation. The reproducibility and peak shape were improved because interaction between the solute and the capillary wall was alleviated. The effects of β -cyclodextrin on the migration time, elution order, peak shape and reproducibility of food additive dyestuffs are discussed in terms of providing a considerable advantage for determining organic anions by capillary electrophoresis. Sequential injection of dyestuffs and β -cyclodextrin into a capillary electrophoresis column was found to be a simple and rapid method for a qualitative comparative study of inclusion complexation phenomena.

1. Introduction

Cyclodextrins (CDs) are well known carrier electrolyte additives in high-performance capillary electrophoretic (HPCE) techniques for improving separation efficiency [1–3] and have been recognized as successful chiral selectors during the last few years [4]. Since research has been concentrated on the above aspects, other applications of CDs based on their inclusion complexation ability with a large number of aromatic ring-containing compounds have yet to receive adequate attention. The role of β -CD in decreasing analysis times and improving the reproducibility during the determination of or-

ganic anions, specifically dyestuff food additives, was investigated in this work.

High-performance liquid chromatography (HPLC) [5,6] and thin-layer chromatography (TLC) [7] are the most popular methods for the determination of dyestuffs. Although HPLC methods can be performed with acceptable sensitivity, most of them are time consuming and suffer from a poor separation ability for the simultaneous determination of a broad range of dyestuffs, and they are not amenable to further methodological development. The appearance of capillary electrophoresis (CE) in the field of separation science [8] with its intrinsic capabilities, i.e., high resolution efficiency and short analysis times, ease of setting up, the small volumes required, the numerous modes for varying the selectivity and the wide range of applica-

* Corresponding author.

tion [9,10], have stimulated many researchers to examine this technique [11].

Some papers on the determination of dyestuffs by CE have been published [12–17]. In this report, we present a study on the simultaneous determination by CE of seven food additive dyestuffs using a method that takes advantage of inclusion complexation with β -CD. The effects of β -CD on analysis time, elution order, peak shape, and reproducibility were investigated. With sequential injection of dyes and β -CD into a CE column, an unusual band broadening was observed, which can be considered in terms of the formation of a mobility gradient along the sample zone due to inclusion complexation. By observing the extent of band broadening, comparison of complex formation ability with β -CD among the various dyes is feasible.

2. Experimental

2.1. Instrumentation

A high-voltage power supply (Model HCZE-30 PNO.25-LDS; Matsusada Precision Devices) was used to generate an electric field up to 30 kV. Separations were performed at 25 kV. For sequential injection studies, a 20 kV electric field was applied. On-column detection of the separated peaks was performed at 245 nm with a Model 875-CE UV-Vis detector (Jasco). Electropherograms were processed and recorded on a Chromatopac model CR3A instrument (Shimadzu). Separations were performed using a fused-silica capillary tube (77 cm long, 60 cm to the detector $\times 50 \mu\text{m}$ I.D. and $375 \mu\text{m}$ O.D.). For sequential injection, a 60 cm long capillary, 40 cm to the detector, was used. Capillaries were obtained from GL Sciences (Tokyo, Japan). Each new capillary was conditioned by flushing for 30 min with 1 M NaOH and for another 30 min with a carrier electrolyte containing 20 mM sodium tetraborate adjusted to pH 7.5 prior to use. For sequential injections studies, 10 mM sodium tetraborate of the same pH was used. Between two runs, when β -CD was absent from the carrier electrolyte, the capillary was flushed

with NaOH and conditioned for 5 min with electrolyte buffer. Hydrodynamic injection was performed by raising the anodic end of the capillary 10 cm higher than the level of the cathodic vial for 5 s.

2.2. Chemicals and reagents

All reagents were of analytical-reagent grade if not stated otherwise. All solutions including carrier electrolytes and standards were prepared using 18-M Ω water generated by a Milli-Q laboratory water purification system (Millipore, Bedford, MA, USA). Dyestuff food additives were received as a gift from the National Institute of Health Sciences, Japan. Stock standard solutions were prepared by dissolving the dyestuffs at $1 \cdot 10^{-4}$ M in distilled water and were diluted to the appropriate concentration with the same solvent prior to use.

3. Results and discussion

In CE, the relative electrophoretic mobility (μ_{rel}), depends on charge (Z) and molecular mass (M_r) and is estimated with the following equation [18]:

$$\mu_{\text{rel}} = ZM_r^{-2/3} \quad (1)$$

Owing to the dependence of mobility on charge density, any manipulation of M_r can affect the mobility and consequently the migration time. Potential approaches are derivatization and complexation. In this regard, to improve the determination of dyestuffs, we checked the effect of β -CD, which has a relatively high molecular mass and a well known ability to form inclusion complexes with organic compounds containing aromatic rings. Although β -CD is neutral, it could alter the electrophoretic mobility of analytes based on differing molecular masses of the complexed and free solutes. New patterns of elution order and resolution were observed, which are dictated by how and to what extent one solute can be included in the β -CD cavity. We investigated the behaviour of the seven food

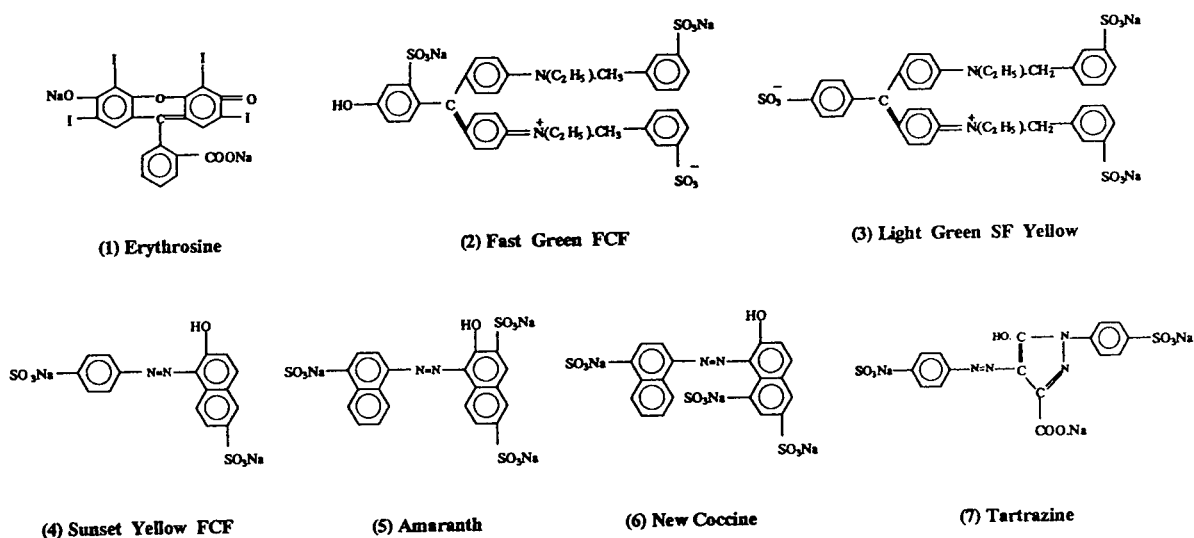


Fig. 1. Structures of the dyestuff food additives studied.

additive dyestuffs shown in Fig. 1 in the presence and absence of β -CD in carrier electrolyte. For this purpose, several analyses were performed at different concentrations of β -CD and the resulting electropherograms are shown in Fig. 2. The migration time, elution order, peak shape and reproducibility were altered as a result of differing extents of complexation of the solutes with β -CD. These parameters are discussed separately.

3.1. Migration time

Owing to formation of inclusion complexes between the dyes and β -CD, which have higher molecular masses than free dyes, the migration time decreased in all cases (see Fig. 2). Since the complex formation constants varied from solute to solute, the retention time was reduced to different extents. With a 20 mM concentration of β -CD in the carrier electrolyte, the greatest decreases were 39% in amaranth and 38% in Sunset Yellow FCF. The migration times of New Coccine, Fast Green FCF, Light Green SF Yellow and tartrazine decreased by 34.6, 34.0, 34.0 and 30.0%, respectively. The migration time of erythrosine decreased by only 9.5%. This small decrease in migration time is evidence of poor complexation with β -CD. The presence of

bulky iodine atoms in the erythrosine molecule may explain this behaviour. Another observation is that although the elution window of dyestuffs decreased from 10 to 5.5 min, complete resolution between peaks could still be established. Narrowing of the elution window not only failed to disturb the resolution between peaks, but even improved it in the case of isomeric pairs: amaranth and New Coccine. Amaranth, which is different from New Coccine only in the position of the sulfonate group (Fig. 1), showed a stronger tendency for inclusion in the β -CD cavity and eluted earlier (39 and 34.6% decrease in migration times for amaranth and New Coccine, respectively). Taking the above results into consideration, a short and qualitative discussion is given below.

The relative stabilities of β -CD and the dyes studied are governed by factors such as hydrophobic interaction and space-filling ability of molecules. Depending on the size and geometry of dyes, in relation to the dimensions of the β -CD cavity, substantial differences in the migration behaviour of dyes were observed. For example, amaranth and Sunset Yellow, bearing a similar naphthoid moiety, showed the strongest binding, which could be explained as being due to the ready inclusion of this part of molecule in the β -CD cavity via Van der Waals

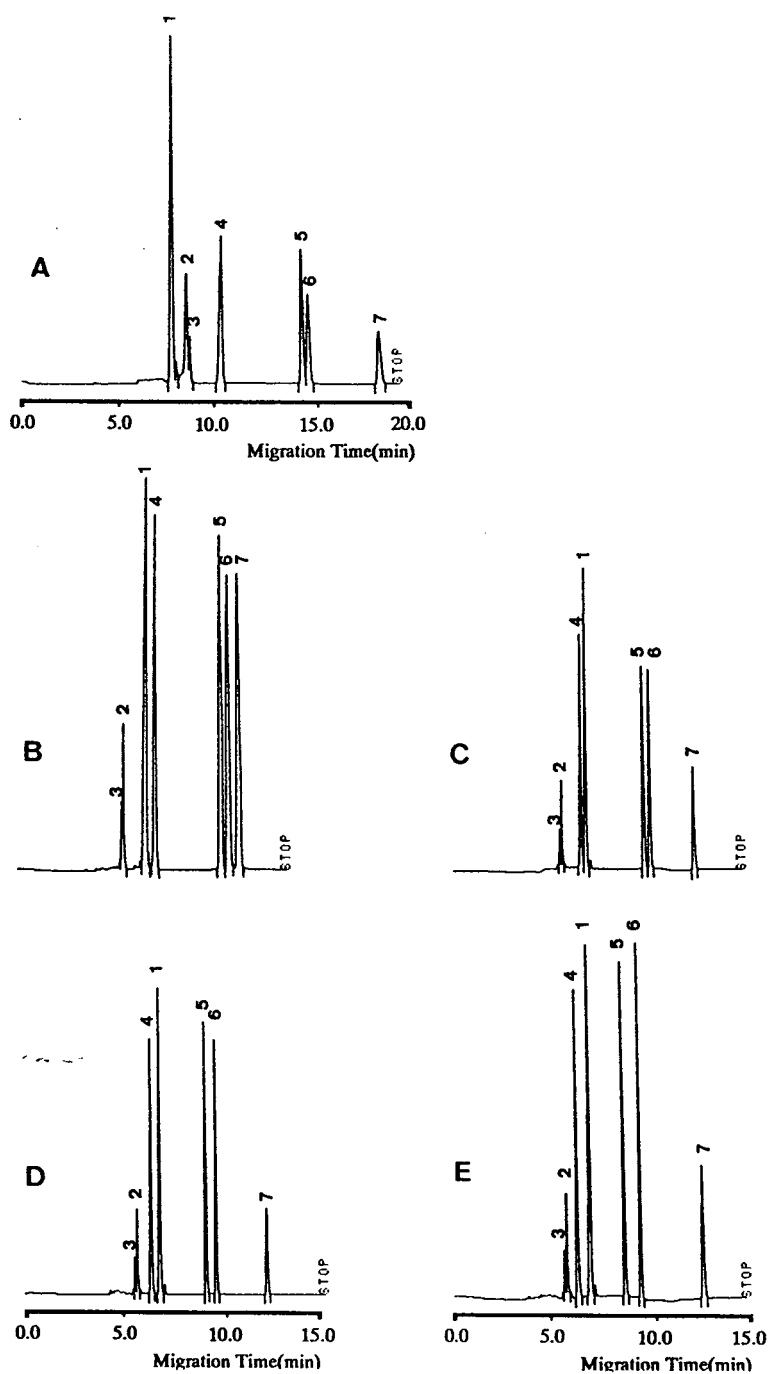


Fig. 2. Electropherograms of the separated dyestuffs and the effect of β -CD concentration on the migration time, separation and elution order. Mixtures of the dyestuffs, each at 10^{-5} M, were injected hydrodynamically for 30 s. Electropherograms: (A) 0, (B) 5, (C) 10, (D) 15 and (E) 20 mM β -CD in the carrier electrolyte. See Experimental for other conditions and Fig. 1 for peak identification.

interactions and cavity size considerations. The isomeric pair of amaranth, i.e., New Coccine, however, showed a weaker interaction owing to the different position of the sulfonate group in the naphthonoid part of the molecule. Again, Fast Green FCF and Light Green SF Yellow showed similar behaviours towards the β -CD cavity owing to the similarity of the included part of these molecules inside the β -CD cavity. In the case of tartrazine, a decrease in the hydrophobicity of molecule tends to weaken the interaction with β -CD. Finally, erythrosine as mentioned previously, showed the weakest interaction with β -CD owing to the size effect.

3.2. Elution order

A change in the elution order of the dyestuffs was observed after the addition of β -CD to the carrier electrolyte (Fig. 2). The tendency for inclusion in the β -CD cavity appears to influence the elution order of dyestuffs. The apparent mobility (μ_{app}) of dyestuffs were calculated using the equation [11]

$$\mu_{app} = L_d L_t / t_{app} V \quad (2)$$

where L_d is the distance from the injector to the detector (cm), L_t is total capillary length (cm), t_{app} is the apparent or observed migration time of dyestuffs (s) and V is the applied voltage (volts). In Fig. 3, the change in the apparent mobility of the dyestuffs is plotted as a function of β -CD concentration. When the concentration of β -CD in the carrier electrolyte increased, the apparent mobility values changed with varying patterns. This phenomenon can change the elution order of the dyestuffs, e.g., in the presence of 20 mM β -CD the elution order of erythrosine shifted from the first to the fourth peak. Fast Green FCF and Light Green SF Yellow were also eluted before erythrosine, owing to a greater tendency for inclusion complex formation. On the other hand, the elution order of erythrosine and Sunset Yellow SCF was reversed when the concentration of β -CD was increased from 5 to 10 mM (see Fig. 2). At this concentration, the interaction of Sunset Yellow SCF with β -CD was

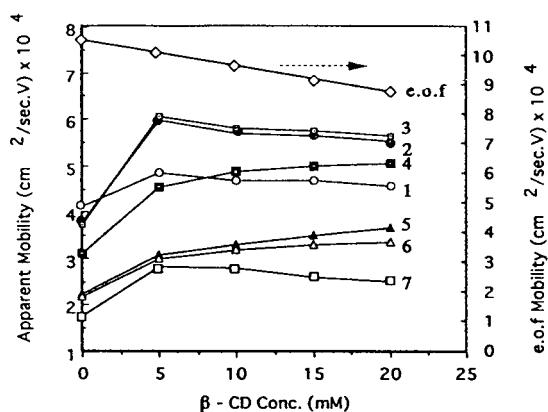


Fig. 3. Change in apparent electrophoretic mobility of dyestuffs as a function of β -CD concentration.

strong enough to change the elution order. In addition, higher concentrations of β -CD up to 20 mM were necessary for a better resolution between the peaks of erythrosine and Sunset Yellow SCF, which was decreased in 5 mM β -CD in the carrier electrolyte. It should be noted that the apparent mobility of erythrosine, Fast Green FCF, Light Green SF and tartrazine showed slight decreases when the concentration of β -CD was increased from 10 to 20 mM. These decreases in mobilities came from the decrease in electroosmotic flow due to the increase of the carrier electrolyte viscosity.

3.3. Peak shape and reproducibility

One of the drawbacks in HPCE is adsorption of analytes by silanol groups on the capillary wall. These groups can be positively charged as SiOH_2^+ , neutral as SiOH or negatively charged as SiO^- , depending on the pH of the carrier electrolyte. The surface exhibits strong adsorption of many compounds, resulting in peak tailing and poor reproducibility of migration times. Besides static or dynamic coating of the interior capillary to diminish the capillary wall effect [19,20], as a general procedure it is recommended to wash out the capillary prior to the next analysis as a capillary wall conditioning step to maintain reproducible results. In this study, owing to inclusion complexation, some part of

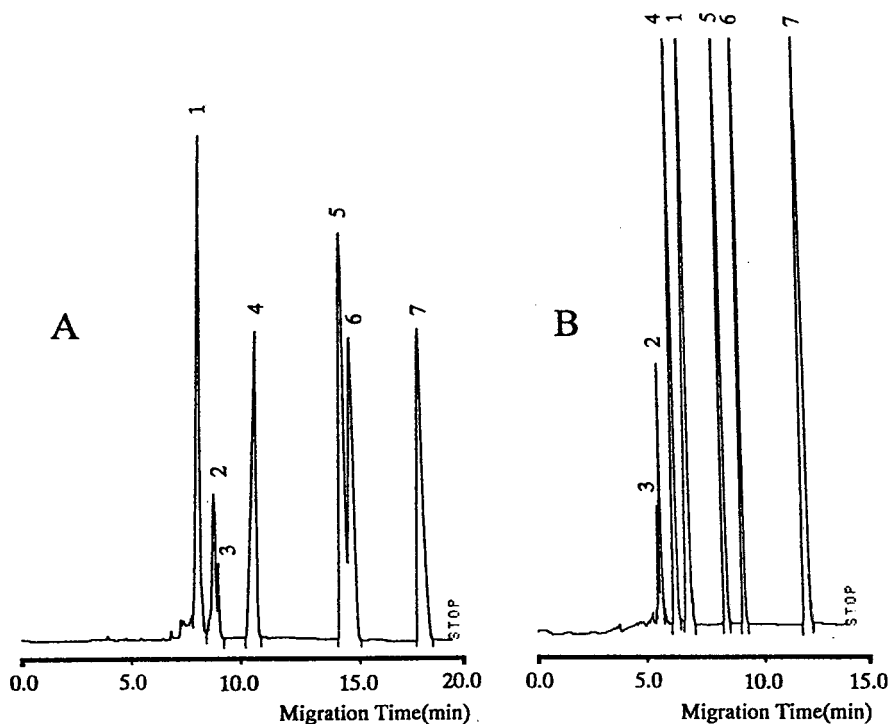


Fig. 4. Effect of β -CD on peak shape of separated dyestuffs; 10^{-4} M dyes were injected. (A) 0 and (B) 20 mM β -CD. See Experimental for other conditions and Fig. 1 for peak identification.

the dyestuffs (yet to be identified) was included in the β -CD cavity and the solute–capillary interaction seems to have been diminished. This effect can be seen in Fig. 4, where in electropherogram B sharper peaks and better resolution are obtained. The peak width at half-height for

each solute were calculated from the data taken from electropherograms A and B in Fig. 4 and provided in Table 1. Decreased peak widths and improved peak symmetry in the presence of β -CD could be evidence for lessening of the interaction with the capillary wall.

Table 1

Effects of inclusion complexation with β -CD on peak area, peak height and peak width at half-height (all in arbitrary units) of dyestuffs shown in Fig. 1

Compound	Without β -CD			With 15 mM β -CD		
	Peak area	Peak height	Peak width	Peak area	Peak height	Peak width
Erythrosine	29450	3171	2.32	46003	5203	2.21
Fast Green FCF	8357	855	2.44	1880	1875	1.08
Light Green SF Yellow	1767	424	1.04	3500	978	0.89
Sunset Yellow FCF	26141	1990	3.28	34985	5001	1.75
Amaranth	41387	2679	3.86	37569	6070	1.55
New Coccine	29187	1987	3.67	46069	9278	1.24
Tartrazine	34183	2049	4.17	51203	4599	2.78

In order to explain the effect of complexation on reproducibility, two sets of experiments with five consecutive analyses were carried out. In the first set, β -CD was present in the carrier electrolyte without the washing step between runs. In the second set, β -CD was absent and the washing step was also omitted. The ordinary procedure without β -CD in the carrier electrolyte but with the washing step between runs was also performed for comparison and the results are given in Table 2. The standard deviation for the migration times of the first set was comparable to that for the ordinary procedure. This comparative study indicates the merit of β -CD as an additive to the carrier electrolyte in CE to counteract the adverse capillary wall effect.

3.4. Sequential injection study

CE can be used for electrophoretically mixing spatially distinct zones of chemical reagents in which ethanol was determined by enzymatic reaction [21]. In our study, selected dyestuffs and β -CD were sequentially injected into a capillary column through the following steps to obtain information about the extent of interaction between the dyes and β -CD. First a mixture of dyes including erythrosine, Sunset Yellow FCF and amaranth was injected. The power supply was turned on to move the sample

zone electrophoretically towards the cathodic end. Then the power supply was turned off and β -CD was injected. Again the power supply was turned on and the main electrophoresis was started. These steps were repeated with different concentrations of β -CD and the electropherograms were recorded. As shown in Fig. 5, the electropherograms obtained had broader than normal CE peaks. The extent of band broadening was different for each solute. One explanation for this observation is that, since β -CD is neutral and the dyestuffs are anionic, after few seconds the β -CD zone can overtake the dyestuff zone and interact with solutes for inclusion complex formation. Any solute that can enter the β -CD cavity due to an increase in molecular mass will move faster than free solutes. By means of this process a velocity difference generated along the sample zone tends to form a broader band. This phenomenon is shown schematically in Fig. 6. Owing to the probability factor, higher β -CD concentrations are more favoured for inclusion complexation, so a wider sample zone and broader bands can be expected when the concentration of β -CD is increased (see Fig. 5). When water was injected instead of β -CD, band broadening was not observed, showing that the major source of band broadening comes from inclusion complex formation. This study also showed that, since in one mixture solutes with different complexation abilities have

Table 2
Reproducibility of migration times (min) for successive analyses with and without a washing step between runs in comparison with the condition of the presence of β -CD in the carrier electrolyte

Compound	No additive			15 mM β -CD	
	Mean	S.D. ^a	S.D. ^b	Mean	S.D. ^a
Erythrosine	7.45	0.38	0.03	6.59	0.05
Fast Green FCF	8.13	0.26	0.04	5.47	0.05
Light Green SF Yellow	8.28	0.28	0.03	5.36	0.03
Sunset Yellow FCF	9.87	0.61	0.04	6.16	0.07
Amaranth	13.73	0.61	0.05	8.79	0.10
New Coccine	14.04	0.33	0.03	9.32	0.05
Tartrazine	17.50	0.33	0.03	11.83	0.06

^a No washing step between runs.

^b With washing step between two runs.

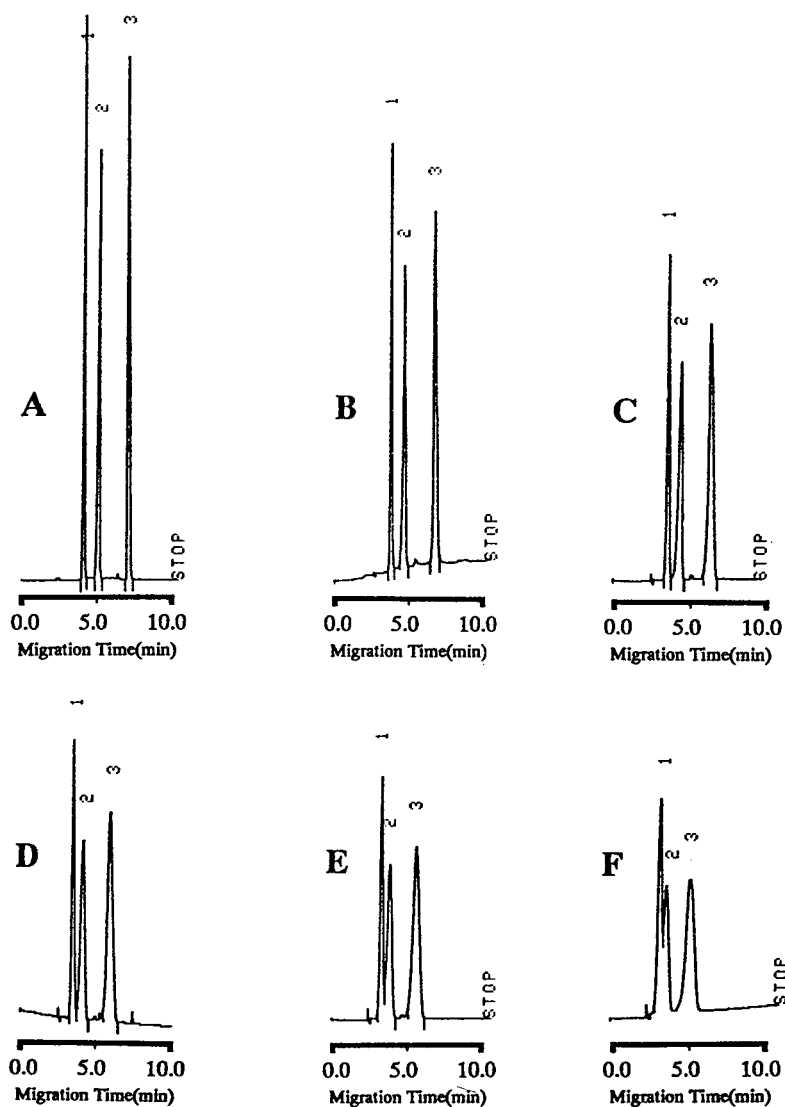


Fig. 5. Electropherograms obtained from sequential injection of dyes and β -CD into a CE column. Peaks: 1 = erythrosine; 2 = Sunset Yellow FCF; 3 = amaranth. Electropherograms: (A) injection of dye mixture only; (B–F) injection of dye mixture followed by injection of (B) 5, (C) 10, (D) 15, (E) 20 and (F) 25 mM β -CD. See Experimental for other conditions.

weaker or stronger interactions with β -CD, various extents of band broadening for each peak could be expected. Amaranth, for example, with its relatively high ability for complex formation, showed the broadest band (see Fig. 5). In fact, the extent of band broadening observed is

directly related to the ability of dyestuffs to form inclusion complexes with β -CD. The sequential injection method can thus provide an easy and rapid method for qualitative comparison of the inclusion complex formation ability of dyestuffs with β -CD. Generally this method can be ap-

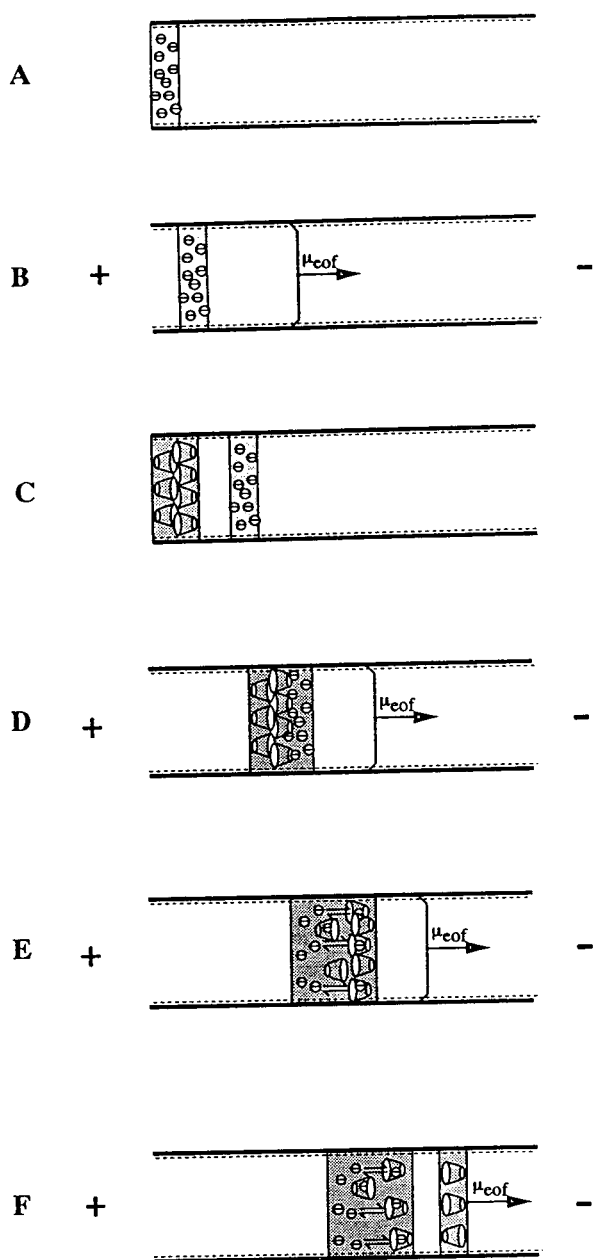


Fig. 6. Schematic representation of different steps in the sequential injection of β -CD and dyestuffs. (A–C) spatial injection of solute and reagent; (D) overtaking of the dyestuff zone by β -CD during the electrophoretic run; (E) equilibration for inclusion complex formation; (F) separation of β -CD zone from dyestuff zone, which becomes broad owing to the formation of a velocity gradient along the solute zone.

plied in any comparative study when the interaction between reagent and solutes can affect the solute's electrophoretic mobility.

4. Conclusion

We have described the advantages of host-guest complexation of food additive dyestuffs with β -CD for the simultaneous determination of these compounds in CE. The complexation with β -CD decreases the charge density and the electrophoretic mobility of the dyestuffs. Consequently, the dyestuffs eluted faster and migration times were decreased by 9.5–39% according to ability of the solutes for complex formation. Although the elution window decreased from 10 to 5.5 min, no loss in separation efficiency was observed. The resolution between the isomeric pairs amaranth and New Coccine was even improved by selective complexation with β -CD. Owing to the diminished interaction of solutes with the capillary wall and faster elution, sharper peaks and improved reproducibility in migration times were observed, which are key points for quantitative studies. Introduction of the sequential injection method described here showed the feasibility of qualitative comparative studies of inclusion complexation phenomena. The extent of band broadening for each solute is directly related to the extent of complexation ability of the solute with β -CD.

Acknowledgement

This study was partly supported by a Grant-in-aid for Scientific Research (No. 06452377) from the Ministry of Education, Science and Culture, Japan.

References

- [1] S. Terabe, H. Ozaki, K. Otsuka and T. Ando, J. Chromatogr., 332 (1985) 211.

- [2] A. Guttman, A. Paulus, A.S. Cohen, N. Grinberg and B.L. Karger, *J. Chromatogr.*, 448 (1988) 41.
- [3] Y.Y. Rawjee and G. Vigh, *Anal. Chem.*, 66 (1994) 619.
- [4] C.A. Monnig and R.T. Kennedy, *Anal. Chem.*, 66 (1994) 280R.
- [5] J.T. Hann, and I.S. Gilkson, *J. Chromatogr.*, 395 (1987) 317.
- [6] K. Korany and K. Gasztonyi, *Elelmiszervizsgalati Kozl.*, 33 (1987) 108; *C.A.*, 107 (1987) 100932f.
- [7] R. Egginger, *Fleischwirtschaft*, 68 (1988) 41; *C.A.*, 109 (1988) 21765n.
- [8] J.W. Jorgenson and K.D. Lukacs, *Anal. Chem.*, 53 (1981) 1298.
- [9] D.N. Heiger, *High Performance Capillary Electrophoresis—An Introduction*, Hewlett-Packard, Avondale, PA, 1992.
- [10] R.A. Wallingford and A.G. Ewing, *Adv. Chromatogr.*, 29 (1990) 1.
- [11] G.M. Laughlin, J.A. Nolan, J.L. Lindahl, R.H. Palmieri, K.W. Anderson, S.C. Morris, J.A. Morrison and T.J. Bronzert, *J. Liq. Chromatogr.*, 15 (1992) 961.
- [12] E.D. Lee, W. Muck and J.D. Henion, *Biomed. Environ. Mass. Spectrom.*, 18 (1989) 253.
- [13] K.P. Evans and G.L. Beaumont, *J. Chromatogr.*, 636 (1993) 153.
- [14] S.M. Burkinshaw, D. Hinks and D.M. Lewis, *J. Chromatogr.*, 640 (1993) 413.
- [15] S.N. Croft and D. Hinks, *Text. Chem. Color.*, 25 (1993) 47.
- [16] J. Varghese and R.B. Cole, *J. Chromatogr.*, 639 (1993) 303.
- [17] S. Suzuki, M. Shirano, M. Aizawa, H. Nakazawa, K. Sasa and H. Sasagawa, *J. Chromatogr. A*, 680 (1994) 541.
- [18] E.C. Rickard, M.N. Strohl and R.G. Nielsen, *Anal. Biochem.*, 197 (1991) 197.
- [19] S. Hjertén, *J. Chromatogr.*, 347 (1985) 189.
- [20] J.E. Wiktorowicz and J.C. Colburn, *Electrophoresis*, 9 (1990) 769.
- [21] J.B. Harmon, H.D. Patterson and F.E. Regnier, *J. Chromatogr. A*, 657 (1993) 429.

Short communication

High-performance liquid chromatographic determination of denatonium benzoate in ethanol with 5% polyvinylpyrrolidone

Arthur Faulkner*, Pierre DeMontigny

Merck Research Laboratories, P.O. Box 4, WP78-110, West Point, PA 19486-0004, USA

First received 31 March 1995; revised manuscript received 2 May 1995; accepted 4 May 1995

Abstract

An analytical method for the determination of denatonium benzoate in ethanol with 5% polyvinylpyrrolidone has been developed using reversed-phase ion-pair high-performance liquid chromatography with ultraviolet (210 nm) detection. The procedure is linear and accurate over the range 1.0–20.0 ppm with a limit of detection of 0.25 ppm (at a signal-to-noise ratio of 3).

1. Introduction

A bitter tasting substance can be added to a product to avoid unwanted ingestion or as a denaturant. Denatonium benzoate (Fig. 1), marketed as Bitrex, is commonly used for this purpose. Bitrex is used in ethanol as a denaturant with typical concentrations in the range 2–10 ppm. The determination of denatonium benzoate has been the subject of several publications. Techniques utilized include colorimetric assay [1,2], thin-layer chromatography (TLC) [3], high-performance liquid chromatography (HPLC) [4,5], and ion-selective potentiometry [6].

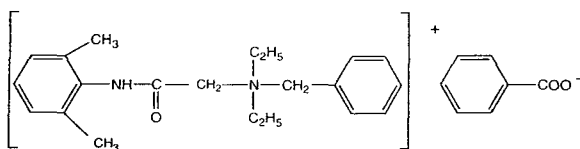


Fig. 1. Structure of denatonium benzoate (Bitrex).

HPLC procedures are especially useful because they provide the required separation to achieve good sensitivity and selectivity for the determination of low-level analytes. This was found to be the case for Bitrex in ethanol with 5% polyvinylpyrrolidone (PVP). Both previously reported HPLC methods were found to be inapplicable due to the lack of resolution between PVP and Bitrex. Therefore, a new HPLC method was required to determine Bitrex at low ppm levels. This paper describes the use of reversed-phase ion-pair chromatography to achieve this goal along with the required validation data to demonstrate the accuracy, precision, and linearity of the method.

2. Experimental

2.1. Instrumentation

The liquid chromatograph consisted of a Shimadzu (Kyoto, Japan) LC-600 pump, a

* Corresponding author.

Shimadzu SIL-6B injector, a SYS-TEC (Minneapolis, MN, USA) column heater, a Shimadzu SPD-6AV Detector, and a Shimadzu CR501 Integrator. The photodiode-array detector was a Hewlett-Packard (Waldbronn, Germany) Model HP 1040M. The chromatographic column was a Waters (Milford, MA, USA) Symmetry C₁₈, 100 Å, 5 µm, 150 × 3.9 mm I.D.

2.2. Reagents and drugs

HPLC-grade acetonitrile and water were obtained from Fisher Scientific (Fair Lawn, NJ, USA). Electrophoresis-grade sodium dodecyl sulfate, reagent-grade sodium phosphate monobasic, and 2 M hydrochloric acid were also obtained from Fisher Scientific. Ethyl alcohol U.S.P., 190 proof, was obtained from Quantum Chemical (Tuscola, IL, USA). The denatonium benzoate was obtained from Macfarlan Smith (Edinburgh, UK). Reagent-grade benzoic acid was obtained from Aldrich (Milwaukee, WI, USA). Denatonium saccharide (min. 95%) was obtained from Sigma (St. Louis, MO, USA). Polyvinylpyrrolidone (Kollidon 30) was obtained from BASF (Mount Olive, NJ, USA).

2.3. Procedure for HPLC

A stock solution of 0.1 M phosphate buffer was prepared by dissolving 13.8 g sodium phosphate monobasic (NaH₂PO₄·H₂O) in 900 ml HPLC-grade water. The pH was adjusted to 3.0 using 2 M HCl and the solution was diluted to 1000 ml with HPLC-grade water. The 0.01 M phosphate buffer solution was prepared by diluting 100 ml of the 0.1 M stock solution to 1000 ml with HPLC-grade water. The mobile phase consisted of acetonitrile–0.01 M phosphate buffer pH 3 (50:50, v/v) containing 25 mM sodium dodecyl sulfate pumped at 1.2 ml/min. The column was thermostated at 35°C and UV detection at 210 nm was used (0.08 AUFS). The injection volume was 20 µl.

2.4. Standard preparation

Accurately weigh 100 mg of denatonium ben-

zoate into a 100-ml volumetric flask. Add about 50 ml ethanol and sonicate until dissolved. Dilute to volume with ethanol and shake well. Pipet 10.0 ml of this solution into a 100-ml volumetric flask and dilute to volume with ethanol. Pipet 10.0 ml of this solution into a 100-ml volumetric flask and dilute to volume with ethanol. Pipet 10.0 ml of this solution into a 100-ml volumetric flask and dilute to volume with acetonitrile–0.01 M phosphate buffer pH 3 (50:50). This is the working standard solution (concentration, 1 µg/ml). Filter this solution through a 0.45-µm acrodisc filter and inject.

2.5. Preparation of samples

The sample solutions should be diluted with acetonitrile–0.01 M phosphate buffer pH 3 (50:50) to give a desired final concentration of about 1 µg/ml denatonium benzoate. For a 10-ppm Bitrex sample, pipet 1.0 ml of the ethanol solution containing 5% PVP into a 10-ml volumetric flask. Dilute to volume with acetonitrile–0.01 M phosphate buffer pH 3 (50:50) and shake well (concentration, 1 µg/ml). Filter this solution through a 0.45-µm acrodisc filter and inject.

3. Results and discussion

During pre-formulation studies, Bitrex (denatonium benzoate) was being evaluated as a deterrent for ingestion of a formulation consisting mainly of ethanol and polyvinylpyrrolidone (5%). Low ppm levels were being tested. Therefore, a sensitive analytical method was needed to determine Bitrex in this solution. Attempts to determine Bitrex were first made using a published HPLC method [4,5]. Results were found to be unsatisfactory due mainly to the presence of PVP, which elutes as a very broad peak overlapping with the Bitrex peak. Using these two methods, the capacity factor for Bitrex was 2.5 and 2.3, respectively, and resolution from PVP was not possible. Thus, further method development was required to obtain the needed separation.

3.1. Physico-chemical characteristics of Bitrex

To optimize the separation and sensitivity for Bitrex, the physico-chemical characteristics of this compound were examined. Because Bitrex is a quaternary ammonium (denatonium) salt of benzoic acid, its hydrophilic nature will not change as a function of pH. However, silanophilic interactions with the bonded stationary phase of the reversed-phase column would be a problem at elevated pH. Neutral-pH mobile phases were found to be inadequate, with a long retention time of denatonium, unless the organic content was increased significantly. However, high organic content was found to give a very broad peak shape for PVP, preventing adequate selectivity to be achieved for the determination of Bitrex. The effect of increasing the ionic strength by using a higher concentration of phosphate buffer was also found to be unsatisfactory. At low pH, denatonium was unretained ($k' = 0.77$) by the reversed-phase column when using a mobile phase of acetonitrile–0.01 M phosphate buffer pH 3 (50:50). This would be expected since residual silanols are protonated at low pH, significantly reducing ionic interactions. Although the denatonium molecule contains hydrophobic groups, the positively charged quaternary amine causes low retention under reversed-phase conditions. Consequently, ion-pair chromatography was evaluated with a low-pH mobile phase to increase the retention of denatonium while achieving separation from PVP.

3.2. Selection of an ion-pair reagent

The mechanism of retention in ion-pair chromatography can be described by two models [7]. In the ion-pair model, a complex is formed between the analyte and the ion-pair reagent, and this complex interacts with the stationary phase in the column. In the dynamic ion-exchange model, the ion-pair reagent coats the stationary phase in the column, resulting in a charged layer that the analyte will interact with. The mechanism of separation can be a combination of these models. These models predict that

the capacity factor of the analyte will increase with higher ion-pair reagent concentration to a limiting value.

Short hydrocarbon chain ion-pairing reagents were first evaluated for use in the mobile phase. With octane sulfonic acid sodium salt for example, denatonium retention was found to be too short and resolution from PVP was not adequate. The relatively high organic content of the mobile phase was needed to prevent the PVP peak from becoming excessively broad. As the organic content of the mobile phase increases, an ion-pair reagent with a longer hydrocarbon chain is needed to achieve an optimal separation. With this mobile phase, sodium dodecyl sulfate (SDS) would be expected to provide the most selectivity based on a compilation of adsorption isotherm and retention data [8]. SDS consists of a very long hydrocarbon chain that provides improved hydrophobic character, thereby increasing concentration of the ion-pair reagent at the surface of the stationary phase.

Experiments were performed to determine the most desirable concentration of the ion-pair reagent. The mobile phase of acetonitrile–0.01 M phosphate buffer pH 3 (50:50) was prepared with various concentrations of sodium dodecyl sulfate. The results are presented in Fig. 2. With the Symmetry column, the capacity factor was found to increase with ion-pair reagent concentration, reaching a plateau at about 25 mM. Theoretical treatment of ion-pair HPLC predicts that selectivity will approach a maximum as the

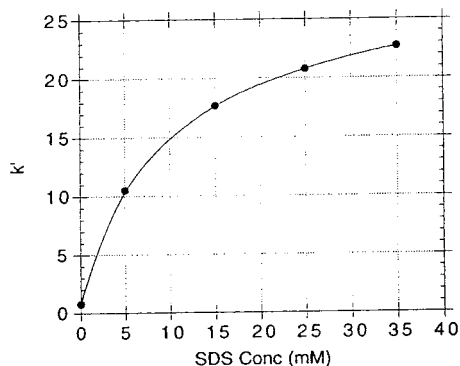


Fig. 2. Capacity factor of Bitrex versus concentration of sodium dodecyl sulfate in the mobile phase.

surface concentration of the ion-pair reagent increases. The curve in Fig. 2 is in good agreement with this prediction [7,8]. The mobile phase was buffered at low pH (3) to protonate residual silanol groups in the stationary phase and to ensure dissociation of denatonium benzoate (benzoic acid $pK_a = 4.19$). The molarity of the phosphate buffer was found to have no effect on the retention of Bitrex when changed from 0.01 to 0.05 M.

3.3. Optimization of the separation

Following the selection of a low-pH mobile phase and ion-pair chromatography to achieve the required separation for the determination of Bitrex, separation of the two ionic species of denatonium benzoate had to be demonstrated. Because a low-pH mobile phase would protonate the benzoate anion to give benzoic acid with increased retention by reversed-phase, two separate solutions were prepared. One solution consisted of benzoic acid and the other was a solution of denatonium saccharide, which is a salt of saccharin in lieu of benzoic acid. HPLC photodiode-array spectra along with the chromatogram of denatonium benzoate are shown in Fig. 3. Clearly, both ionic species were found to be well separated using a mobile phase consisting of acetonitrile–0.01 M phosphate buffer, pH 3 (50:50) containing 25 mM sodium dodecyl sulfate. Benzoic acid was found to elute at 1.4 min

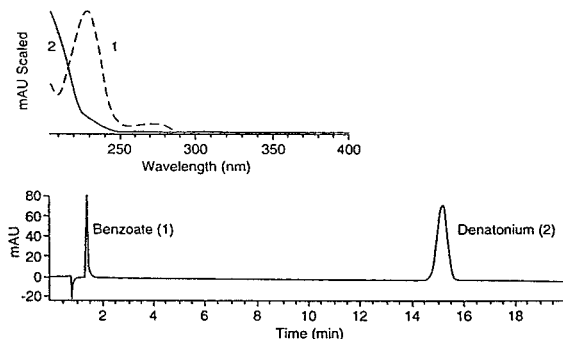


Fig. 3. Diode-array spectra (top) and chromatogram (bottom) of denatonium benzoate (1.0 mg/ml).

and denatonium eluted at 15.2 min. Since denatonium is responsible for bitter taste, there was no need to quantitate benzoic acid; however, the lack of interference was clearly demonstrated. Detection at 210 nm was preferred to other wavelengths to achieve adequate sensitivity for the determination of denatonium at low ppm levels.

The solution of denatonium saccharide was analyzed and compared with a solution of denatonium benzoate. When corrected for the difference in molecular mass, the denatonium peak had an equivalent response in both cases, thus demonstrating complete dissociation of the analyte under the HPLC conditions. Typical chromatograms of a Bitrex standard and an ethanol with 5% PVP sample containing 10.0 ppm Bitrex are shown in Fig. 4. Baseline separation of PVP and denatonium is illustrated.

3.4. Analytical method validation

Validation of the method was conducted by spiking known amounts of Bitrex into ethanol with 5% PVP. Solutions were prepared containing 1, 5, 10, and 20 ppm Bitrex. Results of replicate analyses and recovery are presented in Table 1. Recovery of Bitrex ranged from 95 to

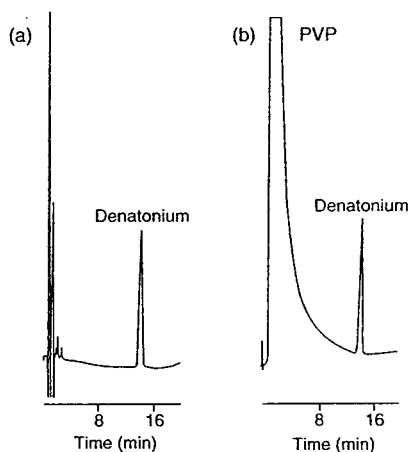


Fig. 4. Chromatogram of (a) Bitrex standard (1 $\mu\text{g/ml}$) and (b) 10.0 ppm Bitrex in ethanol with 5% PVP.

Table 1
Linearity and recovery results for Bitrex in PVP–ethanol solution

Bitrex added (ppm)	Bitrex found (ppm)	Recovery (%)	Mean recovery (%)	R.S.D. recovery (%)
1.03	1.03	99.9	96.7	2.85 (<i>n</i> = 3)
1.03	0.980	94.8		
1.03	0.987	95.5		
5.17	5.06	97.8	98.6	0.72 (<i>n</i> = 3)
5.17	5.11	98.9		
5.17	5.13	99.2		
10.3	10.3	99.7	99.1	0.88 (<i>n</i> = 5)
10.3	10.3	99.5		
10.3	10.2	98.9		
10.3	10.3	99.8		
10.3	10.1	97.7		
20.7	20.5	99.1	99.3	0.19 (<i>n</i> = 3)
20.7	20.6	99.4		
20.7	20.6	99.4		
Mean R.S.D. recovery		1.16		
Slope (standard error)		4201 (± 9)		
Intercept (standard error)		−164 (±103)		
Correlation coefficient		0.9999		
Number of data points		14		
Linear range studied (ppm)		1–20		

100%, thus demonstrating that the method is quantitative. The standard deviation of the results is larger at the lower concentration, as expected. However, the R.S.D. of less than 3% for 1.0 ppm is acceptable at that level. At the target concentration of 10 ppm, the recovery (99.1%) and the precision (0.88%) demonstrate the reliability of the method. Linearity of the method is demonstrated by the correlation coefficient of 0.9999 (*n* = 14), based on the linear regression of response versus concentration of Bitrex from the accuracy data. The intercept is only 0.4% of the response of 10 ppm Bitrex, further supporting the linearity of the method.

Lack of interference was demonstrated by assaying ethanol with 5% PVP. There were no peaks present that would interfere with the quantitation of Bitrex. Based on a signal-to-noise ratio (*S/N*) of 3, the limit of detection for this method is 0.25 ppm. In ethanol solution without

PVP present, where injection without dilution is possible, the limit of detection is 0.025 ppm (*S/N* = 3). The limit of quantitation for this method is 1.0 ppm (*S/N* = 12).

4. Conclusions

A rapid and sensitive analytical procedure for Bitrex in ethanol with 5% PVP was developed. The separation offers improved resolution compared to previously reported methods [4,5]. Also with this method, the retention of Bitrex can be readily optimized to achieve resolution from various components of a formulation by adjusting the concentration of the ion-pair reagent in the mobile phase. The sensitivity is appropriate for most applications in which Bitrex is used as a denaturant.

References

- [1] National Formulary XVII, American Pharmaceutical Association, Washington, DC, 17th ed., 1990, p. 1924.
- [2] K. Helrich (Editor), Official Methods of Analysis of the Association of Official Analytical Chemists, Association of Official Analytical Chemists, Arlington, 15th ed., 1990, pp. 1152–1154.
- [3] M.J. Glover and A.J. Blake, *Analyst*, 97 (1972) 891.
- [4] K. Sugden, T.G. Mayne and C.R. Loscombe, *Analyst*, 103 (1978) 653.
- [5] C.E. Damon and B.C. Pettitt, Jr., *J. Chromatogr.*, 195 (1980) 243.
- [6] O.G.B. Nambiar, K. Gosavi and T. Ravindranathan, *Analyst*, 116 (1991) 1011.
- [7] M.T.W. Hearn (Editor), *Ion-Pair Chromatography*, Marcel Dekker, New York, 1985, Ch. 2.
- [8] A. Bartha, G. Vigh and Z. Varga-Puchony, *J. Chromatogr.*, 499 (1990) 423.



ELSEVIER

Journal of Chromatography A, 715 (1995) 195–198

JOURNAL OF
CHROMATOGRAPHY A

Short communication

Determination of amphoteric surfactants in cosmetic cleansing products by high-performance liquid chromatography on a cation-exchange column

Angela Tegeler, Wolfgang Ruess, Erich Gmahl*

Analytical department of Wella AG, Berliner Allee 65, 64274 Darmstadt, Germany

First received 2 March 1995; revised manuscript received 16 May 1995; accepted 16 May 1995

Abstract

An HPLC method with diode-array detection at 210 nm is described for the routine determination of amphoteric surfactants with a betaine structure in cosmetic cleansing products. In a strongly acidic pH range cocamidopropylbetaine and alkylbetaine are successfully separated from non-ionic and anionic matrix components on a cation-exchange column (Nucleosil 100-5 SA, 5 μm , 250 \times 4 mm I.D.). Chromatographic separation was carried out under isocratic conditions at a flow-rate of 1.0 ml/min. The mobile phase consisted of 70% acetonitrile and 30% 0.05 M lithium hydroxide in water, adjusted to pH 1.6 with phosphoric acid (v/v). As sample preparation the products and standards were simply diluted and subsequently filtered before injection. The method is precise, robust, independent of the shampoo matrix and thus suitable for routine use, such as product quality control.

1. Introduction

Today the use of cosmetic cleansing products, such as shampoos or shower foams and foam baths, has become an important part of our regular habits and, as consumers, it is difficult to imagine life without them. Besides the auxiliary agents, such as thickeners, opacifiers, perfume oils, colourants and preservatives, the detergents are the most important ingredients of such products. From the analytical point of view the present formulations represent extremely complex mixtures on account of their numerous components, of which the surfactants can also exhibit variation in the length of the carbon chain and the degree of ethoxylation.

A typical present-day formula could contain an anionic (e.g. alkyl ether sulfate), a non-ionic (e.g. alkyl polyglucoside) as well as an amphoteric surfactant (e.g. cocamidopropylbetaine) as cleansing agents. As amphoteric surfactants are gentle to the skin and mucous membranes, they particularly influence the quality of a shampoo. For this reason it is absolutely essential to have an efficient but uncomplicated method to quantify them in the appropriate products.

In the past, several papers were published dealing with the solution of this problem using HPLC on different types of columns and with different detection techniques [1–5]. When we repeated these methods in our laboratory we discovered, however, that the determination was highly dependent on the product matrix and was in many cases impossible. Therefore, we de-

* Corresponding author.

veloped a method on a cation-exchange column in the strongly acidic pH range to enhance the selectivity so that neutral or anionic matrix components show no retention, but the amphoteric surfactants are retarded, as they carry a positive charge under these conditions. Thus, the detection and quantitative determination of the two most important members of this class of compounds in our shampoos, i.e. cocamidopropylbetaine and alkylbetaine, are described in the following.

2. Experimental

2.1. Chemicals

Acetonitrile and HPLC grade water were supplied by Zinsser Analytik (Frankfurt, Germany), orthophosphoric acid (85%, p.a.) and lithium hydroxide (approx. 98%) were supplied by Merck (Darmstadt, Germany). Cocamidopropylbetaine (Fig. 1) was obtained from Goldschmidt (Essen, Germany) as the raw material Tego Betain L7 (approx. 30% active substance in water). Alkylbetaine (Fig. 2) was obtained from Kaprolactam (Dzerzhinsk, Russia) as a 30% aqueous solution.

The alkyl chain-lengths of cocamidopropylbetaine are given by the supplier and correspond to the well-known coconut fatty acid distribution. The chain-length distribution of the alkylbetaine raw material was determined by a GC-MS method, where the betaines are pyrolyzed in the injection port of the GC to the

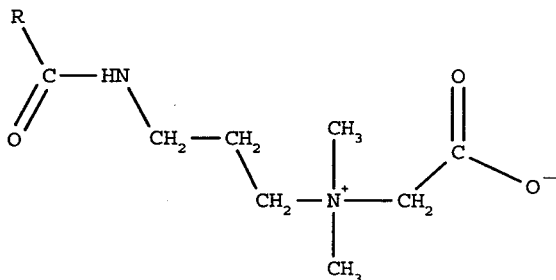


Fig. 1. Structure of cocamidopropylbetaine, R = alkyl chains of coconut fatty acids.

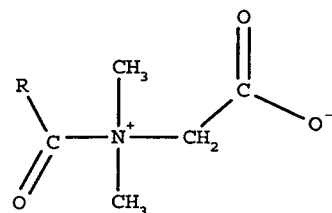


Fig. 2. Structure of alkylbetaine, R = alkyl chains of C₁₂ and C₁₄ fatty acids.

corresponding N,N-dimethylalkylamines which afterwards can be separated and quantified [6].

2.2. Instrumentation

The analyses were carried out on a liquid chromatograph HP 1090 Series M (Hewlett-Packard, Palo Alto, CA, USA) with autosampler, HPLC^{3D} ChemStation (DOS series) and a diode-array detector operated at a wavelength of 210 nm.

2.3. Chromatographic conditions

A cation-exchange column Nucleosil 100-5 SA, 5 μ m, 250 \times 4 mm I.D. (Macherey-Nagel, Düren, Germany) was used. The mobile phase consisted of 70% acetonitrile and 30% 0.05 M lithium hydroxide in water, adjusted to pH 1.6 with phosphoric acid (v/v). Separation was carried out under isocratic conditions at a flow-rate of 1.0 ml/min and a constant temperature of 40°C. The injected sample volumes were 10 μ l in each case.

2.4. Sample preparation

Before injection the shampoos were diluted approximately 1:10 to 1:20 with water and suspended matter was removed by filtration with a membrane syringe filter (0.45 μ m, Hewlett-Packard). The calibration solutions were prepared in the same way. The dilution depends on the expected concentration in the formulations.

3. Results and discussion

Fig. 3 shows a typical chromatogram of commercially available shampoos containing alkylbetaine (left) or cocamidopropylbetaine (right). The distribution of the fatty acid homologues corresponds to the surfactant raw materials used. It is evident that the selectivity of the column achieves excellent separation of the shampoo matrix. Thus all the non-ionic or anionic components are eluted long before the betaines.

Although the cocamidopropylbetaines are separated better than the alkylbetaines under the conditions described, the separation efficiency was satisfactory in both cases.

For the quantitative determination the cali-

bration curves were plotted according to the external standard method based on the areas of the C₁₂ homologues in each case. In the concentration range for shampoos (0.1–2% by weight), when dilution is taken into account, the linearity according to the equation $y = mx + b$ is very good. The regression data for alkylbetaine ($m = 7.21$, $b = -0.608$, correlation coefficient = 0.99991) and cocamidopropylbetaine ($m = 78.92$, $b = 8.84$, correlation coefficient = 0.99984) were obtained with 5 data points each.

The results of the quantitation of the betaines in two commercially available shampoos are summarized in Table 1. Both alkylbetaine in shampoo 1 and cocamidopropylbetaine in shampoo 2 can be determined with a high degree of precision and accuracy.

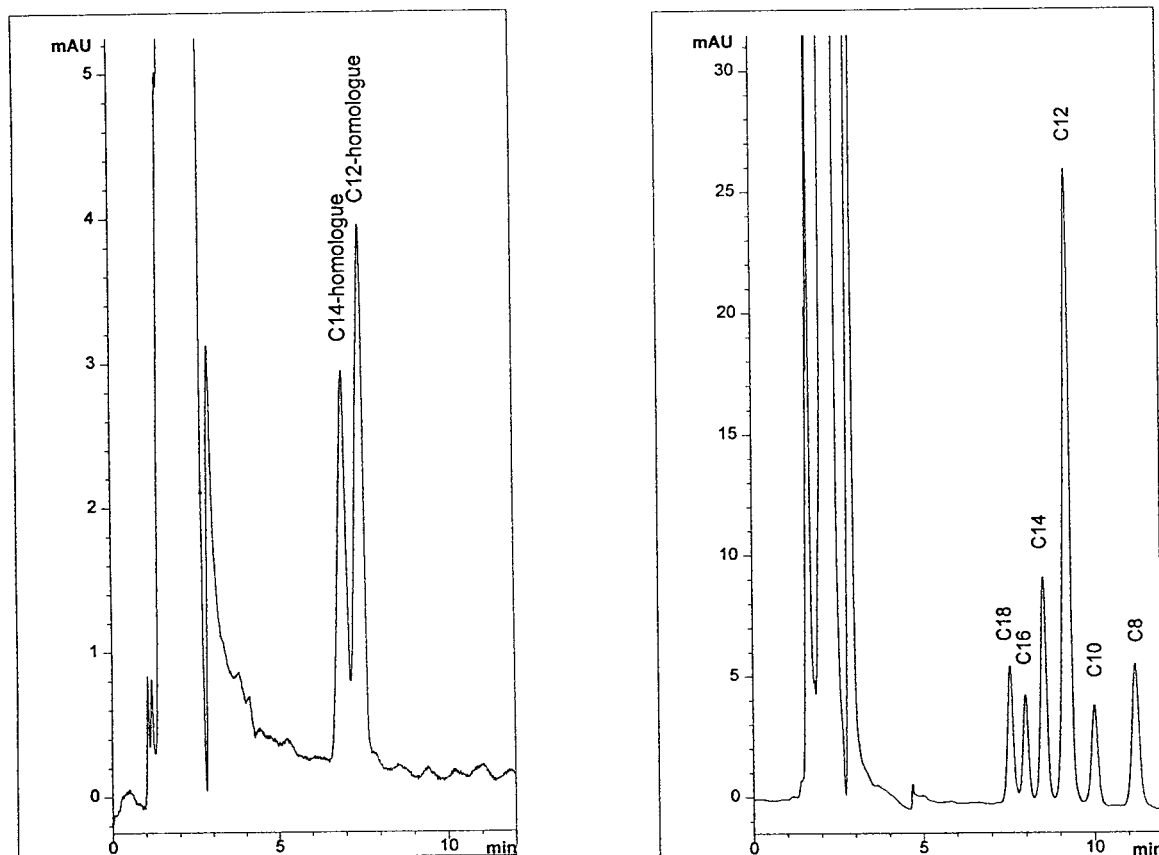


Fig. 3. Chromatograms of shampoos with alkylbetaine (left) and cocamidopropylbetaine (right) under the analytical conditions described above.

Table 1

Values obtained in the determination of alkylbetaine and cocamidopropylbetaine in commercially available shampoos with mean, standard deviation and expected value

Measurement No.	Percentage (w/w) of alkylbetaine in shampoo 1	Percentage (w/w) of cocamidopropylbetaine in shampoo 2
1	5.01	5.04
2	4.88	5.06
3	4.94	5.04
4	4.89	5.03
5	4.96	4.97
6	5.09	5.05
7	4.76	4.99
8	5.08	5.06
Mean	4.95	5.03
S.D.	0.11	0.033
Expected	5.0	5.0

4. Conclusions

The method described here for the determination of the amphoteric surfactants with betaine structure is rapid and uncomplicated on the one hand, and also precise and robust on the other, as we ascertained in the analysis of numerous shampoos and shower foams. For us, this method represented a considerable improvement over the methods previously presented in papers on this subject. It is also eminently suitable for use as a routine method in production quality control.

References

- [1] K. Nakamura and Y. Morikawa, *J. Am. Oil Chem. Soc.*, 61 (1984) 1130.
- [2] Y. Kondoh and S. Takano, *Anal. Sci.*, 2 (1986) 467.
- [3] H. Koenig and W. Strobel, *Proc. 2nd World Surfactants Congress, Paris, Vol. 3, 1988*, p. 108.
- [4] M. Matsuzaki, K. Ishii, H. Yoshimura and S. Hashimoto, *J. Soc. Cosmet. Chem. Jpn.*, 27 (1993) 494.
- [5] A.J. Wilkes, G. Walraven and J.M. Talbot, *Comun. Jorn. Com. Esp. Deterg.*, 25 (1994) 209.
- [6] E. Gmahl and A. Tegeler, unpublished results.



ELSEVIER

Journal of Chromatography A, 715 (1995) 199–200

JOURNAL OF
CHROMATOGRAPHY A

Letter to the Editor

Experiences with HPLC-grade solvents

Chromatographers usually assume that the special HPLC-grade solvents available from several manufacturers provide the level of quality and reproducibility that is needed for high-quality separations. After all, the label specifications spell out the level of merit, and the significant price of the solvent should justify the assumed excellence. Unfortunately, however, in some cases, the quality assumed for these solvents is not provided. I cite recent incidents that suggest that we should always be wary of solvents, particularly when unexplained problems arise.

Acetonitrile

After several months of success, studies with a new prototype column used for the reversed-phase separation of synthetic peptides suddenly went sour. After a brief period with the usual acetonitrile–aqueous trifluoroacetic acid gradients, efficient, well-packed columns quickly developed high back pressure, much lowered plate numbers and poor peak shapes. After two weeks of frustrating work, we concluded that the prototype column packing was not the problem source. During this time the operator attempted to replace the column inlet frit of a column that went “bad”. Much to his surprise, the porous stainless-steel frit was removed only with great difficulty, and when it finally released, about a millimeter of packing was stuck to it. This ridge of packing on the frit was very hard, and particles were essentially glued together. The remaining inlet of the column packed bed was in the same shape. We suspected that a polymeric material was building up in the column inlet.

Having no further ideas as to the cause of this problem, we changed sources for water, trifluoroacetic acid and acetonitrile. When acetonitrile from another manufacturer was used, the problem immediately disappeared.

In discussing the problem with the manufacturer of the original acetonitrile, we learned that this solvent now is purified by an adsorption process, rather than the previous (and traditional) distillation over permanganate. We speculate that the adsorption process, as exercised, failed to remove material (an unsaturate?) that polymerized upon contacting the inlet frit or the packed bed. This undesirable material apparently is removed by permanganate/distillation, and may be removed by adsorption performed properly. Shifting to a solvent made by another manufacturer solved this vexing problem.

Dichloromethane

When using this solvent for normal-phase separations with unmodified silica, we suddenly observed problems with irregular peak shapes and varying retention times. The HPLC instrument was functioning properly, and other checks showed that the columns were appropriately packed. After much frustration, we were suspicious that the solvent may be problem (obtained from the same manufacturer that supplied the tainted acetonitrile above!). Some of this dichloromethane was shaken with an equal volume of water; the aqueous phase became strongly acidic. Based on this result, we speculated that this dichloromethane (tested from several fresh bottles) contained hydrochloric acid, likely

formed by the hydrolysis of phosgene created by the oxidation/degradation of dichloromethane. Again, HPLC-grade solvent from another manufacturer immediately cleared up the problem. We also were able to suitably purify the contaminated solvent by treatment with Florisil.

The lesson learned by these experiences is that solvent purity should never be taken for granted.

If problems occur for no definable reason, a change to solvents from another manufacturer may be the answer.

*Rockland Technologies,
Inc, Newport, DE, USA*

J.J. Kirkland

PUBLICATION SCHEDULE FOR THE 1996 SUBSCRIPTION

Journal of Chromatography A

MONTH	Oct. 1995	Nov. 1995	Dec. 1995 ^a	
Journal of Chromatography A	715/1	715/2 716/1 + 2 717/1 + 2	718/1 718/2	The publication schedule for further issues will be published later.
Bibliography Section				

^a Vol. 701 (Cumulative Indexes Vols. 652–700) expected in December.

INFORMATION FOR AUTHORS

(Detailed *Instructions to Authors* were published in *J. Chromatogr. A*, Vol. 657, pp. 463–469. A free reprint can be obtained by application to the publisher, Elsevier Science B.V., P.O. Box 330, 1000 AH Amsterdam, Netherlands.)

Types of Contributions. The following types of papers are published: Regular research papers (full-length papers), Review articles, Short Communications, Discussions and Letters to the Editor. Short Communications are usually descriptions of short investigations, or they can report minor technical improvements of previously published procedures; they reflect the same quality of research as full-length papers, but should preferably not exceed five printed pages. Discussions (one or two pages) should explain, amplify, correct or otherwise comment substantively upon an article recently published in the journal. Letters to the Editor (max. two printed pages) bring up ideas, comments, opinions, experiences, advice, disagreements, insights, etc. For Review articles, see inside front cover under Submission of Papers.

Submission. Every paper must be accompanied by a letter from the senior author, stating that he/she is submitting the paper for publication in the *Journal of Chromatography A*.

Manuscripts. Manuscripts should be typed in **double spacing** on consecutively numbered pages of uniform size. The manuscript should be preceded by a sheet of manuscript paper carrying the title of the paper and the name and full postal address of the person to whom the proofs are to be sent. As a rule, papers should be divided into sections, headed by a caption (e.g., Abstract, Introduction, Experimental, Results, Discussion, etc.). All illustrations, photographs, tables, etc., should be on separate sheets. Manuscripts should be accompanied by a 5.25- or 3.5-in. disk. Your disk and (**exactly matching**) printed version (printout, hardcopy) should be submitted together to the accepting editor or Editorial Office **according to their request**. Please specify the type of computer and word-processing package used (do not convert your textfile to plain ASCII). Ensure that the letter "l" and digit "1" (also letter "O" and digit "0") have been used properly, and format your article (tabs, indents, etc.) consistently. Characters not available on your word processor (Greek letters, mathematical symbols, etc.) should not be left open but indicated by a unique code (e.g. *gralpha*, @, #, etc., for the Greek letter α). Such codes should be used consistently throughout the entire text. Please make a list of such codes and provide a key. Do not allow your word processor to introduce word splits and do not use a "justified" layout. Please adhere strictly to the general instructions on style/arrangement and, in particular, the reference style of the journal. Further information may be obtained from the Publisher.

Abstract. All articles should have an abstract of 50–100 words which clearly and briefly indicates what is new, different and significant. No references should be given.

Introduction. Every paper must have a concise introduction mentioning what has been done before on the topic described, and stating clearly what is new in the paper now submitted.

Experimental conditions should preferably be given on a *separate* sheet, headed "Conditions". These conditions will, if appropriate, be printed in a block, directly following the heading "Experimental".

Illustrations. The figures should be submitted in a form suitable for reproduction, drawn in Indian ink on drawing or tracing paper. Each illustration should have a caption, all the *captions* being typed (with double spacing) together on a *separate sheet*. If structures are given in the text, the original drawings should be provided. Coloured illustrations are reproduced at the author's expense. The written permission of the author and publisher must be obtained for the use of any figure already published. Its source must be indicated in the legend.

References. References should be numbered in the order in which they are cited in the text, and listed in numerical sequence on a separate sheet at the end of the article. Please check a recent issue for the layout of the reference list. Abbreviations for the titles of journals should follow the system used by *Chemical Abstracts*. Articles not yet published should be given as "in press" (journal should be specified), "submitted for publication" (journal should be specified), "in preparation" or "personal communication".

Vols. 1–651 of the *Journal of Chromatography*; *Journal of Chromatography, Biomedical Applications* and *Journal of Chromatography, Symposium Volumes* should be cited as *J. Chromatogr.* From Vol. 652 on, *Journal of Chromatography A* should be cited as *J. Chromatogr. A* and *Journal of Chromatography B: Biomedical Applications* as *J. Chromatogr. B*.

Dispatch. Before sending the manuscript to the Editor please check that the envelope contains four copies of the paper complete with references, captions and figures. One of the sets of figures must be the originals suitable for direct reproduction. Please also ensure that permission to publish has been obtained from your institute.

Proofs. One set of proofs will be sent to the author to be carefully checked for printer's errors. Corrections must be restricted to instances in which the proof is at variance with the manuscript.

Reprints. Fifty reprints will be supplied free of charge. Additional reprints can be ordered by the authors. An order form containing price quotations will be sent to the authors together with the proofs of their article.

AVAILABLE AT YOUR FINGERTIPS:

NOW AVAILABLE:

THE ELSEVIER SCIENCE COMPLETE CATALOGUE ON INTERNET

THE ELSEVIER SCIENCE COMPLETE CATALOGUE 1995 ON CD-ROM

These catalogues feature all journals, books and major reference works from Elsevier Science. Furthermore they allow you to access information about the electronic and CD-ROM products now published by Elsevier Science.

Demonstration examples of some of these products are included.

Features include:

ELSEVIER SCIENCE



Catalogue on INTERNET

- All the journals, with complete information about journal editors and editorial boards
- Listings of special issues and volumes
- Listings of recently published papers for many journals
- Complete descriptions and contents lists of book titles
- Clippings of independent reviews of published books
- Book series, dictionaries, reference works
- Electronic and CD-ROM products
- Demonstration versions of electronic products
- Free text search facilities
- Ordering facilities
- Print options
- Hypertext features

ELSEVIER SCIENCE



Catalogue on CD-ROM

Extra features with the Catalogue on Internet

- Alerting facility for new & forthcoming publications
- Updated monthly

**ELSEVIER SCIENCE
COMPLETE CATALOGUE
INTERNET: TRY IT TODAY!**

gopher to: gopher.elsevier.nl
WWW: <http://www.elsevier.nl/>

CD-ROM (published yearly, free of charge)

Please contact:

Customer Service Department
Tel.: +31 (20) 485 3757
Fax: +31 (20) 485 3432
e-mail: ninfo-f@elsevier.nl



ELSEVIER



PERGAMON



NORTH
HOLLAND



EXCERPTA
MEDICA



0021-9673(19951027)715:1;1-0